Regulation of BCR-ABL expression via its 3'untranslated region

Bradley Chereda

A thesis submitted for the degree of
Doctor of Philosophy
to the University of Adelaide

December 2012

School of Medicine
Faculty of Health Sciences
University of Adelaide

Leukaemia Biology Group
Centre for Cancer Biology
IMVS, SA Pathology

Declaration

This work contains no material which has been accepted for the award of any other degree or diploma in any university or other tertiary institution to Bradley Chereda and, to the best of my knowledge and belief, contains no material previously published or written by another person, except where due reference has been made in the text.

I give consent to this copy of my thesis, when deposited in the University Library, being made available for loan and photocopying, subject to the provisions of the Copyright Act 1968.

I also give permission for the digital version of my thesis to be made available on the web, via the University's digital research repository, the Library catalogue, the Australasian Digital Theses Program (ADTP) and also through web search engines, unless permission has been granted by the University to restrict access for a period of time.

Bradley Chereda
December 2012

Table of contents

Abstract

In patients with chronic myeloid leukaemia (CML), a translocation between chromosomes 9 and 22 fuses the *BCR* gene with the *ABL1* gene, and gives rise to the *BCR-ABL* gene. Expression of the BCR-ABL protein initiates and drives CML. The level of BCR-ABL expression is associated with disease progression and response to therapy, yet control of BCR-ABL expression is poorly understood. This study has added to this limited knowledge-base by investigating the role that the *BCR-ABL* 3'untranslated region (3'UTR) plays in controlling BCR-ABL expression. Due to the nature of the translocation, the *BCR-ABL* 3'UTR is contributed by the *ABL1* gene. We found that *ABL1* and *BCR-ABL* have similar, but shorter half-lives than *BCR*. This suggests that the *ABL1* moiety influences the stability of the *BCR-ABL* transcript. Addition of the *ABL1* 3'UTR to a *Renilla* reporter gene strongly repressed reporter expression. Furthermore, insertion of a premature poly-adenylation site in the 3'UTR resulted in a rescue of reporter expression, demonstrating that the 3'UTR is required in the transcript for full activity, and thus is indicative of post-transcriptional control. Generation of *ABL1* reporters containing various regions of the 3'UTR revealed that discrete regions of the 3'UTR could strongly influence gene expression. Following these results, we attempted to identify factors involved in the regulation of BCR-ABL expression. We focused on microRNAs-29, 30, 125, 141, 196 and 203, predicted by bioinformatics to interact with the 3'UTR. Although some of these microRNAs interacted with *ABL1* reporters, they did not modulate endogenous BCR-ABL expression. In parallel, we developed an assay that was aimed at identifying RNA-binding proteins that bind to the *ABL1* 3'UTR. Finally, using publically-available datasets, we found data suggesting that RNA-binding proteins; TTP, hnRNP-C, ELAVL-1, TIA-1 and TIAL-1 interact with functional regulatory regions of the *ABL1* 3'UTR.

Taken together, we have shown that the *BCR-ABL* 3'UTR sequence is repressive, and contains discrete regions that can influence gene expression. The 3'UTR is located within a region of the *BCR-ABL* transcript that is responsible for controlling *BCR-ABL* mRNA stability. Although many attempts were made to discover functional *ABL1* 3'UTR binding factors, their identities remain unknown. Further research is required to identify the binding factors involved. We envisage that a comprehensive understanding of how BCR-ABL is controlled will contribute to a better understanding of the biology of CML, and pave the way for innovative forms of targeted therapy.

Acknowledgements

I would first and foremost like to thank my supervisors Prof. Junia Vaz de Melo and Dr Duncan Hewett for taking me on as a PhD student, for your excellent guidance, time, effort and patience committed to ensure I have a thesis to hand in. It was a privilege to be in the trenches (or Bay-One) with you Duncan, I learned all the old-school tricks and tips needed to get by in the lab, and our camaraderie helped me get through my PhD. I am also grateful to Junia for giving me a free-ride to do whatever experiments I thought would add to the project (thought were cool), as well as being our CML-guru. I learned a lot in all these respects. I *leave you* both with the ability to fill in forms.

Secondly, I would like to thank past and present members of the Leukaemia Biology Group. The Lads™ (Jun and Stanley) cheers for your friendship, many laughs and fun were had. Mark, thanks for the banter throughout my second year (I am nearly over 'clone-gate'). Deborà, thanks for your patient ear, as well as your stories of Brazil. Thanks to Ljiljana, as both a member of team-3'UTR and for your wise words. Veera, thanks for keeping the results ticking over during my write-up. I thank all of you and Brett, Vicksta™, Angela, Linda, Tess, Annabel, Gink and Fong for your invaluable support on and off the bench, and making it that much easier to complete my PhD.

I was also fortunate enough to be able to steal plasmids/bounce ideas off: Greg Goodall, Emily Paterson and Cameron Bracken (microRNAs), and Ian Macara, Hidekazu Lioka, Jason Weber, Mary Olanich, Kirk Jenson and Ashwin Unnikrishnan (RNA-binding proteins). Thanks also to the other laboratories within the IMVS that provided equipment/support throughout my research. I'm also appreciative of the Flow-Lab staff for your help with everything relating to FACS in this project, the Proteomics Facility for mass-spectrometry work, and Tony Cambareri for keeping the institute together (even still, I managed to convince Junia that our lab burnt down!).

I would not have been able to complete this PhD without the help of various funding bodies. I was the recipient of a three-year 'Australian Postgraduate Award' from the Australian government. I was able to attend the 17th Congress of the European Hematology Association, in Amsterdam, due to a "coalition" of travel grants from the Adelaide University's 'Postgraduate Travel Fund', a grant from the SPMSFF (SA Pathology), and a travel grant from the conference itself. I also received a travel grant from the European Molecular Biology Organisation to attend the "Complex life of mRNA" symposium in Heidelberg in October 2012. I also thank Junia for keeping me on after my scholarship ended so I could still ~~go for a pint~~ eat during the write up of my thesis.

I am also grateful for the hospitality provided by the members of the various laboratories I visited in Europe. Dankeschön to Alex, Caroline, Leon and Stan; Florian, Roberto and fellow Aussie Keriyn! Grazie tanto to Emanuele, Monica and Simona! And, dekuji pekne to Tereza and Marketa for the wonderful time I had in Prague.

Finally, I express my appreciation to my family and friends that have provided considerable support since embarking on my PhD and throughout my studies.

Abbreviations

2D	2-dimensional
7mG	7'-methyl guanine cap
AANAT	Aralkylamine N-acetyltransferase
ABL1	Abelson gene
AGO	Argonaute
ALL	Acute lymphoblastic leukaemia
AML	Acute myeloid leukaemia
ANKFN1	Ankyrin-repeat and fibronectin type III domain containing 1
AP	Alkaline phosphatase
ASF	see SFRS1
ATP	Adenosine tri-phosphate
AU-RE	AU-rich element
Aza	5-Azacytidine
BC	Blast crisis
BCL2	B-cell lymphoma 2
BCR	Breakpoint cluster region
bone fide	*in good faith, genuine*
BSA	Bovine serum albumin
C/EBPα	CCAAT/enhancer-binding protein alpha
CAGE	Capped analysis of gene expression
CDC42	Cell division control protein 42 homolog
CDCA	Chenodeoxycholic acid
CDK4	Cyclin-dependent kinase 4
cDNA	complementary DNA
CHOP	CCAAT/enhancer-binding protein homologous protein
CID	Collision-induced dissociation
CIP	Alkaline phosphatase
cis	on the same side
CLL	Chronic lymphocytic leukaemia
CML	Chronic myeloid leukaemia
CMP	Common myeloid progenitor
CNL	Chronic neutrophilic leukaemia
COLIa1	Collagen type I alpha1
CP	Chronic phase
CRB3	Crumbs homolog 3
DEPC	Diethylpyrocarbonate
DGCR8	DiGeorge syndrome critical region gene 8
DNA	Deoxy-ribose nucleic acid
DNA-PKcs	DNA-dependent protein kinase, catalytic subunit

DNMT3A	DNA (cytosine-5-)-methyltransferase 3 alpha
DSB	Double-stranded breaks
ELAVL	(Embryonic lethal, abnormal vision, Drosophila)-like
EST	Expressed sequence tag
et al	*and others*
etc	ecetera
ex vivo	*out of the living*
FACS	Fluorescence-activated cell sorting, Flow cytometry
FOXO3	Forkhead box O3
FUS	Fused in sarcoma
GFP	Green fluourescent protein
GMP	Granulocyte-macrophase progenitor
GRP58	see PDIA3
GUS-B	Glucuronidase beta
HNF4α	Hepatocyte nuclear factor 4 alpha
hnRNP	heterogeneous nuclear ribonucleoprotein
HOX-B7	Homeobox B7
HPLC	High-performance liquid chromatography
HSC	Haemopoietic stem cell
HuR	ELAVL-1
IFNγ	Interferon gamma
IGF2BP	Insulin-like growth factor 2 binding protein
IL	Interleukin
IMP	see IGF2BP
IMPDH2	Inosine-5'-monophosphate dehydrogenase 2
in silico	*performed on computer*
in vitro	*in glass*
in vivo	*within the living*
JAK	Janus kinase
kb	kilobases
kDa	kilo dalton
KH	K-homology
KRAS	Kirsten rat sarcoma viral oncogene homolog
LB	Luria broth
LC-eSI-IT	Liquid chromatography-electrospray ionisation ion-trap mass spectrometry
LDLR	Low density lipoprotein receptor
LT-HSC	Long-term HSC
LTR	Long terminal repeat
m/z	mass/charge
max	maximum
MCL	Mantle-cell lymphoma
Me	Methylation

Meg^K	Megakaryocyte
MEP	Megakaryocyte-erythroid progenitor
MMR	Major molecular response
modus operandi	*mode of operation*
MR	Molecular response
mRNA	messenger RNA
MS-MS	Tandem mass spectrometry
next-gen	next-generation
NPM1	Nucleophosmin
nt	nucleotide
NUMB	Numb homolog
Oct4	octamer-binding transcription factor 4
PACT	protein activator of PKR
PAS	Poly adenylation signal
PBA	4-Phenylbutyric acid
PBMNC	Perhiperal blood mononuclear cell
PCR	Polymerase chain reaction
PDIA3	Protein disulphide-isomerase A3
Ph	Philadelphia
PhD	Doctor of philosophy
PI3K	Phosphoinositide 3-kinase
PKCβII	Protein kinase C βII
PMSF	Phenylmethylsulfonyl fluoride
poly-A	poly-adenosine
PP2A	Protein phosphatase 2A
Pre-miRNA	Precursor-microRNA
Pri-miRNA	Primary-microRNA
PTEN	Phosphatase and tensin homolog
PTENP1	PTEN pseudogene 1
qRT-PCR	Quantitative real-time PCR
RACE	Rapid amplification of cDNA ends
RB	Retinoblastoma (gene)
RBC	Red blood cell
RBD	RNA-binding domain
RIP-SEQ	Immunoprecipitation of proteins coupled with next-gen sequencing
RISC	RNA-induced silencing complex
RNA	Ribonucleic acid
ROS	Reactive oxygen species
RRM	RNA-recognition motif
SD	Standard deviation
SEM	Standard error of the mean
SFRS1	Splicing factor, arginine/serine-rich 1

SH1	Src homology domain 1
siRNA	silencing RNA
SILAC	Stable isotope labelling with amino acids in cell culture
SNP	Single nucleotide polymorphisms
ssRNA	single-stranded RNA
STAT5	Signal transducer and activator of transcription 5
ST-HSC	Short-term HSC
TIA-1	T-cell-restricted intracellular antigen-1
TIAL-1	TIA-like-1
TKI	Tyrosine kinase inhibitor
TLS	Translocated in liposarcoma
TNF	Tumour necrosis factor
trans	opposite side
TRBP	HIV transactivating response RNA binding protein
TTP	Tristertaprolin
UTR	Untranslated region
UV	Ultraviolet
vice versa	*the other way around*
vs.	*versus*
ZFP36	see TTP

Chapter 1

Chronic myeloid leukaemia

1.1 Preface

This thesis describes the investigative approach undertaken to characterise the control of BCR-ABL expression by its 3'untranslated region (3'UTR). The *BCR-ABL* gene is the resultant of a chromosomal translocation event, and is observed in all cases of chronic myeloid leukaemia (CML). Expression of the BCR-ABL protein is known to drive early pathogenesis of CML via signal transduction from its tyrosine kinase domain. The expression levels of BCR-ABL have been associated with disease progression and response to therapy, but to date it is not clear how BCR-ABL expression is controlled. Therefore, we envisage that having a deeper insight in to the role of the *BCR-ABL* 3'UTR during BCR-ABL expression will have significant relevance to understanding the biology of this disease.

This thesis comprises five chapters. Chapter 1 introduces CML, and how BCR-ABL is involved in disease pathogenesis. In chapter 2, the *BCR-ABL* 3'UTR is described in terms of published studies and unpublished data from our laboratory. Chapters 3 and 4 introduce microRNAs and RNA-binding proteins respectively, and outline our approach used to investigate if these factors interact with *BCR-ABL*. Then chapter 5 provides discussion and future directions for the work described herein. Each chapter has its own 'Introduction'. In addition, chapters containing 'Result' sections have their own 'Methods' section, with methods common to more than one chapter described in the appendices, in order to avoid repetition. There are a few instances where data or figures that are not my own are used to help explain a particular concept. These instances are clearly referenced and permission was obtained prior to their use.

1.2 Chronic myeloid leukaemia

CML is a myeloproliferative disorder arising in the haemopoietic stem cell (HSC) compartment. It is characterised by a reciprocal t(9;22) chromosomal translocation, resulting in the formation of the Philadelphia (Ph) chromosome containing the *BCR-ABL* gene[1]. The *BCR-ABL* gene is a fusion gene consisting of the 5' end of the *BCR* (breakpoint cluster region) gene and the 3'end of the *ABL1* gene (also known as Abelson) (see Fig 1.2). This gene is transcribed from the *BCR* promoter to form a chimeric *BCR-ABL* transcript that codes for the BCR-ABL protein. It is the BCR-ABL protein, in particular its constitutively active tyrosine kinase activity, that causes the pathogenesis of early-stage disease[2,3]. Aberrant

tyrosine kinase activity from BCR-ABL causes activation of downstream targets, in turn promoting proliferation and evasion of apoptosis - leading to the leukaemic phenotype.

CML patients are often diagnosed in chronic phase (CP)[4]. The natural course of the disease is progression into an acute leukaemia, blast crisis (BC) (in some cases via an intermediate "accelerated phase"). BC is almost always fatal. Current first line therapy, imatinib (Novartis, Switzerland, Gleevec™ or Glivec™), a tyrosine kinase inhibitor (TKI), has greatly improved patient outcome by significantly reducing the frequency of progression to BC, in addition to inducing a remission of CP[5].

Even with imatinib's success, there are a number of challenges which remain for understanding and efficiently treating CML. These include: eradication ('cure') of disease, mutations in BCR-ABL which decrease TKI efficacy, and the biology of disease progression. A body of evidence implicates the level of BCR-ABL expression as having an important role in these events in CML. Our research has therefore focused on improving the knowledge of the mechanisms that govern BCR-ABL expression.

1.3 Disease pathogenesis

The pathogenesis of CML described in Fig 1.1, begins with the *BCR-ABL* gene and CP-CML, followed by progression to a more acute leukaemia. This section provides an overview of the key clinical and biological steps in CML.

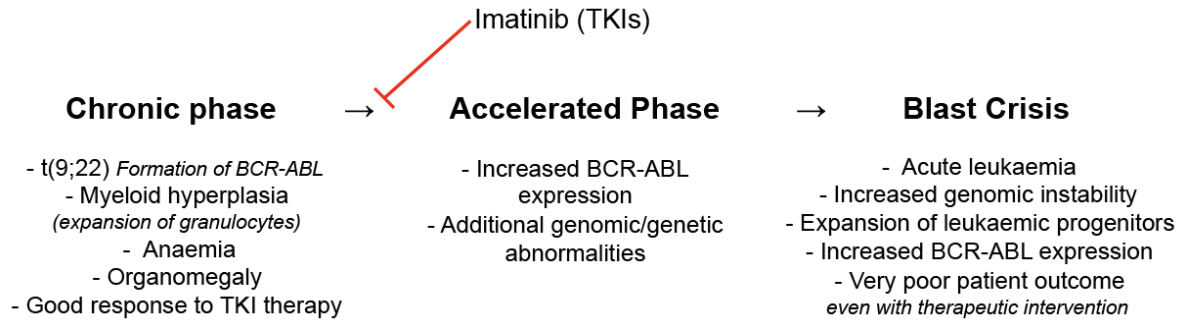

Fig 1.1: Schematic of CML pathogenesis. The diagram above highlights some of the key features in the pathogenesis of CML. Increased BCR-ABL expression and additional genetic abnormalities are positioned between CP and advanced disease as these features mark disease progression. The potential inhibition of disease progression by imatinib is also indicated. TKI: tyrosine kinase inhibitor.

1.3.1 Chronic phase

Most CML patients are diagnosed in CP. Approximately 250 new CML-cases are diagnosed each year in Australia, and the median age at diagnosis is approximately 50 years of age[6]. The main clinical signs are anaemia and splenomegaly, and symptoms of abdominal discomfort, fatigue and increased infections/bleeding predominate at diagnosis[7]. These clinical features are in turn the result of myeloid hyperplasia (granulocyte expansion) caused by the aberrant kinase activity of BCR-ABL[4,8]. In the majority of patients, both the symptoms and signs of disease are rapidly alleviated upon commencement of imatinib treatment.

1.3.2 Blast crisis

Progression into BC is usually fatal, and occurs at an average of 5-7 years from diagnosis if the disease is not efficiently treated in CP. A CML patient is said to be in BC when haemopoietic blasts (undifferentiated cells) make up more than 20% of the peripheral blood count. Currently it is unknown how the transition to BC occurs. However, it is characterised by the expansion of haemopoietic progenitor cells which can no longer differentiate. These progenitor cells gain self-renewal, differentiation arrest and survival properties which lead to their uncontrolled proliferation[9]. In fact their properties are more stem cell-like than CP-myeloid progenitors[10]. In addition to differentiation arrest, genomic instability is observed in advanced disease[11,12]. Extra chromosomal abnormalities (Ph duplication, trisomy 8 or 19, loss of 17p), and altered function of tumour suppressors (e.g., p53, p16, PP2A) or oncogenes (e.g., MYC, RB) have been detected in patients in advanced disease[13]. It is thought that these additional hits are responsible in part for the transition into BC[9,12].

1.3.3 Treatment

The TKI, imatinib, is the first line treatment for CML. Imatinib is a small molecule that specifically targets the constitutive cell-signalling effects of BCR-ABL by selectively binding to the adenosine triphosphate (ATP) binding pocket of ABL's Src homology 1 (SH1) kinase domain[14,15]. As a result, the kinase domain can no longer hydrolyse ATP and is stabilised in an inactive conformation, shutting down the constitutive signalling[14,15]. This inhibition of BCR-ABL kinase signalling restores apoptosis in BCR-ABL expressing cells[8], with gradual reduction of the leukaemic clone and consequent clinical remission. Unfortunately, response

to TKI treatment in BC is poor[16], which may reflect additional abnormalities found in advanced disease and a loss of BCR-ABL dependence.

The most sensitive method for measuring a patient's response to therapy is by performing quantitative polymerase chain reaction (PCR) amplification for BCR-ABL[17,18]. Thresholds of response are defined in log-reductions of *BCR-ABL* transcripts compared to diagnosis (termed molecular response, MR). These measurements, and the time taken to achieve them, are highly predictive of patient outcome[18]. For example, a 3-log reduction in %BCR-ABL (a major MR) is highly predictive of progression free survival[18]. Also, with cessation of therapy being a new goal in CML therapy[19], another milestone, MR4.5 (a 4.5-log reduction of %BCR-ABL), is the current threshold for enrolling patients in TKI-cessation studies[20].

Phase III clinical trials for imatinib therapy in CML demonstrated a progression free (progression to advanced disease) survival of 93% after six years[21]. Unfortunately, a subset of patients are, or become, non-responsive to imatinib therapy. The leading cause of imatinib resistance is the emergence of leukaemic clones with BCR-ABL kinase mutations that decrease imatinib's binding affinity[22,23]. A number of next-generation TKIs are in development for the purpose of improving patient-response in comparison to imatinib, as well as targeting mutant forms of BCR-ABL. With the knowledge that a significant proportion of patients remain who initially do not respond to treatment[5], relapse due to kinase-mutation independent mechanisms[23,24], or develop resistance to next-generation TKIs[25-27], alternate strategies are required to combat CML.

An additional limitation of TKI therapy is that quiescent stem cells within the CD34+ population are resistant to TKIs (residual disease)[28-31]. This prevents the absolute eradication of CML. There is considerable debate surrounding this topic. It is unknown whether kinase inhibition is insufficient for killing stem cells[32-37], or if kinase inhibitors are unable to access the leukaemic stem cell population[38-41].

1.4 BCR-ABL

In 1960, Nowell and Hungerford described a minute chromosome (the Ph chromosome) which was consistently observed in seven patients with 'chronic granulocytic leukaemia' (another term for CML)[42]. More than ten years later, it was found that the Ph chromosome was the result of a t(9;22) translocation[43]. Then in mid 1980s, it was shown that

this translocation involved the fusion of the *BCR* and *ABL1* genes resulting in the expression of a 210 kilo dalton (kDa) BCR-ABL fusion protein[44].

The location of the *BCR* and *ABL1* fusion is highly variable[45], however it usually involves fusion of intron 13 or 14 of *BCR* with a 140 kilobases (kb) region of *ABL1* between exon 1b and exon 2 (Fig 1.2)[45]. The *ABL1* gene has two isoforms resulting from alternate promoter regions (exon 1b and exon 1a) (Fig 1.2). This means that even if the *BCR-ABL* fusion includes the 1a exon, this exon will be spliced-out during messenger RNA (mRNA) maturation, because exon 1a lacks a splice site acceptor. Therefore, the major *BCR-ABL* transcripts are e13a2 (*BCR* exon 13 and *ABL1* exon 2) and e14a2 (these transcripts are also referred to in the literature as b2a2 and b3a2, respectively). Both transcripts result in expression of the 210 kDa BCR-ABL protein. There is much debate regarding the consequence of a patient expressing either the e13a2 or e14a2 transcript[46,47]. The position of the *BCR* breakpoint has been correlated with patient prognosis[48-50], platelet count[46,51,52], and response to therapy[48,53]. However, there is an equal body of evidence which refutes a correlation between *BCR* breakpoint and the aforementioned phenotypes[54-57]. A recent study which reported that patients expressing e14a2 variant have a superior response to imatinib may reignite the e13a2/e14a2 debate[53].

In addition to the 210 kDa BCR-ABL protein, a smaller (190 kDa)[58] and larger (230 kDa)[59] variant of BCR-ABL has been observed in various leukaemias, including CML[47,60]. These proteins are the result of alternate *BCR* and *ABL1* fusions: e1a2 (190 kDa variant) and e19 or e20a2 (230 kDa variant)[58,59]. The 190 kDa variant is rarely found in CML, but is observed in two-thirds of Ph-positive acute lymphoblastic leukaemia[61]. The 230 kDa variant has been associated with neutrophilic-CML which is distinguished from classical CML by a more indolent phenotype[62]. Unless specifically stated, any mention of BCR-ABL refers to the 210 kDa variant.

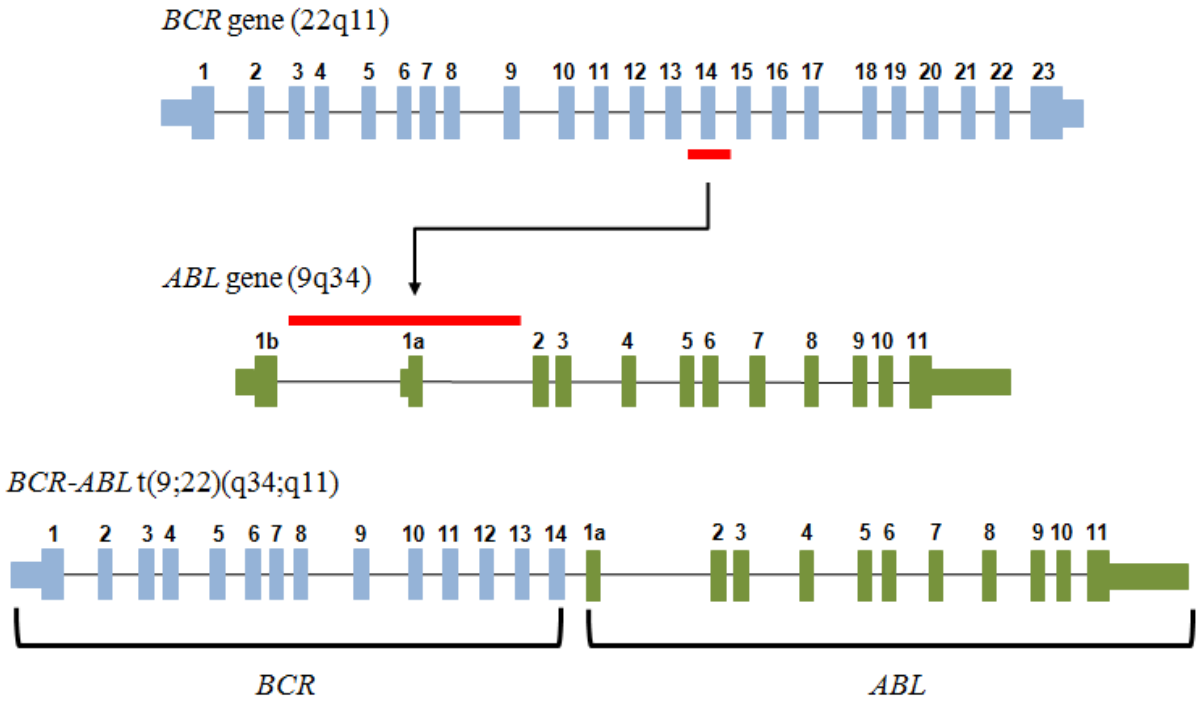

Fig 1.2: Formation of the *BCR-ABL* gene. In CML, the major t(9;22) rearrangements fuse either intron 13 or 14 of *BCR* (green) with intron 1a or intron 1b of *ABL1* (blue) (the example above is a fusion of intron 14 with intron 1b). Red lines indicate the location of characterised breakpoints for BCR-ABL formation in CML[47]. The *ABL1* gene contains two alternate promoters (labelled 1b and 1a above). It must be emphasised that, regardless of the presence of exon 1a, it will be absent from the processed *BCR-ABL* transcript because exon 1a lacks a splice acceptor site. Exons are depicted as rectangles and numbered. Untranslated regions are half as tall as the exonic regions. Introns are depicted as a thin line. The diagram is not to scale.

1.4.1 BCR-ABL signalling in disease

Constitutive BCR-ABL kinase activity changes the cellular environment to promote the disease features of CML. The importance of BCR-ABL signal transduction during CML has led to the understanding of the downstream targets of BCR-ABL (Fig 1.3). Altered activation of these targets by BCR-ABL has been linked with changes in proliferation, apoptosis, growth factor independence, cell adhesion and DNA repair (reviewed in[9]). All of which contribute to CML pathogenesis.

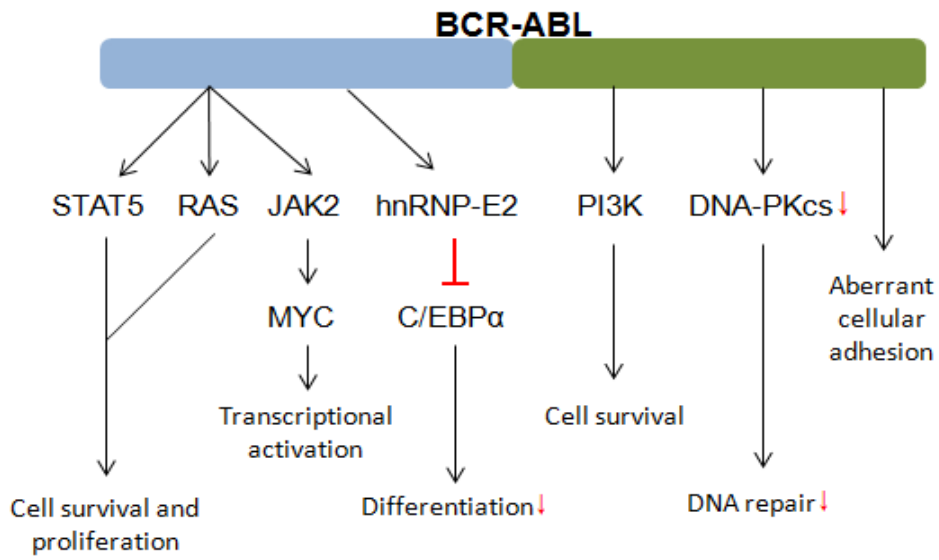

Fig 1.3: Key pathways activated by BCR-ABL signal transduction. The cartoon above highlights some of the key targets and pathways activated by BCR-ABL. STAT5: signal transducer and activator of transcription 5, JAK2: janus kinase 2, hnRNP-E2: heterogeneous nuclear ribonucleoprotein-E2, PI3K: phosphoinositide-3-kinase, DNA-PKcs: catalytic sub-unit of DNA dependent protein kinase, C/EBPα: CAAT/enhancer binding protein alpha.

1.4.1.1 Proliferation and apoptosis

BCR-ABL induces the activation of key cell signalling pathways, such as RAS, MYC, JAK, STAT5 and PI3K (summarised in Fig 1.3). As a result, cells expressing BCR-ABL gain a proliferative and anti-apoptotic advantage[2,63,64], and proliferate in a growth factor independent manner[65,66]. These phenotypes lead to the granulocyte expansion observed in CP-CML[4].

A number of studies have investigated the consequence of STAT5 activation by BCR-ABL. The STAT5 pathway is known to control proliferation and apoptosis in healthy cells, as well as causing oncogenic signalling events in cancer[67,68]. STAT5 activation was originally correlated with BCR-ABL expression in CML cell lines and primary cells[69,70]. This activation was found to be BCR-ABL kinase dependent, as STAT5 activation was completely ablated upon BCR-ABL kinase inhibition by imatinib *in vivo*[71]. Additional studies have demonstrated that STAT5 activation is essential for BCR-ABL induced leukaemia. Deletion of STAT5 in BCR-ABL expressing cells inhibited proliferation and restored apoptotic function[72]. Furthermore, STAT5 deletion prevented transformation and maintenance of BCR-ABL induced leukaemia in murine models[72].

It is also known that BCR-ABL can inhibit the apoptotic pathway[63,64,73]. Inhibition of BCR-ABL kinase activity reinstates apoptosis of CML cells, showing the dependence on kinase activity[3,73,74]. Inversely, increasing BCR-ABL expression makes cells more resistant to apoptotic induction[75-77]. BCR-ABL kinase activity activates the STAT5 and PI3K/AKT pathways[78] – which are key players of apoptosis[79,80]. However, there is evidence that these pathways are redundant for BCR-ABL induced inhibition of apoptosis[81,82]. The exact mechanism behind BCR-ABL's effect on apoptosis still remains unknown.

1.4.1.2 Genomic instability

BCR-ABL has been implicated in facilitating genomic instability via disrupting DNA repair pathways and directly inducing genomic mutations[83]. In addition, it is known that BCR-ABL can inhibit DNA-damage-induced apoptosis[84,85], which may lead to retention of genomic mutations. DNA mutations are features of both BC-CML[9,12] and TKI resistance (BCR-ABL kinase domain mutations)[86]. It is therefore suggested that BCR-ABL provides CML cells with the genomic plasticity required for malignant transformation[12,86,87].

BCR-ABL kinase activity is known to increase the levels of reactive oxygen species (ROS) within the cell[83,88-91]. ROS are responsible for the majority of DNA damage that occurs inside a cell[92], causing genomic point mutations or double-stranded breaks (DSBs). The increase in ROS by BCR-ABL is therefore thought to contribute to the higher rates of oxidised nucleotides (predictors of point mutations) and DSBs found in CML cells compared to (equivalent) healthy cells[89].

Components of the DNA repair machinery are also impeded by BCR-ABL, permitting the accumulation of additional mutations. Two key examples are RAD51 and DNA-PKcs, which are involved in the repair of DSBs[93,94]. CML patients exhibit increased RAD51 expression and activity in a BCR-ABL dependent manner[94]. Increased RAD51 activity has been implicated in negatively affecting fidelity of DSB-repair, thus inducing genomic instability[94]. The expression of DNA-PKcs is reduced upon BCR-ABL expression and in cells taken from CML patients[93]. This accompanied a deficiency in DSB-repair in BCR-ABL positive cells, which was dependent on the expression level of BCR-ABL[93].

1.4.2 Expression patterns of BCR-ABL in CML

Several groups noted differences in BCR-ABL expression between CP and BC, as well as between different haemopoietic cell compartments. These observations led to speculation that BCR-ABL expression levels play a role in CML pathogenesis.

A number of studies have found increased expression of BCR-ABL in BC compared with CP. This increase was observed at both the mRNA[40,95-97] and protein level[95,98,99]. These results are reinforced by a number of reports examining BCR-ABL expression from CP and BC samples from the same patient (i.e. matched CP and BC samples). In these patient-matched samples, an increase in *BCR-ABL* mRNA or protein is consistently observed in the BC samples compared to CP – ranging from 1.5-8.0 fold[95,98,99]. Moreover, the increase of *BCR-ABL* mRNA is attributed to increased transcript levels and not genomic amplification[98]. This finding is indicative of enhanced *BCR-ABL* transcription or increased stability of the *BCR-ABL* transcript during disease progression.

BCR-ABL expression has also been compared between the different haemopoietic cell compartments of the myeloid lineage[10,28,40,97]. These studies show that BCR-ABL expression, both mRNA and protein, decreases as the leukaemic stem cells differentiate (Fig 1.4, A). Of interest, two of these studies also examined the expression of *BCR* in the different cell compartments. Jiang, *et al.* reported that *BCR* mRNA expression was lower in comparison to *BCR-ABL* expression in primitive CD34+ cells[40]. This suggested a mechanism exists which causes upregulation of BCR-ABL, but not BCR in primitive CML cells.

In the other study, Marega, *et al.* examined *BCR* and *ABL1* mRNA expression in HSCs and myeloid progenitors from healthy donors. They observed that *BCR* expression was much higher in HSCs than progenitor cells[97]. However, *ABL1* expression levels remained constant[97], and so only *BCR* and *BCR-ABL* were examined in the context of CML. In CP samples, they observed a similar 'relative' decrease in *BCR* and *BCR-ABL* RNA upon stem cell differentiation. Interestingly, relative *BCR-ABL* expression was 10-fold higher than *BCR*. For example, upon differentiation of HSCs into common myeloid progenitors (CMPs), *BCR-ABL*/GUSB expression decreased from 3.1 to 0.8. Whereas, *BCR* expression decreased from 0.3 to 0.1 (see Fig 1.4, B top). These findings are consistent with Jiang, *et al.*'s[40]. Furthermore, comparison of the CP and BC expression data for *BCR* and *BCR-ABL* in the Marega, *et al.* study, indicates an increase in *BCR-ABL* but not *BCR* expression in the HSC

and granulocyte-macrophase progenitor (GMP) compartments in BC[97] (see Fig 1.4, B bottom).

Taken together, the studies by Jiang, *et al.*[40] and Marega, *et al.*[97] outline a mechanism by which *BCR-ABL* expression does not mimic that of *BCR*. This was found in the context of both myeloid differentiation and disease progression. A reasonable assumption therefore is that the *ABL1* portion of BCR-ABL significantly regulates *BCR-ABL* transcript levels in those contexts. This can be explained by the gain of an *ABL1*-repressive factor, or loss of an *ABL1*-stabilising factor during differentiation and/or disease progression.

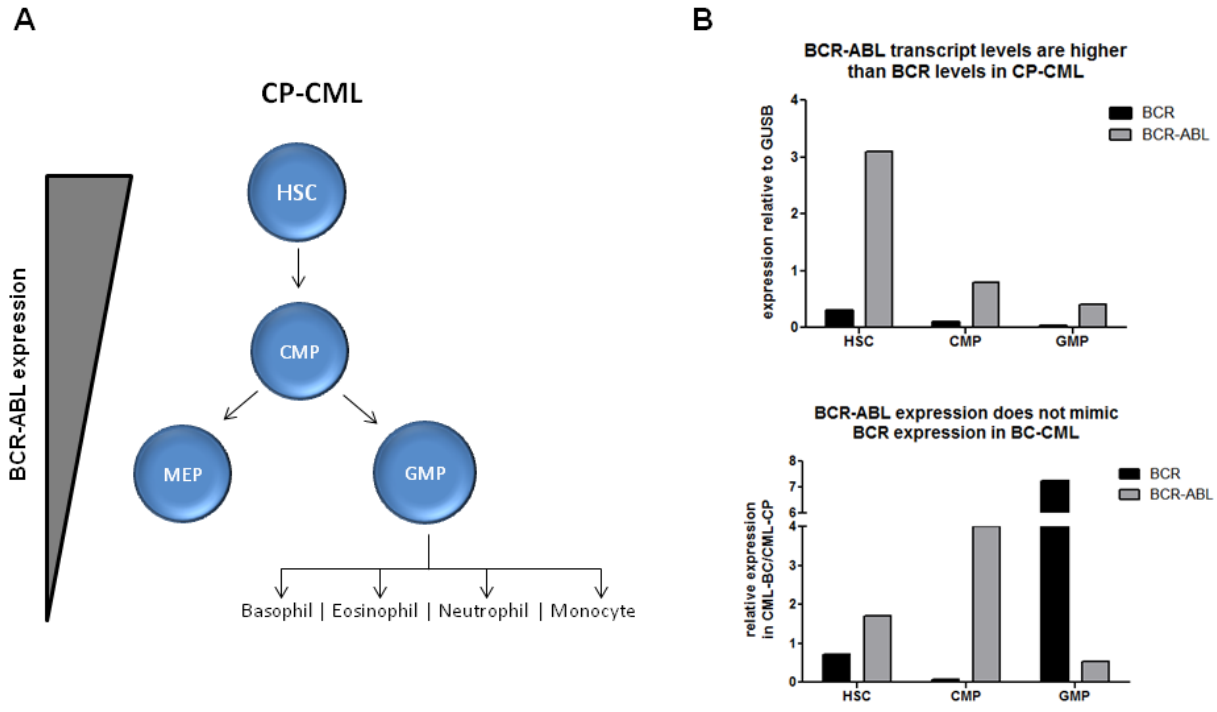

Fig 1.4: BCR-ABL expression patterns in haemopoietic cell compartments. (**A**) This diagram illustrates the observation that BCR-ABL levels decrease upon myeloid differentiation in CP-CML[97]. (**B**) *Top*, using the data from Marega, *et al.*, it can be seen that *BCR-ABL* mRNA is 10-fold higher than *BCR* mRNA relative to GUSB in HSCs and myeloid progenitors in CP[97]. *Bottom*, relative mRNA expression data for *BCR* and *BCR-ABL* in BC was divided by the data in CP from Marega, *et al.*[97]. This analysis shows that *BCR-ABL* expression does not mimic *BCR* expression in BC. HSC: haemopoietic stem cell, CMP: common myeloid progenitor, MEP: megakaryocyte-erythroid progenitor, GMP: granulocyte-macrophage progenitor.

1.4.3 BCR-ABL dosage

The previous section highlighted the differential expression of BCR-ABL in both myeloid differentiation and disease progression. These changes in BCR-ABL expression have led to further studies investigating the consequence of enhanced BCR-ABL expression. Enhanced expression of BCR-ABL has been found to inhibit the apoptotic pathway[77], increase genomic instability[93], block differentiation[100-102], and enhance resistance to TKIs[95,96,103-105]. These observations provide evidence to suggest that high levels of BCR-ABL:

- Promote disease progression: mutations in addition to BCR-ABL and an expansion of leukaemic progenitor cells due to a block in differentiation are key features of advanced disease[106]. Both of these phenotypes are linked with high BCR-ABL levels.
- Contribute to TKI resistance (in general): enhanced BCR-ABL expression reduces the sensitivity of CML cells to TKI-induced cell death[95].
- Contribute to TKI resistance (in primitive cells): primitive cells express more BCR-ABL than mature cells[10,28,40,97], and high levels of BCR-ABL enhance resistance to TKIs[95,96,103-105].

1.4.3.1 Association with blast crisis

As mentioned in the previous section, our laboratory and others have observed an increase in BCR-ABL expression in patients from CP to BC[40,95-99]. Moreover, it has been shown that cells expressing increasing amounts of BCR-ABL have an increase in genomic instability as well as perturbed differentiation, which are intrinsic properties of BC-CML[12,100,106]. Therefore these findings provide evidence that an increase in BCR-ABL from CP to BC is a factor that promotes disease progression.

1.4.3.1.1 Dose-dependent downregulation of C/EBPα

C/EBPα, a protein required for myeloid differentiation[107], was found to be downregulated in cell lines expressing BCR-ABL[101]. In addition, these BCR-ABL expressing cell lines responded poorly to growth-factor induced differentiation[100]. Ectopic expression of C/EBPα and BCR-ABL kinase inhibition was able to reverse the block in differentiation suggesting a role for BCR-ABL in this process[101]. Further experiments then showed that BCR-ABL negatively regulated the expression of C/EBPα via upregulation of hnRNP-E2, an RNA-binding protein which inhibits C/EBPα expression[100]. Interestingly, in cell line models,

hnRNP-E2 upregulation and C/EBPα downregulation were directly proportional to increasing levels of BCR-ABL[100]. Furthermore, in CML patient samples, hnRNP-E2 expression was restricted to BC[100]. To add extra complexity to this pathway, it was recently shown that the microRNA, miR-328, acts in a non-canonical way to block hnRNP-E2 regulation of C/EBPα and promotes myeloid differentiation[102]. The expression of this microRNA negatively correlates with BCR-ABL expression levels, and thus is downregulated in BC, which enhances BCR-ABL's ability to inhibit differentiation[102]. Taken together, these experiments provide evidence of a sophisticated circuit by which enhanced BCR-ABL expression can facilitate a switch to BC by disrupting myeloid differentiation.

1.4.3.1.2 Dose-dependent inhibition of DNA repair

The DNA-dependent kinase complex is a major component of the DNA repair machinery involved in DSB-repair[108]. With the knowledge that ABL disrupts this complex[109], BCR-ABL's role in this pathway was investigated. It was found that high levels of BCR-ABL reduced the expression of DNA-PKcs, a key component of the DNA repair complex[93]. Furthermore, the reduction in DNA-PKcs correlated with a higher incidence of genomic instability and could be reversed by BCR-ABL kinase inhibition[93]. As increased genomic instability is believed to play a role in the transition to BC[12], these findings present another route by which enhanced BCR-ABL expression can promote disease progression.

1.4.3.2 BCR-ABL levels and imatinib resistance

Enhanced BCR-ABL expression has also been linked with imatinib resistance. Ph chromosome duplications (leading to increased BCR-ABL expression) have been associated with TKI resistance in patients[22,110]. Furthermore, a number of cell line models have specifically shown that enhanced BCR-ABL expression confers resistance to TKI-induced cell death[95,103-105].

In our laboratory, a number of murine cell lines were established expressing various amounts of exogenous BCR-ABL. It was found that increasing levels of BCR-ABL led to reduced sensitivity to imatinib[95]. Furthermore, the time taken to acquire kinase domain mutations was significantly reduced[95,105]. This observation is consistent with high levels of BCR-ABL increasing genomic instability[90,95].

Exposure of human CML cell lines (that exogenously express BCR-ABL) to gradually increasing concentrations of imatinib, led to the over-expression of BCR-ABL[95,103,105]. Interestingly, emergence of clones with acquisition of a kinase domain mutation led to a decrease in BCR-ABL expression[104,105]. These experiments inferred that increased BCR-ABL expression is one mechanism for TKI resistance.

In another model, healthy murine myeloid progenitor cells were transformed with BCR-ABL, and selected for high and low BCR-ABL expression. In this model, cell that expressed 'high' levels of BCR-ABL exhibited increased proliferation and reduced apoptosis compared to cells expressing 'low' levels of BCR-ABL[76]. However, the high-expressing cells were more sensitive to imatinib[76]. They speculated that cell line models (where enhanced BCR-ABL levels promoted TKI resistance) were dependent on other abnormalities for increased sensitivity to imatinib in a BCR-ABL dependent manner.

The differences between the cell line and primary cell models can be attributed to the cell type used. The primary cell models, where BCR-ABL expression is the only abnormality, may closely mimic the situation in CP-CML. On the other hand, the cell line models (which contain additional abnormalities) may closely mimic BC-CML. As mentioned, BC features both additional mutations and enhanced BCR-ABL expression. So the findings from the cell line (BC-like) experiments may explain why BC-patients respond poorly to TKI therapy[16].

1.4.3.3 BCR-ABL expression and TKI-sensitivity in leukaemic stem cells

There is a large body of evidence showing that quiescent CML stem cells are refractory to TKI therapy[28-31]. Currently, the mechanism for residual disease is not completely understood, and is a key question in CML. It is important to answer this question as stem cell refractoriness to TKI therapy makes it difficult to completely eradicate CML[111].

The observation that BCR-ABL levels are higher in the primitive and stem-cell population[10,28,40,97], and cell line models showing that increased BCR-ABL expression decreases imatinib sensitivity[22,95,103-105,110], led to the hypothesis that increased BCR-ABL expression could play a role in stem-cell resistance to imatinib.

Surprisingly, two reports have observed that following imatinib treatment, persistent leukaemic stem cells showed a bias for *low* BCR-ABL expression[112,113]. These studies compared BCR-ABL expression in CML patients at diagnosis (in CP) and after they achieved

MMR. Although BCR-ABL expression was markedly reduced in 'persistent' cells[112,113], the overall BCR-ABL expression pattern mimicked that of untreated cells. That is, HSCs had the highest levels of BCR-ABL, which reduced upon differentiation (Fig 1.4, A).

It remains unknown whether or not 'high' or 'low' BCR-ABL levels facilitate residual disease. Did the persistent cells once express high levels of BCR-ABL, which was then tempered by imatinib treatment? Or were persistent cells in fact selected by their low expression of BCR-ABL? This discrepancy regarding the role of high or low BCR-ABL levels in residual disease does not take away from the fact that BCR-ABL dosage appears to be involved. Therefore it is anticipated that the biology of residual disease will also benefit from understanding how BCR-ABL expression is controlled.

1.4.4 Control of BCR-ABL expression

By virtue of the *BCR-ABL* translocation, transcription of *BCR-ABL* is under the control of the *BCR* promoter, and post-transcriptional control of *BCR-ABL* is likely to involve the *ABL1* 3'UTR. To date, both transcriptional and post-transcriptional control of *BCR-ABL* is poorly understood. By understanding how BCR-ABL expression is controlled, and identifying the factors involved, we anticipate these findings would have direct application to CML in providing:

- A rationale behind the increased *BCR-ABL* expression levels in leukaemic stem cells compared to mature leukaemic cells, including the consequence this has for TKI therapy.
- A greater understanding of BC transformation: *BCR-ABL* expression increases from CP to BC. Understanding how BCR-ABL is controlled will help determine if enhanced BCR-ABL expression precedes or follows disease progression. It will also outline some of the mechanisms that promote advanced disease.
- Additional therapeutic targets to combat CML: several studies have demonstrated the potency of specifically targeting *BCR-ABL* mRNA levels in both cell lines and a CML patient using small RNAs[114-121]. Targeting *BCR-ABL* expression could circumvent TKI resistance, and/or synergise with TKI inhibition of its kinase activity, leading to a deeper therapeutic response in CML patients.
- Prognostic tools to predict disease progression: regulators of BCR-ABL expression can be used to monitor patient prognosis if they predict disease progression. Changes

in the expression of such factors would precede changes in BCR-ABL expression and allow for earlier clinical intervention.

Another application for understanding BCR-ABL expression relates to the modelling of CML. Current models of BCR-ABL transformation use a plasmid containing BCR-ABL complementary DNA (cDNA) whose expression is driven by a long terminal repeat (LTR) promoter, containing the last 152 nt of the 5'UTR, and the first 800 nt of the 3'UTR[122]. Therefore BCR-ABL expression levels are under the control of exogenous elements, and will be different from those achieved by the endogenous *BCR-ABL* locus. Once elements that are important for BCR-ABL expression are mapped, they could be included in the *BCR-ABL* transgene to more closely mimic BCR-ABL expression. A transgene containing the 190 kDa variant of BCR-ABL has been generated under the control of the *BCR* promoter using homologous recombination (the length of the 3'UTR in that transgene was not reported)[123]. However, the 190 kDa BCR-ABL variant is rarely found in human CML and so this study does not contribute to the understanding of CML. More importantly, this example highlights the possibility of constructing a transgene for the 210 kDa BCR-ABL variant that contains relevant *BCR* and *ABL1* sequence required to more closely mimic BCR-ABL expression.

1.4.4.1 The BCR Promoter

Characterisation of the *BCR* promoter is the focus of another project within our laboratory, which is separate from the work presented in this thesis. Therefore discussion related to this topic will be limited. Transcription of *BCR-ABL* is controlled by the *BCR* promoter. Published data suggest that the proximal sequence required for BCR expression is located within a region 1.0 to 1.5 kb upstream of the *BCR* open reading frame[97,124,125]. Our laboratory has narrowed down this sequence to a 120 bp region located 0.5 kb upstream of the *BCR* open reading frame (Dr. Brett Johnson, unpublished data). This 120 bp region had a similar effect on luciferase expression as the previously annotated minimal-promoter sequences. After identifying a small region responsible for the majority of *BCR* transcriptional activity, the current focus is to identify the factors responsible for gene transcription.

1.4.4.2 DNA/histone modifications relative to BCR-ABL

Methyl groups on DNA are associated with the maintenance of DNA in a heterochromatin state, which is transcriptionally inactive[126], Fig 1.5, A). During cancer, this process is hijacked, allowing de-methylation of oncogenes, and silencing of tumour suppressor genes[127]. Histones are involved in forming compact DNA structures required to fit 2 m of DNA inside the nucleus in each cell[128], Fig 1.5, B). Histone modifications, acetylation and methylation, can either unpack the local DNA structure, which is permissive of transcription, or promote DNA compaction and silencing of gene expression[128]. Similar to DNA modifications, histone modifications are also altered in cancer[127].

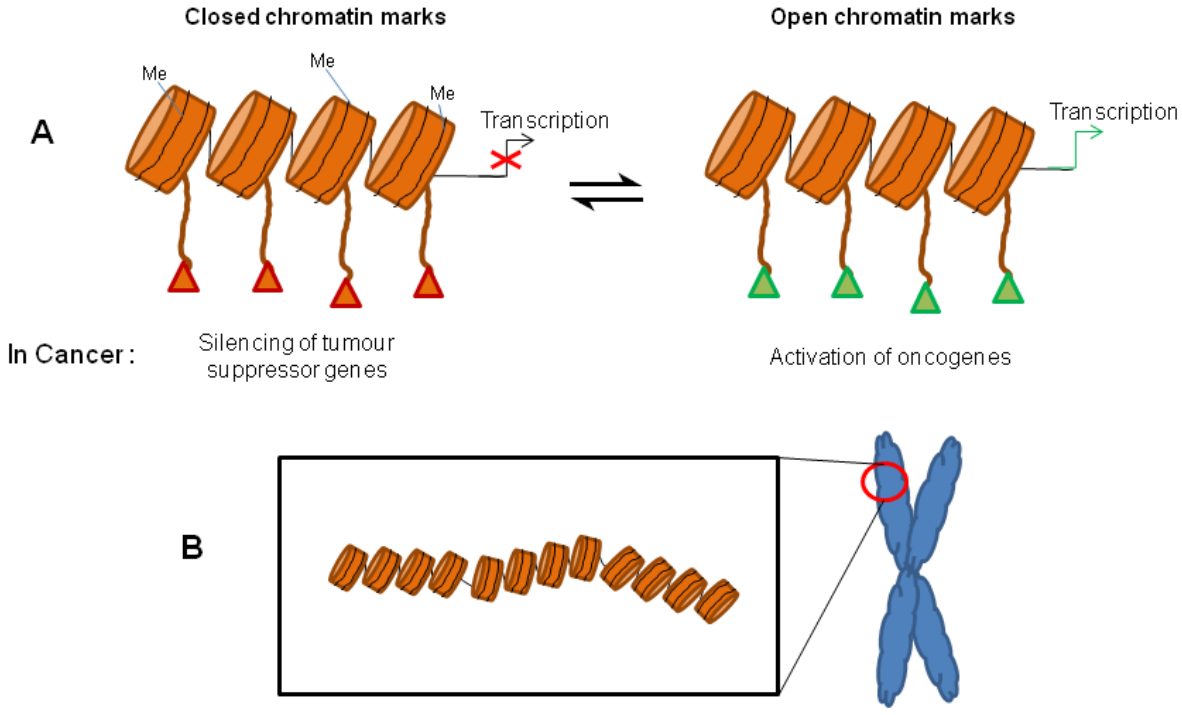

Fig 1.5: DNA/Histone modifications control gene expression. (**A**) Modifications of histone tails (triangles) can alter the way in which chromatin modelling affects transcription. These modifications can silence gene expression (left, red triangles) as well as promoting DNA methylation (Me) also associated with gene silencing. Alternatively, other histone modifications can prevent gene silencing and are permissive of transcription (right, green triangles). Both these states can play a role during cancer. Histones are depicted by orange cylinders, with the black lines representing DNA. (**B**) Histones organise DNA in a compact structure giving rise to the chromosome structure (blue), required to organise the large amount of DNA located in the nucleus.

DNA and histone modifications are poorly characterised in CML. However, with the technology becoming more robust and cheaper, it would be anticipated that epigenome sequencing will be performed more frequently in the context of CML in the near future. Such experiments would not only uncover how the *BCR* promoter is regulated by epigenetic modifications, but how the CML epigenome as a whole differs from that of healthy cells, as well as which epigenetic changes occur during disease progression.

1.4.4.3 The *BCR-ABL* 3'UTR

The 3'UTR acts as a barcode that can contribute to RNA localisation, stability and translation, and therefore plays a critical role during gene expression[129,130]. To date, little is known about the *BCR-ABL* 3'UTR's involvement in the fate of *BCR-ABL* mRNA. Therefore, our laboratory is interested in understanding the function of the *BCR-ABL* 3'UTR, as well as identifying binding-factors that mitigate this function. The most common binding-factors are microRNAs and RNA-binding proteins – discussed in detail in chapters 3 and 4, respectively. The 3'UTR barcode determines which of these factors interact with the transcript, and therefore governs where the RNA will localise, how stable (or unstable) the RNA becomes, and the level of protein translated from the gene. Preliminary data from our laboratory showed that the *BCR-ABL* 3'UTR was repressive, which led us to investigate the significance of this observation in the context of CML.

1.4.4.4 BCR-ABL is abnormal

It must be reiterated that the *BCR-ABL* gene is not found in healthy cells. Our approach to identify regulators of BCR-ABL involves discrete examination of the promoter or the 3'UTR. A caveat for this approach is that regulators of *BCR* and *ABL1* expression could have reduced, similar, or enhanced effects in the context of BCR-ABL expression. It may be too simplistic to assume that the *BCR* promoter functions identically to that of the *BCR-ABL* promoter. It is known that transcriptional-enhancers can be located hundreds of kb upstream and downstream of genes[131,132]. So downstream enhancers for *BCR* may not be present in the *BCR-ABL* gene, or *BCR-ABL* may come under the control of *ABL1* enhancers. Likewise, the *BCR-ABL* 3'UTR may act differently from the *ABL1* 3'UTR. For example, cross-talk between the 5'UTR and 3'UTR is known to control gene expression, which would obviously differ between *ABL1* and *BCR-ABL*[133,134]. That said, our approach is still a valid strategy to identify

regulators of BCR-ABL. However, one should be aware of potential contextual differences between *BCR*, *ABL1* and *BCR-ABL*.

1.4.4.5 The key regulators of BCR-ABL expression are known, now what?

Once the major transcription factors, microRNAs and RNA-binding proteins that modulate BCR-ABL expression have been identified, the next step is to determine their role in CML, followed by determining their possible role as therapeutic targets.

With respect to control of BCR-ABL by the 3'UTR, it is imperative to first determine how the 3'UTR functions (Fig 1.5, A), that is, how the 3'UTR influences BCR-ABL expression. Then the search can then begin for the regulators that functionally interact with the 3'UTR. Finally, it is important to show the relevance of these interactions in the context of CML (Fig 1.5, B). For example, if a microRNA is found to interact with the *BCR-ABL* 3'UTR, the expression of the microRNA would be scrutinised in CML:

- Is this microRNA differentially expressed in CML compared to healthy myeloid cells?
- Is this microRNA differentially expressed between CP and BC (where an increase in BCR-ABL expression is observed)?
- Is this microRNA differentially expressed between different myeloid compartments (i.e. HSC *vs*. GMP etc) where changes in BCR-ABL expression are observed?
- Is this microRNA aberrantly expressed in patients who poorly respond to therapy?
- Do changes in microRNA expression translate into significant changes in BCR-ABL expression *in CML*?
- How are these microRNA(s) regulated?
- Can we modulate the expression of these microRNA(s) in a therapeutic setting?

This pipeline is outlined in Fig 1.5, and is identical in the case of identification of a functional RNA-binding protein interaction with the *BCR-ABL* 3'UTR, or a transcription factor interaction with the *BCR-ABL* promoter. The ultimate goals are to: 1) apply the knowledge of BCR-ABL expression to the biology of CML, and 2) identify a regulator(s) of BCR-ABL that can modulate BCR-ABL expression in CML patients together with TKI therapy to produce a deeper/more effective therapeutic response.

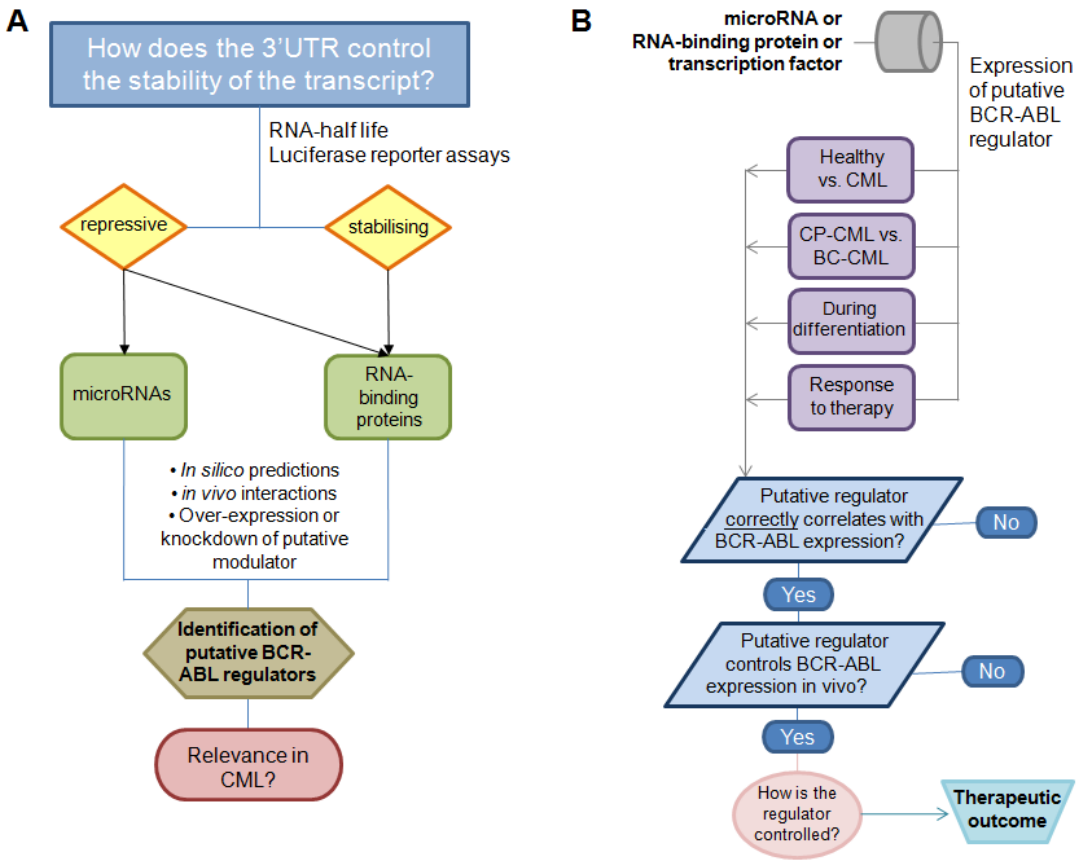

Fig 1.5: Experimental pipeline to identify factors that control BCR-ABL expression in the context of CML. (**A**) It is first required to determine what role the 3'UTR has during the expression of BCR-ABL, that is repressive or stabilising. This leads to investigation of the factors involved in facilitating the 3'UTR's effect on expression. Then, the relevance of these regulators is CML would need to be established. (**B**) Establishing the expression pattern of the putative regulator will provide evidence for its biological function in CML. This would be followed by manipulation of the regulator in CML primary cells to demonstrate the ability to alter BCR-ABL expression in vivo. If the regulator itself can be therapeutically targeted, it may be possible to modulate BCR-ABL expression in CML patients to synergise with current TKI therapies.

1.5 Specific aims

This chapter introduced the concept that BCR-ABL expression levels contribute to the biology of disease progression, TKI-therapy and residual disease. Surprisingly little is known about how BCR-ABL expression is controlled. The previous section explained how such knowledge could contribute to biological and clinical aspects of CML.

Within the time-frame of a PhD project, it is not realistic to expect the completion of the entire experimental pipeline from Fig 1.5. Instead, this study aimed to complete the left hand side of the pipeline, that is:

1. Determine the function of the *BCR-ABL* 3'UTR for the control of BCR-ABL expression
2. Identify regulators that functionally interact with the 3'UTR, namely
    a. MicroRNAs
    b. RNA-binding proteins
3. Pre-determine the significance of such interactions in the context of CML
    a. Does the putative regulator have a known role in CML?
    b. Are expression data available for this regulator in the context of CML that would correctly correlate with BCR-ABL expression levels?

Chapter 2

Characterisation of the *ABL1* 3'UTR

2.1 Introduction

The importance of understanding how BCR-ABL expression is controlled was highlighted in the previous chapter. There is a large body of literature describing 3'UTR-mediated control of gene expression in development and disease, yet the *BCR-ABL* 3'UTR is poorly understood. The main aim of this study is to address the gap in the literature surrounding the significance of the *BCR-ABL* 3'UTR's effect on BCR-ABL expression. This chapter describes the search for alternate *BCR-ABL* 3'UTR species, followed by our investigation into the effect of the 3'UTR on gene expression. Finally, several bioinformatics approaches are used in an attempt to identify putative regulatory elements within the *BCR-ABL* 3'UTR, as well as potential *trans*-factor interactions. Of note, as the *BCR-ABL* 3'UTR is identical to the *ABL1* 3'UTR, the expressions "*BCR-ABL* 3'UTR" and "*ABL1* 3'UTR" are interchangeable.

2.1.1 The 3'UTR

The 3'UTR spans from the nucleotide following the stop-codon until the end of the transcript (Fig 2.1). The 3'UTR plays a critical role in post-transcriptional regulation. This is facilitated by binding of regulatory molecules to specific elements present within the 3'UTR that affect gene expression. Important elements include the poly adenylation signal (PAS), and binding sites for microRNAs and RNA-binding proteins (Fig 2.1).

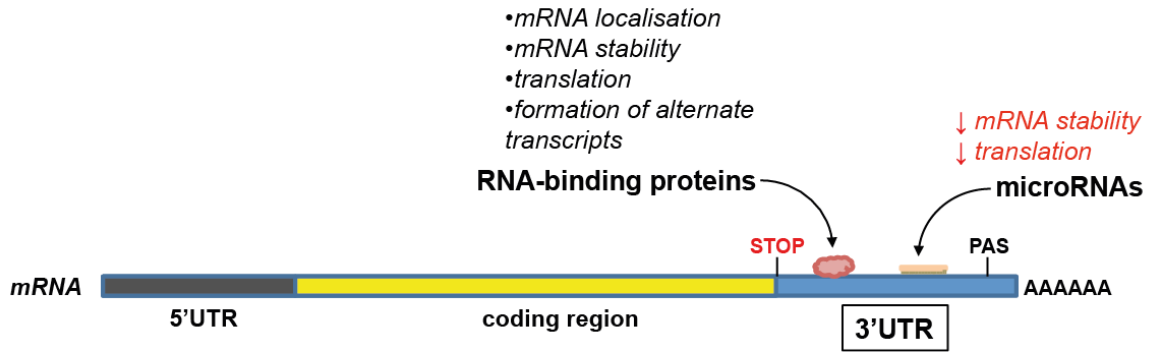

Fig 2.1: The 3'UTR contains a number of important regulatory elements. The 3'UTR (blue) consists of the sequence downstream of the stop-codon. It contains a PAS (poly adenylation site) within the last 10-30 nt of the transcript which directs transcription termination and polyadenylation[135]. The 3'UTR is also a target for *trans*-factors that play a critical role in post-transcriptional regulation, such as RNA-binding proteins and microRNAs. MicroRNAs repress gene-expression by interactions with complementary sequences generally within the 3'UTR. Although RNA-binding proteins bind throughout the transcript, they have a well-documented role of controlling gene expression via interactions with the 3'UTR. They affect a number of mechanisms involved in RNA biogenesis, and act as repressors or enhancers of gene-expression.

2.1.1.1 The PAS

Every transcript (with the exception of replication-dependent histone genes[136]) contains a PAS[135]. The PAS determines the site for pre-mRNA cleavage and addition of the poly-A tail[135]. Therefore, the PAS is a determinant of 3'UTR length. The most common eukaryotic PAS sequence is AAUAAA, with single nucleotide variants accounting for most of the remaining annotated PAS[137]. Poly-adenylation is involved in mRNA transport, translation and stability[138]. In particular the poly-A tail is required for circularisation of mRNA, which is essential for efficient translation[139]. While the PAS plays a role in general gene expression, some genes are known to contain alternate PASs which change the fate of the transcript (discussed later).

2.1.1.2 MicroRNAs

MicroRNAs (discussed in chapter 3) are a class of small non-coding RNAs, important for post-transcriptional regulation of gene expression. Their role is to fine-tune gene expression during important cellular events[140]. MicroRNAs reduce the expression of their targets by altering mRNA stability or translation, or both[141]. MicroRNAs bind to complementary regions located generally within the 3'UTR; however, it is the proteins that are complexed with the

microRNA that facilitate repression of gene expression. MicroRNA binding sites consist of at least six consecutive nucleotides with 100% homology to their target.

MicroRNA involvement in 3'UTR-mediated gene regulation has been intensively studied since their discovery over ten years ago. They play a crucial role in coordinating gene expression during development. Interference of microRNA-networks are known to contribute to a number of diseases[142]. We therefore aim to explore direct microRNA interactions with the *BCR-ABL* transcript, and understand what role such microRNAs play in the context of CML.

2.1.1.3 RNA-binding proteins

RNA-binding proteins (discussed in chapter 4) play a number of key roles during the life of a transcript. They are included in general RNA biogenesis as well as post-transcriptional control of RNA-fate. The 3'UTR is a known target for protein interactions involved in post-transcriptional regulation. Similar to microRNAs, RNA-binding proteins play key roles during development and disease[143].

RNA-binding proteins contain RNA-binding domains (RBDs) that facilitate their interaction with RNA[144]. The protein-RNA interaction usually involves ambiguous or short sequences[145]. Therefore, prediction of RNA-protein interactions is difficult. Our initial aim was to develop a method to isolate RNA-binding proteins that interact with the *BCR-ABL* 3'UTR. The desired outcome was to identify proteins that are important as post-transcriptional mediators of BCR-ABL expression.

2.1.1.4 3'UTR avoidance

In humans, the average length of the 3'UTR is approximately 1000 nt[146]. The main inference from the length of the 3'UTR is that the number of factors that interact with the 3'UTR should increase with size. This is demonstrated by the shortening of 3'UTRs in some cancers, which allow for the escape of 3'UTR-mediated regulatory control[147]. A number of mechanisms have been observed that overcome 3'UTR-mediated gene regulation. These include genomic mutations within the 3'UTR, 3'UTR shortening, and decoy 3'UTRs (Fig 2.2, A-B).

3'UTR single nucleotide polymorphisms (SNPs) (Fig 2.2, A) have been noted in various diseases[148]. A number of functionally relevant SNPs have been mapped to microRNA

binding sites, whereby the microRNA can no longer interact with the mutated 3'UTR[149-152]. By mapping SNPs to predicted microRNA sites, Gong, *et al.* showed that of the 2 million predicted microRNA binding sites, around 90,000 would be disturbed by a SNP, whilst 90,000 potential microRNA sites would be formed[152]. These same principles apply to RNA-binding proteins, but their ambiguous sequence affinity makes it difficult to predict how 3'UTR SNPs could affect RNA-binding protein interactions.

Alterations in the 3'UTR, in particular 3'UTR shortening, provide a mechanism for evading regulation by microRNAs and RNA-binding proteins (Fig 2.2, A;[153]). The main mechanisms that give rise to 3'UTR alterations are the use of alternate PAS[147] and alternate splicing[154,155]. These events have been observed in both healthy[156] and in cancer cells[147]. Shortening of the *CyclinD1* 3'UTR has been observed in mantle-cell lymphoma (MCL), and is also a prognostic indicator – a shortened 3'UTR is associated with poor prognosis[157]. Interestingly, a number of mechanisms have been observed that cause *CyclinD1* 3'UTR shortening. Wiestner, *et al.* found a number of genetic alterations in MCL patients resulting in the formation of premature PASs in the 3'UTR[157]. Mayr, *et al.* also observed the usage of a non-canonical PAS (AAGAAA) in the 3'UTR, which led to *CyclinD1* truncations[147]. *CyclinD1* 3'UTR truncations were found to increase *CyclinD1* stability and protein expression due to the loss of an AUUUA-motif and microRNA binding sites[158].

Poliseno, *et al.* described the use of decoy 3'UTRs in pseudogenes as a method for escaping 3'UTR-mediated regulation (Fig 2.2, B;[159]). This study investigated the *PTENP1* gene, which is a pseudogene (see Fig 2.2 legend) for *PTEN*. *PTENP1*'s coding sequence differs from *PTEN* by 18 nucleotides; however the start codon is disrupted preventing translation. The 3'UTR of *PTENP1* is around 2 kb, and the first 1.2 kb are identical to that of *PTEN*[159]. It was observed that *PTENP1* enhanced expression of PTEN, and that the *PTENP1* 3'UTR acted as a decoy for *PTEN*-targeting microRNAs[159]. That study also examined the role of other pseudogenes acting as 3'UTR decoys, for example *PTEN*, *KRAS*, *Oct4*, *CDK4*, *FOXO3*, *NPM1*, *E2F3* and *DNMT3A*[159]. Although that study focused on disruptions of microRNA interactions, the *NPM1* 3'UTR is a known target for RNA-binding proteins[160], providing evidence that pseudogenes may also act as a sink for RNA-binding proteins.

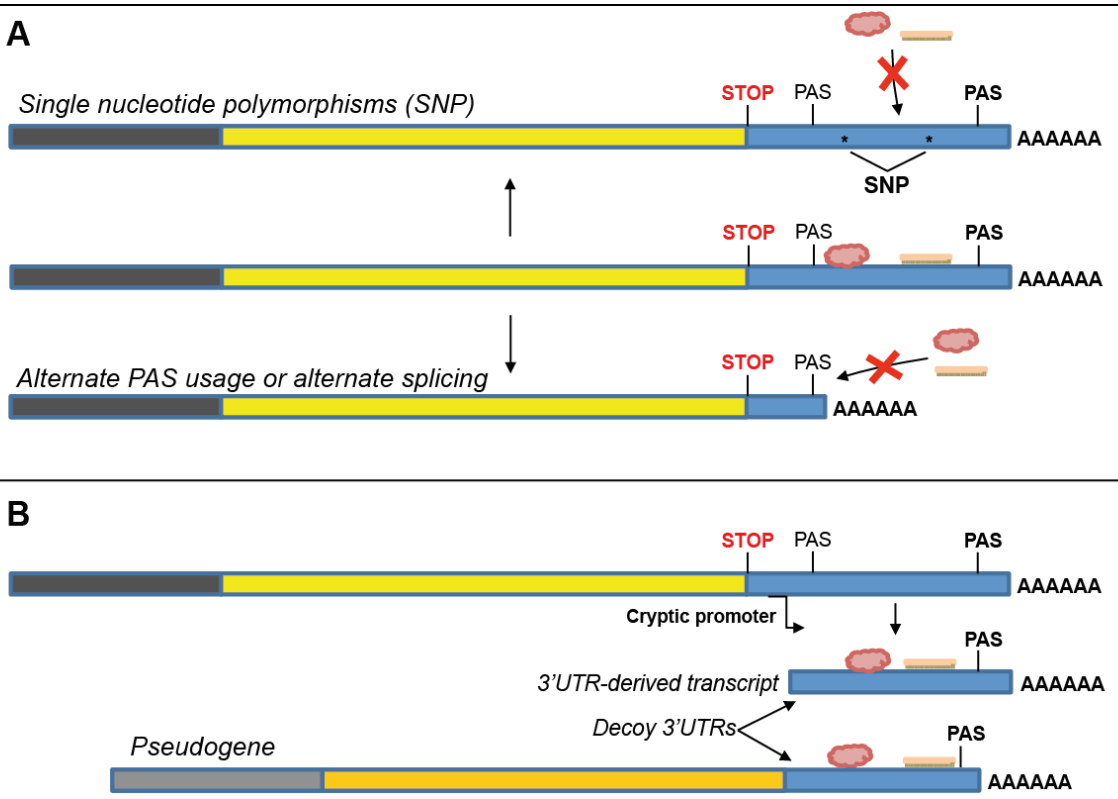

Fig 2.2: Mechanisms for evasion of 3'UTR regulatory control. (**A**) 3'UTR alterations and alternate PAS usage/splicing are known to disrupt regulatory elements within the 3'UTR. For example, polymorphisms within binding sites for *trans*-acting factors can prevent these factors from interacting with the 3'UTR. Likewise, 3'UTR-shortening via alternate splicing and PAS usage can result in the exclusion of regulatory elements present in the full-length 3'UTR. (**B**) 3'UTR-decoys contain portions of 3'UTR sequence, and are formed from discrete (cryptic promoters) within 3'UTRs or expressed as a part of a pseudogene* (see below). Decoy 3'UTRs can compete for microRNAs and RNA-binding proteins, thus abating regulatory control of the "functional" coding gene. *Pseudogenes are loci that contain homology to a functional gene, but the gene is disrupted in a way that prevents expression of a functional gene. For example, Altered promoter regions, lack of a start-codon, inclusion of a premature stop codon, etc. They are thought to have arisen via retrotransposition and tandem gene duplication, with over 8000 found in the human genome[161].

Mercer, *et al.* used a database of capped analysis of gene expression (CAGE) tags to map 5' mRNA caps (start of transcripts) within the human and mouse genome[162]. These CAGE tags were over-represented in promoter regions, as would be expected. However the next highest representation was within 3'UTRs. These data raise the possibility that the 3'UTR is transcribed independent of the coding gene. 3'UTR-derived transcripts could therefore act as 3'UTR decoys for the full length transcript.

2.1.2 The *BCR-ABL* 3'UTR

This study aimed to characterise the *BCR-ABL* 3'UTR. By knowing how the 3'UTR regulates BCR-ABL expression, we can examine its importance in CML (Fig 1.5). Our focus was to determine if the 3'UTR was activating or repressive, if it is altered, and to what extent it is regulated by *cis*/*trans*-acting factors.

Although this study focused on the *BCR-ABL* 3'UTR and CML, *ABL1* has also been implicated in a number of other diseases (interestingly, all of which are leukaemias) (Table 2.1). Moreover BCR-ABL variants have been found in other leukaemias[61,62,163]. Therefore we anticipate that the findings of this study will have relevance to those diseases as well.

Table 2.1: Examples of *ABL1* involvement in other diseases

Gene	Disease	Reference
BCR-ABL (excluding CML)	AML, ALL, CNL	61,62,163
(*ETV6*)*TEL-ABL1*	CML, AML, ALL	164-166
NUP214-ABL1	T-cell ALL, B-cell ALL	167,168
EML1-ABL1	T-cell ALL	169
RCSD1-ABL1	ALL	170

2.1.2.1 What is known about the *BCR-ABL* 3'UTR

The *BCR-ABL* fusion gene contains the 3'UTR from *ABL1* (see chapter 1, Fig 1.2, pg 7). The *ABL1* gene has two alternate transcripts (RefSeq NM_005157, and NM_007313), whose 3'UTRs are identical, and only differ by alternate promoter-usage. The *ABL1* 3'UTR was cloned and sequenced in 1990 by Andrews, *et al.*[171]. Even with the primitive knowledge on how 3'UTRs regulated gene expression at that time, the importance of this region was flagged in the opening paragraph by Andrews, *et al.*[171] '*Untranslated regions at the 3'end of mRNA transcripts (3'utrs) are important in determining certain mRNA transcript characteristics and more particularly are involved in regulating transcript half-life'*. It is for these very same reasons we are also investigating the *ABL1* 3'UTR.

The annotated *ABL1* 3'UTR on the NCBI (www.ncbi.nlm.nih.gov/), Ensembl (www.ensembl.org/) and UCSC (www.genome.ucsc.edu/) genome browsers is 1992-nt long. Therefore, the *ABL1* 3'UTR is approximately twice the average length of a human 3'UTR. There are two PASs present within the *ABL1* 3'UTR sequence: a canonical PAS (AAUAAA),

at the 1969th nucleotide of the 3'UTR (giving rise to the 1992 nt 3'UTR), and a non-canonical (AAGAAA) PAS at the 780th nucleotide. However, there is no evidence (from EST data, on the UCSC browser) that the latter PAS is used.

It is widely accepted that cross-species sequence conservation relates to function, especially in non-coding regions[172]. Therefore, we examined the cross-species sequence conservation of the *ABL1* 3'UTR using the UCSC genome browser (human genome assembly 18, or hg18). This database identified six hotspots in the *ABL1* 3'UTR with high cross species-conservation. However the major part of the 3'UTR is not highly conserved (Fig 2.3). Two of the hotspots are located at the 3' end, with one of these containing the annotated PAS. Interestingly, the last five nucleotides of the non-canonical PAS exhibit cross-species conservation (Fig 2.3).

To date, the only *trans*-acting factors known to regulate BCR-ABL via the 3'UTR are microRNAs. miR-203[173,174], and miRs-451, 515 and 760[174] have been reported to regulate BCR-ABL expression. Transcriptome-wide mapping of RNA-binding protein/RNA interactions identified protein interactions with the *ABL1* 3'UTR (see 2.3.11.2.2, pg 79). These mapping experiments do not assess the possible functional significance of the putative interactions and, thus, it is unknown if these proteins affect BCR-ABL expression.

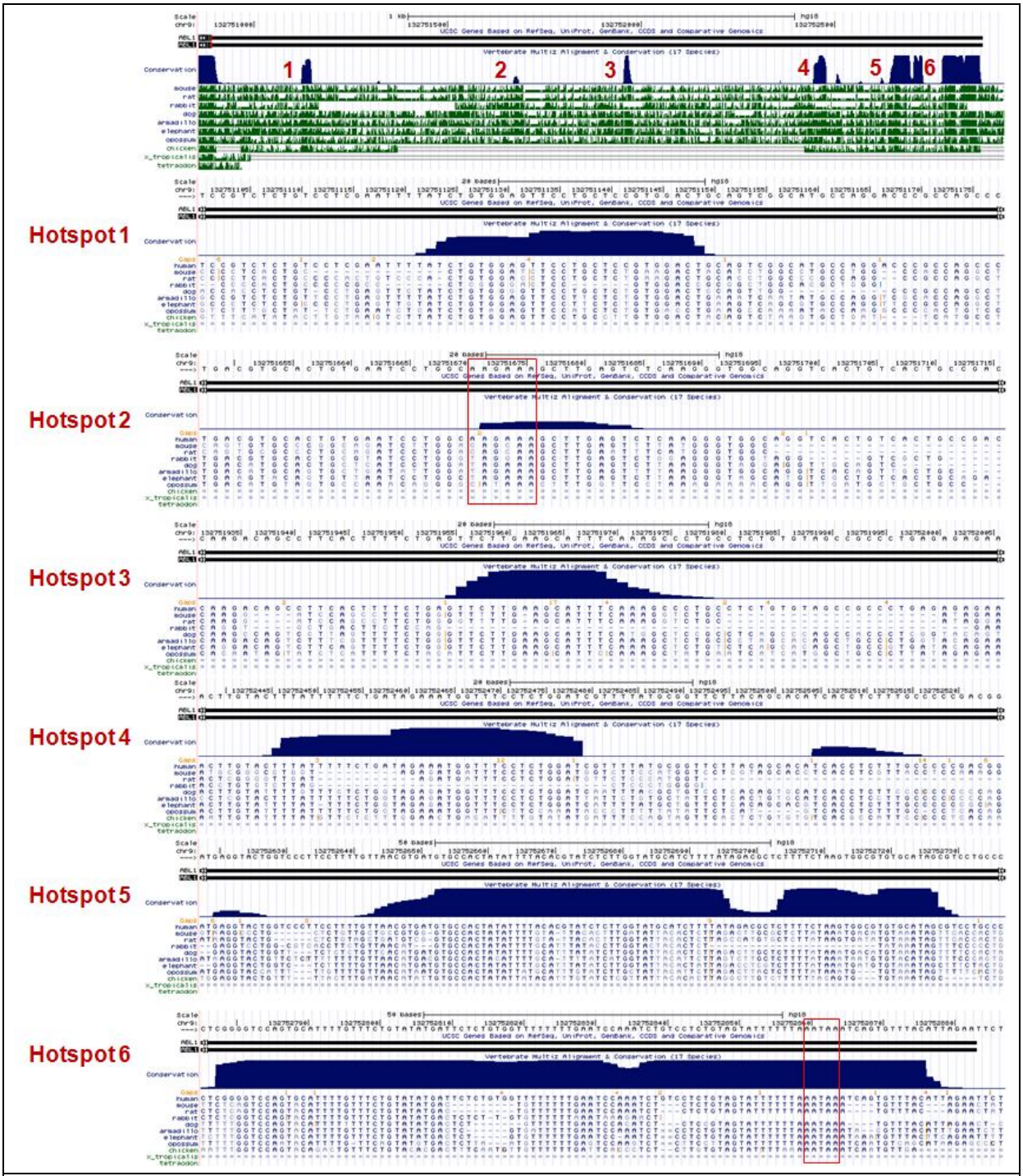

Fig 2.3: Cross-species conservation data for the *ABL1* 3'UTR. Using the hg18 assembly on the UCSC genome browser, six hotspots of sequence conservation were observed across seventeen species for the *ABL1* 3'UTR. The annotated PAS is located within hotspot 6 (AATAAA), and a non-canonical PAS (AAGAAA) is located within hotspot 2 (red rectangles). These data show that, in general, the *ABL1* 3'UTR is not highly conserved.

2.1.2.2 3'UTR shortening of *ABL1*

Shortening of *ABL1* transcripts has been observed in both human[175-177], and mouse[178-180]. Moreover, shortening of the human *ABL1* transcript has been observed in haematopoietic cells[177], and in BC-CML cells[175,176]. In the case of human *ABL1*, it is unknown if this shortening is due to splicing or alternate PAS usage. However, shortened murine *ABL1* transcripts were found to arise via 3'UTR-shortening, a result of non-canonical PAS usage[180]. These shortened *murine ABL1* transcripts were only observed in the mouse testis, and were more stable than full length *ABL1* transcripts[180].

The tissue specificity of shortened *ABL1* transcripts suggests that a specialised mechanism exists in the mouse testis to regulate *ABL1* transcript length. This is of particular interest in CML. If *ABL1*-shortening occurs in humans and alters BCR-ABL expression, this may explain how BCR-ABL levels differ between haematopoietic compartments and disease progression (1.4.2).

After observing shortened *ABL* and *BCR-ABL* human transcripts, Andrews, *et al.* cloned and sequenced the *ABL1* 3'UTR[171]. Their study also showed that the non-canonical PAS was not present in the human *ABL1* gene[171]. In addition they found no evidence for *BCR-ABL* and *ABL1* 3'UTR shortening in human CML cell lines[171]. As the data for those conclusions were not shown, and more sensitive approaches for mapping 3' end formation are now available, we revisited the prospect of 3'UTR shortening in *ABL1* and *BCR-ABL*.

2.1.2.3 Investigating the *BCR-ABL* 3'UTR

We aimed to characterise the *ABL1* 3'UTR based on the mechanisms of 3'UTR-mediated gene regulation discussed in 2.1.1. This will involve, defining the *ABL1* 3'UTR, and looking for 3'UTR variants. Then we will examine the effect of the 3'UTR on gene expression, and identify and *cis* or *trans* elements that facilitate regulatory control. Our approach is summarised in Table 2.2.

Table 2.2: *ABL1* 3'UTR characterisation scheme

	Aim	Experiments involved
Defining the *ABL1* 3'UTR	- Confirm genome browser annotation - Search for *ABL1* 3'UTR variants	- 3'RACE - Bioinformatics/data mining
***ABL1* 3'UTR's role during gene expression**	- Investigate the net effect of the 3'UTR on gene expression - Investigate mechanisms for 3'UTR regulatory effects - Determine if the effect is cell-specific	- mRNA halflife - Luciferase reporter assays
Identification of cis/trans regulatory elements	- Map regions in the 3'UTR which may be affected by *cis* or *trans* factors	- Luciferase reporter assays - Bioinformatics/data mining
Identification of factors that interact with the *ABL1* 3'UTR	- MicroRNAs (chapter 3) - RNA-binding proteins (chapter 4)	
***ABL1* 3'UTR in CML**	- Search for *ABL1* 3'UTR variants in disease - *ABL1* 3'UTR SNP analysis	- 3'RACE - Bioinformatics/data mining - Conventional sequencing

2.2 Methods

2.2.1 Renilla reporter constructs

The *ABL1* 3'UTR was cloned into the *Xba*I sites of pCIneo-hRL (kindly provided by Prof. Greg Goodall, Centre for Cancer Biology, Adelaide (Fig 2.4, A;[181]), using a PCR-based approach (2.2.1.1). This plasmid was named phRL-ABL1 3'UTR (Fig 2.4, B). *Most* of the *Renilla*-reporters harbouring different regions of the *ABL1* 3'UTR were constructed by one of three methods: PCR-cloning, restriction digest of phRL-ABL 3'UTR, or insertion of a unique restriction site into phRL-ABL1 3'UTR. The different *ABL1* 3'UTR reporter constructs are listed in Table 2.3, and their modes of construction are described in the following sub-sections.

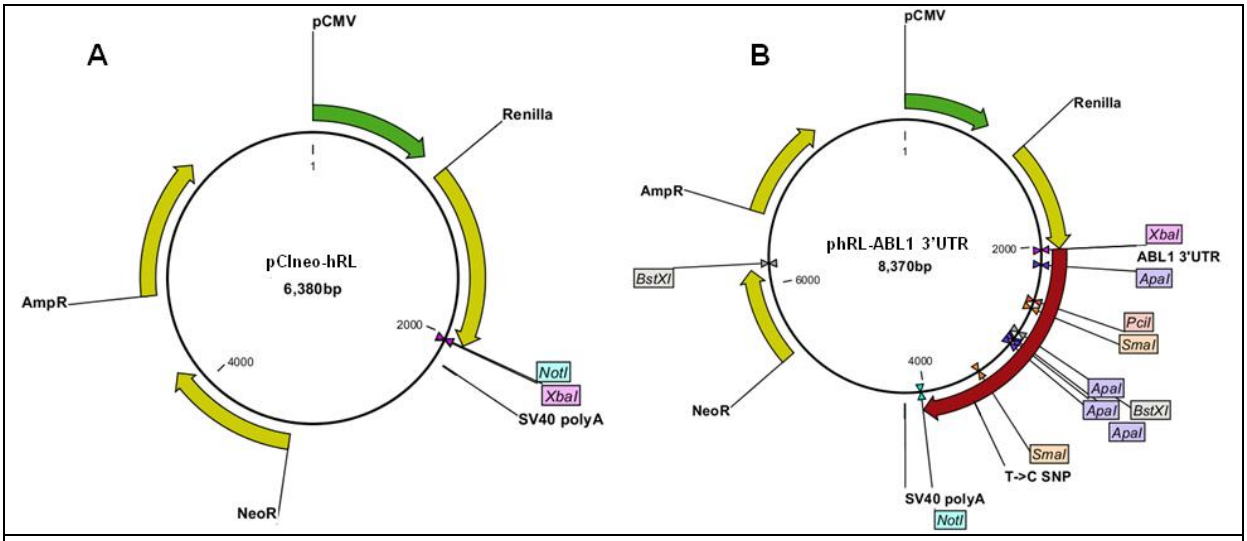

Fig 2.4: Renilla-based *ABL1* 3'UTR reporter vectors. (**A**) pCIneo-hRL is the parental vector used to generate *ABL1* 3'UTR-reporters. It contained a human-codon optimised Renilla gene[182] driven by the CMV promoter. Restriction sites used for cloning are indicated by coloured boxes. (**B**) Cloning of the *ABL1* 3'UTR into pCIneo-hRL generated the plasmid phRL-ABL1 3'UTR. Although the 3'UTR was cloned into the *Xba*I restriction site in pCIneo-hRL, the 3' *Xba*I site was destroyed during cloning. Note: the 3'UTR contains a T to C mutation at the 1557th nucleotide. This mutation is not an annotated SNP, and was most likely introduced during PCR amplification of the 3'UTR, as AmpliTaq® Gold has an error-rate of 1.5 nt for a fragment of 1992 bp (according to manufacturer). Vector map created using CLC bio Workbench v6.5 (CLC bio, Aarhus, Denmark).

Table 2.3: pCIneo-hRL-based *ABL1* 3'UTR reporter constructs

Plasmid name (phRL-)	**Mode of construction**		
	PCR 2.2.1.1	Restr.site 2.2.1.2	Restr.site ins 2.2.1.3
ABL1 3'UTR	✓		
ABL1 3'UTR(reverse)	✓		
ABL1 (-124)		✓	
ABL1 (1-225)*	✓		
ABL1 (1-579)		✓	
ABL1 (1-755)	✓		
ABL1 (1-840)	Blunt cloning (see 2.2.1.4)		
ABL1 (1-935)	✓		
ABL1 (1-1116)	✓		
ABL1 (1-1249)			✓
ABL1 (1-1572)			✓
ABL1 (242-1992)			✓
ABL1 (499-1992)		✓	
ABL1 (981-1992)		✓	
ABL1 (1116-1992)	✓		
ABL1 (1257-1992)			✓
ABL1 (1387-1992)		✓	
ABL1 (1576-1992)			✓
ABL1 (1889-1992)†	✓		
FL_ABL1 (PAS)	See 2.2.1.5		
FL_ABL1 (SAP)	See 2.2.1.5		
ABL1 3'UTR Δ1116-1253			✓
ABL1 3'UTR Δ840-935			✓
ABL1 3'UTR ΔTTP	Mutagenesis (see 2.2.3)		
ABL1 (1116-1257)	See 2.2.1.6		
ABL1 (1116-1257)ΔTTP	Mutagenesis (see 2.2.1.6)		
ABL1 (1116-1287)	✓		
ABL1 (821-939)	✓		
ABL1 (821-1287)	✓		

The plasmids' name relates to the region of the *ABL1* 3'UTR it contains
* also called Renilla-miR196 (see 3.2.3.1)
† also called Renilla-miR30 (see 3.2.3.1)

2.2.1.1 *ABL1* 3'UTR reporters (PCR-based)

2.2.1.1.1 PCR

The *ABL1* 3'UTR was amplified using AmpliTaq® Gold (Applied Biosystems; Foster City, CA, USA) according to Appendix A.1, using the primer set (Geneworks; Thebarton,

Australia) in Table 2.4 and genomic DNA template (isolated from a healthy control blood sample). The PCR conditions were: 96°C for 10 min, then 30 cycles of 94°C for 30 sec, 55°C for 45 sec, and 72°C for 2 min; then 72°C for 10 min.

Subsequent PCRs were performed using Phusion® High-Fidelity DNA Polymerase (Finnzymes; Vantaa, Finland) according to Appendix A.2, using phRL-ABL1 3'UTR as a template, and the primers in Table 2.4. PCR conditions were: 96°C for 30 sec, then 30 cycles of 96°C for 10 sec, 55°C for 15 sec, and 72°C for 15 sec/kb; then 72°C for 10 min.

Table 2.4: Primers used to amplify regions of the *ABL1* 3'UTR

ABL1 3'UTR reporter (phRL-)	**Sequence** (5' – 3') (Upper line: forward primer; Lower line: reverse primer)
ABL1 3'UTR	GTGCAG**TCTAGA**CAGCAGTCAGGGGTCAGGTG ATCTGC**TCTAGA**TTCTAATGTAAACACTGATTTATTTA
ABL1 3'UTR(reverse)^	GTGCAG**TCTAGA**CAGCAGTCAGGGGTCAGGTG ATCTGC**TCTAGA**TTCTAATGTAAACACTGATTTATTTA
ABL1 (1-225)	GTGCAG**TCTAGA**CAGCAGTCAGGGGTCAGGTG ACAGAT**TCTAGA**CGAGGACAGAGAC
ABL1 (1-755)	GTGCAG**TCTAGA**CAGCAGTCAGGGGTCAGGTG CACGTC**TCTAGA**GAGCAAGAGCTGGGCTCTGG
ABL1 (1-933)	GTGCAG**TCTAGA**CAGCAGTCAGGGGTCAGGTG GTTCAC**TCTAGA**CCCTTGCAGACCTG
ABL1 (1-1116)	GTGCAG**TCTAGA**CAGCAGTCAGGGGTCAGGTG GCAGGT**TCTAGA**TGGCAGCTCTATTCTCTCTC
ABL1 (1117-1992)	GAGAGAG**TCTAGA**GCTGCCACTGGGCACCT ATCTGC**TCTAGA**TTCTAATGTAAACACTGATTTATTTA
ABL1 (1889-1992)	TCTGCT**TCTAGA**GGTCCAGTGCATTTTG ATCTGC**TCTAGA**TTCTAATGTAAACACTGATTTATTTA
ABL1 (1889-1992)	TCTGCT**TCTAGA**GGTCCAGTGCATTTTG ATCTGC**TCTAGA**TTCTAATGTAAACACTGATTTATTTA
ABL1 (1116-1287)	GAGAGAG**TCTAGA**GCTGCCACTGGGCACCT GCTTTC**CGCCGGCG**CGTTTGTGGTTTTCCTAACC
ABL1 (821-939)	CAGG**TCTAGA**TCACTGCCGACATCC GTTCAC**TCTAGA**CCCTTGCAGACCTG
ABL1 (821-1287)	CAGG**TCTAGA**TCACTGCCGACATCC GCTTTC**CGCCGGCG**CGTTTGTGGTTTTCCTAACC
Restriction sites in bold ^ derived from a Phusion-based PCR (Appendix A.2), the *ABL1* 3'UTR does not contain any mutations, and the 3'UTR-flanking *Xba*I sites are both intact	

2.2.1.1.2 Restriction digest cloning

All restriction enzymes were purchased from New England Biolabs (Ipswich, MA, USA), and were supplied with 10x NEB buffer and 10x Bovine Serum Albumin (BSA). The PCR products and pCIneo-hRL were digested with *Xba*I (or *Xba*I and *Not*I-HF) in 1x NEB buffer 4 and 1x BSA. The digestion reactions were incubated at 37^{o}C for 2 h. To prevent self-ligation of the vector backbone, the terminal phosphate groups were removed by calf intestinal alkaline phosphatase (CIP) (Finnzymes). CIP (10 U) was added to the plasmid digest, which was incubated at 37^{o}C for a further 15 min. The vector backbone and digested PCR products were then purified by gel extraction (Appendix A.9) for ligation. The purified insert and vector were ligated (ratio 3:1) as per Appendix A.10, for transformation (2.2.1.7).

2.2.1.2 *ABL1* 3'UTR reporters (restriction site-based)

The 3' *Xba*I site in phRL-ABL1 3'UTR was destroyed during the cloning procedure. This became advantageous for constructing different *ABL1* 3'UTR reporters using *ABL1* 3'UTR-specific restriction sites (Fig 2.4, B). phRL-ABL1 3'UTR digests were set up as per Table 2.5, using 10 U of each enzyme in 1x NEB buffer and 1x BSA. The reactions were incubated at 37^{o}C for 2 h. The DNA was blunt-ended for circularisation using T4 polymerase (New England Biolabs) (Appendix A.17). Blunt-ended DNA was ligated as per Appendix A.10 for transformation (2.2.1.7).

Table 2.5: *ABL1* 3'UTR restriction sites used to make alternative *ABL1* 3'UTR reporters

ABL1 3'UTR reporter (phRL-)	**5' cutter**	**3' cutter**	**NEB buffer**
ABL1 (1-124)	*Apa*I	*Not*I-HF	4
ABL1 (1-579)	*Sma*I	*Not*I-HF	4
ABL1 (499-1992)	*Xba*I	*Pci*I	3
ABL1 (981-1992)	*Xba*I	*Apa*I	4
ABL1 (1387-1992)	*Xba*I	*Sma*I	4

2.2.1.3 *ABL1* 3'UTR reporters (restriction site insertion-based)

Due to difficulties during PCR-cloning, some of the *ABL1* reporters were constructed via insertion of an *Eco*RI site into phRL-ABL1 3'UTR (which does not contain an *Eco*RI site)

(Fig 2.5, A). The restriction site was placed at a position of interest within the 3'UTR. The site was shifted slightly adjacent if there was a sequence resembling an *Eco*RI site – requiring fewer nucleotide changes. This intermediate plasmid was then digested with either *Xba*I/*Eco*RI or *Eco*RI/*Not*I to form alternate ABL1 reporters. To specifically splice out regions of the *ABL1* 3'UTR, the region was flanked by *Eco*RI sites (Fig 2.5, B) introduced by PCR mutagenesis Appendix A.3, using the primers in Table 2.6.

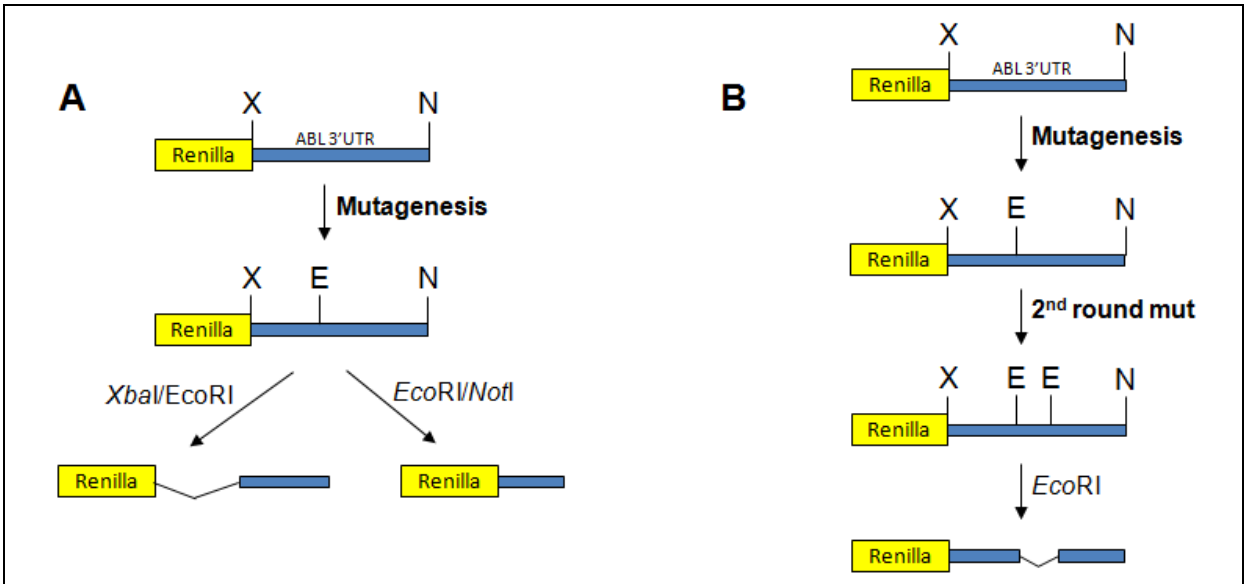

Fig 2.5: Restriction site insertion-based cloning strategy. (**A**) Insertion of an *Eco*RI site into the *ABL1* 3'UTR sequence of phRL-ABL1 3'UTR allowed for generation of alternate 3'UTR reporters. The entire region before the *Eco*RI site can be excised by a *Xba*I/*Eco*RI digest, or the region following the *Eco*RI site can be excised by a *Eco*RI/*Not*I digest. (**B**) In order to splice out regions of the 3'UTR, the region was flanked by *Eco*RI sites by two rounds of mutagenesis, followed by an *Eco*RI digest. X, *Xba*I site. E, *Eco*RI site. N, *Not*I site.

Table 2.6: Restriction site insertion-based mutagenesis primers

ABL1 3'UTR reporter (phRL-)	**Sequence (5' – 3')** (Upper line: forward primer; Lower line: reverse primer)
ABL1 (1-1249*)	GCCTCATGTTCTGTGGGG**GAATTC**AGGGAGGGTTAGGAAAA TTTTCCTAACCCTCCCT**GAATTC**CCCCACAGAACATGAGGC
ABL1 (1-1572*)	CTTGTACTTTATTTTTCTGATA**GAATTC**GTTTCCTCTGGATCGTTTTATGC GCATAAAACGATCCAGAGGAAAC**GAATTC**TATCAGAAAAATAAAGTACAAG
ABL1 (242*-1992)	TGTGACGTGCACTGT**GAATTC**TGGCAAGAAAGCTT AAGCTTTCTTGCCA**GAATTC**ACAGTGCACGTCACA
ABL1 (1257*-1992+)	Same as phRL-ABL1 (0-1249)
ABL1 (1576*-1992)	Same as phRL-ABL1 (0-1572)
ABL1 3'UTR Δ1117*-1253*	*Eco*RI pos.1117: CCCTGAGAGA**GAATTC**AGCTGCCACTGGGC GCCCAGTGGCAGCT**GAATTC**TCTCTCAGGG *Eco*RI pos.1253: Same as phRL-ABL1 (0-1249)
ABL1 3'UTR Δ840*-935*	*Eco*RI pos.840: CGACATCCCTCCCCCA**GAATTC**TGGAGGCAGGGACAAG CTTGTCCCTGCCTCCA**GAATTC**TGGGGGAGGGATGTCG *Eco*RI pos.935: CTGGGCCCAGGCAGGTCTGCA**GAATTC**CAGAGTGAACCGTCCTTT AAAGGACGGTTCACTCTG**GAATTC**TGCAGACCTGCCTGGGCCCAG

Restriction site in bold.
Mutated nucleotides underlined.
+ The digestion should have produced phRL-ABL1 (1253-1992), however four 3' nucleotides were removed unintentionally during the endfill step.
* location of restriction site insertion.

After the restriction site was inserted, the plasmids were digested as per Table 2.7, using 10 U of each enzyme in 1x NEB buffer and 1x BSA. The reactions were incubated at 37^{o}C for 2 h. The DNA was blunt ended for circularisation using T4 polymerase (Appendix A.17). Blunt-ended DNA was ligated as per Appendix A.10 for transformation (2.2.1.7).

Table 2.7: Restriction enzymes used to construct the following *ABL1* 3'UTR reporters

ABL1 3'UTR reporter (phRL-)	**5' cutter**	**3' cutter**	**NEB buffer**
ABL1 (1-1257)	*Eco*RI	*Not*I-HF	4
ABL1 (1-1576)	*Eco*RI	*Not*I-HF	4
ABL1 (242-1992)	*Xba*I	*Eco*RI	4
ABL1 (1257-1992)	*Xba*I	*Eco*RI	4
ABL1 (1572-1992)	*Xba*I	*Eco*RI	4
ABL1 3'UTR Δ1117-1253	*Eco*RI	*Eco*RI	*Eco*RI
ABL1 3'UTR Δ840-935	*Eco*RI	*Eco*RI	*Eco*RI

2.2.1.4 Blunt-end cloning: phRL-ABL1 3'UTR (1-840)

Construction of phRL-ABL1 3'UTR (1-839) involved an *Xba*I/*Bst*XI digest of phRL-ABL1 3'UTR (1-840), which generates a DNA fragment containing 1-840 nt of the *ABL1* 3'UTR. *Bst*XI also cuts in the vector backbone, so this 839 nt fragment was isolated and blunt-end cloned into pCIneo-hRL.

phRL-ABL1 3'UTR (1-935) was digested with 20 U of *Xba*I and *Bst*XI in 1x NEB buffer 3 and 1x BSA, and pCIneo-hRL with 20 U of *Xba*I in 1x NEB buffer 4 and 1x BSA, for 1 h at 37^{o}C. The digests were treated with T4 polymerase to generate blunt ends (Appendix A.17). CIP (10 U) was added to the pCIneo-hRL end-fill reaction and incubated at 37^{o}C for 15 min. pCIneo-hRL (*Xba*I-digested) and the 840 nt 3'UTR fragment were then gel purified as per Appendix A.9. The purified insert and vector were ligated (ratio 3:1) as per Appendix A.10, for transformation (2.2.1.7).

2.2.1.5 Duplex insertion: phRL-FL_ABL1 (PAS) and phRL-FL_ABL1 (SAP)

Complementary oligonucleotides were designed that contained a PAS[183] flanked by *Eco*RI half sites (Table 2.8). The complementary oligonucleotides were annealed and cloned into phRL-ABL1 3'UTR (containing an introduced *Eco*RI site at the 242nd nt of the *ABL1* 3'UTR, phRL-ABL1 3'UTR (EcoRI.242)). The PAS was also cloned in the reverse orientation (SAP) as a control for insertion of DNA into the 3'UTR.

2.2.1.5.1 Oligo-duplex annealing

To form a DNA duplex containing the PAS flanked by *Eco*RI half sites, the forward and reverse oligonucleotides were flanked with AATTC at the 5' end and G at the 3' end (Table 2.8). The two complementary oligonucleotides were first annealed to form a double stranded duplex. Lyophilised PAS-EcoRI_F and PAS-EcoRI_R oligonucleotides were diluted to 200nM in TE (Appendix B). Each oligonucleotide (25 µL) were placed in a single 1.5 mL micro-centrifuge tube, heated to 90°C for 20 min and allowed to cool to room temperature for approximately 3 h (switching off the heat block). Synthesised oligonucleotides lack 5' phosphate groups, so T4 polynucleotide kinase (10 U) (New England Biolabs) was added to 8 µL of the oligo-duplex in 1x ligase buffer (containing ATP) at 37°C for 2 h. The enzyme was then inactivated at 65°C for 20 min.

Table 2.8: Oligonucleotides used to generate EcoRI-flanked PAS DNA

Oligonucleotide*	**Sequence (5' – 3')** (Upper line: forward primer; Lower line: reverse primer)
PAS-EcoRI_F	**AATTC**TGGCCGCAATAAAATATCTTTATTTTCATTACAT C*TGTGTGTTGGTTTTTTGTGTG*A**G**
PAS-EcoRI_R	**AATTC**TCACACAAAAAACCAACACACAGATGTAATGAAA ATAAAGATATTTTATTGCGGCCA**G**
Restriction half-site in bold PAS site underlined on the forward strand G/U rich element italicised on the forward strand *Once these oligonucleotides are annealed, the duplex will appear as though cut at both ends by *Eco*RI. However, as mentioned the duplex will require addition of 5' phosphate groups to ligate with other DNA. Creating half-sites eliminates the need to flank the 5' and 3' ends with *Eco*RI sites plus an additional 6 nt required for *Eco*RI recognition. This reduces the length of the oligonucleotide by 18 nt, which not only reduces cost, but also increases the % of full-length DNA (manufacturer's instructions) – increasing cloning efficiency.	

2.2.1.5.2 Restriction digest cloning

phRL-ABL1 3'UTR(EcoRI.242) was digested with 20 U *Eco*RI-HF in 1x NEB buffer 4 and 1 x BSA at 37^{o}C for 2 h. CIP (10 U) was added to the plasmid digest to prevent self ligation, and incubated at 37°C for a further 15 min. The vector backbone was then purified by gel

extraction (Appendix A.9). Finally, the vector backbone and oligo-duplex DNA was ligated as per Appendix A.10, and transformed (2.2.1.7).

2.2.1.6 phRL-ABL1 (1116-1257) and phRL-ABL1 (1116-1257)ΔTTP

phRL-ABL1 (1116-1257) and phRL-ABL1 (1116-1257)ΔTTP were generated using a plasmid with three copies of the 1116-1257 region cloned into pCIneo-hRL (phRL-ABL1 (1116-1257)x3, provided by Mark Cutting, Centre for Cancer Biology, Adelaide). The phRL-ABL1 (1116-1257)x3 vector was first subjected to PCR mutagenesis to mutate a putative tristetraprolin (TTP) binding site at the 1206th nucleotide within the *ABL1* 3'UTR (see 2.2.4). This resulted in a vector containing three copies of the 1116-1257 nt region, of which two had mutated TTP binding sites (Fig 2.6).

The mutagenised vector and pCIneo-hRL were digested with *Xba*I (20 U) in 1x NEB buffer 4 and 1x BSA for 1 h at 37°C. CIP (10 U) was added to the pCIneo-hRL digest to prevent self ligation, and incubated at 37°C for a further 15 min. *Xba*I digested pCIneo-hRL DNA and the 142 nt 3'UTR-fragment were purified by gel extraction (Appendix A.9). Finally, the 142 nt fragments were ligated with pCIneo-hRL as per (Appendix A.10), and transformed (2.2.1.7) (Fig 2.6).

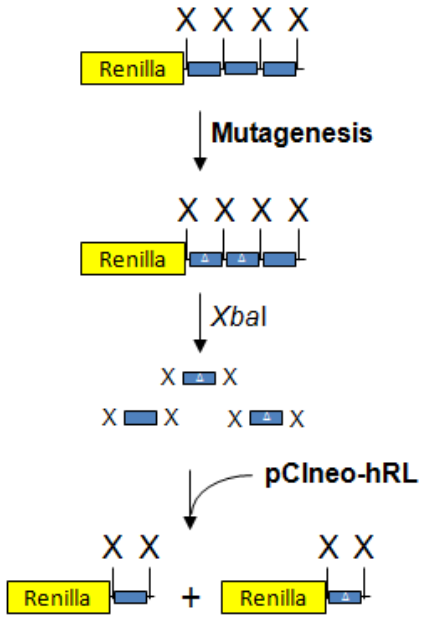

Fig 2.6: Generation of phRL-ABL1 (1116-1257) and phRL-ABL1 (1116-1257)ΔTTP. Mutagenesis of a putative TTP site within the *ABL1* 3'UTR was performed on a vector containing three copies of nt 1116-1257 of the *ABL1* 3'UTR. A clone was isolated which had mutations in two of the TTP binding sites (depicted as triangles). This vector was then digested to obtain isolated 142 nt fragments containing either wildtype or mutated TTP binding sites. These DNA fragments were purified and then cloned into the *Xba*I site of pCIneo-hRL. Single copies of the wildtype or mutated TTP binding site (5' → 3') were screened for via sequencing. X, *Xba*I site.

2.2.1.7 Transformation

Each ligation was transformed into electrocompetent cells as per Appendix A.11.

2.2.1.8 DNA plasmid prep

Desired clones were obtained using the DNA plasmid prep method as per Appendix A.13**.** Presence and orientation of binding site were confirmed by sequencing Appendix A.4.

2.2.1.9 Plasmid amplification

Following sequence confirmation, bulk quantities of the selected clones were obtained using the HiSpeed® Plasmid Midi Kit (QIAGEN, Chadstone, Australia) according to the manufacturer's instructions.

2.2.2 Firefly reporter constructs

The *ABL1* 3'UTR was also cloned downstream of a firefly gene under the control of 1.55 kb of the *BCR* promoter proximal to the transcription start site (pGL4.10-5BCR, Fig 2.7, A; kindly provided by Dr Brett Johnson, Centre for Cancer Biology, Adelaide). This plasmid was called pGL4.10-5BCR/3ABL (Fig 2.7, B). phRL-ABL1 3'UTR(reverse) and pGL4.10-5BCR were digested with *Xba*I (20 U) in 1x NEB 4 buffer and 1x BSA at 37°C for 1 h. CIP (10 U) was added to the vector backbone to prevent self ligation, and incubated at 37°C for a further 15 min. The vector backbone and *ABL1* 3'UTR DNA were gel-purified as per Appendix A.9. Then the 3'UTR DNA was ligated into pGL4.10-5BCR as per (Appendix A.10), and plasmid preparations were obtained as per 2.2.1.7-2.2.1.9.

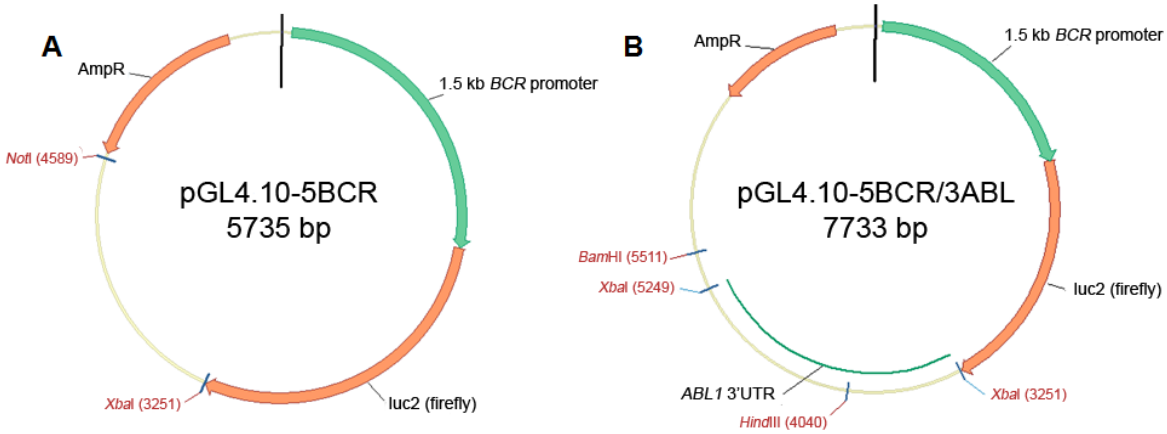

Fig 2.7: Firefly-based *ABL1* 3'UTR reporter vectors. (**A**) pGL4.10-5UTR contains 1.55 kb of the *BCR* gene upstream the transcription start site, upstream of the luc2 *Firefly* gene. (**B**) pGL4.10-5BCR/3ABL was generated by inserting the *ABL1* 3'UTR into the *Xba*I site of pGL4.10-5BCR. The 3'UTR was sourced from phRL-ABL1 3'UTR(reverse), which contains the full-length 3'UTR flanked by *Xba*I sites. Vector map created using Vector NTI® software (Invitrogen).

2.2.3 PCR (qualitative)

Qualitative PCRs were performed using Phusion® High-Fidelity DNA Polymerase according to Appendix A.2, and using the primers in Table 2.9. These PCRs used genomic DNA or cDNA as templates prepared as per Appendix A.6 and A.7 respectively.

Table 2.9: Primers used for qualitative PCR (Distal PAS experiments)

Primer	Sequence (5' – 3')
Forward primer-orange	AGGTACTGGTCCCTTCCTTT
Forward primer-red	GTGCAGTCTAGACAGCAGTCAGGGGTCAGGTG
Reverse-proximal	ATCTGCTCTAGATTCTAATGTAAACACTGATTTATTTA
Reverse-distal	GGCACCTTGGAGTATTTCACAGTG

2.2.4 PCR (mutagenesis)

Mutagenesis of the predicted TTP binding site in *ABL1* 3'UTR reporters was performed using PCR Mutagenesis as per Appendix A.3, with the primers in Table 2.10. For phRL-ABL1 3'UTR ΔTTP, phRL-ABL1 3'UTR was used as the template. For phRL-ABL1 (1116-1257)ΔTTP, phRL-ABL1 (1116-1257)x3 was used as the template (see 2.2.1.6).

Table 2.10: Primers used for mutagenesis of a putative TTP binding site at the 1206th nucleotide within the *ABL1* 3'UTR.

ABL1 3'UTR reporter (phRL-)	**Sequence (5' – 3')** (Upper line: forward primer; Lower line: reverse primer)
ABL1 3'UTR ΔTTP	CTTGAACTGGGCGAATGTCTTACGCAATTACCGTGAGTGACATAGCC
ABL1 (1116-1257)ΔTTP	GGCTATGTCACTCACGGTAATTGCGTAAGACATTCGCCCAGTTCAAG
Mutated nucleotides underlined	

2.2.5 PCR (quantitative)

BCR-ABL and *GUS-B* mRNAs were quantified by TaqMan® real-time PCR (qRT-PCR). Custom qRT-PCR assays were designed for *BCR-ABL* and *GUS-B* (Table 2.11). The qRT-PCR was performed as per Appendix A.8 using random-hexamer primed cDNA (see Appendix A.7). *GUS-B* served as a housekeeping gene for quantification of *BCR-ABL*[184]. The PCR was performed using the 7900HT Real-Time PCR machine using the standard curve method.

Table 2.11: Primer and probe sequences for quantifying *BCR-ABL* and *GUS-B* RNA

	Sequence (5' – 3')
*BCR-ABL**	
Forward primer	TCCGCTGACCATCAATAAGGA
Reverse primer	CACTCAGACCCTGAGGCTCAA
Probe	*FAM*–CCCTTCAGCGGCCAGTAGCATCTGATA–*TAMRA*
GUS-B	
Forward primer	GAAAATATGTGGTTGGAGAGCT
Reverse primer	CCGAGTGAAGATCCCCTTTTTA
Probe	*FAM*–TGAACAGTCACCGACGAGAGTGCTGGT–*TAMRA*
* Forward primer complementary to exon 13 of *BCR*, and reverse primer exon 2 of *ABL1*. Therefore this assay can be used to detect the majority of *BCR-ABL* variants. FAM: 5' fluorophore; TAMRA: 3' quencher	

2.2.6 Protein expression analysis

BCR-ABL and actin expression was quantified by Western blotting.

2.2.6.1 Protein lysates

From the 2 mL of cells harvested, 1 mL was collected for protein extraction (the other 1 mL was used for RNA isolation). Cells were washed twice with Phosphate-Buffered Saline (PBS) (Invitrogen, Mulgrave, Australia) then resuspended in 50 µL NP40 lysis buffer (Invitrogen) supplemented with 1 x protease inhibitor cocktail (Roche; Penzberg, Germany) and phenylmethylsulfonyl fluoride (PMSF) (Sigma; Sydney, Australia). Lysates were kept on ice and vortex-mixed every 10 min for 30 min. Then the lysates were centrifuged (15700g, 10 min, 4^{o}C), and the supernatant collected in a fresh tube. Protein amount was determined using the Bradford assay (BIO-RAD; Gladesville, Australia) according to the manufacturer's instructions.

2.2.6.2 SDS PAGE and Western transfer

Prior to electrophoresis, 10 µL protein sample buffer (2x) (Appendix B) was added to each sample (20 µg), and made up to 20 µL with water. Then the sample was boiled for 5 min at 95^{o}C, and loaded on an 8 x 5 cm, 7.5% SDS polyacrylamide gel. The Full-Range Rainbow™ molecular weight marker (GE Healthcare; Rydalmere, Australia) (10 µL) was also loaded to estimate protein size. Samples were electrophoresed for 65 min at 150 V using the Mini-PROTEAN® Tetra Cell apparatus (BIO-RAD) in tris-glycine running buffer (Appendix B). Proteins were then transferred to a PDVF membrane (GE Healthcare) using the Trans-Blot® SD Semi-Dry Electrophoretic Transfer Cell apparatus (BIO-RAD) at 15 V for 30 min. The PDVF membrane was prepared by placing in methanol (Merck; Kilsyth, Australia) for 2 min, water for 5 min, then soaked in western transfer buffer (Appendix B) until the transfer. Following the transfer, the membrane was blocked in 5% skim milk in TBS-T (Appendix B).

2.2.6.3 Western blotting

Because the antibody raised against c-ABL interferes with visualising β-Actin, the membrane was cut in half prior to staining with the primary antibody. The antibodies used and incubation conditions are outlined in Table 2.12. Following each antibody incubation, the membrane was washed thrice with TBS-T for 5 min.

The Typhoon™ 9400 scanner (GE healthcare) was used for band detection using the ECF substrate (GE healthcare). Band intensity was quantified using ImageQuant™ TL software (GE healthcare).

Table 2.12: Antibodies and conditions used to quantify BCR-ABL and actin expression

Primary Antibodies		Incubation	Dilution
High molecular weight half	mouse anti-c-ABL (Calbiochem^)	4°C, overnight	1/2500
Low molecular weight half	rabbit anti-Actin (Sigma)	4°C, overnight	1/5000
Secondary antibodies			
High molecular weight half	Goat, anti-mouse IgG-AP (Santa-Cruz*)	RT, 1.5 h	1/5000
Low molecular weight half	Goat, anti-rabbit IgG-AP (Invitrogen)	RT, 1.5 h	1/7500
Incubations carried out in TBS-T/5% skim milk. *Santa Cruz Biotechnology (Santa Cruz, CA, USA) ^Calbiochem (EMD Millipore, Billerica, MA, USA) AP, alkaline phosphatase			

2.2.7 Cell culture

BV-173, HEL, HeLa, HL-60, Jurkat-LT, K-562, KCL-22, KYO-1, LAMA-84, THP-1, and U-937 cells were cultured as per Appendix A.14.

2.2.7.1 Imatinib treatment

To monitor BCR-ABL expression upon imatinib exposure, $4x10^5$ cells were plated in three wells of a 24-well plate in 2 mL of fresh media. These cells were then exposed to 1 µM imatinib (Novartis; Basel, Switzerland). Every 24 h, one well was harvested for RNA (see 2.2.5.1) and protein isolation. For a baseline measurement of BCR-ABL expression, $4x10^5$ cells which were not exposed to imatinib, were collected for RNA and protein isolation.

2.2.8 Transient transfection

Cell lines were transfected with either FuGene® 6 (Roche), X-tremeGENE™ (-HP) (Roche), or Lipofectamine™ (Invitrogen). The specific reagent used is detailed in the figure legends in the results section. For experiments involving imatinib: 24 h post-transfection, Imatinib (1 µM) was added to the respective wells. Statistical analysis was carried out using the one-tailed t-test using GraphPad® Prism software, version 5 (GraphPad Software Inc; La Jolla, CA, USA).

2.2.8.1 FuGene 6

Cells were plated in 6 or 24-well plates at a final confluence of 50% just prior to transfection. The cells were then transfected as per Table 2.13 using FuGene® 6 transfection reagent according to the manufacturer's instructions. Cells were harvested 48 h post-transfection and luciferase readings obtained as per Appendix A.15.

Table 2.13: FuGene 6 transfection conditions (per well)

Renilla-based		**Firefly-based**	
Renilla construct	3.2 fmol	Firefly construct	200 fmol
pGL3-control*	500 ng	pCMV-RL*	20 ng
pUC19+	up to 1 µg DNA	pUC19+	up to 1 µg DNA
FuGene® 6	6 µL	FuGene® 6	6 µL
Volume	2 mL	Volume	2 mL
n^	quadruplicate	n^	at least 3
*Firefly transfection control (Promega) +DNA filler ^A master mix of (x)n + 0.5 was made for each transfection, where x is the number of cell lines transfected.		*Renilla transfection control +DNA filler ^A master mix of (x)n + 0.5 was made for each transfection, where x is the number of cell lines transfected.	

2.2.8.2 X-tremeGENE and X-tremeGENE HP

Cells were plated in 6 or 24-well plates at a final confluence of 50% just prior to transfection. The next day, cells were transfected as per Table 2.14 using X-tremeGENE™ or X-tremeGENE™-HP transfection reagent according to the manufacturer's instructions. Cells were harvested 48 h post-transfection and luciferase readings obtained as per Appendix A.15.

Table 2.14: X-tremeGENE™ (HP) transfection conditions (per well)

Renilla construct	0.8 fmol
pGL3-control*	240 ng
X-tremeGENE™ (HP)	0.75 µL (3:1 ratio)
Volume	0.5 mL
n^	quadruplicate
*Firefly transfection control, made up to the 3:1 ratio, i.e. eliminating the need for filler DNA. ^A master mix of (x)n + 0.5 was made for each transfection, where x is the number of cell lines transfected.	

2.2.8.3 Lipofectamine

Lipofectamine™ is recommended for transfection of the adherent HeLa cell line. HeLa cells were seeded in 24 well plates 18 hours pre-transfection (10^5 cells per well in 1 mL). The following day, cells were transfected as per Table 2.15 using the Lipofectamine™ transfection reagent according to the manufacturer's instructions. Cells were harvested 48 h post-transfection and luciferase readings obtained as per Appendix A.15.

Table 2.15: Lipofectamine transfection conditions (per well)

Renilla construct	3.2 fmol
pGL3-control*	500 ng
pUC19+	Up to 1 µg DNA
Lipofectamine™	3 µL
n^	quadruplicate
*Firefly transfection control +DNA filler ^A master mix of n + 0.5 was made for each transfection.	

2.2.8.4 MicroRNA induction

Pre-miR™, or microRNA mimics (Applied Biosystems), were used to induce microRNA levels during transient transfections. The Pre-miR™ (30 or 100 nM) was included along with the DNA during the transfection setup procedure. See 3.2.3.3, pg 103, for further details.

2.2.9 Bioinformatics

MicroRNA binding sites within the *ABL1* 3'UTR were predicted using TargetScan software (www.targetscan.org). RNA-binding protein consensus sites in the *ABL1* 3'UTR were annotated by RBPDB v1.2.1 (http://rbpdb.ccbr.utoronto.ca/). Experimental evidence for RNA-binding protein interactions was shown in the doRiNA database (http://dorina.mdc-berlin.de/rbp_browser/dorina.html).

2.3 Results

2.3.1 *BCR-ABL* and *ABL1* have similar and shorter half-lives than *BCR*

The half-lives of *BCR-ABL*, *ABL1* and *BCR* were determined to investigate the relative stabilities for each transcript. These experiments were performed by Dr Duncan Hewett (Centre for Cancer Biology, Adelaide). K-562 cells were treated for 8 h with actinomycin D (which inhibits transcription) and collected (for RNA isolation). *BCR-ABL*, *ABL1*, and *BCR* mRNA levels were quantified by qRT-PCR and normalised against 18s RNA (which has a half life of 65 h, thus remaining relatively stable over 8 h[185]). The equation in Fig 2.8, A was used to calculate the half-lives of the three mRNAs. Prism software was used to find *a* (y-axis intercept) and *b* (rate of decay) from the exponential growth function. These values are displayed below the equation in Fig 2.8, A. *ABL* and *BCR-ABL* had similar half-lives, 2.08 and 2.29 h respectively, which were shorter than that of *BCR* (8.44 h) (Fig 2.8, B). From these data we speculate that the stability of the *BCR-ABL* transcript is influenced by the *ABL1* moiety because of their similar decay trends. However, we are also mindful that these results do not exclude the possibility of a stabilising element within the 3' moiety of *BCR* that is not present in *BCR-ABL*.

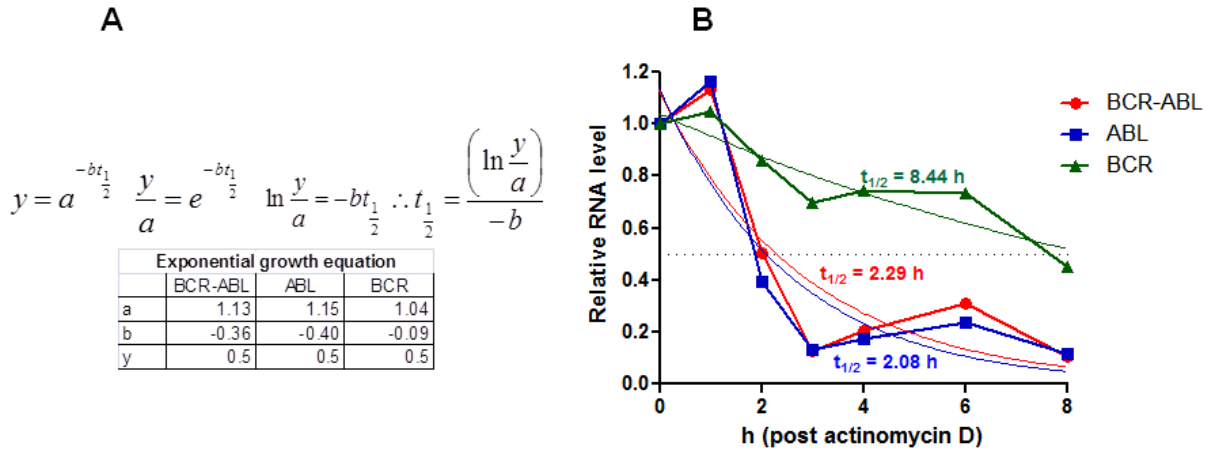

Fig 2.8: *BCR-ABL* and *ABL1* have similar, but shorter half-lives than *BCR*. (**A**) The equation used to calculate the half lives of each transcript where *a* is the y-axis intercept, b is the rate constant, and y is 0.5 or 50% RNA remaining. The table below shows the values for each of the factors in the equation. These values were calculated from the graph in **B**, using the exponential growth equation using Prism 5 software. (**B**) K-562 cells were treated with actinomycin D, and then an RNA sample was collected over 8 h. The relative levels of the three genes and 18s were determined by TaqMan quantitative PCR. The graph shows the mean 'relative RNA amount' for *BCR-ABL*, *ABL* and *BCR* normalised to 1 against 18s RNA. The half-life values shown ($t_{1/2}$) correspond by colour to the appropriate gene. The results are from a single experiment, with the qRT-PCR performed in triplicate.

2.3.2 Defining the *ABL1* 3'UTR

The previous half-life experiments provided the rationale to investigate the *ABL1* 3'UTR. One of our aims was to define the 3'UTR and look for 3'UTR-variants or decoys known to play an important role during gene expression (2.1.1.5). We specifically looked for alternate *ABL1* 3'UTR species using 3'RACE (3' rapid-amplification of cDNA ends).

2.3.2.1 3' RACE identifies a number of putative *ABL1* 3'UTR products

Knowing that the murine *ABL1* gene is truncated in the mouse testis resulting in the deletion of a portion of the 3'UTR[179], we investigated the possibility that the *ABL1*/*BCR-ABL* 3'UTR is truncated in humans using 3'RACE. *ABL1*/*BCR-ABL* 3'RACE was performed by Duncan Hewett, following a recently described protocol (Fig 2.9, A;[186]). This method used an *ABL1* specific primer (binding just upstream of the *ABL1* stop-codon) and an oligo-dT primer (binding to the poly-A tail) in order to amplify the 3'-end of *ABL1* containing transcripts. 3'RACE was performed on RNA obtained from peripheral blood mononuclear cells (PBMNCs) from ten CP-CML and eight healthy control samples. The 3'RACE-amplicons

were then electrophoresed on an agarose gel with a representative experiment shown in (Fig 2.9, A). We found three 3'RACE-products that were common for most CML (and healthy control) samples: a 900 nt band, a 2 kb band and a band >2 kb.

The presence of a 900 bp product was of interest because the 780th nt of the *ABL1* 3'UTR contains a non-canonical PAS. We prioritised our efforts on investigating 3'UTR-shortening due to its importance for evading 3'UTR-mediated control (2.1.1.5), therefore the >2 kb product was not sequenced. However, we did look for evidence of larger *ABL1* 3'UTR species (2.3.2.3). We confirmed that the 2 kb band corresponded to the annotated *ABL1* 3'UTR (Fig 2.9, B), validating our 3'RACE protocol. The sequence of the ~900 bp band was identical in each sample, and corresponded to a shortened *ABL1* 3'UTR. However, instead of alternate PAS-usage, an intra-3'UTR splicing event removed 328-1571 nt of the *ABL1* 3'UTR (forming a 748 nt 3'UTR species, historically referred to here as "900") (Fig 2.9, C). The sequence results also showed that the splice junction contained canonical splice donor and acceptor sites (Fig 2.9, C). This was of interest, because the experiment performed by Andrews, *et al.* – to rule out *ABL1* 3' shortening in humans, used radiolabelled probes binding to the start and end of the 3'UTR[171]. Therefore, their experiments may not detect intra-3'UTR splicing of *ABL1*.

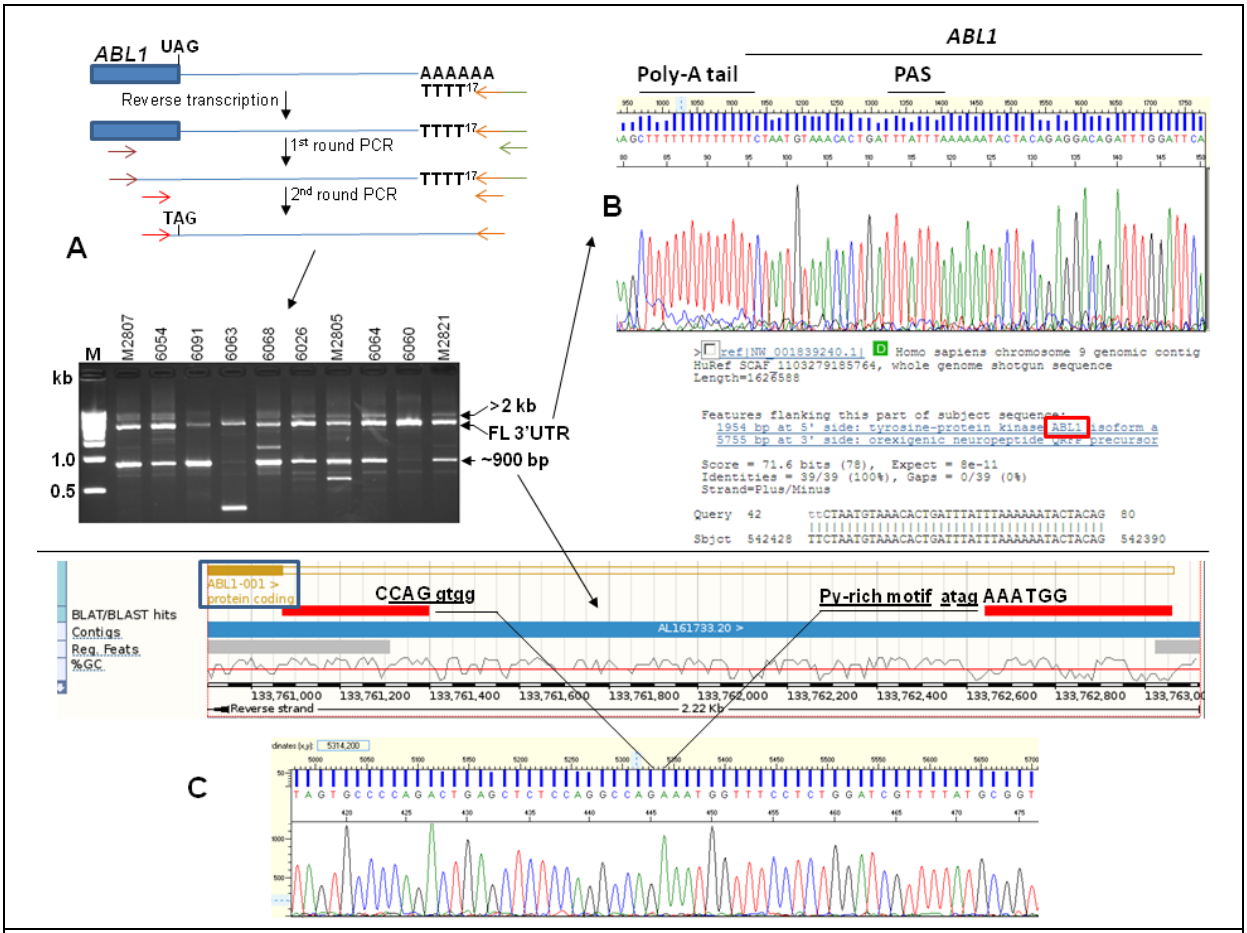

Fig 2.9: 3'RACE identifies a putative splice event in the *ABL1* 3'UTR. (**A**) The 3'RACE experiment. (top) Cartoon of the 3'RACE protocol based from[186]. First, RNA was reverse transcribed using an oligo-dT primer (orange-green) containing 17 thymidines at the 3' end and two primer binding sites for downstream PCRs (orange and green). Next, 1st round PCR was performed on the reverse transcribed RNA using a forward primer specific for *ABL1* (purple, just upstream of the stop codon), and a reverse primer (green) which is complementary to the green region of the reverse transcribed RNA. A 2nd round of PCR was performed to ensure specificity to the *ABL1* 3' end. This used a primer set (red and orange) which bound just inside the primers used in the 1st round PCR. This 3'RACE product was then electrophoresed on a 1% agarose gel (bottom). Marker bands were annotated on the left hand side (in kb). The three dominant 3'RACE sizes were annotated on the right hand side. (**B**) Sequencing of the 2 kb 3'RACE product corresponded to the annotated 1992 nt *ABL1* 3'UTR. Note this was sequenced using a reverse primer, hence the poly-A tail are indicated by thymidines, and the PAS is in the reverse orientation. A blast search (NCBI-BLAST) of the sequencing trace confirmed the product was *ABL1*, and corresponded to the 1992 nt 3'UTR. (**C**) Blast analysis (Ensembl; top) showed that the ~900 nt 3'RACE product was identical for each sample, and corresponded to an intra-3'UTR (329-1570) deletion. The blast-sequence is shown in red, and aligned to the *ABL1* gene (brown). The hollow section of the *ABL1* gene is the 1992 nt 3' UTR. A representative sequence trace is shown below, with the boundary of the deletion shown on the blast output above. The capital letters highlight the splice boundary. Lowercase letters highlight genomic sequence adjacent to the deletion. The underlined sequences denote the sequences which match consensus donor and acceptor splice sites.

2.3.2.2 The shortened 3'UTR is found in less than 2% of all *ABL1* 3'UTR containing transcripts

Both the levels of short and full-length *ABL1* 3'UTR species were quantified in order to calculate the frequency of the splice event. The qRT-PCR assay outlined in Fig 2.10 was performed by Dr Duncan Hewett using PBMNCs from CP-CML patients. The ratio of ABL900/ABL3'UTR showed that the shortened *ABL1* 3'UTR was rare, accounting for less than 2% of all *ABL1* 3'UTR containing transcripts (Fig 2.10) (that is, both *ABL1* and *BCR-ABL*; this method could not distinguish between the two transcripts). The shortened 3'UTR was also quantified in seven BC-CML PBMNC samples. A similar frequency of the shortened 3'UTR (2%) was observed (data not shown).

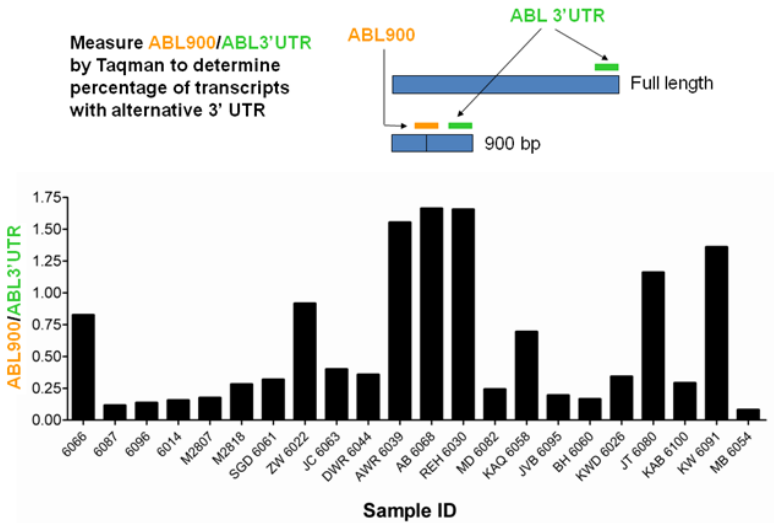

Fig 2.10: The shortened *ABL1* 3'UTR is present in less than 2% of *ABL1*-containing transcripts. (top) Diagram of the qRT-PCR assays used to quantify the shortened 3'UTR species. A short 3'UTR-specific qRT-PCR assay was designed across the splice junction (orange), in addition to an assay designed at the end of the 3'UTR (common to the full length and shortened 3'UTR species) (green). These assays allow for calculating the ratio of short *vs.* total *ABL1* 3'UTR species, in order to determine the abundance of the short 3'UTR. (bottom) Ratio of short vs total *ABL1* 3'UTR species for twenty-two CP-CML samples. Both ABL900 (orange) and ABL3'UTR (green) assays were quantified using the standard curve method, with the graph showing the mean of triplicate PCRs.

2.3.2.3 No evidence of a distal poly-adenylation site for *ABL1*

Some of the 3'RACE products were larger than 2 kb. These products were not sequenced because our focus was on shortened 3'UTR species. Interestingly, however, we noted a

canonical PAS downstream of the annotated *ABL1* transcript and within a region that was highly conserved across species. A number of ESTs (expressed sequence tags) were also mapped to this region (Fig 2.11, A). These observations were similar to a recent study that found a distal PAS for the *HNF4α* gene (Fig 2.11, B;[187]). Therefore we looked for evidence that this distal PAS was used by *ABL1*.

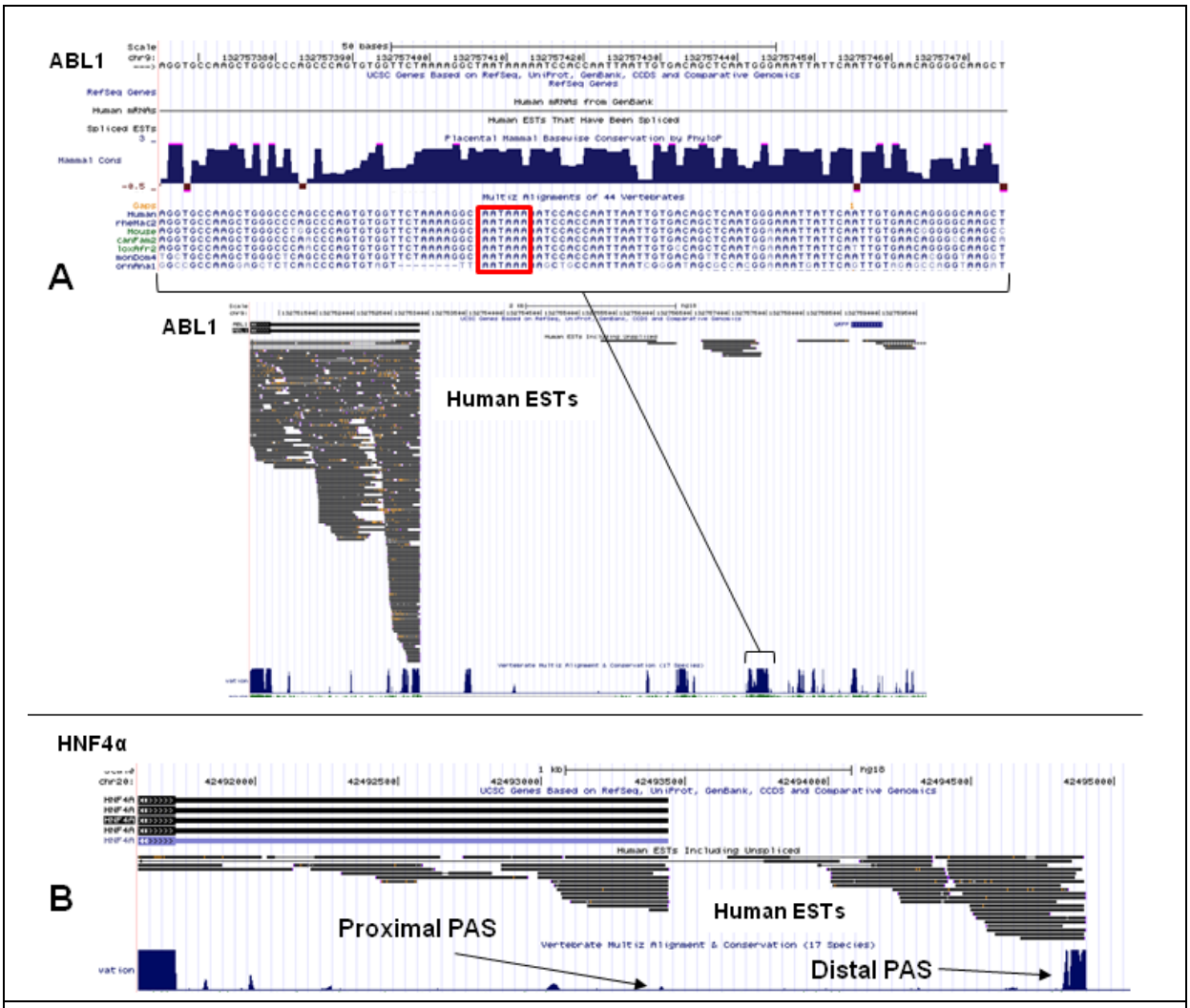

Fig 2.11: A species-conserved region located 6 kb downstream of the *ABL1* stop-codon contains a putative *ABL1* PAS. (**A**) A number of regions downstream of the ABL1 gene exhibit cross-species conservation. Within one of these regions is the canonical PAS sequence AATAAA (red box). Furthermore, there are a number of ESTs which map to the PAS. (**B**) Recently, a distal PAS was found for the *HNF4α* gene[187]. The UCSC genome browser shows a trend for *HNF4α* similar to that for *ABL1*. That is, there is a species conserved region located downstream of *HNF4α*'s annotated PAS, and this region contains a canonical PAS sequence. Furthermore, EST hits are found to extend past the proximal PAS to this putative distal PAS.

Our strategy to show that the distal PAS was used by *ABL1* involved amplification of cDNA using a primer inside the *ABL1* 3'UTR and one just upstream of the distal PAS (Fig 2.12, A). We also included a reverse primer just 5' of the annotated ('proximal') *ABL1* PAS as a control for the PCR. These primer sets were used to amplify cDNA from K-562 and KYO-1 (CML cell lines). In this experiment, the distal PAS primer set failed to amplify the cDNA template (Fig 2.12, A). On the other hand, a 400 bp PCR product was observed in the PCR using the proximal PAS primer set. These results were indicative that the distal PAS was not used by *ABL1*.

However, it was also possible that the polymerase could not amplify 5 kb fragments. To show that the polymerase can amplify large PCR products, a similar PCR was performed using a K-562 genomic DNA template control. In this PCR the forward primer was shifted back to the start of the 3'UTR to show (in the proximal PAS PCR) that larger cDNA species were produced (Fig 2.12, B). For the distal PAS primer set, an amplicon of approximately 6 kb was only observed in the PCR containing genomic DNA template. Whereas, a ~2 kb amplicon was observed in the genomic DNA and cDNA PCRs using the proximal primer set. Interestingly there was a ~900 bp product for these samples which may correspond to the spliced 3'UTR variant. These data show that the polymerase can amplify large PCR products. However we did not find evidence supporting the usage of the distal PAS by *ABL1*.

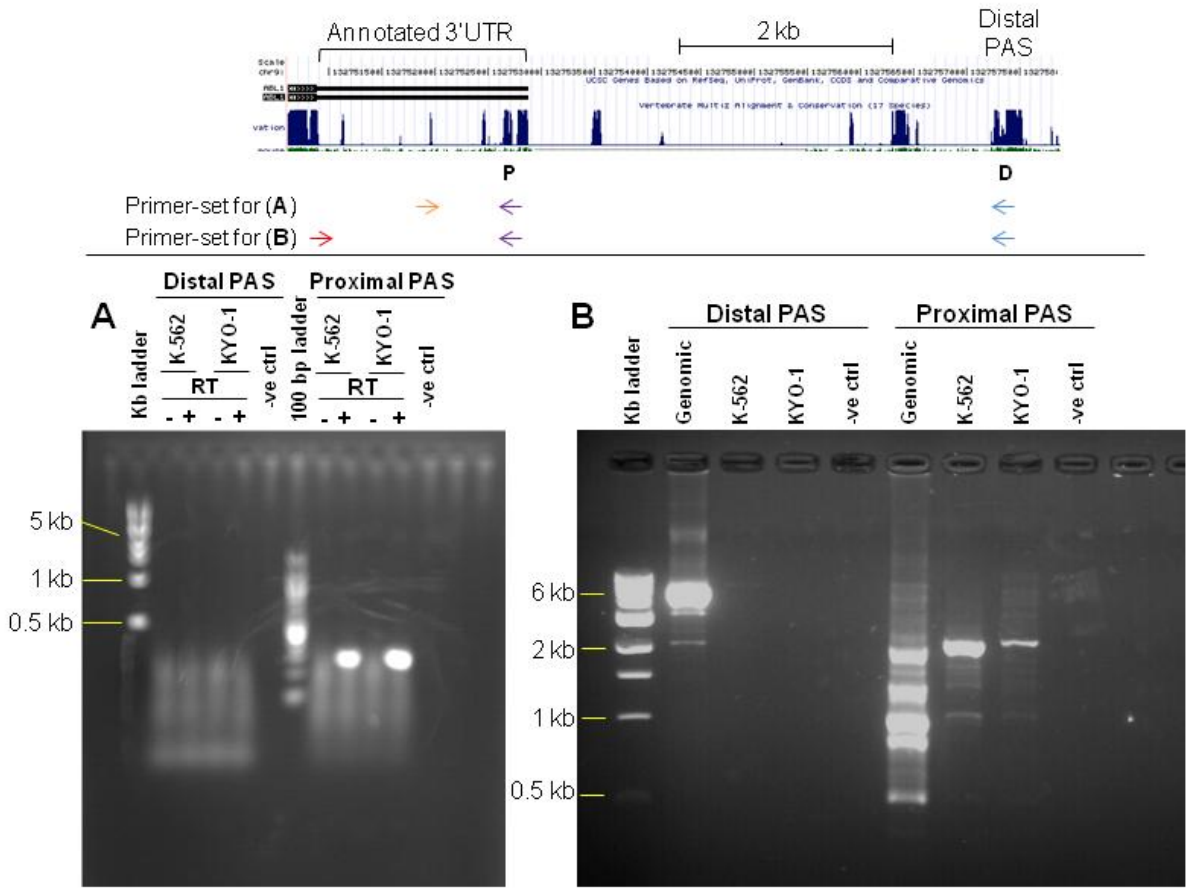

Fig 2.12: The *ABL1* gene does not use a distal PAS 6 kb from the *ABL1* stop-codon. (top) Primer design for the PCRs performed in **A** and **B**, shown against a representation of the *ABL1* gene from the UCSC browser. (**A**) A qualitative PCR was performed on cDNA from K-562 or KYO-1 cells using a primer set specific to the distal PAS (orange and blue) or the proximal (annotated) PAS (orange and purple). A reverse-transcriptase minus control was included to show that any bands observed were due to cDNA and not genomic DNA amplification. (**B**) The same RT+ cDNAs in **A** (free of genomic contamination) were amplified as previously, except that the forward primer (red) was moved to the start of the *ABL1* 3'UTR, and a K-562 genomic DNA sample was included as a control for the PCR reaction.

2.3.3 Optimising transient transfections in haemopoietic cell lines

A dual-luciferase-based system was used to examine *ABL1* 3'UTR's effect on gene expression. The majority of the luciferase work involves a *Renilla* reporter for the *ABL1* 3'UTR, and a *Firefly* luciferase transfection control. Our experiments involved transiently transfecting these plasmids into haemopoietic cells. It is known that these cell types have poor transfection rates[188]. Therefore, we determined which cell lines were suitable for transient transfection of plasmid DNA.

A cell line's transfection status was based either on raw luciferase readings and reproducibility of the relative luciferase activity or GFP-based transfection efficiency. A Renilla luciferase signal reading of >100 was 'satisfactory', and >1000 'good' (based on background readings of <10). Firefly readings (except in U-937 cells, data not shown) were always much lower than Renilla (Fig 2.13, A). So for Firefly, >40 was 'satisfactory' and >100 was 'good' (based on background readings of <2). In order to observe small changes in relative Renilla activity, a standard deviation of <10% was considered optimal, and 10-15% 'satisfactory'.

During this study the supplier ceased production of FuGene 6, so we switched to the X-tremeGENE-HP transfection reagent.

2.3.3.1 FuGene 6

FuGene 6 was used routinely to transfect suspension cell lines in our laboratory. The standard conditions were: FuGene:DNA (6 µL : 1 µg), which was the maximum amount of FuGene 6 recommended by the manufacturer. The KYO-1, K-562, KCL-22, U-937 cell lines were successfully transfected with luciferase reporters using (unless stated) the standard conditions (Table 2.13).

In the HEL cell line, the raw luciferase readings were satisfactory (Renilla >100 and Firefly ~100) (Fig 2.13, A), but the reproducibility of inter-experiment triplicates was poor (>20% SD) (Fig 2.13, B). Renilla readings in LAMA-84 cells were good, however some of the Firefly readings were poor (Fig 2.13, A). In the THP-1, HL-60 and Jurkat-LT cell lines, the Firefly readings were poor at the maximum sensitivity (Fig 2.13, A). Transfection of the HL-60 cell line with either twice the amount of DNA or twice the amount of total DNA:lipid complex failed to improve luciferase signal (data not shown). A GFP reporter was transfected into BV-173 and HL-60 cells, however FACS analysis of these cells 48 h post-transfection showed 0% GFP positivity (data not shown). These findings are summarised in Table 2.16.

Table 2.16: Summary of FuGene 6 transient transfections in haemopoietic cell lines

Cell line	Ph	Transfectable	Signal*	Reproducible^
KYO-1	+	Yes	Good	Good
K-562	+	satisfactory	Good	satisfactory
KCL-22	+	satisfactory	Good	satisfactory
LAMA-84	+	No	Poor^{F}	n/a
U-937	-	Yes	Good	Good
HEL	-	Not ideal	Satisfactory^{F}	Not ideal
Jurkat-LT	-	No	Poor^{F}	n/t
BV-173	-	No	Very poor^{G}	n/t
HL-60	-	No	Very poor^{GFR}	n/t
THP-1	-	No	Very poor^{FR}	n/t
*superscript denotes which reporter reading resulted in a sub-optimal signal. ^for relative Renilla luciferase activity ^{G}, GFP. ^{F}, Firefly. ^{R}, Renilla. n/t, not tested				

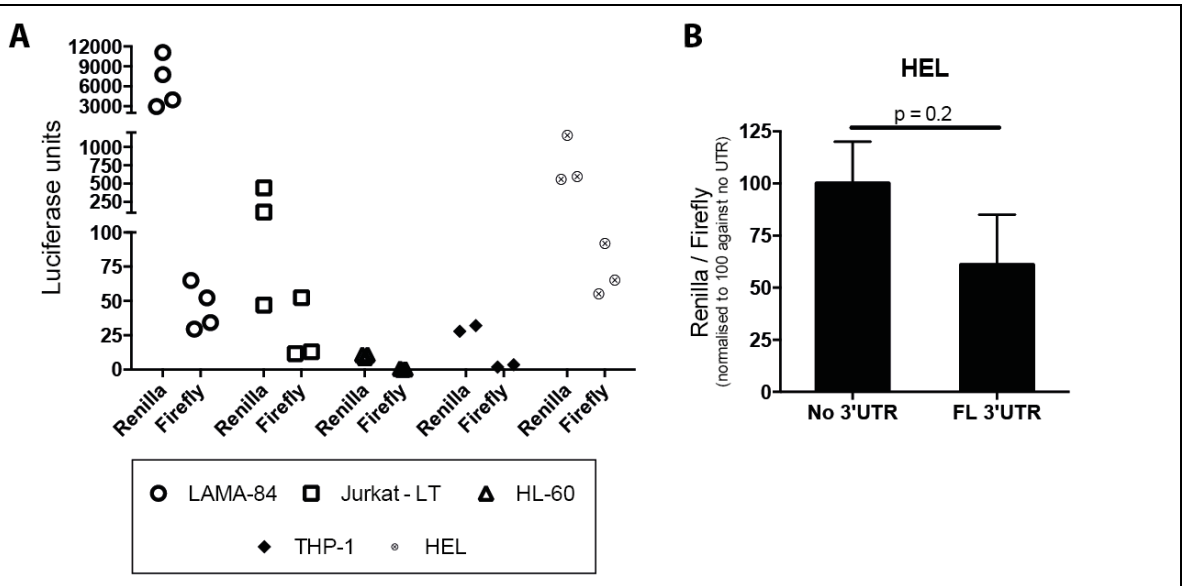

Fig 2.13: LAMA-84, Jurkat-LT, HL-60, THP-1, and HEL cell lines do not transfect well using FuGene 6 at a ratio of 6:1. (**A**) Graph represents raw luciferase values for a dual-luciferase assay in five cell lines from a single experiment performed in quadruplicate (LAMA-84), triplicate (Jurkat-LT, HEL and HL-60) or duplicate (THP-1). Data were obtained using 100% sensitivity on the TL-20/20 luminometer 48 h post-transfection. (**B**) Graph shows the Renilla luciferase activity for pCIneo-hRL (No 3'UTR) and phRL-ABL1 3'UTR (FL 3'UTR) relative to Firefly luciferase activity and normalised to 100 against No 3'UTR. Data are from a single triplicate transfection performed in the HEL cell line. p-value calculated using Prism software. Error bars represent mean ± SD

2.3.3.2 X-tremeGENE-HP

The X-tremeGENE-HP transfection reagent improved both signal and reproducibility in the LAMA-84, KYO-1, K-562, and HEL cell lines compared to FuGene 6 (Fig 2.14, A-B; Table 2.17). Furthermore, transfections performed in the HeLa cell line achieved high luciferase signals (data not shown). Therefore the transfection procedure was streamlined to one product. Unfortunately X-tremeGENE-HP did not improve the transfection efficiency for the HL-60 or BV-173 cell lines (data not shown). KT-1 cells were used following cessation of FuGene 6, therefore there are no data for that reagent. This cell line exhibited extreme variability in transfection efficiency using the X-tremeGENE-HP reagent. Within a quadruplicate transfection, a portion of the replicates would have no luciferase reading, while the remainder had 'satisfactory' or 'good' luciferase signal (data not shown). Therefore this cell line is not appropriate for luciferase experiments.

Our results suggest that X-tremeGENE-HP can boost the transfection efficiency of cells which exhibited some degree of transfection with FuGene 6. For example, in LAMA-84 cells X-tremeGENE-HP enhanced the luciferase signal so that readings could be obtained at 75% sensitivity rather than 100%. Firefly luciferase signal was also boosted above 150, a "good" signal (Fig 2.14, A).

Interestingly, a DNA:reagent ratio 3:1 out performed 6:1 for both transfection reagents (This was only examined after changing to X-tremeGENE-HP) (Fig 2.14, B). Therefore the 3:1 ratio was used for subsequent experiments.

Table 2.17: Summary of X-tremeGENE-HP transient transfections in haemopoietic cell lines

Cell line	Ph	Transfectable	Signal*	Reproducible^
KYO-1	+	Yes	Good	Good
KCL-22	+	Yes	Good	Good
K-562	+	Yes	Good	Good
LAMA-84	+	Yes	Good	Good
KT-1	+	No	Poor-Good^{FR}	Very Poor
U-937	-	Yes	Good	Good
HEL	-	Yes	Good	Good
BV-173	-	No	Very poor^{G}	n/t
HL-60	-	No	Very poor^{GFR}	n/t

*superscript denotes which reporter reading resulted in a sub-optimal signal.
^Intra-experimental reproducibility considered.
^{G}, GFP. ^{F}, Firefly. ^{R}, Renilla. n/t, not tested.

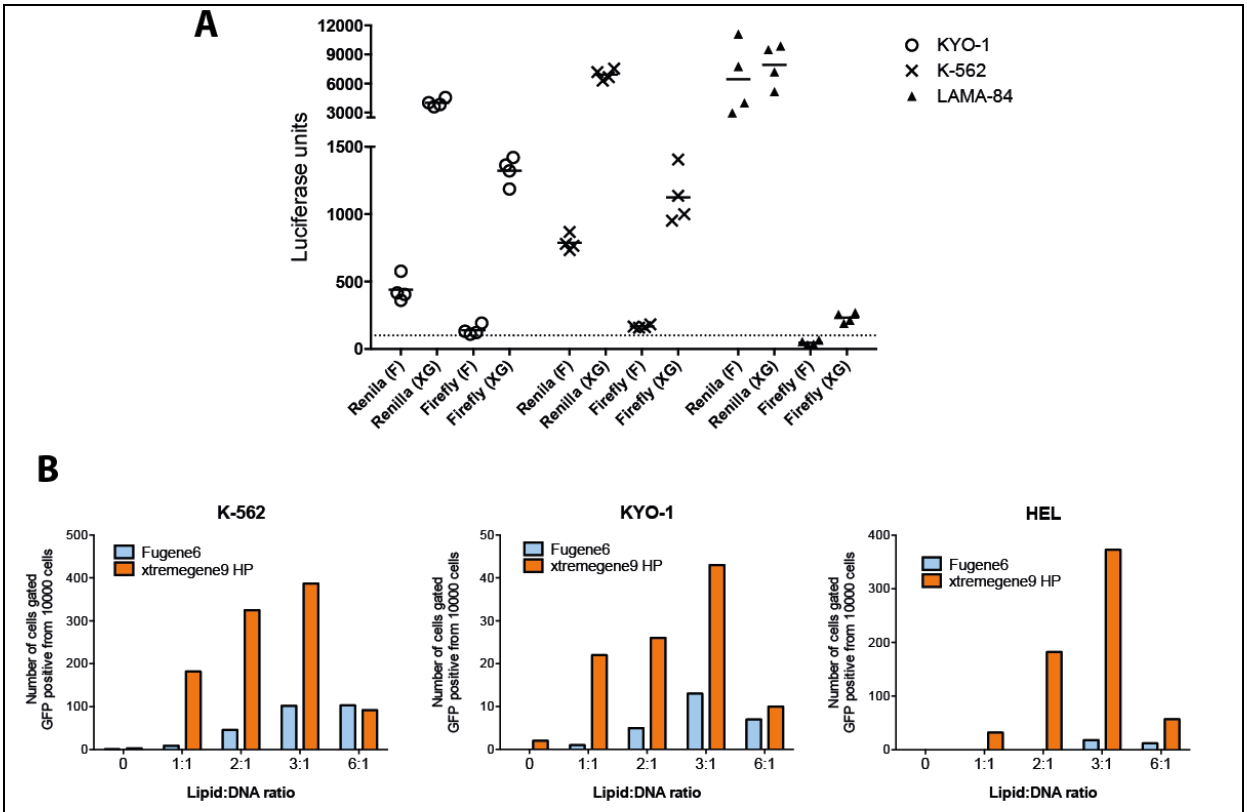

Fig 2.14: X-tremeGENE-HP improves luciferase signal and a ratio of 3:1 is more effective than 6:1. (**A**) Graph shows raw luciferase readings obtained for a dual-luciferase assay performed in quadruplicate; in KYO-1, K-562 and LAMA-84 cells using FuGene 6 (F) or X-tremeGENE-HP (XG) at a 3:1 ratio. Luciferase activity was then obtained 48 h post-transfection. Dotted line denotes 100 luciferase units (a poor signal for Firefly) (**B**) One microgram of pMSCV-puro-GFP was transfected into K-562, KYO-1 and HEL cells using FuGene 6 (blue) or X-tremeGENE-HP (orange) at the described ratios. Note: at ratio 0, the media contained 1 µg of pMSCV-puro-GFP. Cells were measured for GFP expression by FACS 48 h post-transfection; the graph shows GFP+ cells per 10000 cells counted.

2.3.4 The full-length *ABL1* 3'UTR is repressive

To examine the effect of the *ABL1* 3'UTR on gene expression, it was cloned into an expression vector downstream of the *Renilla* luciferase gene. Presence of the *ABL1* 3'UTR reduced Renilla protein expression by approximately 50% in a number of cell lines (Fig 2.15). Interestingly the *ABL1* 3'UTR did not reduce Renilla expression in the KCL-22 (imatinib resistant[73]) cell line. These results show that, in general, the *ABL1* 3'UTR has a net repressive effect on gene expression.

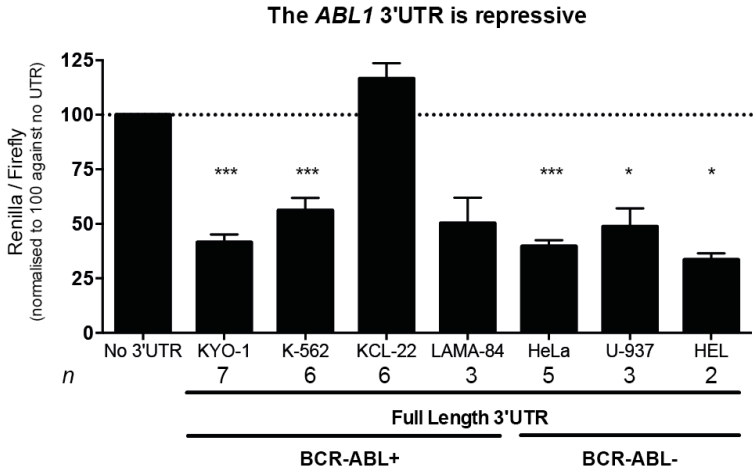

Fig 2.15: The *ABL1* 3'UTR reduces expression of the Renilla reporter gene. The cell lines above were transfected with pCIneo-hRL (No 3'UTR) or phRL-ABL1 3'UTR (Full length 3'UTR) using FuGene 6 (KYO-1, K-562), X-tremeGENE-HP (KCL-22, U-937, HEL, LAMA-84) or Lipofectamine (HeLa). Luciferase activities were obtained 48 h post-transfection. Graph shows relative Renilla luciferase activity (Renilla/Firefly) normalised to 100 against No 3'UTR. The first bar No 3'UTR is shown as a reference; the other bars show the *ABL1* 3'UTR reporter activity from seven cell lines (four BCR-ABL positive and three BCR-ABL negative). Data represent the mean ± SEM of *n* independent experiments of quadruplicates. *** $p < 0.001$, ** $p < 0.01$, * $p < 0.05$; one sample t-test (Prism software).

2.3.4.1 Imatinib-exposure alters BCR-ABL expression

Patient response to imatinib treatment is measured by qRT-PCR of BCR-ABL levels, which predicts leukaemic burden. If a patient is responsive to treatment, BCR-ABL positive cells will undergo apoptosis, which will thus result in an overall "reduction" in BCR-ABL transcripts. However, this reduction is the result of BCR-ABL cells dying. It was unknown at the time of our experiments, if imatinib exposure (at a concentration equivalent to patient trough levels, 1 µM) had a transient effect on BCR-ABL expression, i.e., did BCR-ABL signal transduction alter its own expression? To examine this possibility, four CML cell lines (K-562, KYO-1, LAMA-84, and KCL-22) were exposed to 1 µM imatinib for 72 h and BCR-ABL or ABL protein and RNA levels examined (Fig 2.16, A-B). BCR-ABL protein level decreased over the 72 h exposure in the three imatinib sensitive cell lines (K-562, KYO-1, LAMA-84) (Fig 2.16, A), whereas BCR-ABL expression increased in KCL-22 cells (Fig 2.16, A; right). This was an interesting result as KCL-22 cells are resistant to imatinib and in this cell line the 3'UTR is not repressive (Fig 2.15). The results for the imatinib sensitive lines are accurate until 48 h, after which less than 50% viability was observed (data not shown).

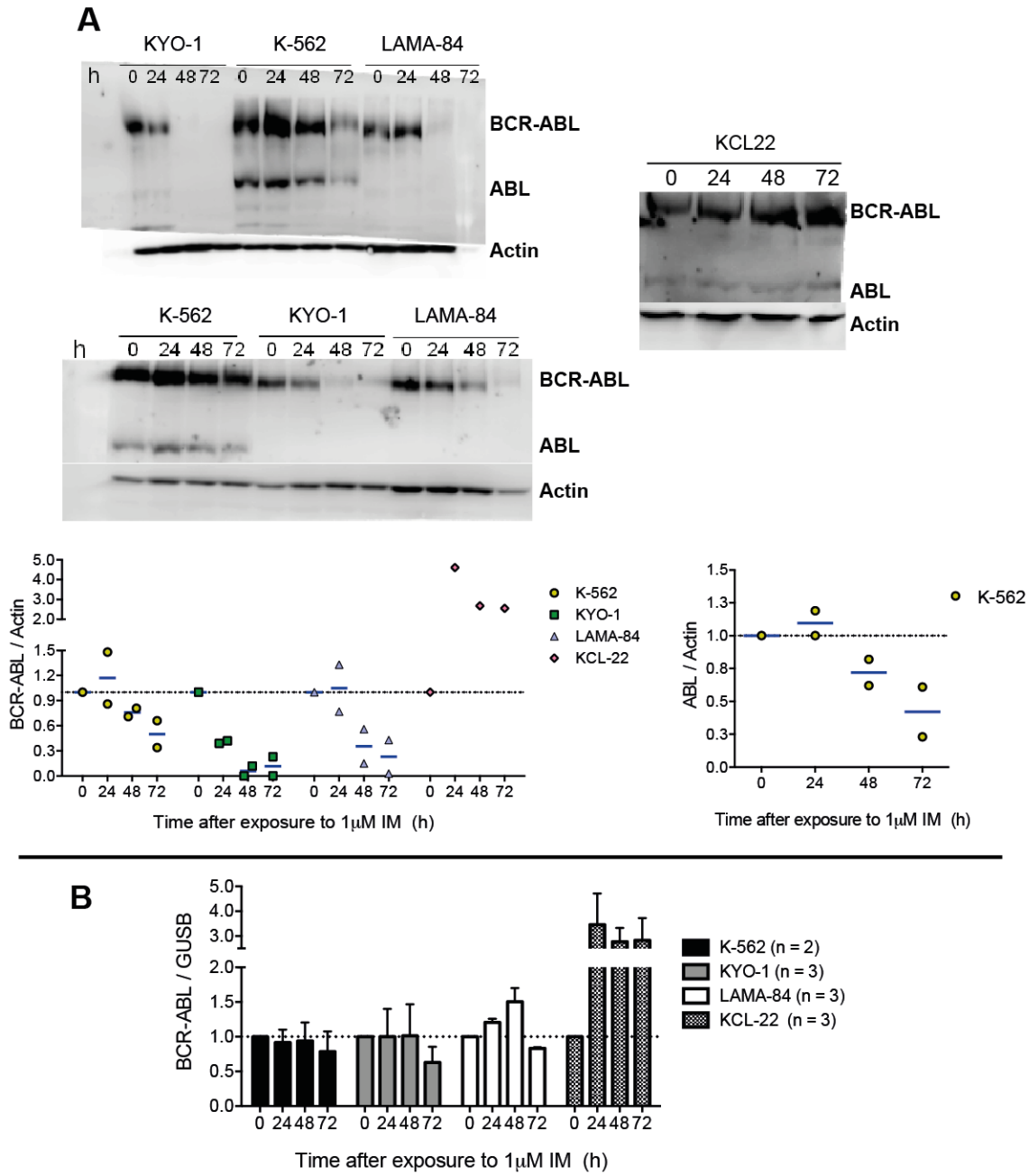

Fig 2.16: Imatinib exposure affects BCR-ABL expression. (**A**) BCR-ABL protein expression was measured in four CML cell lines following exposure to 1 μM imatinib over 72 h, with protein samples obtained every 24 h. BCR-ABL levels were then measured by western blotting, and normalised to Actin expression. Two experiments were performed for K-562, KYO-1 and LAMA-84 cells and one for KCL-22 cells. Each data point was plotted in the lower graph for normalised BCR-ABL (left) and ABL (right) expression. The blue lines indicate the mean of multiple experiments. *ABL1* is not present in KYO-1 and LAMA-84 cells at the genomic level. (**B**) *BCR-ABL* mRNA was measured from the same samples as in (**A**) (additional experiments were performed in KYO-1, LAMA-84 and KCL-22 cells). BCR-ABL expression was measured by TaqMan qRT-PCR, and normalised to *GUSB* expression. The data represent the mean ± SEM of *n* independent experiments. Each PCR was performed in triplicate.

In KCL-22 cells, an increase in *BCR-ABL* RNA was observed upon imatinib treatment, which corresponded to protein expression data (Fig 2.16, B). In contrast, imatinib exposure had little effect on *BCR-ABL* RNA levels in the K-562 and KYO-1 cell lines, despite a reduction in protein expression (Fig 2.16, B). Also *BCR-ABL* RNA levels appeared to increase in LAMA-84 cells, which did not correlate with protein expression (Fig 2.16, B). Therefore it is possible that BCR-ABL expression may involve a feedback loop for self-regulation that may involve post-transcriptional regulation, such as via the 3'UTR.

To explore the possibility that the *ABL1* 3'UTR was involved in BCR-ABL auto-regulation, KYO-1 cells were transfected with a Firefly luciferase gene under the control of the BCR promoter (1.5 kb upstream of the BCR transcription start site), in the presence or absence of the *ABL1* 3'UTR. These transfections were also performed in the presence or absence of 1 μM imatinib. Expression of the BCR-driven Firefly gene was reduced around 60% in the presence of imatinib (Fig 2.17, A). Interestingly, addition of the *ABL1* 3'UTR did not exacerbate the reduction of Firefly expression upon treatment of imatinib (Fig 2.17, A). Addition of the *ABL1* 3'UTR (5'BCR 3'ABL) reduced Firefly expression compared to no 3'UTR (5'BCR) (keeping in line with the observation that the 3'UTR is repressive). However these data were normalised to the 0 μM imatinib experiment, in order to specifically show the effect of the 5'UTR and 3'UTR during gene expression after BCR-ABL kinase inhibition.

The above experiment was repeated in U-937 (BCR-ABL negative) cells in order to show that the reduction of reporter expression was not due to an off-target effect of imatinib[4]. In this experiment there was no change in expression of either *Firefly* reporter upon exposure to imatinib (Fig 2.17, B).

These data suggest that BCR-ABL kinase inhibition reduces gene expression. This effect does not involve the *ABL1* 3'UTR, but may involve the 5'UTR of *BCR*. It is also possible that the *Firefly* coding region or distal elements upstream of the inserted *BCR*-promoter may be responsible for the change in Firefly expression in response to BCR-ABL kinase inhibition. However, it is reasonable to conclude that the *BCR*-5'UTR is responsive to BCR-ABL kinase inhibition with the knowledge that BCR-ABL expression changes upon imatinib treatment (Fig 2.16).

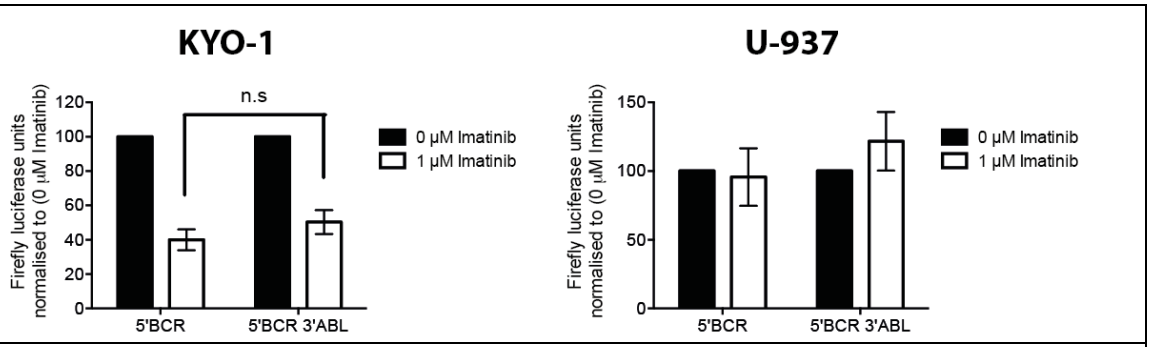

Fig 2.17: A reduction of reporter expression by BCR-ABL kinase inhibition may be dependent on *BCR*, but not the *ABL1* 3'UTR. (**A**) A *BCR*-driven Firefly reporter (5'BCR) and a *BCR*-driven Firefly reporter containing the 3'UTR of *ABL1* (5'BCR 3'ABL) were transfected into KYO-1 cells using FuGene 6. Imatinib was added 24 h post-transfection, and luciferase activity was obtained 48 h post-transfection. The graph shows raw Renilla luciferase activity, with the activity of each luciferase reporter normalised to 0 µM imatinib. Data represent the mean ± SEM of three independent triplicate experiments. Raw luciferase activity was used because imatinib exposure altered the expression of the transfection control, pCMV-RL. (**B**) Same as **A**, but the experiment carried out in U-937 cells.

2.3.5 *ABL1* 3'UTR-mediated repression occurs at the RNA level

To further understand how the *ABL1* 3'UTR represses gene expression, we examined if the reduction in Renilla expression was at the RNA or protein level. To do this, we first attempted to quantify *Renilla* RNA by qRT-PCR. However, a limitation in this approach was that there are no introns in the *Renilla* transcript. Therefore the PCR will detect both Renilla plasmid-DNA as well as *Renilla* mRNA. This also applied to the control luciferase, *Firefly* mRNA, which also has no intronic regions. To address this problem, RNA samples were treated with DNase in the step prior to cDNA synthesis to remove plasmid DNA. In addition, a separate cDNA reaction was performed without reverse-transcriptase to determine how much of the TaqMan signal was due to plasmid DNA. Despite the use of different DNAse enzymes in increasing unit concentrations, we could not detect *Renilla* RNA. Each luciferase qRT-PCR had identical signals for cDNA samples in the presence or absence of reverse transcriptase (data not shown).

To work around the difficulty of quantifying luciferase RNA, we inserted a premature polyadenylation site in the *ABL1* 3'UTR, based on two recent studies[183,187]. Insertion of a PAS at the 242nd nt of the *ABL1* 3'UTR meant that the entire 3'UTR was present in the DNA, however the *Renilla* transcript only contained the first 242 nt of the 3'UTR (Fig 2.18, A) (which does not affect reporter activity *alone* (Fig 2.20; 2.3.6.2)). To show that the insertion

did not disrupt the function of the 3'UTR, the PAS-motif was also cloned in the reverse orientation. Insertion of the premature PAS rescued luciferase activity over 1.5-fold (Fig 2.18, B) compared to wildtype 3'UTR reporter, whereas, the 3'UTR-reporter containing the reverse orientation PAS had a similar reporter activity as the wildtype 3'UTR (Fig 2.18, B). These results provide evidence that the *ABL1* 3'UTR is required in the transcript for repressive activity, and is suggestive of a post-transcriptional effect on gene expression.

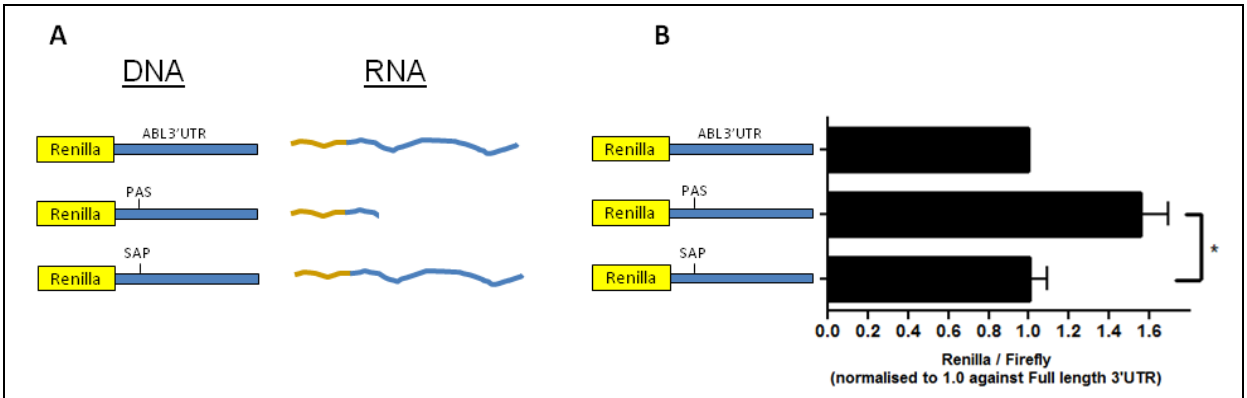

Fig 2.18: The *ABL1* 3'UTR is required in the RNA in order to repress Renilla expression. (**A**) Cartoon showing the experimental design. The wildtype *ABL1* 3'UTR and PAS insertion (3' → 5') both contain the full length 3'UTR in both the DNA and RNA. In contrast, the PAS insertion (5' → 3') reporter has the full length 3'UTR at the DNA level, but the resultant transcript only contains the first 242 nt of the 3'UTR. (**B**) The three reporter constructs above were transfected into KYO-1 cells using X-tremeGENE-HP, and luciferase activities obtained 48 h post-transfection. The graph shows relative Renilla luciferase activity (Renilla/Firefly) normalised to 1 against the wildtype 3'UTR. Data represent the mean ± SEM of three independent experiments of quadruplicates, using KYO-1 cells. * $p < 0.05$; t-test (Prism software).

2.3.6 Discrete regions of the *ABL1* 3'UTR affect reporter expression

Various portions of the *ABL1* 3'UTR were fused with the *Renilla* gene in order to map regulatory regions within the 3'UTR. Identification of regions contributing to changes in gene expression may also help identify those factors involved. These ABL1-reporters were transfected into a number of cell lines

2.3.6.1 5' truncations of the *ABL1* 3'UTR

We investigated the effect that gradual 5'deletions of the *ABL1* 3'UTR had on reporter expression. A series of 5' truncation constructs were transfected into the KYO-1, K-562,

KCL-22, and HeLa cell lines (Fig 2.19, A). In the KYO-1 cell line, deletion of the first 242 nt of the 3'UTR resulted in a loss of reporter activity, suggesting that this region can enhance expression. Further deletions up to the 1116th nt had little effect on reporter activity. Interestingly, a 142 nt truncation, deleting nt 1116-1257 resulted in a 4-fold increase of reporter expression. After deletion of the 142 nt region, further truncations had little effect on reporter activity. These observations show that in KYO-1 cells, nt 1-242 and 1116-1257 of the *ABL1* 3'UTR are responsible for most of the 3'UTR's effect on reporter expression.

In the K-562 experiments, deletion of 242-499 nt of the 3'UTR resulted in a loss of reporter activity, and so this region may enhance expression. Further deletions up to the 1116th nt had little effect on reporter activity. However, similar to KYO-1 cells, deletion of nt 1116-1257 resulted in a 4-fold rescue of reporter expression. Subsequent deletions past the 142 nt region, mapped a repressive region in the last 103 nt of the 3'UTR. This region represses reporter activity by around 50%. These observations showed that several regions in the *ABL1* 3'UTR (242-499, 1116-1257 and 1889-1992) strongly control reporter expression in K-562 cells.

The HeLa experiments showed that the first 242 nt of the 3'UTR may contain an enhancing element, also observed in the KYO-1 cell line. Further deletions up to the 1116th nt had little effect on reporter activity. Again, deletion of the 1116-1257 regions caused a rescue of reporter expression (2-fold). Subsequent deletions mapped another repressive element located between nt 1576-1889 of the 3'UTR. Close to a 2-fold rescue of reporter activity was observed upon deleting this region. These observations showed that several regions in the *ABL1* 3'UTR (1-242, 1116-1257 and 1576-1889) strongly control reporter expression in HeLa cells.

A number of interesting observations were found in the KCL-22 experiments. In KCL-22 cells, the full length 3'UTR is not repressive (Fig 2.15, 2.19, A). However, deletion of the first 499 nt restores the repressive effect of the *ABL1* 3'UTR. This suggests that a sequence within the first 499 nt is responsible for the full length 3'UTR having no net effect on reporter expression in the KCL-22 cell line. In addition, further 5' deletions show a similar luciferase profile to the KYO-1 and K-562 cell lines. In particular, deletion of 1116-1257 reveals that the 142 nt repressive region is also active in the KCL-22 cell line.

In summary, these experiments mapped a 142 nt region (1116-1257) as having a strong effect on reporter expression in all three cell lines. Also, deletion of the first 499 nt of

the 3'UTR restores the repressive function of the 3'UTR in the KCL-22 cell line. It was also shown that the 5' end (in general) promoted gene expression, and the 3'end (in general) inhibited gene expression (Fig 2.19, B).

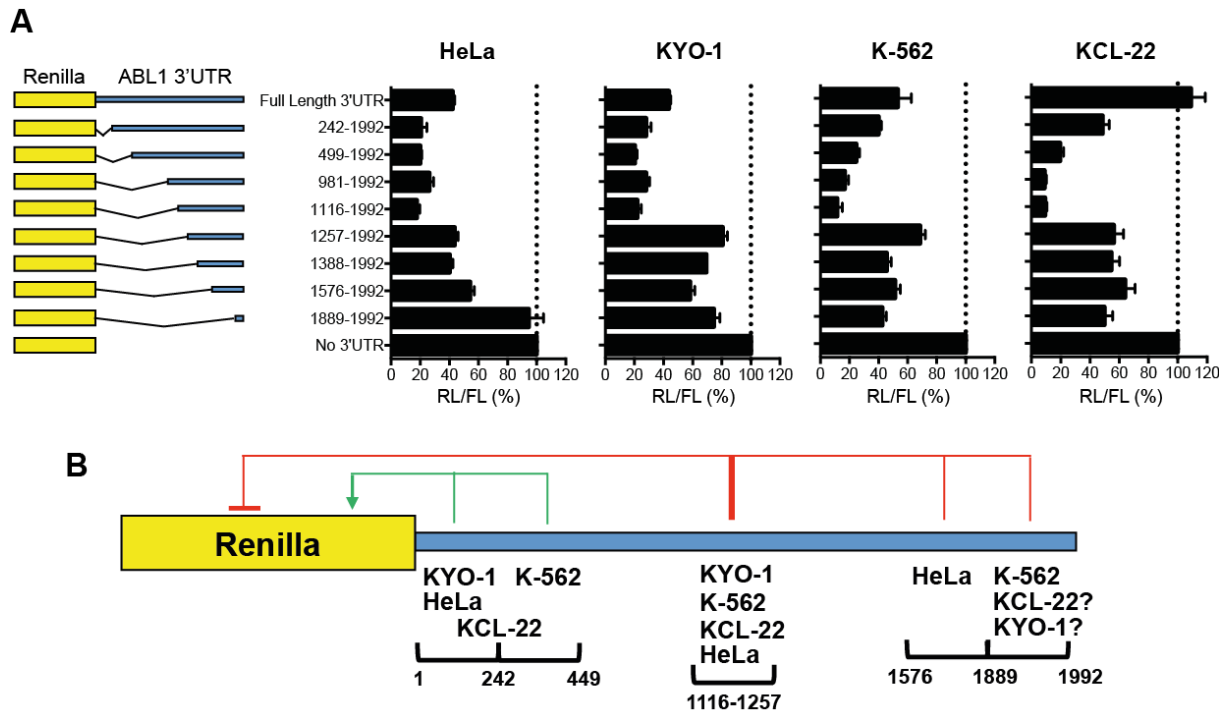

Fig 2.19: Mapping regulatory elements in the *ABL1* 3'UTR by serial deletions at the 5' end of the 3'UTR. KYO-1, K-562, KCL-22 and HeLa cell lines were transfected with a number of *ABL1* 3'UTR reporter vectors using FuGene 6 (KYO-1, K-562 and KCL-22) or Lipofectamine (HeLa). Luciferase activities were obtained 48 h post-transfection. The graph shows relative Renilla luciferase activity (Renilla/Firefly; RL/FL) normalised to 100 against No 3'UTR. Data represent the mean ± SEM of three independent experiments of quadruplicates.

2.3.6.2 3' sequential additions of the *ABL1* 3'UTR

Given the presence of a strong repressor (1116-1257), we also examined how sequential 3' additions of the 3'UTR affected reporter expression (Fig 2.20, A). It was possible that the strong repressor masked the effect of other regulatory elements located in the 5' end.

In KYO-1 cells, addition of up to the first 755 nt had a nominal effect on reporter activity. However, addition of 225 nt (1-755 *vs.* 1-935) resulted in a similar repression effect to that of the full length 3'UTR. Subsequent 3' additions from nt 935 until the full length 3'UTR completed the full repressive activity of the 3'UTR in a gradient-like manner. We

further mapped the 755-935 region by testing a construct containing the first 840 nt of the 3'UTR. This construct showed no reduction in reporter expression, suggesting that the repressive effect was due to a sequence within nt 840-935 of the 3'UTR.

The results for HeLa and K-562 experiments were again comparable (similar to the 5'truncation work) to that of the KYO-1 experiments. That is, the first 755 nt of the 3'UTR showed little effect on reporter expression, but inclusion of the first 935 nt effectively restored the repressive nature of the 3'UTR. We did not test the 1-840 construct in these cell lines due to time constraints, but if required this construct could be used to further map the repressive region in K-562 and HeLa cells.

The results for the KCL-22 cell line again highlighted a separate mechanism by which the *ABL1* 3'UTR controls expression. In these experiments, the first 755 nt caused a 50% increase in reporter expression. Addition of nt 755-935 reduced reporter expression back to baseline (in accordance with this region having a repressive effect). Interestingly, subsequent additions until nt 1576 caused a gradual increase in reporter expression. Finally, the full length 3'UTR reporter showed a similar level of expression as no 3'UTR.

In summary, the 3' additions mapped a region between nt 755(840) and 935 which has repressive activity, thus identifying a region in addition to that spanning nt 1116-1257 (from 5'truncations) that has a striking effect on gene expression. The experiments for KCL-22 provided an interesting insight into the nature of the 3'UTR in these cells.

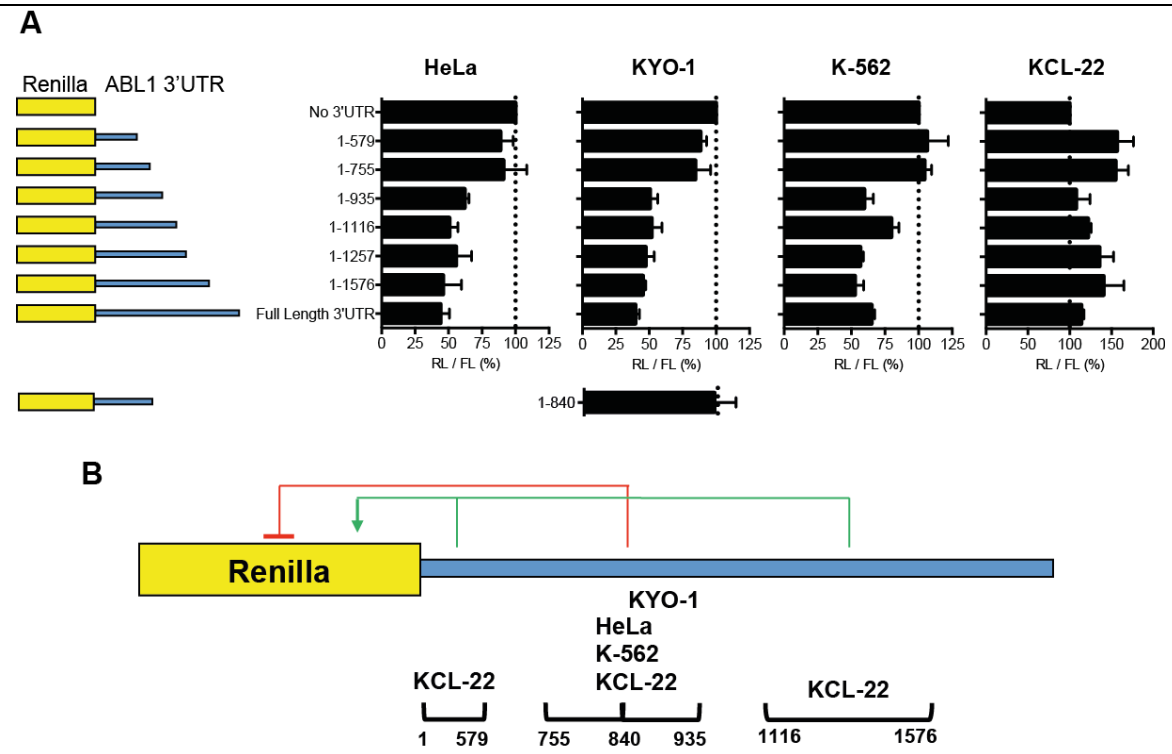

Fig 2.20: Mapping regulatory elements in the *ABL1* 3'UTR by serial deletions at the 3' end of the 3'UTR. KYO-1, K-562, KCL-22 and HeLa cell lines were transfected with a number of *ABL1* 3'UTR reporter vectors using FuGene 6 (KYO-1) or X-tremeGENE–HP (KCL-22, K-562 and HeLa). An additional construct, phRL-ABL1(1-840), was tested in the KYO-1 cell line to further map a region of interest. Luciferase activities were obtained 48 h post-transfection. The graph shows relative Renilla luciferase activity (Renilla/Firefly; RL/FL) normalised to 100 against No 3'UTR. Data represent the mean ± SEM of three independent experiments of quadruplicates. Note that the x-axis for KCL-22 is independent of the other three for clarity.

2.3.7 The region spanning nt 1116-1287 of the *ABL1* 3'UTR is repressive

The 5' truncation experiments mapped a repressive element to a 142 nt region (1116-1257) (Fig 2.19, A). Interestingly, this region contains a canonical binding site for TTP (known as zfp-36 or tristetraprolin) 'UUAUUUAAU'. TTP is an RNA-binding protein that has a well-documented role in controlling RNA stability[189]. This site is also encompasses an AU-rich element (AU-RE) (AUUUA). There is only one TTP/AU-RE predicted within the *ABL1* 3'UTR (Table 2.18). In addition, there was a predicted microRNA binding site for miR-125 within this region (chapter 3, Fig 3.7, pg 110). Therefore we performed pilot experiments to search for evidence that these factors functionally interact with the *ABL1* 3'UTR (Fig 2.21 and 2.22 respectively). We also examined if region alone could alter gene expression. The

sequence 1116-1287 was cloned downstream of *Renilla* (because the 5' truncation experiments only defined the 5' boundary, we included an extra 30 nt). This construct was transfected into KYO-1 and KCL-22 cells. In KYO-1 cells, this region alone reduced reporter expression by 40% and, surprisingly, this region was also repressive in KCL-22 cells (Fig 2.23, pg 73).

2.3.7.1 TTP binding site

The putative TTP binding site/AU-RE encompasses nt 1206-1214 of the *ABL1* 3'UTR (Table 2.18). In order to examine its effect on reporter expression, this binding site was mutated from UUAUUUAAU to UUAGCGAAU in the full length *ABL1* 3'UTR reporter and in a reporter harbouring the 1116-1257 region. There was an overall increase of reporter expression upon deletion of the putative site (Fig 2.21). However this increase was not significant: full length 1.00 *vs.* 1.15 (p = 0.4); 142 nt region 1.00 *vs.* 1.41 (p = 0.07). These data show that the site does not heavily influence gene expression via the *ABL1* 3'UTR, but may allow for fine tuning of (BCR-)ABL expression.

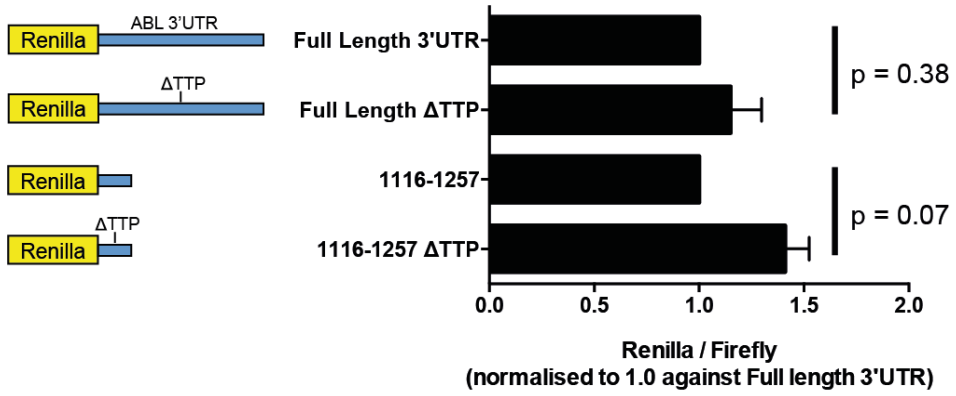

Fig 2.21: Deletion of the AU-RE within the *ABL1* 3'UTR. The putative TTP-binding site/AU-RE was mutated in the full length and 1116-1257 *ABL1* 3'UTR reporters by PCR mutagenesis. Wildtype and mutation reporters were then transfected into KYO-1 cells (using FuGene 6), and luciferase activity obtained 48 h post-transfection. The graph shows relative Renilla luciferase activity normalised to 1 against the wildtype binding-site reporters. Data represent the mean ± SEM of three independent experiments of quadruplicates. The p-values comparing wildtype and mutated binding site were 0.38 and 0.07 for the full length and 1116-1257 constructs respectively and were derived using a two-tailed, one sample t-test (Prism software).

2.3.7.2 MicroRNA-125

The predicted binding site for miR-125 comprises of nt 1253 to 1259, which is inclusive of the 3' deletion site (1257). Therefore, in order to investigate if miR-125 interacts with this putative site, the miR-125a Pre-miR (microRNA mimic) was co-transfected into HeLa cells with 1116-1257 and 1116-1287 reporters. The 1116-1287 reporter harbours the putative miR-125 site, whereas the 1116-1257 reporter does not.

If miR-125a interacts with the predicted site downstream of the luciferase gene, we would expect to observe a reduction in reporter activity. However, there was a dose-response increase in luciferase activity, which was not indicative of a functional interaction between miR-125a and nt 1116-1287 of the *ABL1* 3'UTR (Fig 2.22; left). Moreover, a similar pattern of reporter expression was observed in the absence of the predicted miR-125 binding site. Therefore these results suggest that miR-125 does not functionally interact within the 1116-1287 region of the *ABL1* 3'UTR. To completely dismiss an interaction between miR-125 and the 3'UTR, future work should confirm that there is an induction of miR-125 to a biologically relevant level, and that this results in altered expression of a known miR-125 target.

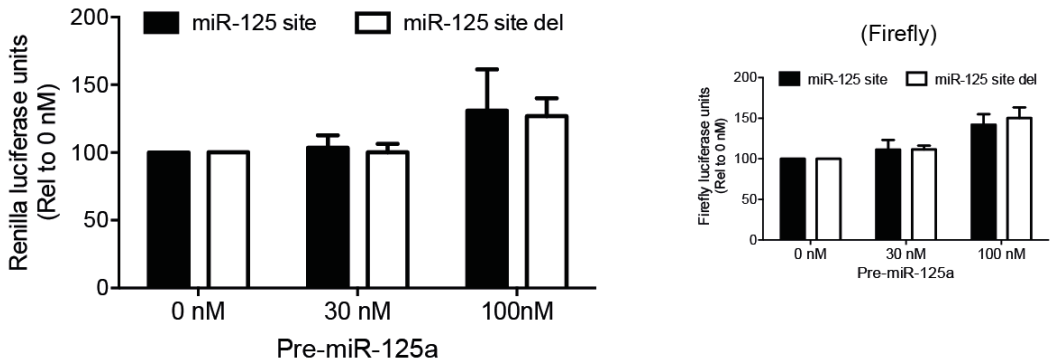

Fig 2.22: MiR-125a does not interact within the 1116-1258 region of the *ABL1* 3'UTR. HeLa cells were transfected (using X-tremeGENE-HP) with an *ABL1* 3'UTR reporter containing the region 1116-1280 (miR-125 site) or 1116-1257 (miR-125 site del). The cells were also transfected with varying amounts of miR-125a Pre-miR (as indicated above). Luciferase activity was then obtained 48 h post-transfection. The graph (left) shows raw Renilla luciferase activity normalised to 100 against 0 nM Pre-miR. Data represent the mean ± SEM of three independent triplicate experiments. Raw Renilla values were used because miR-125a altered the expression of Firefly luciferase (right).

2.3.8 The region spanning nt 821-940 of the ABL1 3'UTR is repressive

3' mapping experiments (2.3.6.2) identified a putative 96 nt repressive region (840-935) of the *ABL1* 3'UTR (Fig 2.20). Therefore, like the 1116-1257 region, it was cloned downstream of the *Renilla* reporter gene to test if it could affect reporter expression alone (20 extra nt were included at the 5' end as in 2.3.7). In KYO-1 and KCL-22 cells, this region alone reduced reporter expression by approximately 30% (Fig 2.23, A), consistent with the mapping experiments (Fig 2.20).

2.3.8.1 The 96 and 142 nt repressors have an additive effect on reporter expression

The 96 nt (840-935) and 142 nt (1116-1257) repressive regions are separated by 180 nt, so we examined the possibility of cross-talk between these regions. The region 821-1287 was cloned downstream of *Renilla* and then transfected into KYO-1 and KCL-22 cells. In both cell lines, the reporter activity was lower for the dual-repressor construct than each repressor alone (Fig 2.23, A). These data are consistent with an additive effect for each repressor (acting as two separate repressive regions); they do not seem to interfere or enhance each other's repressive nature.

We then spliced out these repressive regions from the full length 3'UTR reporter. It was anticipated that removal of these repressive regions would increase reporter activity. In KYO-1 cells, removal of the 142 nt (1116-1257) repressive region rescued reporter expression by 1.3-fold compared to the wildtype 3'UTR (n = 3) (Fig 2.23, B), although the increase was not significant ($p = 0.14$). Interestingly, we saw a similar result upon deletion of the putative TTP-binding site (Fig 2.21), which may suggest that this AU-RE plays a small but functional role during BCR-ABL expression. Upon deletion of the 96 nt (840-935) repressive region, there was no difference in reporter expression compared with the full length 3'UTR (n = 2) (Fig 2.23, B).

These results suggest that these regions are not significantly repressive in the context of the full length 3'UTR. This could be due to redundancy (repressive saturation), interplay with other regions in the 3'UTR, or these regions were repressive (or not) due to a structural artefact due to the nature of this 'synthetic' 3'UTR reporter system.

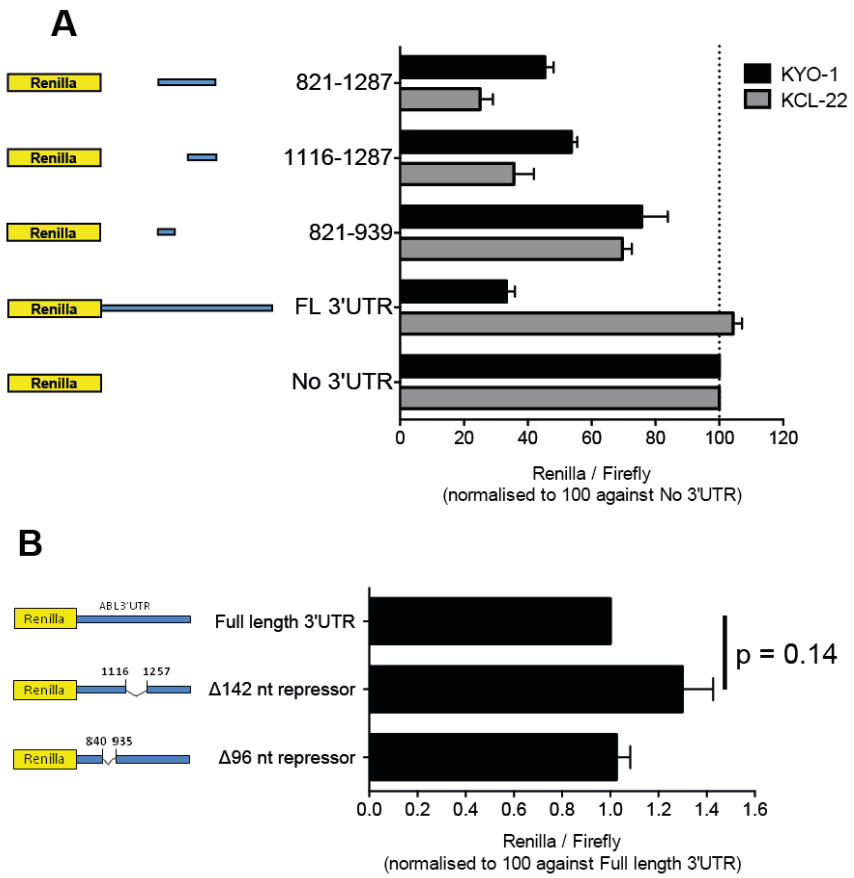

Fig 2.23: The 96 and 142 nt repressors alone reduce reporter expression, however their repressive activity is redundant in the context of the full length *ABL1* 3'UTR. (**A**) KYO-1 and KCL-22 cell lines were transfected with reporters harbouring the 96 and 142 nt repressors, or a reporter containing both using X-tremeGENE–HP. Luciferase activity was measured 48 h post-transfection. The graph shows relative Renilla luciferase activity normalised to 100 against No 3'UTR. Data represent the mean ± SEM of three independent experiments of quadruplicates. (**B**) KYO-1 cells were transfected with reporters harbouring deletions of the 96 or 142 nt repressive regions using X-tremeGENE–HP. Luciferase activity was measured 48 h post-transfection. The graph shows relative Renilla luciferase activity normalised to 1 against full length 3'UTR. Data represent the mean ± SEM of at least two independent experiments of quadruplicates. The p-value was derived using a two-tailed, one sample t-test (Prism software).

2.3.9 Merging the deletion mapping data

With exception to the KCL-22 experiments, there is little overlap in regulatory regions between the 5' (Fig 2.19, B) and 3' (Fig 2.20, B) mapping experiments. This was a suprise, particularly for the regions with strong regulatory activity (735-935) and (1116-1257). It is possible that because these truncated 3'UTRs do not exist in nature, they may adopt a

different structure resulting in cryptic regulatory sites. Alternatively, some of the regulatory regions may require up or downstream elements to function, and these elements are disrupted in the truncated-3'UTR species.

In the KCL-22 experiments, the 3' and 5' mapping data are compatible considering what is known about the 3'UTR. The 5' mapping results show that the first 499 nt contains one or more regions which are stabilising or activating (Fig 2.19, A). Upon deletion of this region, the 3'UTR behaves in a way similar to that observed in KYO-1, K-562 and HeLa cells. In the 3' mapping experiments, the first 579 nt are activating, which is in agreement with the 5' mapping results. The 755-935 region has a repressive effect (which is also observed in the other three cell lines). However, the 1116-1257 repressive region has no effect on reporter expression (unlike what was found in the other three cell lines). One possible explanation involves our observation that the 1116-1257 region is active following deletion of the 1-499 region in KCL-22 cells (Fig 2.19, A). Therefore, the 1-499 region may control the repressive nature of the 1116-1257 region.

A similar mechanism has been proposed for the *HNF4α* 3'UTR, where an upstream 'balancer' region appeared to control a downstream repressive element[187]. Luciferase-mapping of the *HNF4α* 3'UTR identified two regions that repressed reporter expression. Interestingly, splicing out these regions from the 3'UTR had little effect on reporter activity (similar to the *ABL1* 3'UTR repressors in this study, Fig 2.23). They then found an upstream element (40 nt) that could completely ablate the repressive activity of one of the repressive regions. Their study did not identify the regulator(s) involved, but it is possible that the *HNF4α* and *ABL1* 3'UTRs are regulated in a similar manner.

2.3.10 3'UTR avoidance

As discussed in 2.1.1.5, decoy 3'UTRs are known to provide a mechanism which alleviates 3'UTR-mediated regulation of the coding gene. Decoy 3'UTRs can exist in pseudogenes or as discrete transcripts of the full length gene (see Fig 2.2, B).We used bioinformatics approaches to investigate the possibility that decoy 3'UTRs exist for *ABL1*.

2.3.10.1 No evidence for *ABL1* 3'UTR-containing pseudogenes

To search for *ABL1* 3'UTR-containing pseudogenes, a blast search using the *ABL1* 3'UTR sequence was performed against the human genome (hg19) using CLC main workbench v6.5

software. The only major hits were for chromosome 9, and all corresponded to the *ABL1* gene (Fig 2.24, A). There were four separate entries for the *ABL1* gene in the blast-database, hence the display of four hits. This approach was validated by performing the same analysis for the *PTEN* 3'UTR sequence, which has a known pseudogene: *PTENP1*. The blast hits for the *PTEN* 3'UTR included the *PTEN* gene (chromosome 10), the pseudogene *PTENP1* (chromosome 9) and the intron of the *ANKFN1* gene (known to contain the 3'end of *PTEN*)[190] (Fig 2.24, B). Together these findings suggest that *ABL1* 3'UTR decoys are not present in the form of a pseudogene.

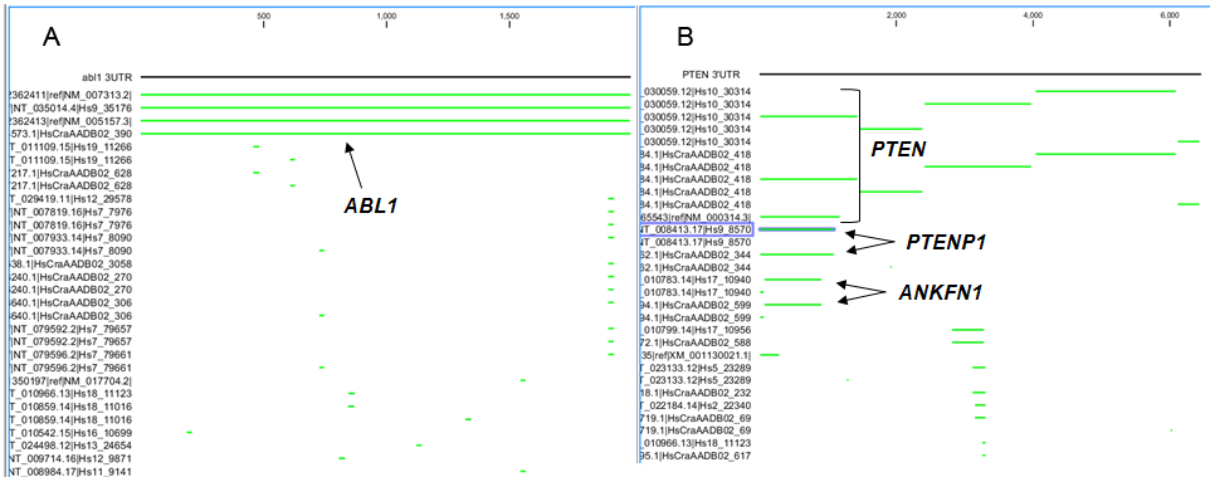

Fig 2.24: Search for *ABL1* 3'UTR pseudogenes. (**A**) The *ABL1* 3'UTR sequence was blasted against the human genome (hg19) to search for *ABL1* 3'UTR pseudogenes. The blast was performed using CLC Main Workbench v6.5 using the blastn engine based on NCBI blast. (**B**) The analysis from **A**, was performed for the *PTEN* 3'UTR sequence. Output in **A** and **B** show the input sequence (black line), with sequence length displayed along the top (in nucleotides). The blast hit contig (green lines) correspond to human genomic sequences that align to the input sequence. Alignments of interest are annotated.

2.3.10.2 The *ABL1* 3'UTR is unlikely to be independently transcribed from *ABL1*.

CAGE tags are able to identify the 5' end of transcripts. When these tags were mapped to the human genome (hg17), they were over represented in the promoters of genes, as would be expected, with the next highest representation being in 3'UTRs. If the *ABL1* 3'UTR is independently transcribed from the *ABL1* gene, it can act as a decoy 3'UTR. Therefore we used the CAGE tag viewer (http://gerg02.gsc.riken.jp/gev-promoter/gbrowse/hg17/)[191] in order to search for CAGE tags located in the *ABL1* 3'UTR, indicative of 5' termini of mRNA.

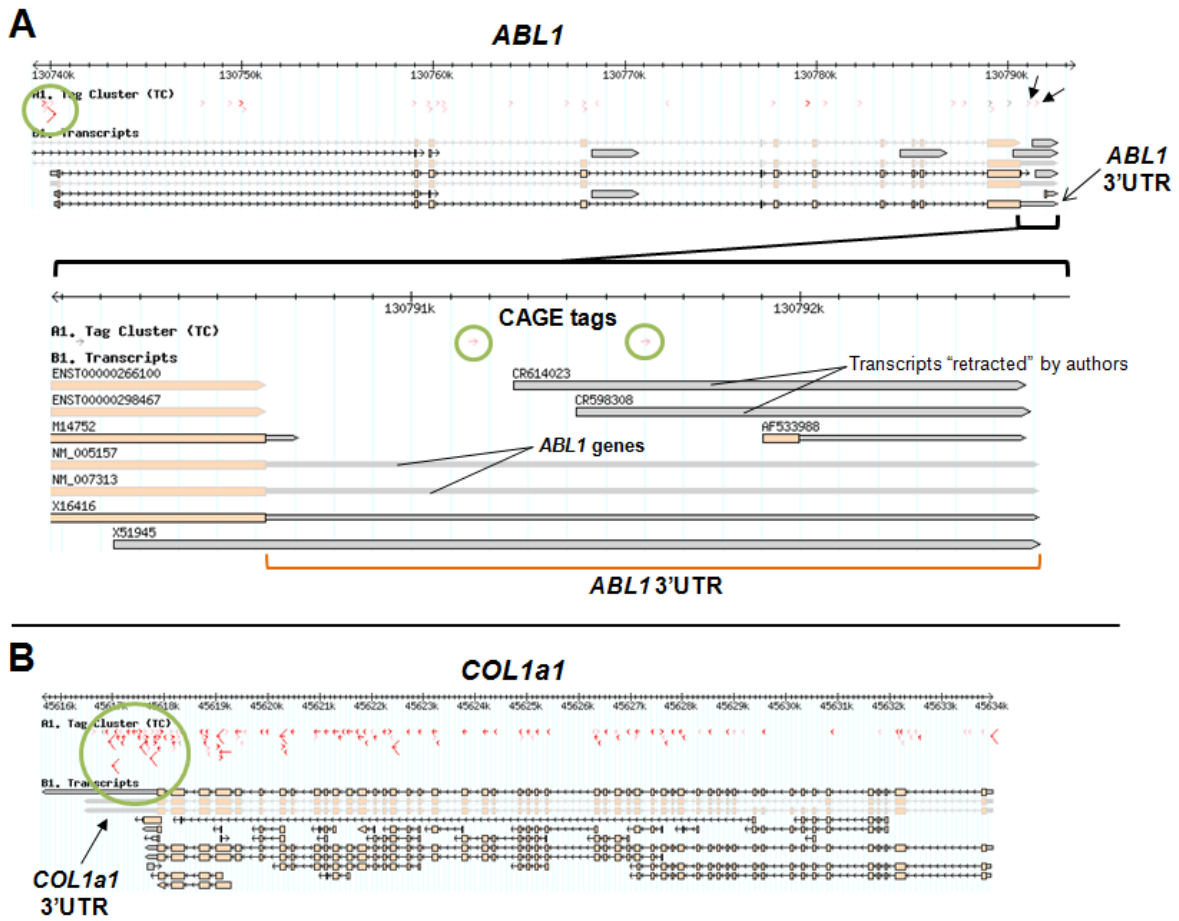

Fig 2.25: CAGE tag hits for the *ABL1* 3'UTR. (**A**) CAGE tags aligning to *ABL1* (ref seq NM_005157) are displayed as red arrows (size of arrow relates to CAGE-tag density). Ref seq NM_007313 was not included because the first intron is ~100 kb, therefore the image would be zoomed out too far to interpret. On the top diagram, the CAGE tags that align to the promoter region are circled in green, whereas the arrow heads highlight two CAGE-tags which are located in the *ABL1* 3'UTR. The bottom scheme zooms in on the *ABL1* 3'UTR. Here, the two CAGE-tags in the 3'UTR are circled in green. This figure also illustrates that both *ABL1* transcripts (NM_005157 and NM_007313) share identical 3'UTRs. (**B**) CAGE-tag alignment for *COL1a1*. The *COL1a1* 3'UTR is expressed as a discrete transcript[162]. Therefore the CAGE-tag alignment was shown for this gene as a point of reference for independently transcribed 3'UTRs (the *COL1a1* gene is located on the minus strand).

There were two CAGE tags which mapped to the *ABL1* 3'UTR (Fig 2.25, A). However *bone fide* transcription start sites are marked by a hotspot of tags (see the *ABL1* promoter). This is further highlighted in *COL1a1*, a gene known to independently transcribe its 3'UTR[162]. There is a hotspot of CAGE tags located in the *COL1a1* 3'UTR (even more so than on its promoter) (Fig 2.25, B). Taken together, these data do not provide strong evidence that the *ABL1* 3'UTR

is contained in transcripts discrete from the full length *ABL1* gene. To completely rule this out, it would be recommended to perform 5'RACE for the *ABL1* gene.

2.3.11 *In silico* screen for *ABL1* 3'UTR regulatory elements

Initially the *ABL1* 3'UTR was examined on the UCSC and Ensembl genome browsers to obtain sequence and conservation information as discussed in 2.1.2.1. During this study, a number of databases were used or became available to predict regulatory regions within the *ABL1* 3'UTR.

2.3.11.1 Predicted microRNA binding sites in the *ABL1* 3'UTR

Targetscan was used to predict microRNA that target the *ABL1* 3'UTR. These predictions are based on sequence homology between the microRNA. This program also considers the cross-species conservation of the predicted binding site. Five microRNAs, miR29/30/125/196 and 203, were predicted to interact with conserved regions of the *ABL1* 3'UTR, as discussed in detail in chapter 3.

2.3.11.2 RNA-binding proteins

RBPDB is analogous to TargetScan, but finds consensus binding sites for RNA-binding proteins within a submitted sequence. Recently, immunoprecipitation of RNA-binding proteins has been coupled with next-generation (next-gen) sequencing to map RNA-protein interactions (this approach is referred to in this thesis as 'RIP-SEQ'). The doRiNA database has pooled data from a number of published datasets and incorporated them into the UCSC genome browser. These databases were not available at the commencement of this project, therefore they were used to attempt to look for RNA-binding protein hits within regions of interest that were mapped in the luciferase mapping experiments.

2.3.11.2.1 Predicted RNA-binding protein binding sites

Using RBPDB, a query for the *ABL1* 3'UTR produced over 1250 potential RNA-binding protein binding sites. These were filtered by: more than a five bp consensus site with a relative score of 100%, a six bp consensus site with relative score of >83%, or all hits for consensus sites of seven bp or greater (Table 2.18). The top hits were SFRS1/ASF, ZFP36/TTP and ELAVL-2. The predicted sites for SFRS1 and TTP are located in regions of

the *ABL1* 3'UTR found to have a regulatory role from the 3'UTR mapping experiments (Fig 2.19 and 2.20). The putative binding site for TTP was deleted in *ABL1* 3'UTR reporters, because of TTP's role in regulating RNA stability[189]. Deletion of the TTP site resulted in a modest increase in reporter activity (Fig 2.21). Therefore, TTP may function as a fine-tuner of BCR-ABL. The putative SFRS1 sites were not deleted because SFRS1 RIP-SEQ data showed no hits for *ABL1* (Fig 2.26).

Table 2.18: RNA-binding protein consensus sites within the *ABL1* 3'UTR

Score*	Relative Score#	Gene name	Start	End	Matching sequence
13.47	91%	SFRS1	1681	1690	AAGACAGAGC
13.01	95%	ZFP36	1206	1214	UUAUUUAAU
12.30	83%	SFRS1	1405	1414	UUGACAGAGC
11.96	93%	ELAVL-2	355	363	UUUCAUUUU
9.80	81%	SNRPA	171	178	UUUGCACC
8.95	100%	NONO	1382	1386	AGGGA
8.95	100%	NONO	859	863	AGGGA
8.95	100%	NONO	1255	1259	AGGGA
8.95	100%	NONO	1650	1654	AGGGA
8.95	100%	NONO	85	89	AGGGA
8.67	100%	RBMY1A1	794	798	CUCAA
8.65	100%	a2bp1	537	541	GCAUG
8.65	100%	a2bp1	527	531	GCAUG
8.65	100%	a2bp1	705	709	GCAUG
8.65	100%	a2bp1	266	270	GCAUG
8.65	100%	a2bp1	698	702	GCAUG
8.63	100%	RBMY1A1	794	798	CUCAA
8.41	89%	EIF4B	1034	1040	UUUGGAA
7.75	96%	SNRPA	171	177	UUUGCAC
7.59	80%	EIF4B	1263	1269	UUAGGAA
7.59	83%	EIF4B	608	614	GCAGGAC
7.56	86%	sap-49	754	759	UUGUGA
7.35	100%	ACO1	1894	1899	CAGUGC
7.09	100%	SFRS9	273	277	AGGAC
7.09	100%	SFRS9	610	614	AGGAC
6.57	89%	ACO1	1976	1981	CAGUGU
6.34	100%	YBX1	1134	1139	CCUGCG
5.94	93%	YBX1	119	124	UCUGCG

Score*	Relative Score#	Gene name	Start	End	Matching sequence
5.88	94%	YTHDC1	537	542	GCAUGC
5.88	94%	YTHDC1	527	532	GCAUGC
5.88	94%	YTHDC1	266	271	GCAUGC
5.28	84%	YTHDC1	1713	1718	GACUGC
5.28	84%	YTHDC1	255	260	GACUGC
5.06	98%	SFRS13A	1153	1159	AAAGGGC
5.06	98%	SFRS13A	973	979	AAAGGGC
4.72	92%	SFRS13A	687	693	AAAGGAU
4.37	93%	KHDRBS3	1209	1214	UUUAAU
4.33	92%	KHDRBS3	1969	1974	AAUAAA
4.24	82%	SFRS13A	505	511	CAAGAAC
4.19	81%	SFRS13A	928	934	CAAGGGC
4.17	81%	SFRS13A	1110	1116	AGAGAAU
4.09	88%	KHDRBS3	1542	1547	CCUAAA
4.04	86%	KHDRBS3	1965	1970	UUUAAA
3.94	84%	KHDRBS3	643	648	GCUAAA

* The score of the binding site is the sum of the scores for each nucleotide compared to the consensus site. This takes into consideration that some RNA-binding proteins interact with ambiguous sequences.
# The relative score is the score divided by the maximum score possible.

2.3.11.2.2 RNA-immunoprecipitation data

The doRiNA browser showed a number of hits for proteins bound to the *ABL1* 3'UTR. These included: AGO, TIA-1, TIAL-1, hnRNP C, ELAVL-1 (also known as HuR) and IGF2BP1-3 (Fig 2.26). From these data, there are four hotspots within the *ABL1* 3'UTR that show binding of numerous RNA-binding proteins (Fig 2.26 and Fig 2.27).

Hotspot 1 has three overlapping reads for the AGO proteins which are indicative of microRNA-RNA interactions (AGO proteins are a core component of the microRNA machinery). A less stringent TargetScan search was performed for this region given its small size. This search predicted binding sites for miR-19, 196, 378, and 411 within the overlapping reads (Fig 2.27, A).

Hotspot 2 has two overlapping reads for TIA-1 and TIAL-1, three for ELAVL-1 and one read for hnRNP C and AGO (Fig 2.27, B). Interestingly an ELAVL-2 binding site, which

shares the same binding site as ELAVL-1[192], was predicted by RBPDB within the overlapping regions for ELAVL-1 (Table 2.18).

Hotspot 3 contains two overlapping reads for TIA-1 and TIAL-1, four reads (three overlapping) for AGO, and two overlapping reads for ELAVL-1 (Fig 2.27, C). A Targetscan search predicted a binding site for miR-361 within the three overlapping AGO reads (Fig 2.27, C).

Hotspot 4 encompasses the last 200 nt of the *ABL1* 3'UTR. It contains three TIA-1 and TIAL-1 reads (two overlapping), and five AGO reads (two sets of overlapping reads with two and three reads respectively) (Fig 2.27, D). The Targetscan database predicted a binding site for miR-30 and the miR-141/200 family within the region containing three overlapping AGO reads (Fig 2.27, D).

The doRiNA database also displayed hits for RNA bound by SFRS1. RBPDB predicted two SRFS1 binding sites within the *ABL1* 3'UTR (Table 2.18), but there were no SFRS1-hits within the *ABL1* 3'UTR (Fig 2.26, termed therein as SF2/ASF). Prior to using this bioinformatics data, we examined miR-30, 141 and 196's potential for regulating BCR-ABL, because the predicted binding sites for these microRNAs were species conserved (results are discussed in chapter 3).

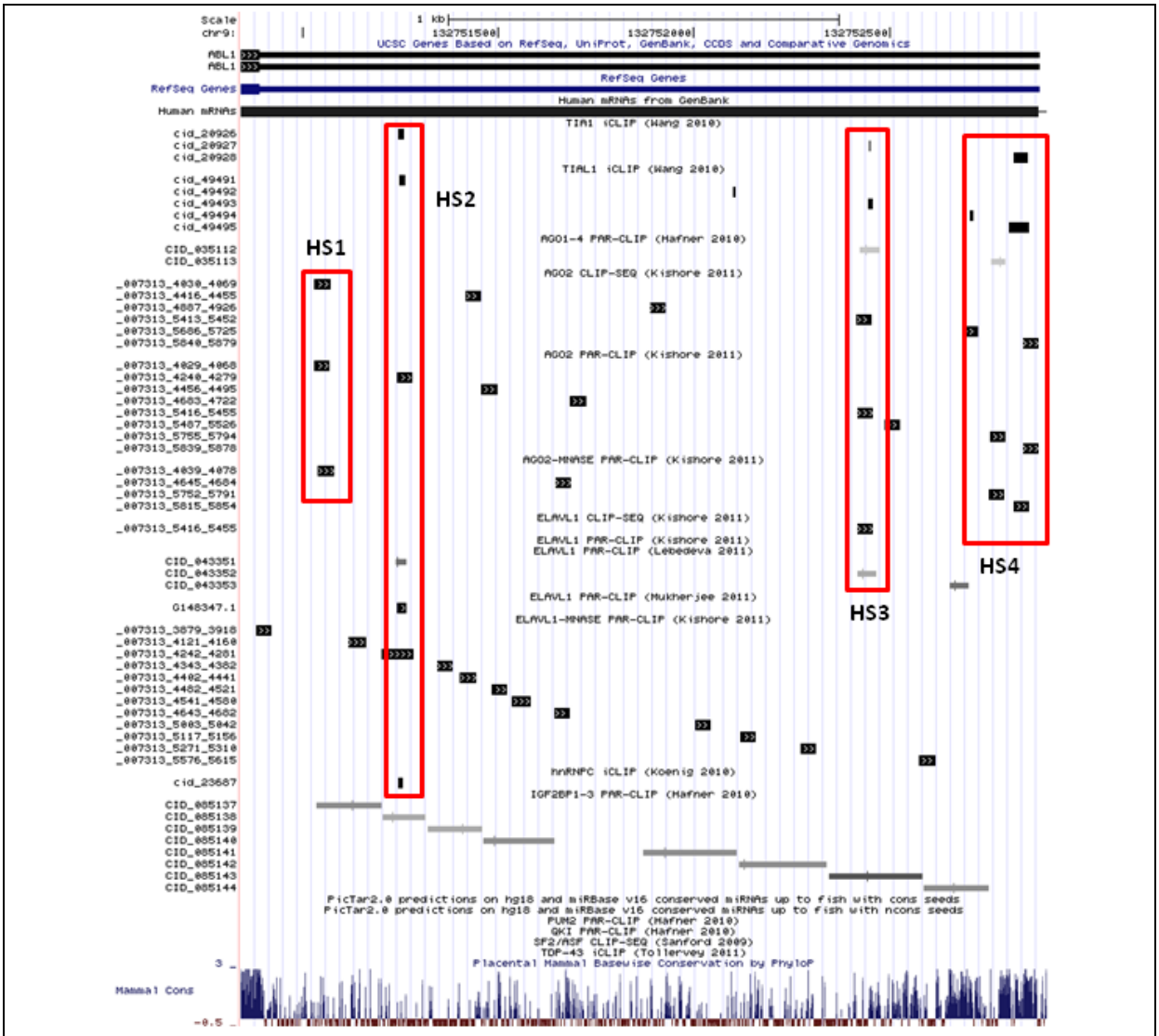

Fig 2.26: RNA-binding protein RIP-SEQ data for the *ABL1* 3'UTR. (**A**) The doRiNA database was used to search for RIP-SEQ data regarding RNA-protein interactions for the *ABL1* 3'UTR. The figure above shows these data input into the UCSC genome browser (hg 19), and centred on the *ABL1* 3'UTR sequence. These data included hits for TIA-1/TIAL-1, AGO2, ELAV1, hnRNP-C, IGF2BP 1-3. There were no hits for PUM2, QK1, SF2/ASF, or TDP-43. Apparent RNA-binding protein hotspots were boxed in red, labelled HS1-HS4.

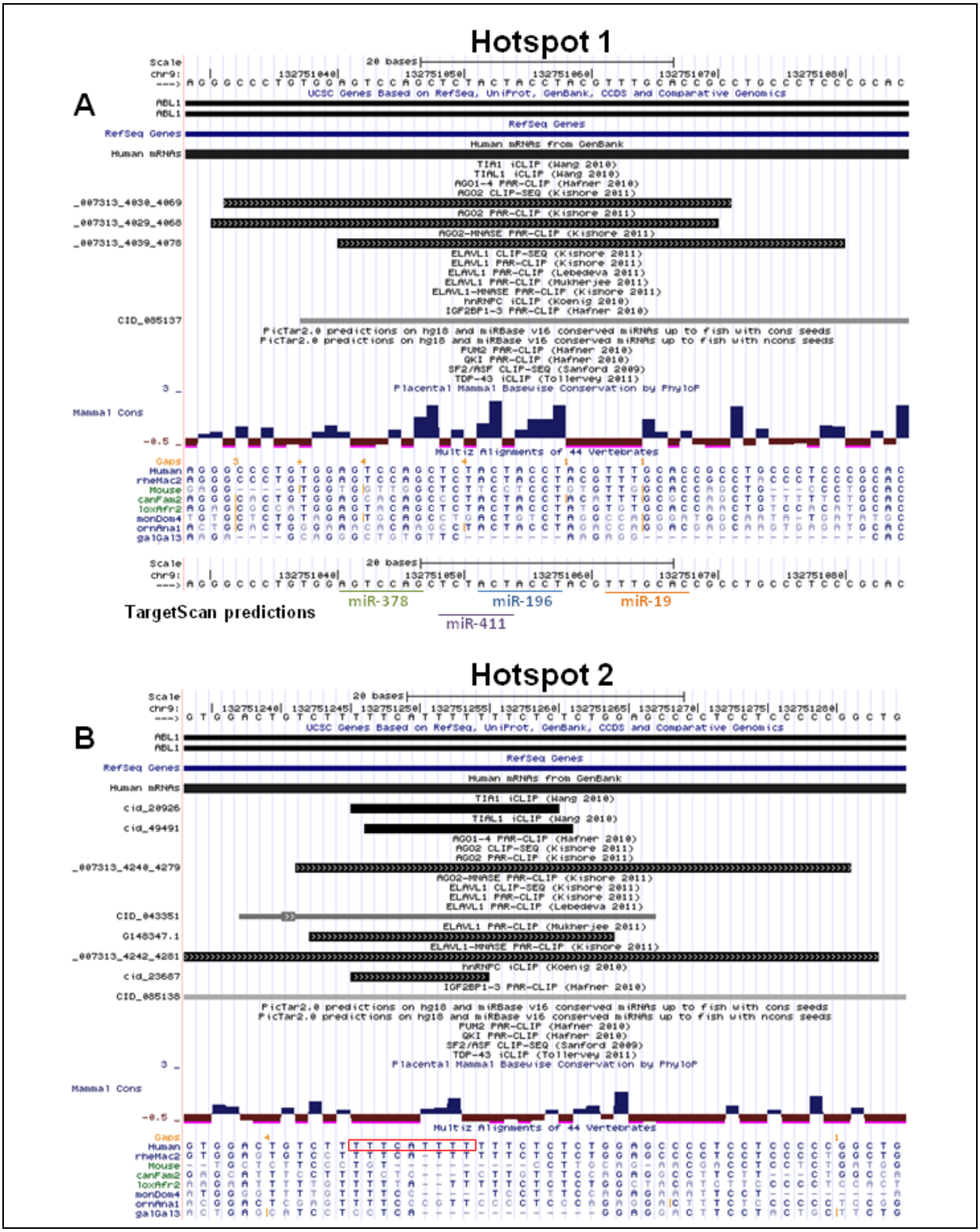
Hotspot 1
A
UCSC Genes Based on RefSeq, UniProt, GenBank, CCDS and Comparative Genomics
RefSeq Genes
Human mRNAs from GenBank
TIA1 iCLIP (Wang 2010)
TIAL1 iCLIP (Wang 2010)
AGO1-4 PAR-CLIP (Hafner 2010)
AGO2 CLIP-SEQ (Kishore 2011)
AGO2 PAR-CLIP (Kishore 2011)
AGO2-MNASE PAR-CLIP (Kishore 2011)
ELAVL1 CLIP-SEQ (Kishore 2011)
ELAVL1 PAR-CLIP (Kishore 2011)
ELAVL1 PAR-CLIP (Lebedeva 2011)
ELAVL1 PAR-CLIP (Mukherjee 2011)
ELAVL1-MNASE PAR-CLIP (Kishore 2011)
hnRNPC iCLIP (Koenig 2010)
IGF2BP1-3 PAR-CLIP (Hafner 2010)
PicTar2.0 predictions on hg18 and miRBase v16 conserved miRNAs up to fish with cons seeds
PicTar2.0 predictions on hg18 and miRBase v16 conserved miRNAs up to fish with ncons seeds
PUM2 PAR-CLIP (Hafner 2010)
QKI PAR-CLIP (Hafner 2010)
SF2/ASF CLIP-SEQ (Sanford 2009)
TDP-43 iCLIP (Tollervey 2011)
Placental Mammal Basewise Conservation by PhyloP
Mammal Cons
Multiz Alignments of 44 Vertebrates
Human
rheMac2
Mouse
canFam2
loxAfr2
monDom4
ornAna1
galGal3
TargetScan predictions
miR-378
miR-196
miR-19
miR-411
Hotspot 2
B
UCSC Genes Based on RefSeq, UniProt, GenBank, CCDS and Comparative Genomics
RefSeq Genes
Human mRNAs from GenBank
TIA1 iCLIP (Wang 2010)
TIAL1 iCLIP (Wang 2010)
AGO1-4 PAR-CLIP (Hafner 2010)
AGO2 CLIP-SEQ (Kishore 2011)
AGO2 PAR-CLIP (Kishore 2011)
AGO2-MNASE PAR-CLIP (Kishore 2011)
ELAVL1 CLIP-SEQ (Kishore 2011)
ELAVL1 PAR-CLIP (Kishore 2011)
ELAVL1 PAR-CLIP (Lebedeva 2011)
ELAVL1 PAR-CLIP (Mukherjee 2011)
ELAVL1-MNASE PAR-CLIP (Kishore 2011)
hnRNPC iCLIP (Koenig 2010)
IGF2BP1-3 PAR-CLIP (Hafner 2010)
PicTar2.0 predictions on hg18 and miRBase v16 conserved miRNAs up to fish with cons seeds
PicTar2.0 predictions on hg18 and miRBase v16 conserved miRNAs up to fish with ncons seeds
PUM2 PAR-CLIP (Hafner 2010)
QKI PAR-CLIP (Hafner 2010)
SF2/ASF CLIP-SEQ (Sanford 2009)
TDP-43 iCLIP (Tollervey 2011)
Placental Mammal Basewise Conservation by PhyloP
Mammal Cons
Multiz Alignments of 44 Vertebrates
Human
rheMac2
Mouse
canFam2
loxAfr2
monDom4
ornAna1
galGal3

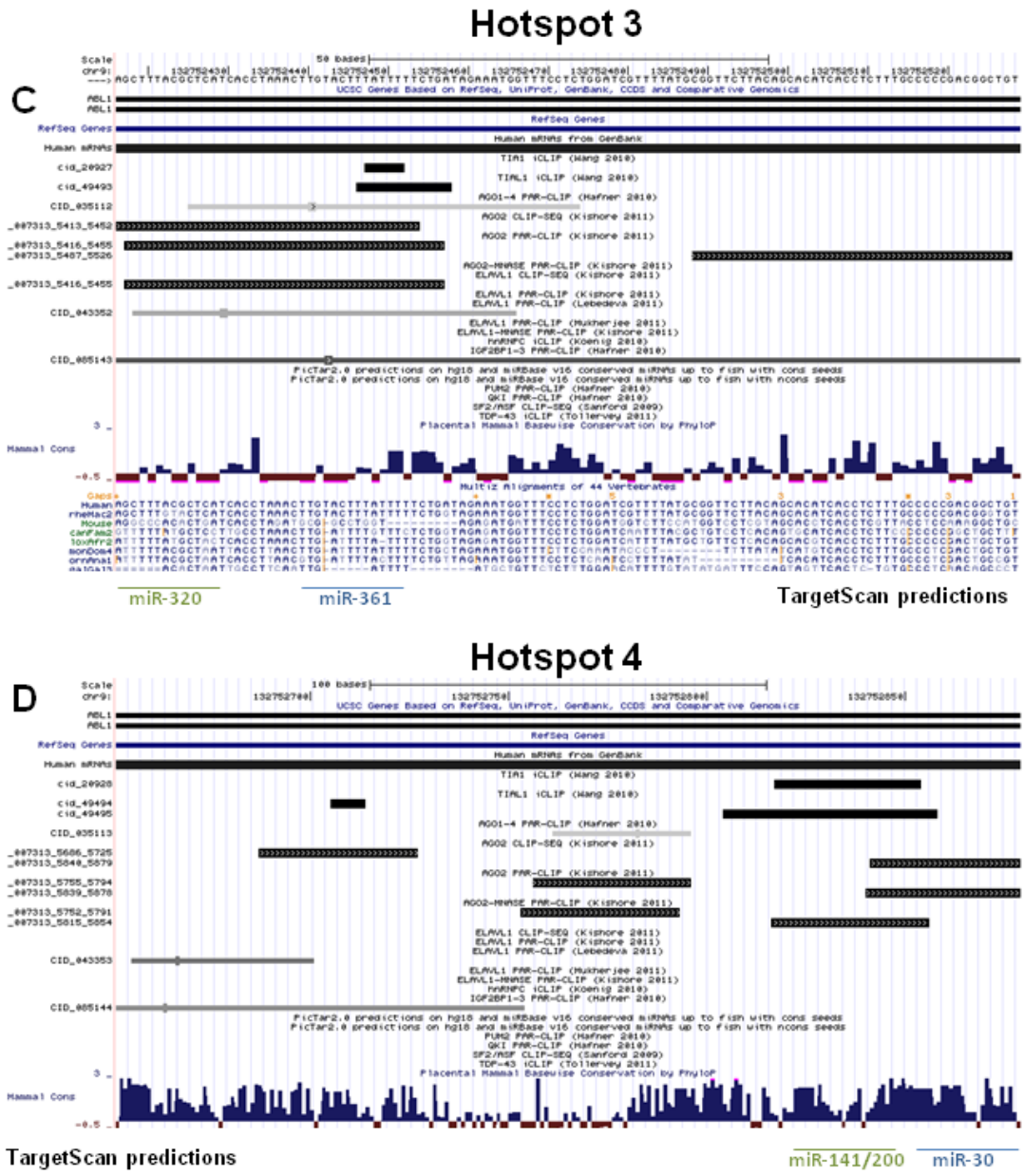

Fig 2.27: High resolution focus on the RNA-binding protein hotspots for the *ABL1* 3'UTR defined in Fig 2.26. Same data as from Fig 2.26, A, however the hotspots defined in the previous figure are displayed in higher resolution to show in detail how the RIP-SEQ data maps to the *ABL1* 3'UTR. (**A**) "Hotspot 1", includes Targetscan microRNA predictions located within AGO2 reads. *Note: these reads map to a species conserved region of the 3'UTR*. (**B**) "Hotspot 2", red box indicates ELAVL-1 binding site[192]. (**C**) "Hotspot 3", includes Targetscan microRNA predictions located within AGO2 reads. (**D**) "Hotspot 4", includes Targetscan microRNA predictions located within AGO2 reads. As the AGO reads map to discrete regions, species conservation of the 3'UTR sequence was ignored for Targetscan annotations.

2.4 Discussion

Defining the *ABL1* 3'UTR

With numerous reports of 3'UTR alterations playing a functional role in cancer[147,148], and the observation that the mouse *ABL1* 3'UTR is truncated[178-180], we looked for the occurrence of human *ABL1 (and therefore BCR-ABL)* 3'UTR-alterations. Using 3'RACE, we identified >2 kb species, a 1992 nt species (the annotated *ABL1* 3'UTR), and a ~900 nt 3'UTR species for *ABL1* (Fig 2.9). The ~900 nt species was identified as a shortened variant of the 3'UTR, the resultant of a splicing event that removes 328 to 1571 nt of the 3'UTR (Fig 2.9). This shortened 3'UTR was observed in the majority of the CML samples tested, but it was only present in <2% of *ABL1* containing transcripts (Fig 2.10). We also looked for evidence that the *ABL1* gene used a canonical PAS located in a species conserved region 6 kb downstream of the *ABL1* stop codon. However, we did not find any evidence that this PAS was used by *ABL1* (Fig 2.12).

Recently, Lin, *et al.* developed a database that used RNA-seq data to map PASs (in the human genome) (xPAD[193]). For the *ABL1* gene, a cluster of reads are found 2 kb downstream of the stop codon (at the annotated *ABL1* 3'UTR) (Fig 2.28). There are no other reads observed within the 2 kb *ABL1* 3'UTR (Fig 2.28), which supports our findings for the 3'RACE experiments that the ABL1 3'UTR is not truncated. However, there is a small cluster of reads aligning to the investigated distal PAS (Fig 2.28). As we did not observe an RNA species that extended from *ABL1* to the distal PAS, it is possible that another gene uses the distal PAS.

Taken together, our findings show that the annotated 2 kb 3'UTR for *ABL1* is the dominant 3'UTR species. These results are consistent with the 1990 study by Andrews, *et al.*, which also found no evidence for alternate *ABL1* 3'UTR species[171].

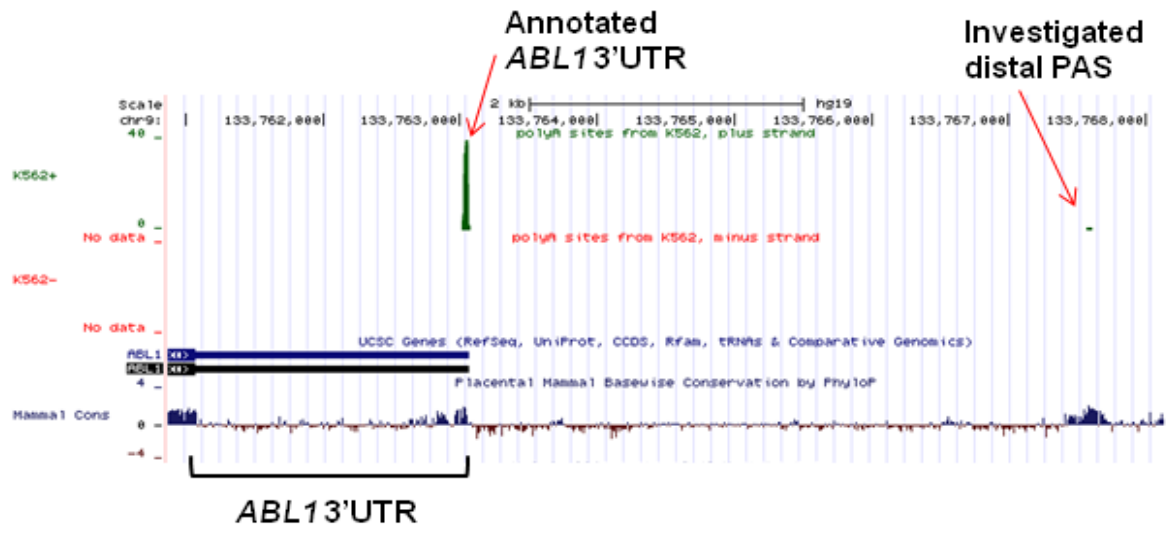

Fig 2.28: xPAD (expression and polyadenylation database) results for the *ABL1* 3'UTR and investigated distal PAS. The xPAD, UCSC genome browser plug-in (http://www.johnlab.org/xpad/) was used to search for PAS within the *ABL1* gene. Data tracks are from K-562 plus and minus strand RNA. The *ABL1* 3'UTR, annotated *ABL1* PAS and the distal PAS investigated in Fig 2.12 are also labelled above. Notably, there are no PAS sequence reads within the *ABL1* 3'UTR. This is indicative that in K-562 cells alternate PAS usage does not occur.

The *ABL1* 3'UTR is repressive

3'UTRs are known to play an important role in controlling gene expression, therefore we wanted to understand to what extent this happened in the case of the *ABL1* 3'UTR. By measuring the half life of *ABL*, *BCR* and *BCR-ABL*, we found that *ABL1* and *BCR-ABL* have similar half-lives – shorter than *BCR*'s (Fig 2.8). Therefore, either the *ABL1* sequence common to *BCR-ABL* and *ABL* (which includes *ABL1* 3'UTR) can reduce transcript stability, or, there is a stabilising element within the *BCR* transcript that is not in the *BCR-ABL* transcript. The half life experiment was a key experiment, because it is one of a few experiments in this thesis that specifically looks at the endogenous transcripts. Marega, *et al*.[97] and Collins, *et al*.[194] have also performed similar experiments. Marega, *et al*. looked at *BCR* and *BCR-ABL* half lives in K-562 cells, and in CP and BC primary cells[97]. They found that in K-562 and CP cells, *BCR* is more stable than *BCR-ABL*, but in BC cells *BCR* and *BCR-ABL* have similar stability profiles[97]. Therefore, a loss of repression via the *ABL1* portion of BCR-ABL during BC may account for enhanced BCR-ABL expression in BC. Interestingly, Collins, *et al*. found that in KCL-22 cells, the *BCR* and *BCR-ABL* transcripts are more stable than *ABL1*[194]. From this, they concluded that *BCR* dictated the expression of *BCR-ABL*.

However, other studies show that *BCR* expression does not always mimic *BCR-ABL* expression[40,97,98]. Furthermore, addition of the *ABL1* 3'UTR to the *Renilla* luciferase gene had no effect on reporter expression in the KCL-22 cell line (Fig 2.15). Taken together, we hypothesise that the *ABL1* moiety is a key contributor to the expression levels of BCR-ABL.

Fusing the *ABL1* 3'UTR with the *Renilla* reporter gene caused strong repression of reporter protein expression (Fig 2.15), outlining the repressive nature of the 3'UTR. We also showed that the 3'UTR can act at the RNA-level (Fig 2.18). The half life and luciferase data suggest that the *ABL* 3'UTR controls BCR-ABL expression at the post-transcriptional level.

We also examined the possibility that BCR-ABL has a feedback mechanism on its own expression. We exposed several CML cell lines to imatinib and monitored endogenous BCR-ABL expression over three days. In imatinib sensitive cell lines (K-562, KYO-1 and LAMA-84) a reduction in protein expression was observed over time (Fig 2.16, A). Of interest, mRNA levels did not correlate with BCR-ABL expression, BCR-ABL transcripts were higher than protein levels. In contrast, both mRNA and protein levels increased in the imatinib resistant KCL-22 cell line. These data suggested that inhibition of BCR-ABL kinase activity can alter BCR-ABL expression. In the case of KCL-22, this appeared to be at the transcriptional level due to the correlation of mRNA and protein levels. The disunity between BCR-ABL mRNA and protein levels in the imatinib sensitive lines were indicative of post-transcriptional regulation, which may involve the 3'UTR.

In order to establish a link between the *ABL1* 3'UTR and changes in BCR-ABL expression during imatinib treatment, *BCR*-promoter driven Firefly reporters with or without the *ABL1* 3'UTR were transfected into KYO-1 cells in the presence or absence of imatinib. Interestingly, Firefly expression was reduced in an *ABL1* 3'UTR-independent manner (Fig 2.17, A), suggesting that the *BCR* promoter or 5'UTR was responsive to imatinib treatment (in KYO-1 cells). Performing this experiment in a non-CML cell line demonstrated that these changes in reporter expression were dependent on BCR-ABL kinase inhibition (Fig 2.17, B). These results are suggestive that imatinib treatment has a dual-targeting role against BCR-ABL (at the protein and expression level). One of the anticipated benefits of these experiments was the possibility that imatinib exposure could serve as a tool for identifying regulators of BCR-ABL. For example, a differential display of factors that interact with the *BCR* promoter or 5'UTR dependent on imatinib treatment may allow for easy identification of

regulators of BCR-ABL. A similar approach demonstrated that the *FUSE-1* RNA binding protein bound and regulated nucleophosmin translation following rapamycin exposure[160].

There are two other studies which also measured BCR-ABL expression after imatinib exposure in K-562 and KCL-22 cells. Suresh *et al*. also observed a decrease in BCR-ABL protein expression after 3 days of imatinib treatment in K-562 cells[195]. In contrast to our results, Yuan *et al*. found reduced BCR-ABL expression in KCL-22 cells following imatinib treatment[196]. However, in this study the duration of imatinib treatment was unclear, in fact it appears to be "long term culture". They also noted rapid accumulation of BCR-ABL kinase mutations. Therefore it is possible that there is an initial increase in BCR-ABL expression followed by a reduction following emergence of BCR-ABL kinase mutant clones, as was the observation for the K-562 and KU178 cell lines[105].

Mapping the *ABL1* 3'UTR

After showing that the *ABL1* 3'UTR was repressive, we expanded our investigation to identifying regions that facilitated gene repression. Luciferase mapping of the *ABL1* 3'UTR identified a number of discrete regions which may contribute to the 3'UTR's repressive effect (Fig 2.29; end of this section). Comparison of the results from the 5' and 3' mapping experiments showed little overlap, which made our data difficult to interpret. So far we have focused on two regions which had an obvious effect on reporter expression, a 142 nt sequence (1116-1257) and a 96 nt sequence (840-935).

The 5' mapping experiments showed that deleting the 142 nt region greatly restored luciferase activity (Fig 2.19, A). This region alone could reduce reporter expression by around 50% (Fig 2.23, A), which validated the observations in the mapping experiments. Bioinformatics data provided evidence that TTP and miR-125 interacted with this region. We found evidence that the AU-RE/TTP site may regulate BCR-ABL in functional studies (Fig 2.21 and Fig 2.22). Deletion or mutation of this site resulted in a modest rescue of reporter activity (Fig 2.21). Therefore this sequence could have a fine-tuning role for BCR-ABL expression. This finding was of interest because TTP expression is reduced during progression from CP to BC[197]. If TTP reduces BCR-ABL expression, a reduction of TTP in BC may help explain how BCR-ABL expression increases in BC[40,95-99]. These data justify inclusion of TTP into the experimental pipeline described in chapter 1 (1.4.4.5), i.e., to validate a functional interaction between TTP and BCR-ABL, followed by studying TTP's

relevance in CML. As the TTP-site also encompasses an AU-RE, it is also possible that other proteins that bind to AU-REs[197] may (also) be responsible for our proposed fine-tuning model.

The 96 nt region (840-935) was identified in the 3' mapping experiments (Fig 2.20, A). This region alone reduced Renilla expression by 30% (Fig 2.23, A), again validating the mapping experiments. Unlike the 142 region, there was no evidence from bioinformatics data that microRNAs interacted with the 96 nt region. There were two predicted RNA-binding sites within this region for NONO and SRFS13A (Table 2.18), but these proteins do not have a described role in RNA stability (as opposed to TTP). Therefore, investigation of these proteins was not prioritised. It would be of interest to determine the role of these proteins with respect to the *ABL1* 3'UTR in future work.

Our data regarding the first 840 nt of the 3'UTR showed that, alone this region had no effect on reporter expression (Fig 2.20, A), but deletion of this region from the full length 3'UTR increased the repressive activity of the remaining 3'UTR sequence (Fig 2.19, A). We propose that this region stabilises the repressive nature of the 3'UTR. The mapping experiments in the KCL-22 cell line provide further support for this model. In KCL-22 cells, the first 499 nt of the 3'UTR appear responsible for the 3'UTR having no repressive activity. Furthermore, the 1116-1257 repressive region is only active in KCL-22 in the absence of the first 499 nt. As previously discussed, our observations for the *ABL1* 3'UTR are remarkably similar to those from a study of the *HNF4α* 3'UTR[187]. However, in either case it is unknown which factors are involved. It is known that RNA-binding proteins and non-coding RNAs can inhibit interactions of microRNAs[198-201] and other proteins[102] with their targets. Therefore, this region may provide properties that alter accessibility of factors to the 3'UTR. Interestingly, RIP-SEQ data show that hnRNP-C binds within the first 500 nt (Fig 2.27, B). This protein is known to stabilise mRNA and promote translation[202-204]. A proposed mechanism for hnRNP-C is the inhibition of mRNA sequestration to P-bodies[203] (which repress translation, a mechanism associated with microRNAs[205]). This would be consistent with this region inhibiting a repressor. It is currently unknown if hnRNP-C regulates BCR-ABL expression and/or plays a role in CML. Another protein, ELAVL-1, has been shown to bind within the first 840 nt of the 3'UTR from RIP-SEQ data (Fig 2.27, B). ELAVL-1 is a protein known to interact with AU-REs[192] and enhance gene expression[206,207]. In CML, it has been reported that ELAVL-1 is upregulated in BC[197]. So if ELAVL-1 stabilises BCR-ABL,

this protein may play a role in the increase of BCR-ABL expression in BC-CML. Similar to TTP, the hnRNP-C and ELAVL-1 findings warrant further investigation to determine their relevance in CML.

The other region of interest was 1576-1992. This region alone had a repressive effect on reporter expression (Fig 2.19, A). There are a number of AGO hits throughout this region, in addition to ELAVL-1 and TIA-1/TIAL-1 (Fig 2.27, C-D). The AGO hits in conserved regions of the 3'UTR contain predicted binding sites for miR-30 and the miR-141/200 family (Fig 2.27, D). Chapter 3 describes our experiments to examine the function of these microRNAs against BCR-ABL. These experiments suggest that miR-30 and 141 did not functionally interact with *BCR-ABL*.

Luciferase reporter strategy for 3'UTR mapping

Although uncommon, there is a precedent to use a reporter-gene system to map regions of interest within the 3'UTR[187,208-211]. We expected that identifying key factor(s) involved in 3'UTR-mediated regulation of BCR-ABL would be made easier if we could focus on discrete regions rather than the entire 3'UTR. For example, we focused on miR-125 and TTP interactions with the 1116-1257 region based on 3' mapping experiments.

Some of the published studies combined their mapping experiments with a particular treatment or gene knockout. These examples also show future applications for our established 3'UTR mapping system for the *ABL1* 3'UTR. Wirsing, *et al.* coupled this approach with the knockdown of Dicer to provide evidence of microRNA interactions with regions of the 3'UTR[187]. Thomas, *et al.* used 3'UTR mapping experiments to identify a region of the *NKX3.1* gene that was responsible for changes in NKX3.1 expression following 5α-dihydrotestosterone treatment[208]. Yashiro, *et al.* performed a similar experiment to identify a region of the *LDLR* gene that was responsive to chenodeoxycholic acid (CDCA) exposure[210]. They then identified a protein that bound to the 3'UTR following CDCA treatment[210].

At present, the reporter-gene system is a simple but crude technique to identify regions of interest within a 3'UTR. As more RIP-SEQ mapping of microRNA and RNA-binding protein interactions becomes more widely available, it is possible that our luciferase data could assist in highlighting other functional interactions with *BCR-ABL*. It is also recommended to perform the Dicer knockout experiments to provide evidence for microRNA-mediated regulation of BCR-ABL. Although we are yet to go one level deeper in

terms of Dicer knockout or drug treatment, our luciferase data did yield some insights into the regions important for controlling BCR-ABL expression. We combined our luciferase data with published RIP-SEQ experiments to try and add an extra dimension to our results. This allowed for identification of TTP, hnRNP-C and ELAVL-1 as potential regulators of BCR-ABL.

3'UTR avoidance

We have shown that the *ABL1* 3'UTR strongly represses gene expression (Fig 2.15). Therefore, there is scope for 3'UTR avoidance to play a potent role in the regulation of *ABL1* 3'UTR-containing RNAs. Bioinformatics experiments failed to identify putative pseudogenes for *ABL1* (Fig 2.24), or an over-representation of CAGE-tags that are indicative of canonical-*ABL1* promoter-independent expression of the *ABL1* 3'UTR (Fig 2.25, A). We also conducted a pilot study to examine polymorphisms within the *ABL1* 3'UTR, but there was no striking SNP pattern found in the 10 CP-CML and 10 BC-CML patients analysed (most likely due to the low power of the experiment) (data not shown). Thus, these findings failed to uncover mechanisms for *ABL1* 3'UTR avoidance.

A shortened *ABL1* 3'UTR was found by 3'RACE, but it only accounts for 2% of *ABL1*-containing transcripts. Interestingly, based on RIP-SEQ data TIA-1 and TIAL-1 localise around the shortened-3'UTR splice sites, nt 328 and 1571 (Fig 2.27, B-C). These proteins have a well-known role in the regulation of splicing[212]. The RIP-SEQ data also show that ELAVL-1 and hnRNP-C co-localise with TIA-1 and TIAL-1 (Fig 2.26, A). This is of interest as Izquierdo has shown that ELAVL-1 is an antagonist of TIA-mediated splicing[213], and this antagonism is mediated by hnRNP-C[214]. This may explain why the splice event is rare. If this were the case for BCR-ABL, it would mean that ELAVL-1 and hnRNP-C would prevent 3'UTR shortening, and therefore prevent avoidance of repressors mapped in the spliced-out region. Monitoring the levels of the shortened *ABL1* 3'UTR following knockdown of ELAVL-1 and/or hnRNP-C would be one strategy to examine this further. This could also be coupled with actinomycin-D half-life experiments to determine if the shortened variant is more stable than the full length 3'UTR.

Although enhanced BCR-ABL expression is observed in CML (1.4.2), and this expression is advantageous for leukaemogenesis (1.4.3), we have not found evidence that

3'UTR avoidance is a major mechanism by which BCR-ABL expression is aberrantly controlled in CML.

MicroRNA regulation of the *ABL1* 3'UTR

Interestingly a number of hits for the AGO protein were found throughout the *ABL1* 3'UTR. MicroRNAs are specifically discussed in the next chapter (with the exception of miR-125, for which we did not find evidence for interaction with the 142 nt repressive region (Fig 2.22)). The majority of the AGO hits fell outside mapped repressive regions, or within stabilising regions (Fig 2.29). However, both the RIP-SEQ and luciferase experiments are limited to detection of endogenously expressed factors in the particular cell line.

Final remarks

From the data in this chapter, we conclude that the *BCR-ABL* 3'UTR is an important region that controls BCR-ABL expression. We show that this region strongly inhibits gene expression (Fig 2.15), and that the *BCR-ABL* 3'UTR is within a region that is known to dictate *BCR-ABL* mRNA stability (Fig 2.8). We then focused on characterising the function of the *BCR-ABL* 3'UTR by coupling 3'UTR mapping experiments with published bioinformatics and experimental data. These findings are illustrated in Fig 2.29. They identify a number of regions with regulatory potential within the 3'UTR, and shortlist TTP, hnRNP-C, ELAVL-1, TIA-1 and TIAL-1 as proteins which may play a role in the regulation of BCR-ABL expression via the *BCR-ABL* 3'UTR.

The next step in our experimental pipeline was to identify regulators responsible for the repressive nature of the *ABL1* 3'UTR. This key step would allow us to examine the significance of these regulators (and the 3'UTR itself) in CML. The five aforementioned shortlisted-proteins were identified only recently, and therefore we have yet to establish their importance in CML. However, we have been actively searching for regulators that interact with the 3'UTR. The next two chapters describe our approach to identify putative functional interactions of microRNAs (chapter 3) and RNA-binding proteins (chapter 4).

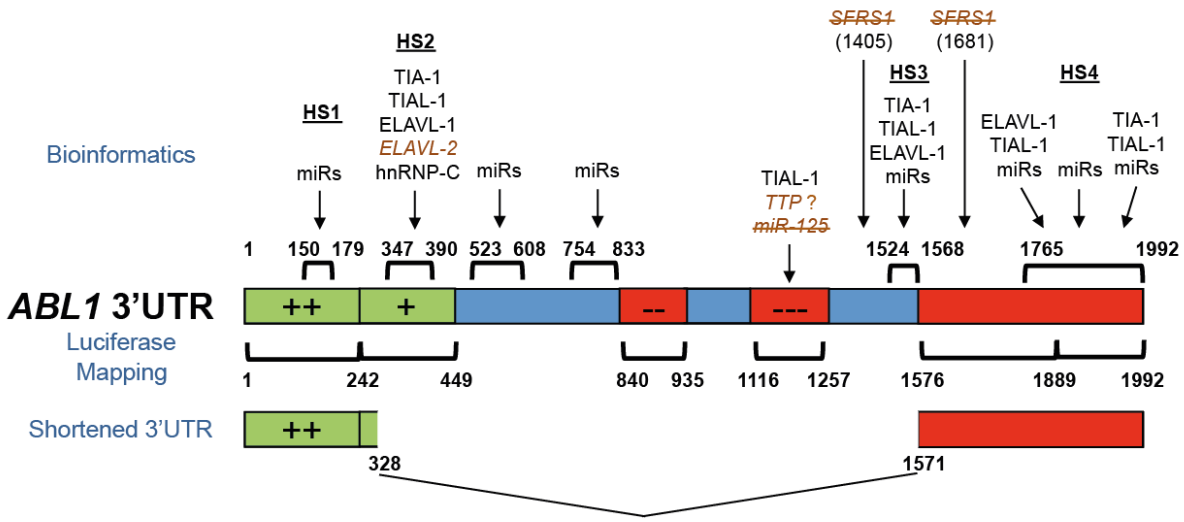

Fig 2.29: Characterisation of the *ABL1* 3'UTR. This diagram highlights key regions which were mapped to alter gene expression (green: activating regions, red: repressive regions). The shortened 3'UTR (identified in Fig 2.9) was displayed underneath the full length 3'UTR. Bioinformatics-evidence for *trans*-factor interactions are overlayed above the 3'UTR caricature, along with the hotspots for RIP-SEQ-mapped interactions (from Fig 2.27). *Trans*-factors in black text are from RIP-SEQ data, where as factors in brown are sequence-based predictions. Evidence against a particular interaction is denoted by strikethrough font. Numbers above the 3'UTR denote the position of the 3'UTR for putative factor-3'UTR interactions. Numbers below the 3'UTR denote the luciferase mapping boundaries. The number 1 relates to the first nucleotide of the *ABL1* 3'UTR.

Chapter 3

MicroRNA regulation of BCR-ABL

3.1 Introduction

3.1.1 MicroRNA

MicroRNAs are small, approximately 22 nt, non-coding RNAs that negatively regulate gene expression[140]. MicroRNAs interact with target mRNAs by Watson-Crick base pairing, subsequently causing destabilisation of the mRNA and/or reducing the rate of mRNA translation. It is predicted that microRNAs regulate around half of all coding genes in humans[215]. To date, there are over 1,500 microRNAs identified in humans[216]. Each of those microRNAs are expected to target hundreds of genes[217]. So it is of no surprise that microRNAs play a crucial and complex role in the regulation of gene-networks during development and disease.

MicroRNAs were first described in 1993[218,219]. Two groups simultaneously reported that expression of lin-*4*, a non-coding gene, repressed expression of the LIN-14 protein, a protein involved in *C. elegans* development. It was also noted that *lin-4* shared inverse homology to a repeated sequence in the *lin-14* 3'UTR. Furthermore, two transcripts were identified for *lin-4*, one was 61 nt in length (later termed 'pre-miRNA') and the other 22 nt (the mature microRNA). These studies also described the gradient-inverse expression profiles of *lin-4* and *lin-14*, which demonstrated a switch-like ability for microRNAs to govern organism development (Fig 3.1). Surprisingly, it was almost ten years later before the importance of microRNAs was discovered.[220]. Since then, their role in a wide range of species and during key developmental events has been well established[221].

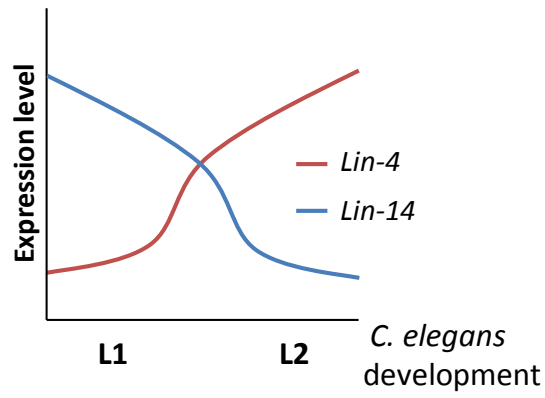

Fig 3.1: MicroRNAs govern key processes. The diagram above is an example for microRNA involvement in development. *Lin-4* expression gradually increases during the transition from first stage larva (L1) to second stage larva (L2) in *C.elegans*. This gradient expression profile controls the timing of the L1 to L2 transition, and maintains the silencing of lin-14 which is required for L2 transition[222].

Haemopoiesis is an example of one of the key events that are governed by microRNAs[223,224]. MicroRNAs help control cell-differentiation into the different haemopoietic compartments[223], as well as maintaining self-renewal capacity of HSCs and progenitor cells[225,226]. Disruption of this network has also been implicated in leukaemia[227], including CML[102,174,195,228-230]. From this knowledge there are only two studies describing microRNAs that control BCR-ABL: miR-203[173,174] and miR-451, 515 and 760[174]. There are however, proof-of-principle experiments to show that microRNA regulation of BCR-ABL can be used as a therapeutic strategy to tackle CML[114-121]. Therefore, we aimed to achieve a greater understanding about microRNAs that regulate BCR-ABL and explore their relevance in CML.

3.1.2 MicroRNA biogenesis

MicroRNA biogenesis and silencing of targets is a complicated process. This process differs between plant, mammals and lower species[231]. Within species there are also exceptions to the canonical pathway[102,232,233]. This section's aim is to provide a general overview for the mechanism of microRNAs in humans, and is summarised in Fig 3.2.

3.1.2.1 Transcription and export

A microRNA can exist in the genome as a classical gene – under the control of its own promoter[234], or located in intronic or exonic sequences of other genes[235]. There is also evidence that intragenic microRNAs have their own promoters[236]. In addition, a single transcript can harbour multiple microRNAs, for example the miR-17/92 cluster, which contains six microRNAs (miR-17, 18, 19a, 20a, 19b-1 and 92)[237].

MicroRNAs are processed from large RNAs to give rise to mature (functional) microRNAs. These larger RNA-species are called 'primary-microRNAs' (pri-miRNAs). RNA polymerase II is generally involved in pri-miRNA transcription[234]. If the pri-miRNA is transcribed by its own promoter, it will be 7-mG capped and polyadenylated[238]. Pri-miRNAs derived from introns are either spliced out to form the pri-miRNA, or processed by Drosha directly from pre-spliced RNA[239].

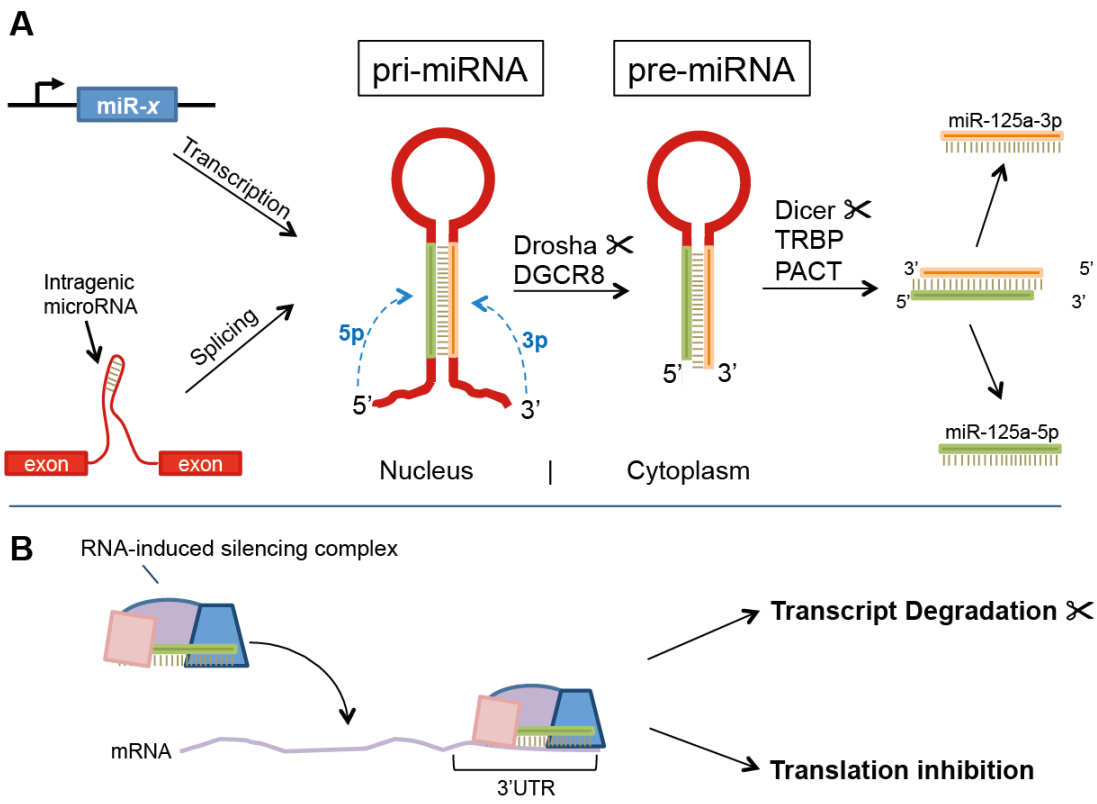

Fig 3.2: MicroRNA biogenesis and function. (**A**) MicroRNAs begin as a pri-miRNA following transcription, or after being spliced from an intron within another gene. The blue (5p) and (3p) denote naming of the mature microRNA. For example, the green strand, from the 5' "arm" of the stem-loop is termed 5p, where as the orange strand from the 3' "arm" is termed 3p. The stem-loop is cleaved by Drosha and DGCR8, giving rise to the pre-miRNA. The pre-miRNA is then exported into the cytoplasm where a Dicer/TRBP/PACT complex cleaves the loop, forming a duplex containing, in this example, miR-125a-3p and miR-125a-5p. Either strand is incorporated into the RISC to silence gene targets. (**B**) Following biogenesis, the mature microRNA, in complex with the RISC, interacts with mRNA via complementary base-pairing between the microRNA and mRNA. This leads to either degradation of the transcript, or silencing of translation, ultimately leading to the downregulation of protein expression.

Pri-miRNAs form a stem-loop structure encompassing the mature microRNA sequence. This structure is efficiently recognised by the microprocessor complex, comprising of Drosha (an RNase III endonuclease) and DiGeorge syndrome critical region 8 gene (DGCR8) (an RNA-binding protein)[240,241]}. The microprocessor cleaves 5' and 3' tails off the pri-miRNA stem-loop (Fig 3.2, A,[234,242]. This generates a 60-70nt RNA-hairpin with a 3' 2 nt overhang; termed the 'precursor microRNA' (pre-miRNA). The pre-miRNA is then exported into the cytoplasm by exportin-5 in a GTP-dependent manner[243].

3.1.2.2 Formation of the mature microRNA

Once in the cytoplasm, another RNase III endonuclease, Dicer, cleaves the loop region to form a microRNA duplex[244]. This step is dependent on Dicer forming a complex with HIV transactivating response RNA binding protein (TRBP) and protein activator of PKR (PACT)[245-249]. Each strand of the microRNA duplex is now the size of the mature microRNA (~22 nt) and has a 2 nt 3' overhang.

TRBP is also responsible for recruitment of Argonaute2 with Dicer and the microRNA duplex[248]. Only one of the strands of the microRNA duplex (guide strand) is incorporated into the AGO2-driven RNA-induced-silencing complex (RISC). The determinant of strand selection is poorly understood. It is thought that the selection is based on thermodynamic stability and microRNA-sequence[250,251], and in certain cases it can be cell-specific[252].

3.1.2.3 MicroRNA modus operandi

A key consideration for microRNA silencing is that some microRNA interactions destabilise target mRNAs, while other microRNA-mRNA interactions only inhibit protein expression (Fig 3.2, B;[141]). However, the exact mechanism of microRNA silencing remains controversial. There are a number of hypotheses that explain microRNA-mediated gene silencing, for example, mRNA deadenylation[253,254], recruitment of the RISC bound mRNA to processing-bodies (P-bodies)[255], and disruption of the 7mG cap-polyA tail interaction[256].

3.1.2.4 MicroRNA seed sequence

Interaction between bases 2-7 of the microRNA and the mRNA target are critical for a functional microRNA-mRNA interaction (Fig 3.3, A;[217]). This region of the microRNA is called the seed sequence (see 3.3.1). There are a number of canonical seed sequence types which are considered in microRNA target prediction programs. These include: 7mer-A1, 7mer-m8 and 8mer[217] (Fig 3.3, B). The A1 refers to an adenosine in the 3'UTR opposite to position 1 of the microRNA (Fig 3.3, B). The over-representation of this adenosine is predictive of *bone fide* binding sites[257]. The m8 refers to a Watson-Crick base pairing at position 8 of the microRNA and 3'UTR.

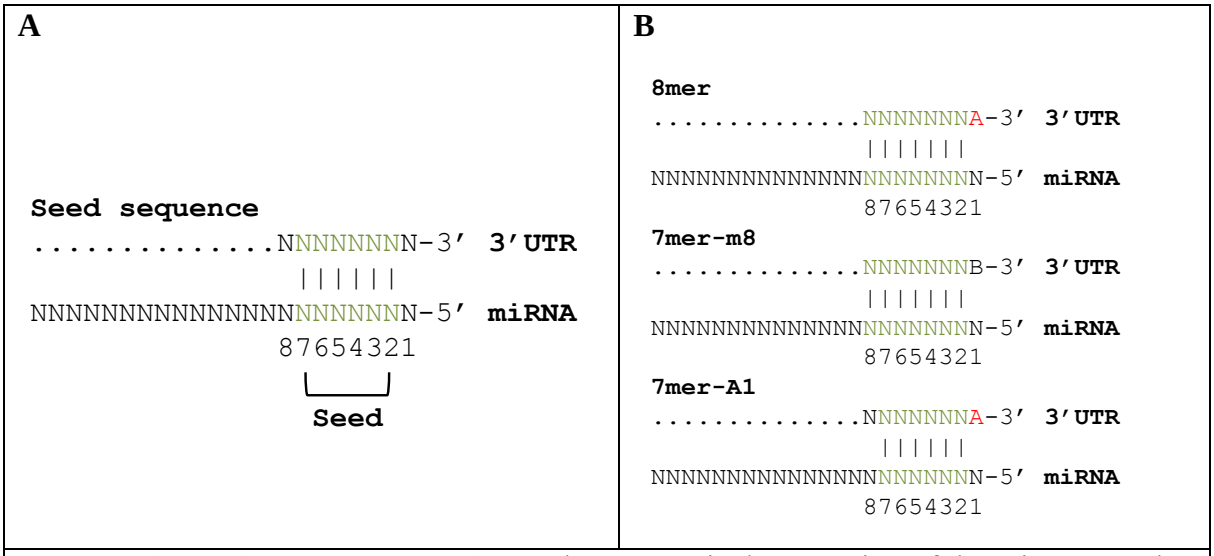

Fig 3.3: The seed sequence. (**A**) The seed sequence is the 5' region of the microRNA that has 100% complementarity between positions 2 to 7 (or 8) of the microRNA and the target mRNA. This region is essential for a functional microRNA:mRNA interaction. (**B**) The three main seed-sequence types are: 8mer (7 bp seed with an adenosine adjacent to position 1 of the microRNA, 7mer-m8 (7 bp seed without the adjacent adenosine) and 7mer-A1 (6 bp seed with the adjacent adenosine). B = C, G or U.

3.1.2.5 Nomenclature

The nomenclature for microRNAs was outlined in 2003[258]. MicroRNAs are almost always named using the "miR-" prefix followed by a number. Exceptions include *lin-* and *let-* which were named before microRNAs were defined. The species code is also added before the miR prefix, e.g. hsa-miR-1 (human microRNA-1), mmu-miR-1 (mouse microRNA-1), and the numbering across species is generally informative of orthologous microRNAs. However, in this thesis only human microRNAs are referred to, and thus the species code is omitted.

MicroRNAs sharing identical seed sequences, but differing in 3' sequence share the same number; a letter following the number is used to differentiates the two microRNAs. For example, miR-29a and miR-29c have an identical seed sequence, but differ by one nucleotide. The tenth base is either a C (miR-29a) or a U (miR-29c). MicroRNAs with identical mature sequences, but at different chromosomal locations are identified with a hyphen-separated number, e.g. miR-196a-1 and miR-196a-2. Finally, -5p and -3p are identifiers of the strands in the microRNA duplex (see Fig 3.2).

3.1.2.6 MicroRNA target prediction

A number of algorithms have been developed in order to predict mRNA-microRNA interactions. These programs are freely available via the internet. In our study, we primarily used the program TargetScan (www.targetscan.org), but we also used the MicroCosm (www.ebi.ac.uk/enright-srv/microcosm/), miRanda (www.microrna.org) and DIANA LAB (http://diana.cslab.ece.ntua.gr) programs to compare with TargetScan (Appendix C). The programs can predict mRNA targets for a particular microRNA, or microRNA targets of a 3'UTR.

Targetscan[257,259] searches for 7mer or 8mer microRNA sites (Fig 3.3, B) within 3'UTRs. Predictions are ranked by species conservation (of the site), number of sites for a particular microRNA, the type of site (7mer or 8mer), local AU content, and position within the 3'UTR. miRanda[260] predicts sites based on microRNA-mRNA complementarity, thermodynamic folding of the duplex, and cross-species conservation in addition to 'likelihood of mRNA downregulation' or mirSVR score[261]. The mirSVR score was determined by a series of experiments which assessed mRNA expression changes following a particular microRNA's induction and adds an interesting parameter to this algorithm. The DIANA-mT[262] algorithm looks for 7-9mer sites from the first or second nucleotide at the 5' end of the microRNA. These sites are ranked by microRNA-mRNA complementarity, cross-species conservation, and considers a unique signal-noise-ratio factor. The signal-noise-ratio involves a mock microRNA, which is an artificial microRNA sequence that is predicted to interact with a similar number of targets as the microRNA in question and is used to calculate precision and false-discovery rates. MicroCosm[263] predictions are ranked by microRNA-mRNA complementarity, thermodynamic folding of the duplex, and cross-species conservation.

3.1.2.7 MicroRNAs in haemopoiesis

Human and mouse models of haemopoiesis have highlighted a key role for microRNAs within this process. Some of the microRNA network is outlined below (Fig 3.4). Self-renewal capacity of haemopoietic stem cells involves miR-29 and miR-125 by promoting cell proliferation and inhibiting apoptosis respectively[225,226]. The differentiation of progenitor cells is in part controlled by miR-15a and miR-155[264,265]. MicroRNAs have also been shown to direct terminal differentiation. Expression of miR-150 directs megakaryocyte-erythroid

progenitors into megakaryocytes[266], and miR-223 blocks GMP differentiation into granulocytes and monocytes[267].

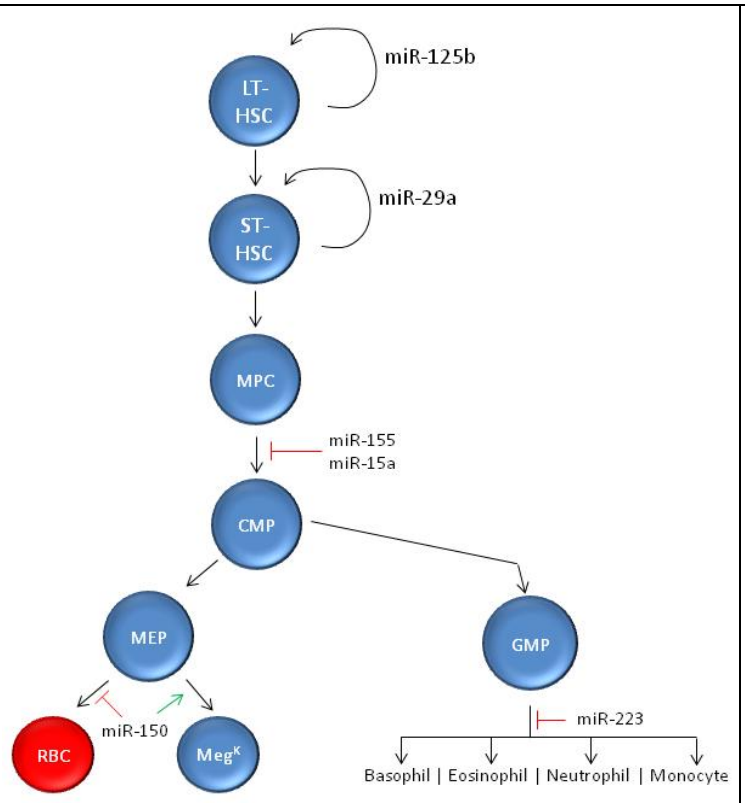

Fig 3.4: Examples of microRNA involvement in haemopoiesis. Critical stages of haemopoiesis require microRNAs. A few examples include microRNAs involved in stem cell maintenance (miR-29a, 125b), differentiation arrest (miR-155, 15a), as well as directing terminal differentiation (miR-10, 223). LT-HSC, long-term haemopoietic stem cell. ST-HSC, short-term haemopoietic stem cell. MPC, multipotent progenitor cell. CMP, common myeloid progenitor. MEP, megakaryocyte-erythroid progenitor. GMP, granulocyte-macrophage progenitor. RBC, red blood cell. Meg^K, Megakaryocyte.

3.1.2.8 Leukaemia

The complex microRNA network in haemopoiesis allows for intricate control of cell lineage fate. On the other hand, disruption of this network can result in leukaemia. Aberrant expression of microRNA in leukaemia not only correlates with leukaemic phenotype[227], but can also correlate with disease stage or prognosis[268-270]. Chronic lymphoid leukaemia (CLL) and 5q- syndrome (a subtype of myelodysplastic syndrome) both feature altered microRNA expression. In CLL, a chromosomal deletion containing the microRNA-15a and miR-16-1 genes is responsible for the de-regulation of BCL2 expression, which is important for the pathogenesis of CLL[271]. 5q- syndrome is characterised by an interstitial deletion in chromosome 5, resulting in the loss of miR-145 and 146a. The loss of these microRNAs in a mouse-model recapitulated some of the key events that occur in 5q- syndrome, outlining their importance in this disease[272]. Another example is the miR-17/92 cluster, comprised of six

microRNAs on a poly-cistronic transcript. Expression of these microRNAs is frequently disrupted in disease, including B-cell lymphoma[273], AML[274], and CML[228]. The miR-17/92 cluster is known to play a role in regulating genes involved in proliferation and apoptosis[274,275], and can act as a tumour suppressor or an oncogene[276].

3.1.2.8.1 MicroRNAs and CML

To date, there is limited knowledge regarding microRNA involvement in CML. MicroRNA profiling has been performed comparing progenitor and mononuclear cells from CML patients[277], CP *vs.* BC[229] and response to therapy[229,230]. A few studies have also investigated microRNA function in the context of CML.

The majority of the functional work has centred on microRNAs regulated by BCR-ABL. Venturini, *et al.* found that upregulation of the miR-17/92 cluster is regulated by BCR-ABL (via Myc)[228]. The expression of these microRNAs was increased in CML cell lines and patient samples[228]. They also showed that these microRNAs increase proliferation of CML cell lines. Suresh, *et al.* demonstrated that downregulation of BCR-ABL by silencing RNA (siRNA) or kinase inhibition by imatinib reduced miR-130a/b expression[195]. These microRNAs downregulate CCN3 expression[195] (CCN3 negatively regulates cell proliferation). Similarly, Lopotová, *et al.* observed a reduction of miR-451 expression upon BCR-ABL kinase inhibition with imatinib[278]. This was of interest because miR-451 may target BCR-ABL expression[174], and miR-451 expression inversely correlated with BCR-ABL expression[229]. Ering, *et al.* showed that BCR-ABL levels inversely correlated with miR-328, with a relationship that higher levels of BCR-ABL and loss of miR-328 expression promoted differentiation arrest – important in blast crisis[102]. Agirre, *et al.* found a decrease of miR-10a levels in CML mononuclear and CD34+ cells[277]. It was further shown that loss of miR-10a can increase cell proliferation of CML cell lines[277].

More relevant to BCR-ABL regulation, Bueno, *et al.* reported that miR-203 directly controlled the expression of BCR-ABL[173]. Their data suggest that over-expression of miR-203 halted proliferation of CML cell lines via inhibition of BCR-ABL expression[173]. In addition, they examined methylation of miR-203, observing that miR-203 was epigenetically silenced in CML patient cells[173]. Because miR-203 was predicted by TargetScan to interact with the *BCR-ABL* 3'UTR, our laboratory also investigated this microRNA. We attempted to replicate their results (to serve as a positive control), however the results from our laboratory

were contradictory to the Bueno, *et al.* findings (3.4.2.2 and 3.4.3.3). Another group reported in an abstract that miR-203/451/515-3p/760 can interact with the *BCR-ABL* 3'UTR, reducing BCR-ABL protein levels[174]. These microRNAs were predicted by another bioinformatics program, mirBASE. However, the data for those findings are yet to be published in a peer-reviewed journal.

A number of proof-of-principle experiments have been performed to highlight the functional relevance of identifying microRNAs that target BCR-ABL. McLaughlin, *et al.* have demonstrated that miRNA-mimics designed to bind to BCR-ABL can reduce BCR-ABL protein levels, and increase survival of mice injected with BCR-ABL+ tumours[121]. In addition, siRNA molecules against BCR-ABL have been used in an attempt to treat a CML patient. The siRNAs reduced BCR-ABL levels initially, but the patient generated (immunological) resistance to the siRNAs upon repeated administration[118,120]. There is a current desire to establish microRNA-based therapeutics[279-281]. Therefore, these experiments provide a rationale to include BCR-ABL targeting in such pipelines.

3.2 Methods

3.2.1 Bioinformatics prediction of microRNA interactions with *ABL1*

Targetscan v4.2, v5.0 and v6.0 was used for prediction of microRNA binding sites within the *ABL1* (and thus *BCR-ABL*) 3'UTR. MicroRNAs were selected based on predicted binding sites within species-conserved regions of the *BCR-ABL* 3'UTR, and the conservation of the microRNA itself across species.

3.2.2 Cell culture

KYO-1, KCL-22, K-562, HL-60, 293T and HeLa cells were cultured as per Appendix A.14.

3.2.3 Luciferase reporter system for screening putative microRNA interactions with the *BCR-ABL* 3'UTR

The microRNA binding sites predicted by TargetScan were cloned downstream of the *Renilla* luciferase gene in pCIneo-hRL. An initial cell-line based luciferase screen looked for evidence of microRNA-binding site interactions. Thereafter, the binding site was deleted to provide further evidence that the microRNA specifically interacted with its predicted site.

3.2.3.1 Construction of luciferase reporters

3.2.3.1.1 PCR

Putative microRNA binding sites (and ~100 nt either side) were amplified by PCR using the Phusion® High-Fidelity DNA Polymerase. The PCR was setup according to Appendix A.2 using phRL-ABL1 3'UTR as a template, and the primers in Table 3.1. PCR conditions were: 96^{o}C for 30 sec, then 30 cycles of 96^{o}C for 10 sec, 55^{o}C for 15 sec, and 72^{o}C for 15 sec; then 72^{o}C for 10 min.

Table 3.1: Primers used to amplify putative microRNA binding sites in the *ABL1* 3'UTR

Luciferase construct	**Sequence** (5' – 3') (Upper line: forward primer; Lower line: reverse primer)
Renilla-miR29 (551-711)*	CATGCA**TCTAGA**TGGTCACTCTGCCC ACAGAT**TCTAGA**ACATGCCCATGCC
Renilla-miR30 (1890-1992)	TCTGCT**TCTAGA**GGTCCAGTGCATTTTG ATCTGC**TCTAGA**TTCTAATGTAAACACTGATTTATTTA
Renilla-miR196 (0-225)	GTGCAG**TCTAGA**CAGCAGTCAGGGGTCAGGTG ACAGAT**TCTAGA**CGAGGACAGAGAC
Renilla-miR203 (993-1123)	CCCTCC**TCTAGA**CCCACTCCTCTAAGACAAAG GCAGGT**TCTAGA**TGGCAGCTCTATTCTCTCTC
*Xba*I restriction site in bold *Numbers in parentheses refer to the region of the *ABL1* 3'UTR amplified.	

3.2.3.1.2 Restriction digest

For each binding site, *Xba*I (8 U) was added to 80 µL of the PCR product from 3.3.2.1.1, in 1x NEB buffer 4 and 1 x BSA. The reaction was incubated at 37^{o}C for 2 h. For the pCIneo-hRL vector backbone, *Xba*I (4 U) was added to 2 µg of pCIneo-hRL in 1x NEB buffer 4, 1 x BSA and made up to 20 µL with water. The reaction was incubated at 37^{o}C for 2 h. To remove phosphates from the vector backbone following digestion, 10 U of CIP was added to the reaction, which was incubated at 37^{o}C for a further 15 min.

3.2.3.1.3 Cloning procedure

Following digestion, the vector backbone DNA and PCR products (containing each putative binding site) were gel purified as per Appendix A.9. The PCR products were separately

ligated into the *Xba*I site in pCIneo-hRL as per Appendix A.10 and then transformed into electrocompetent cells as per Appendix A.11.

Desired clones were obtained using the DNA plasmid prep method (Appendix A.13)**.** The presence and orientation of the binding site were confirmed by sequencing (see Appendix A.4). Following sequence confirmation, bulk quantities of desired clones were obtained using the HiSpeed® Plasmid Midi Kit according to the manufacturer's instructions.

3.2.3.1.4 Mutagenesis of predicted microRNA binding sites

Deleting the putative binding site downstream of *Renilla* demonstrates that the microRNA specifically interacts with its predicted binding site within the *ABL1* 3'UTR. PCR mutagenesis was used to remove the binding site as per Appendix A.3, using the primers in Table 3.2.

Table 3.2: Primers used for mutagenesis of putative microRNA binding sites

Luciferase construct	**Sequence** (5' – 3') (Upper line: forward primer; Lower line: reverse primer)
Renilla-miR29del	GGATGGTTGGCTTTCTGTTTTCCACCCAAATCAA TGGGTGGAAAACAGAAAGCCAACCAGCCTTTGG
Renilla-miR30del	CTGTAGTATTTTTTAAATAAATCAGATTAGAGCGGCCGCTTCCC GGGAAGCGGCCGCTCTAATCTGATTTATTTAAAAAATACTACAG
Renilla-miR196del	GCCCTGTGGAGTCCAGCTCTACGTTTGCACC GGTGCAAACGTAGAGCTGGACTCCACAGGGC
Renilla-miR203del	CACTTTTCTGAGTTCTTGAAGAAAGCCCTGCCTCTGTGTAGCCG ACACAGAGGCAGGGCTTTCTTCAAGAACTCAGAAAAGTGAAGGC
Binding site deletion junction underlined	

3.2.3.2 Transient transfection (Lipofectamine)

HeLa cells (10^5/mL/well) were seeded in 24-well plates 18 h prior to transfection. The luciferase constructs and Pre-miRs were transfected into HeLa cells using the Lipofectamine transfection reagent at a ratio of 3:1 (lipid:DNA) according to the manufacturer's instructions. Each well contained: 3.2 fmol of the Renilla construct, 500 ng of pGL3 (Firefly luciferase, used as a loading control), and the DNA amount made up to 1µg with pUC19 and, if present, microRNA. Each transfection was carried out in quadruplicate. Cells were harvested 24 h

post-transfection and luciferase readings obtained as per Appendix A.15. Statistical analysis was carried out using the one-tailed t-test with GraphPad Prism® 5 software.

3.2.3.3 Transient transfection of K-562 cells with microRNA mimics

K-562 cells ($5x10^5$/mL/well) were seeded in 12-well plates 18 h prior to transfection. Ten and one-hundred millimoles of Cy3 labelled Pre-miR™ (Ambion), miR-141 miRNA mimic (GenePharma, Shanghai, China), or negative control miRNA (GenePharma) were transfected into K-562 cells using X-tremegene™-HP (3 μL) according to the manufacturer's instructions. Cells were harvested 48 h post-transfection and BCR-ABL/Actin expression determined as per 2.2.6 (chapter 2, pg 44). The GenePharma miRNAs were kindly provided by Dr. Cameron Bracken (Centre for Cancer Biology, Adelaide).

3.2.4 MicroRNA over-expression in CML cell lines

Stable over-expression of miR-196b was established in the KYO-1, KCL-22 and HL-60 cell lines. Protein samples for the following cell lines were kindly provided by Dr. Duncan Hewett:

K-562/29a	K-562/29b_1	K-562/29b_2	K-562/29c	K-562/30a
K-562/30b	K-562/30c_1	K-562/30c_2	K-562/30d	K-562/30e

3.2.4.1 MicroRNA expression constructs

Mammalian expression vectors containing miR-29b-1 (chromosome 7) or miR-29b-2 (chromosome 1) were constructed in order to over express these microRNAs in the K-562 cell line. The cloning method was based on that described on 3.2.3.1. The mature microRNA sequence (and 200 nt either side) was amplified by PCR using primers in Table 3.3, and cloned into the *Bam*HI and *Eco*RI sites in pBABE-puro (Fig 3.5, A).

A miR-196b expression vector was also made based on the method in 3.3.2.1. The mature microRNA sequence ± 200 nt was amplified by PCR using primers in Table 3.3, and cloned into the *Not*I and *Eco*RI sites in pMSCV-gfp-puro (Fig 3.5, B). The GFP cassette allowed for GFP selection of microRNA induced cells.

Table 3.3: Primers used to clone miR-29b-1, 29b-2, 196a-1 and 196b into mammalian expression vectors.

microRNA expression construct	**Sequence** (5' – 3') (Upper line: forward primer; Lower line: reverse primer)
pBABE-puro-miR29b_1	TCTCCC**GGATCC**AACAAATTCAGTGACATCAG GTGCAG**GAATTC**GACTGCCATTTGTGATATAT
pBABE-puro-miR29b_2	AGCATC**GGATCC**GCCTTTCATGTTGCCTTGTG ACCTCT**GAATTC**GCTCAAGCCACTGTGTTTAT
pMSCV-puro-gfp-miR196b†	CTGCAAGATTTGGGAAAGCG CCAGCCTTACAAGAGAATGG
Restriction sites in bold. †microRNA-196b genomic DNA contains endogenous *Not*I and *Eco*RI sites and thus are not included in the primer.	

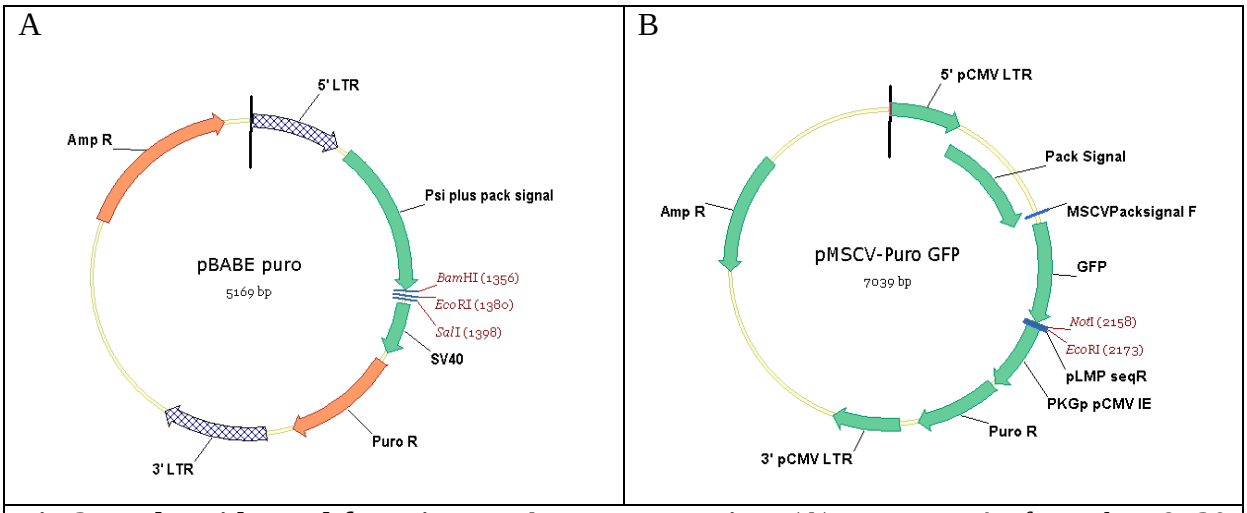

Fig 3.5: Plasmids used for microRNA over-expression. (**A**). MicroRNAs from the 29, 30 and 203 families were cloned into the *Bam*HI and *Eco*RI restriction sites of pBABE-puro. (**B**) MiR-196b was cloned into the *Not*I and *Eco*RI restriction sites of pMSCV-Puro-GFP located immediately downstream of the GFP open reading frame. Plasmid maps drawn using Vector NTI® software.

3.2.4.2 Cell line over-expression

3.2.4.2.1 Over-expression of miR-196b

Stable over-expression of miR-196b was established in the KYO-1, KCL-22 and HL-60 cell lines via retroviral transduction. These cell lines were named: KYO-1/196b, KCL-22/196b and HL-60/196b. The parental cell lines were also transduced with the parental pMSCV-gfp-puro plasmid as a transduction control. These cell lines were named: KYO-1/GFP, KCL-22/GFP and HL-60/GFP.

For production of viral supernatant, 293T cells (10^5/2mL/well) were seeded in 6-well plates the day before transfection. One microgram of pMSCV-puro-gfp-miR196b or pMSCV-gfp-puro, and packaging vector pCI-ampho (1 µg) were transfected into 293T cells using FuGene® 6 at a ratio of 3:1 (lipid:DNA), according to the manufacturer's instructions. The following day, the supernatant was replaced with fresh media. On day 2 post-transfection, the (viral) supernatant was aspirated and filtered through a 0.42 µm filter (Millipore), and stored at -80^{o}C.

For stable cell line establishment, 10^6 cells were resuspended in retrovirus supernatant (2 mL), placed into one well of a 6-well plate, then spinfected (320g, 45 min). Following the spin, fresh media (1 mL) was added and cells returned to 37^{o}C/5% CO_2. Three days post-spinfection, transduced cells were selected based on GFP expression using the Aria™ cell sorter (Becton Dickinson Aria), with FACSDiva™ Software version 6.1.3 (BD Biosciences, San Diego, CA, USA). Cells were then cultured in the presence of puromycin (Sigma) (1 µg/mL).

3.2.5 MicroRNA expression analysis

MicroRNA over-expression in the transduced cell lines was confirmed by qRT-PCR. RNA isolation was carried out as per Appendix A.5**,** and the yield determined using the NanoDrop™ 1000 spectrophotometer. Unless otherwise stated, harvesting of cells for microRNA expression analysis was done 6 days after selection (the last time point in the proliferation work). *RNU6B*, a small RNA, was used as a housekeeping gene for microRNA expression.

3.2.5.1 cDNA synthesis

Each small RNA has a unique stem-loop primer for cDNA synthesis (Fig 3.6). Therefore, a separate cDNA reaction is required for each RNA sample. Each cDNA synthesis reaction contained 100 ng RNA template, and was synthesised using the TaqMan® MicroRNA Reverse Transcription Kit, with TaqMan® small RNA assay: RT primers, according to the manufacturer's instructions (Applied Biosystems). Each TaqMan® small RNA assay contains the 5x RT (reverse transcription) primer mix, and 20x real-time mix. The assay part numbers for all of the assays are in Appendix A.8.

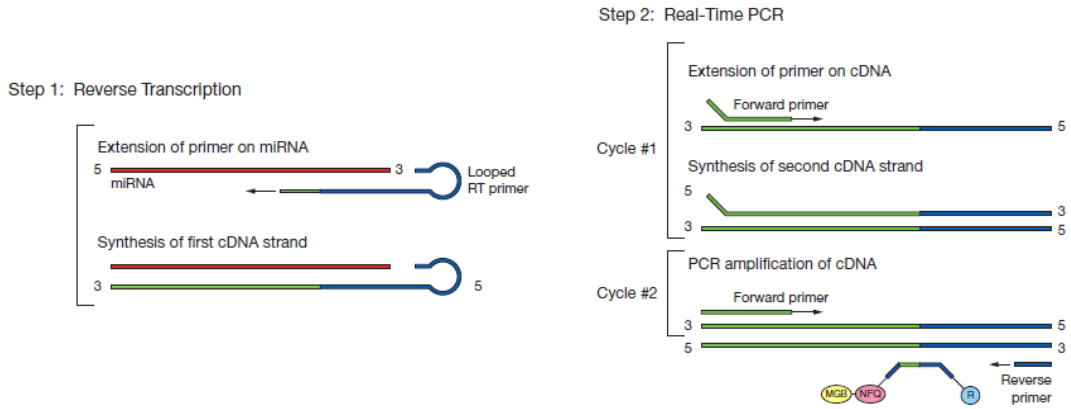

Fig 3.6: MicroRNA-cDNA synthesis and qRT-PCR. MicroRNAs are much smaller in length than coding genes, and therefore require alternative methods for qRT-PCR. Firstly, a microRNA-specific looped RT primer is used in cDNA synthesis (left). This requires a separate cDNA synthesis step for each microRNA to be quantified in a sample, using a different primer for each microRNA. The 3' end of the stem-loop primer binds to the microRNA, and then first cDNA strand synthesis is performed extending the primer until the 5' end of the microRNA. The resultant product is a primer-microRNA sequence hybrid, which is the required length for amplification using TaqMan® PCR, and specific for each microRNA. The qRT-PCR itself (right) is identical to standard qRT-PCR for coding genes. The assay is designed so that the probe binds to the junction of the primer-microRNA cDNA product, and is flanked by forward and reverse primers. This method is also used to quantify small RNAs, for example the *RNU6B* small RNA endogenous control. Image obtained from the Applied Biosystems website (www.appliedbiosystems.com) and used with permission (Appendix D).

3.2.5.2 Small RNA quantification

Quantification of microRNAs and *RNU6B* was performed using Taqman® small RNA assay: real-time reagents, and the TaqMan® universal mastermix II (Applied Biosystems). Each PCR was carried out in triplicate according to the manufacturer's instructions. The PCR was performed on the ABI 7900HT machine using SDS 2.3 software (Applied Biosystems) and the $\Delta\Delta C_T$ method. PCR data from the 7900HT machine was analysed using SDS 2.3 and RQ manager 1.2 software (Applied Biosystems).

3.2.6 Protein expression analysis

BCR-ABL and actin expression was quantified by Western blotting as per chapter 2: 2.2.6, pg 44.

3.2.7 Proliferation assays

Immediately after FACS sorting based on GFP expression, microRNA over-expressing or empty-vector control cell lines were seeded at 50,000 cells per well (2 mL), in 24-well plates in triplicate. Three hours after seeding, the day-0 time point for cell proliferation was obtained for each well (in triplicate) using the Cell-Titer-Glo® assay system (Promega) according to the manufacturer's instructions. Assays were read on the GloMax®-Multi Microplate Multimode Reader (Promega), using the Cell-Titer-Glo program. Cell proliferation was measured every 24 h for the next 6 days.

3.3 Results

3.3.1 Bioinformatics

We initially used TargetScan 4.2 to predict microRNAs targeting the *BCR-ABL* 3'UTR. The software predicted three species-conserved microRNA families that interacted with species-conserved regions of the *BCR-ABL* 3'UTR. These were: miR-29a/b/c, miR-203, and miR-30a/b/c/d/e (Fig 3.7). Subsequent versions of TargetScan revised predictions for the *BCR-ABL* 3'UTR. TargetScan 5.0 (no longer retrievable) added miR-196a/b, and removed the miR-29 family. The miR-29 family was removed from that database because the binding site was no longer considered to reside in a species conserved region of the 3'UTR.

TargetScan
Prediction of microRNA targets
Release 4.2: April 2008

Human ABL1 3' UTR

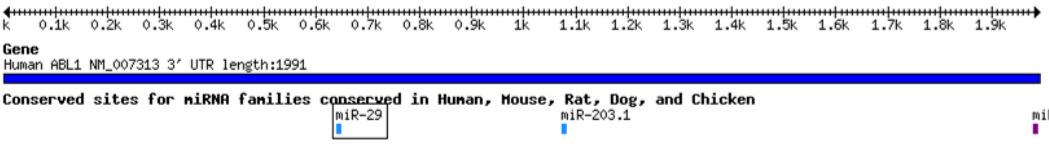

TargetScanHuman
Prediction of microRNA targets
Release 6.0: November 2011

Human ABL1 3' UTR

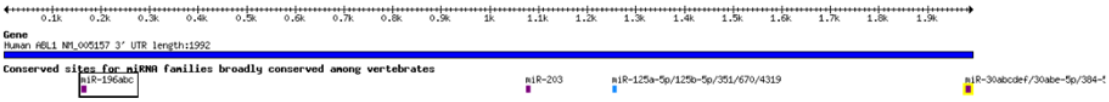

	predicted consequential pairing of target region (top) and miRNA (bottom)	seed match	site-type contribution	3' pairing contribution	local AU contribution	position contribution	TA contribution	SPS contribution	context+ score	context+ score percentile	conserved branch length	PCT
Position 161-168 of ABL1 3' UTR hsa-miR-196b	5' ...GUGGAGUCCAGCUCUACUACCUA... 3' GGGUUGUUGUCCUUUGAUGGAU	8mer	-0.247	-0.008	0.073	-0.074	-0.046	-0.013	-0.32	94	1.874	0.64
Position 161-168 of ABL1 3' UTR hsa-miR-196a	5' ...GUGGAGUCCAGCUCUACUACCUA... 3' GGGUUGUUGUACUUUGAUGGAU	8mer	-0.247	0.003	0.073	-0.074	-0.046	-0.013	-0.30	93	1.874	0.64
Position 640-646 of ABL1 3' UTR hsa-miR-29b	5' ...UUGGGUGGAAAACAGGGUGCUAA... 3' UUGUGACUAAAGUUUACCACGAU	7mer-1A	-0.074	0.004	0.009	0.020	-0.002	-0.066	-0.11	39	1.003	< 0.1
Position 640-646 of ABL1 3' UTR hsa-miR-29c	5' ...UUGGGUGGAAAACAGGGUGCUAA... 3' AUUGGCUAAAGUUUACCACGAU	7mer-1A	-0.074	0.004	0.009	0.020	-0.002	-0.066	-0.11	39	1.003	< 0.1
Position 640-646 of ABL1 3' UTR hsa-miR-29a	5' ...UUGGGUGGAAAACAGGGUGCUAA... 3' AUUGGCUAAAGUCUACCACGAU	7mer-1A	-0.074	0.004	0.009	0.020	-0.002	-0.066	-0.11	39	1.003	< 0.1
Position 1074-1081 of ABL1 3' UTR hsa-miR-203	5' ...UCUGAGUUCUUGAAGCAUUUCAA... 3' GAUCACCAGGAUUUGUAAAGUG	8mer	-0.247	0.003	0.060	0.116	0.051	0.105	> -0.03	23	1.227	0.21
Position 1253-1259 of ABL1 3' UTR hsa-miR-4319	5' ...GUUCUGUGGGGGUCAUCAGGGAG... 3' CACCGAAACGAGUCCCU	7mer-1A	-0.074	-0.009	0.050	0.030	0.013	-0.065	-0.06	25	1.672	0.52
Position 1253-1259 of ABL1 3' UTR hsa-miR-125a-5p	5' ...GUUCUGUGGGGGUCAUCAGGGAG... 3' AGUGUCCAAUUUCCCAGAGUCCCU	7mer-1A	-0.074	-0.002	0.050	0.030	0.013	-0.065	-0.05	24	1.672	0.52
Position 1253-1259 of ABL1 3' UTR hsa-miR-125b	5' ...GUUCUGUGGGGGUCAUCAGGGAG... 3' AGUGUUCAAUCCCAGAGUCCCU	7mer-1A	-0.074	-0.002	0.050	0.030	0.013	-0.065	-0.05	23	1.672	0.52
Position 1979-1986 of ABL1 3' UTR hsa-miR-30e	5' ...UUUUAAAUAAAUCAGUGUUUACA... 3' GAAGGUCAGUUCCUACAAAUGU	8mer	-0.247	-0.008	-0.036	-0.113	0.015	0.096	-0.29	97	2.249	0.88
Position 1979-1986 of ABL1 3' UTR hsa-miR-30a	5' ...UUUUAAAUAAAUCAGUGUUUACA... 3' GAAGGUCAGCUCCUACAAAUGU	8mer	-0.247	0.013	-0.036	-0.113	0.015	0.096	-0.27	97	2.249	0.88
Position 1979-1986 of ABL1 3' UTR hsa-miR-30d	5' ...UUUUAAAUAAAUCAGUGUUUACA... 3' GAAGGUCAGCCCCUACAAAUGU	8mer	-0.247	0.013	-0.036	-0.113	0.015	0.096	-0.27	97	2.249	0.88
Position 1979-1986 of ABL1 3' UTR hsa-miR-30b	5' ...UUUUAAAUAAAUCAGUGUUUACA... 3' UCGACUCACAUCCUACAAAUGU	8mer	-0.247	0.024	-0.036	-0.113	0.015	0.096	-0.26	95	2.249	0.88
Position 1979-1986 of ABL1 3' UTR hsa-miR-30c	5' ...UUUUAAAUAAAUCAGUGUUUACA... 3' CGACUCUCACAUCCUACAAAUGU	8mer	-0.247	0.024	-0.036	-0.113	0.015	0.096	-0.26	95	2.249	0.88

Fig 3.7: MicroRNA-*ABL1* 3'UTR interactions as predicted by TargetScan (from previous page). Targetscan v4.2 and 6.0 (www.targetscan.org) were used to predict microRNA interactions with the *ABL1* 3'UTR. Predictions were restricted to interactions with species-conserved regions of the *ABL1* 3'UTR, by species-conserved microRNAs. TargetScan v4.2 predicted three putative microRNA-*ABL1* interactions: miR-29, 203 and 30. A new version of TargetScan v 6.0 predicted miR-196, 203, 125 and 30. TargetScan software also shows the predicted base-pairing between the microRNA and *ABL1*; this is shown below for all five microRNAs predicted in either TargetScan release. The entire table was included for completeness, however except the 'seed match' column, the other columns are not discussed (the TargetScan website provides detailed explanations of the other columns).

The latest version of TargetScan (6.0) added hsa-miR-125a-5p, hsa-miR-125b and hsa-miR-4319 (Fig 3.7). Of interest, all of the predicted sites in the 3'UTR have an adenosine adjacent to position one of the microRNA, which is over-represented in microRNA binding sites (see 3.2.1.1.4).

In addition to the species-conserved microRNAs interacting with species-conserved regions of the *ABL1* 3'UTR, TargetScan v.6.0 predicts over 300 microRNA binding sites in non-species conserved regions of this 3'UTR.

3.3.2 *BCR-ABL* 3'UTR reporter response to microRNA induction

A luciferase-based approach was used to test the bioinformatics predictions. A number of constructs were generated consisting of *Renilla* luciferase fused with the microRNA binding sites ± 100 bp. We used segments of the 3'UTR rather than the full length because we aimed to limit off target effects of microRNA induction (i.e., if a microRNA regulated a regulator of the 3'UTR). This method is widely used to study microRNA targets[271] (including the miR-203/ABL1 study[173]).

Luciferase constructs harbouring the predicted microRNA binding sites were co-transfected with a microRNA mimic (Pre-miR). A reduction of luciferase activity in the presence of the Pre-miR was indicative of the microRNA interacting with the predicted site. The microRNA seed sequence was then deleted to show that any change in reporter expression was specific to the predicted binding site.

3.3.2.1 Transfection optimisation: Pre-miR

To show that our luciferase system was working, HeLa cells were transfected with a construct harbouring three let-7a binding sites downstream of the *Renilla* luciferase gene (pCIneo-hRL-

Let7a) in the presence of absence of let-7a Pre-miR (9.2 nM). We observed a 20% reduction of luciferase activity in the presence of let-7a (Fig 3.8). Finally, a scrambled Pre-miR was co-transfected with the miR-29 binding site reporter (pCIneo-hRL-miR29). No significant reporter loss was observed (Fig 3.8), demonstrating that Pre-miR induction does not have non-specific effects on luciferase activity.

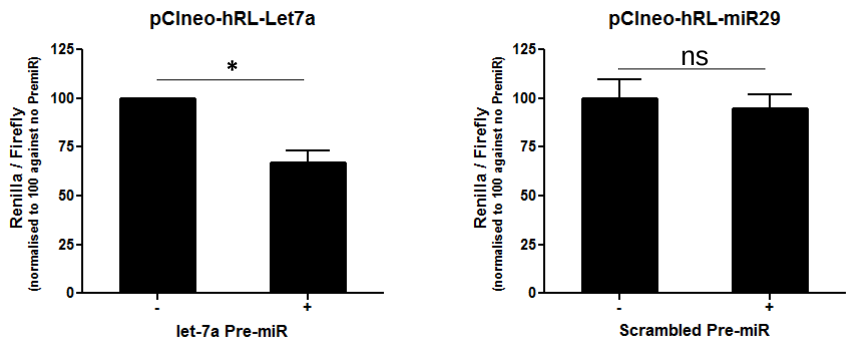

Fig 3.8: Optimisation of Pre-miR transfection. HeLa cells (10^5 per well) were transfected with 3.2 fmol of either pCIneo-hRL-Let7a or pCIneo-hRL-miR29, in addition to 500 ng pGL3 (Firefly luciferase – transfection control), and pUC19 (DNA filler) in the presence or absence of 9.2 nM Pre-miR. Transient transfections were performed using Lipofectamine in triplicate, and luciferase activity measured 48 h post-transfection. Renilla activity was divided by Firefly activity, and normalised to 100 against no Pre-miR. The let-7a transfection was performed thrice and expressed as the mean ± SEM. The scrambled experiment was performed once and expressed as mean ± SD. * $p<0.05$ (t-test). ns (not significant).

3.3.2.2 Transfection optimisation: time

To optimise for the ideal time to harvest transfected cells, HeLa cells were transfected with pCIneo-hRL-Let7a and let-7a Pre-miR and harvested 24, 48 and 72h post-transfection. There was no drastic change observed in the mean reduction of reporter activity by let-7a over time (Fig 3.9, left). However, it can be seen that the Firefly and Renilla luciferase activities decay over time (Fig 3.9, right). In addition there is an increased error in the 72 h experiment (Fig 3.9, left) that changes the interpretation of the experiment – that let-7a does not reduce reporter activity of pCIneo-hRL-Let7a. These experiments show that 24 h post-transfection is the optimal time to read luciferase activity in this system. This time point has the highest luciferase activity, largest microRNA-mediated change in reporter expression and lowest error.

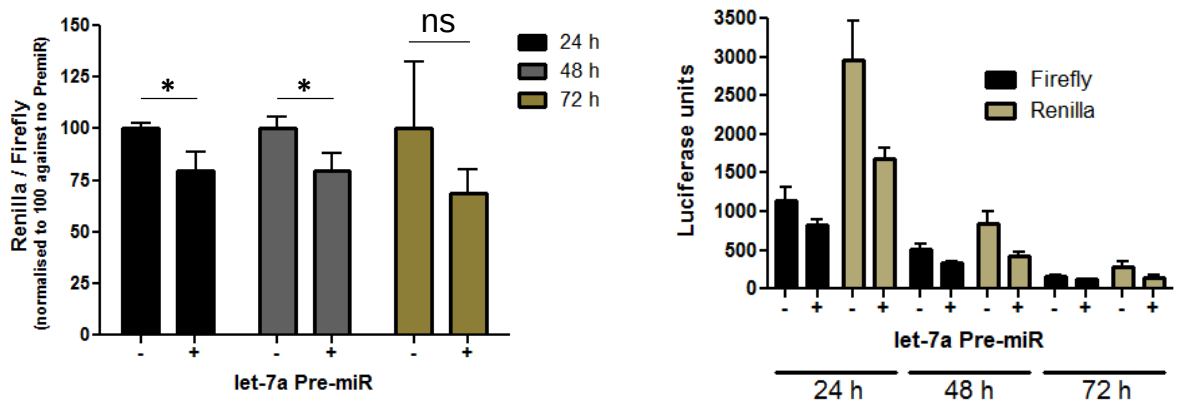

Fig 3.9: Optimisation: luciferase-reading time point. HeLa cells (10^5 per well) were transfected with 3.2 fmol of pCIneo-hRL-Let7a, in addition to 500 ng pGL3 (Firefly luciferase – transfection control), and pUC19 (DNA filler) in the presence or absence of 9.2 nM Pre-miR. Transient transfections were performed using Lipofectamine in triplicate, and luciferase activity measured 24 to 72 h post-transfection. The graph on the left shows Renilla activity divided by Firefly activity, and normalised to 100 against no Pre-miR. The graph on the right shows raw luciferase units for Firefly and Renilla. Both data sets are represented as mean ± SD. * $p<0.05$ (t-test). ns (not significant).

3.3.2.3 Apart from miR-30a, the miR-30 family and miR-203 do not specifically interact with *BCR-ABL* 3'UTR luciferase reporters

Induction of any miR-30 microRNA reduced the luciferase activity of the miR-30 binding site reporter. Upon deletion of the putative site, only miR-30a showed a rescue of luciferase activity (Fig 3.10), although this was not significant ($p = 0.09$).

Surprisingly, miR-203 did not show a specific interaction with its predicted binding site (Fig 3.10). These results are in contrast to a study by Bueno, *et al.* who reported that miR-203 specifically targets BCR-ABL expression via this predicted miR-203 binding site[173]. We also found a lack of effect on a full length *ABL1* 3'UTR reporter by miR-203 (data not shown).

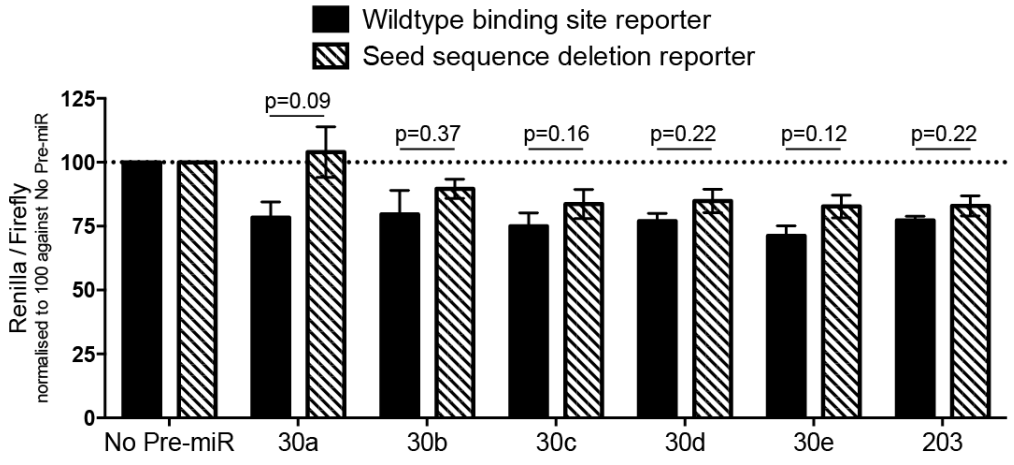

Fig 3.10: *ABL1* 3'UTR reporter assays for miR-30 and 203. HeLa cells (10^5 per well) were transfected with wildtype or seed-sequence deletion reporters for miR-30 or 203 (3.2 fmol), in addition to 500 ng pGL3 (Firefly luciferase – transfection control), and pUC19 (DNA filler) in the presence or absence of 9.2 nM Pre-miR. Transient transfections were performed using Lipofectamine in triplicate, and luciferase activity measured 24 h post-transfection. Renilla activity was divided by Firefly activity, and normalised to 100 against no Pre-miR. These data are expressed as the mean ± SEM of three independent experiments and the p-values are derived from a t-test (Prism software).

3.3.2.4 The miR-29 and 196 families specifically interact with *BCR-ABL* 3'UTR luciferase reporters

Induction of miR-29a/b/c all reduced the luciferase activity of the miR-29 binding site reporter by approximately 25% (Fig 3.11, left). Deletion of the binding site restored luciferase activity, providing evidence that these microRNAs may interact with the predicted binding site ($p<0.05$, except miR-29a). The result for miR-29a does not reach significance because of the large error in the deletion-construct experiments. The means for these experiments were 74, 95 and 117, showing that two of the three experiments had a rescue of luciferase activity.

The most potent reduction of luciferase activity was in the miR-196a/b experiments. MiR-196a reduced luciferase activity of the miR-196 reporter by 25%, and deletion of the seed sequence completely restored luciferase activity ($p<0.01$). Similarly, miR-196b reduced luciferase activity of the wildtype reporter by around 40%, and luciferase activity was completely restored upon deletion of the binding site ($p<0.01$) (Fig 3.11, right).

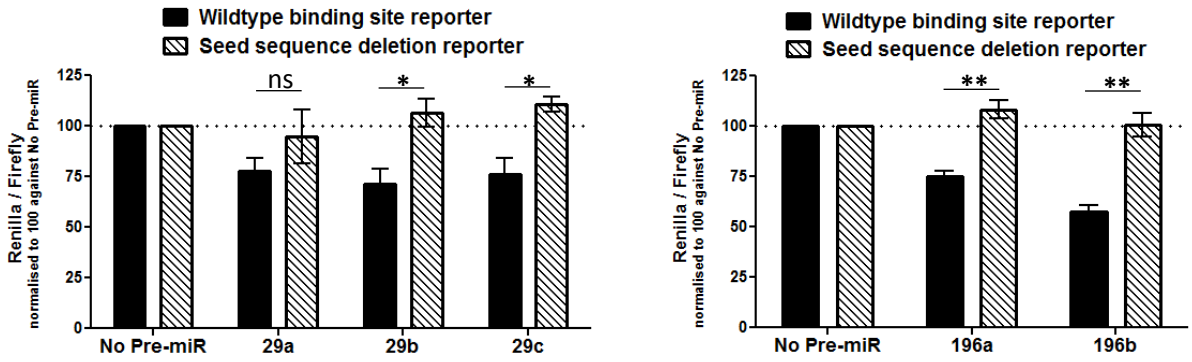

Fig 3.11: MiR-29 and 196 specifically interact with their predicted binding sites in the *ABL1* 3'UTR. HeLa cells (10^5 per well) were transfected with wildtype or seed-sequence deletion reporters for miR-29 or 196 (3.2 fmol), in addition to 500 ng pGL3 (Firefly luciferase – transfection control), and pUC19 (DNA filler) in the presence or absence of 9.2 nM Pre-miR. Transient transfections were performed using Lipofectamine in triplicate, and luciferase activity measured 24 h post-transfection. Renilla activity was divided by Firefly activity, and normalised to 100 against no Pre-miR. These data are expressed as the mean ± SEM of three independent experiments. ** $p<0.01$. * $p<0.05$. ns (not significant) (t-test, Prism software).

3.3.3 MicroRNA over-expression in CML cell lines

The microRNAs were also over-expressed in CML cell lines in order to examine their effect on endogenous BCR-ABL expression.

3.3.3.1 Over-expression of miR-29

We generated K-562 cell lines that over-expressed the miR-29 family, achieving a 3-16 fold induction (Fig 3.12, A). However, over-expression of the miR-29 family did not reduce BCR-ABL expression in K-562 cells (Fig 3.12, B-C). Compared to the empty vector control cell line, the mean BCR-ABL expression ranged from 100-150%. Furthermore, the miR-29 over expressing cell lines survived long-term in culture, and required splitting at a similar rate as the parental K-562 cell line (data not shown). This suggested that miR-29 did not alter cell proliferation.

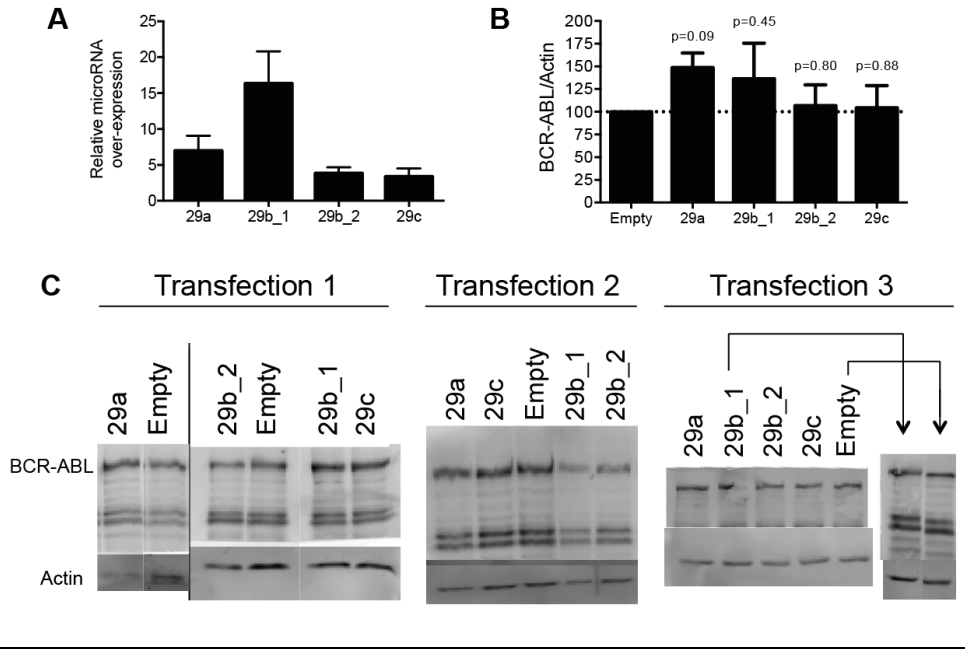

Fig 3.12: Over-expression of the miR-29 family did not change endogenous BCR-ABL expression. pBABE-puro-miR-29 expression vectors were used to stably over-express the miR-29 family in the K562 cell line. (A) Fold over-expression of miR-29 was examined by qRT-PCR. Data represent mean ± SD and were normalised to 1 against empty vector. (B) BCR-ABL expression relative to actin for the three experiments. Data represent mean ± SEM relative to empty vector; p-values were calculated using Prism software. (C) Western blots show BCR-ABL and Actin expression for three independent transfections. The miR-29b_1 experiment in transfection 3 was repeated to obtain a clearer band.

3.3.3.2 Over-expression of miR-30

The luciferase results for miR-30 suggested that miR-30a might interact with the *ABL1* 3'UTR (Fig 3.10). We achieved a 5-18 fold induction of the miR-30 family (Fig 3.13, A). However, when miR-30 was over expressed in the K-562 cell line, there was no significant decrease in BCR-ABL expression (Fig 3.13, B-C). Similar to the miR-29 experiments, the miR-30 over expressing cell lines survived long-term in culture, and required splitting at a similar rate as that for the parental K-562 cell line (data not shown). This suggested that miR-30 did not alter cell proliferation.

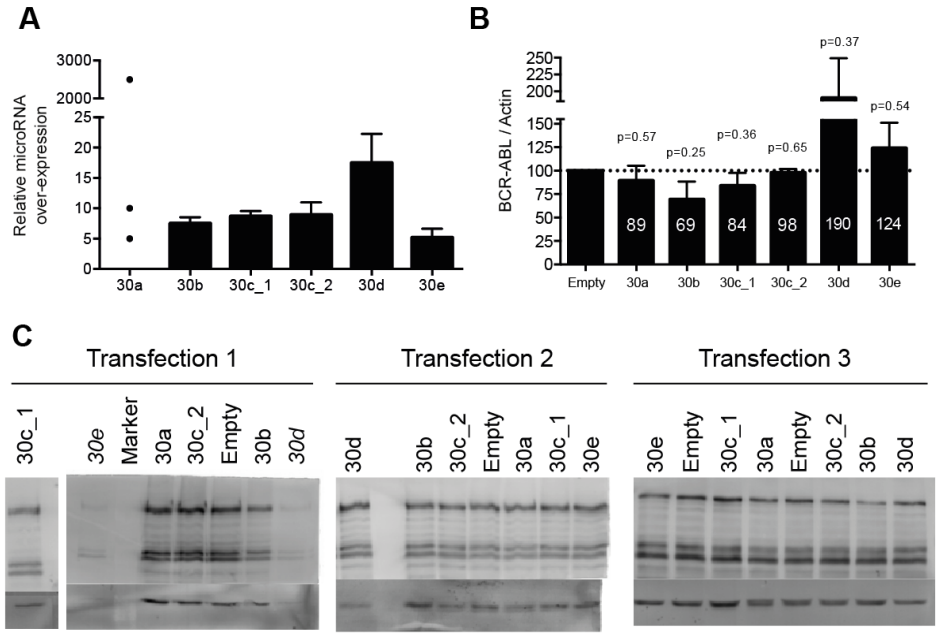

Fig 3.13: Over-expression of the miR-30 family did not change endogenous BCR-ABL expression. pBABE-puro-miR-30 expression vectors were used to stably over-express the miR-30 family in the K562 cell line. (A) Fold over-expression of miR-30 was examined by qRT-PCR. Data represent mean ± SD and were normalised to 1 against empty vector. (B) BCR-ABL expression relative to actin for the three experiments. Data represent mean ± SEM relative to empty vector; p-values were calculated using Prism software. (C) Western blots show BCR-ABL and Actin expression for three independent transfections.

3.3.3.3 Over-expression of miR-203

Data mentioned in this section was provided by Dr. Duncan Hewett and Ms. Ljiljana Vidovic (Centre for Cancer Biology, Adelaide), and is required for discussion of the miR-203 experiments. MiR-203 was previously shown to affect BCR-ABL expression[173]. Our laboratory attempted to replicate some of those experiments to serve as a positive control.

Over-expression of miR-203 was performed in the K-562, KCL-22 and 32Dp210[282] cell lines using the same pBABE-puro-203 vector from the Bueno *et al.* study[173]. 32Dp210 is a murine cell line transduced with a BCR-ABL expression vector that does not contain the miR-203 binding site. We used this cell line as a negative control for miR-203 binding. Our luciferase experiments failed to show an interaction between miR-203 and the predicted binding site (Fig 3.10). Furthermore, over-expression of miR-203 did not affect BCR-ABL protein levels (Fig 3.13, A, centre), and only slightly reduced proliferation in the K-562/miR203 cell line (Fig 3.13, A, left). The lack of phenotype was not due to poor induction

of miR-203, because the K-562 over-expressing cell line had robust levels of miR-203 expression (Fig 3.14, right).

Our results were in contrast to the Bueno, *et al.*[173] study. They reported miR-203 specifically interacted with a segment of the *ABL1* 3'UTR harbouring the predicted miR-203 binding site (Fig 3.14, B, left), and over-expression of miR-203 can reduce BCR-ABL protein levels (Fig 3.14, B, right), as well as causing a dramatic reduction in cell proliferation (Fig 3.14, B, centre).

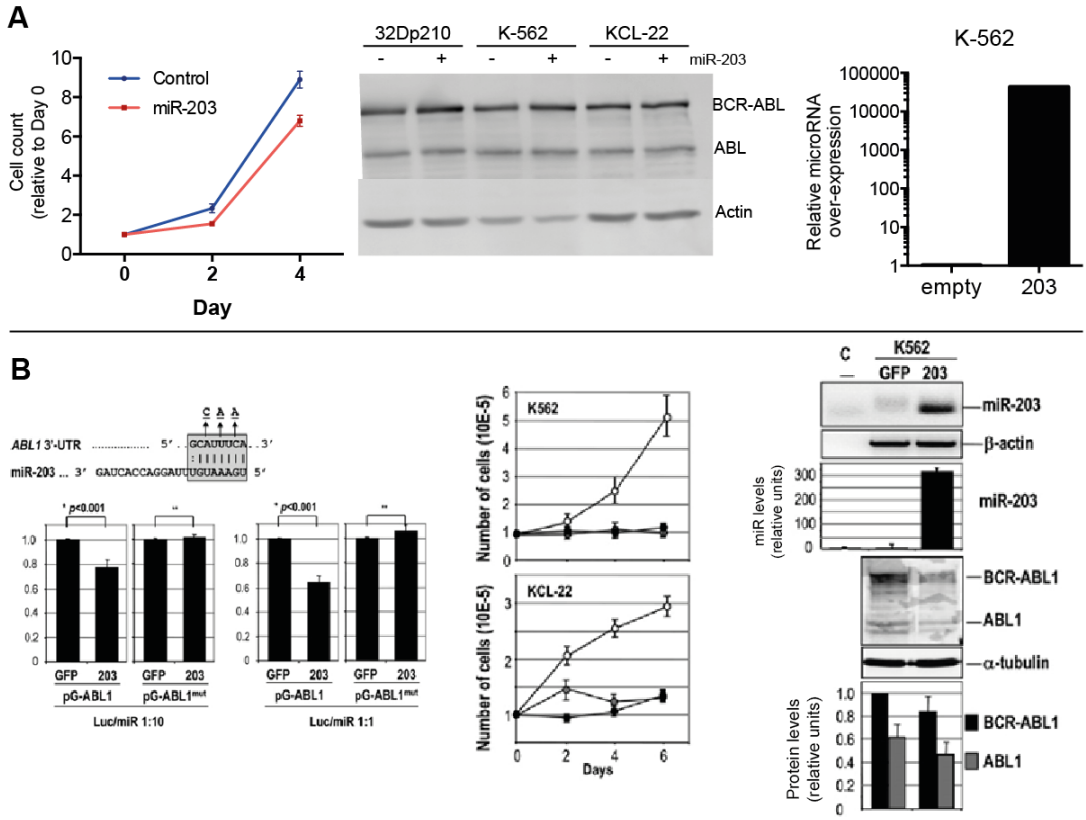

Fig 3.14: Our laboratories results for miR-203 differed from published data. (**A**) We used the same pBABE-puro-miR203 expression vector as Bueno *et al.*[173], to stably over-express miR-203 in BCR-ABL+ cell lines. Trypan-blue cell counts measured proliferation of K-562 cells over-expressing miR-203 relative to empty vector control for four days (left). Protein expression of BCR-ABL, ABL and Actin was measured upon miR-203 over-expression in three BCR-ABL+ cell lines (middle). In addition, we show by qPCR that we achieved a $4x10^5$-fold increase in miR-203 expression in the K-562 cell line (right). (**B**) Bueno, *et al.* report a dramatic effect on BCR-ABL expression by miR-203[173]. Briefly: (left) luciferase experiments show that miR-203 specifically binds its predicted binding site in the *ABL1* 3'UTR. (Middle) over-expression of miR-203 (black circles) completely arrests cell proliferation in K-562 and KCL-22 cell lines compared to empty control (open circles). (Right) over-expression of miR-203 reduces BCR-ABL protein expression in K-562 cells. Image obtained from Bueno, *et al.*[173], and used with permission (Appendix D).

3.3.3.4 Over-expression of miR-196b

Over-expression of miR-196b was performed in the KYO-1 and KCL-22 CML cell lines, and in the HL-60 cell line (myeloid, BCR-ABL negative). This microRNA was chosen because it led to the largest reduction in the luciferase experiments. Induction of miR-196b was achieved in all three cell lines: KYO-1 (50-fold induction), KCL-22 (10^4 to 10^5-fold induction), and HL-60 (20-fold induction) (Fig 3.15, top). These data also show that the KCL-22 parental cell line does not endogenously express miR-196b. The Ct for KCL-22/GFP is ~35 (Fig 3.15, bottom). The amplification plots confirm that the changes observed are due to miR-196b induction rather than changes in the control RNA (Fig 3.15, bottom).

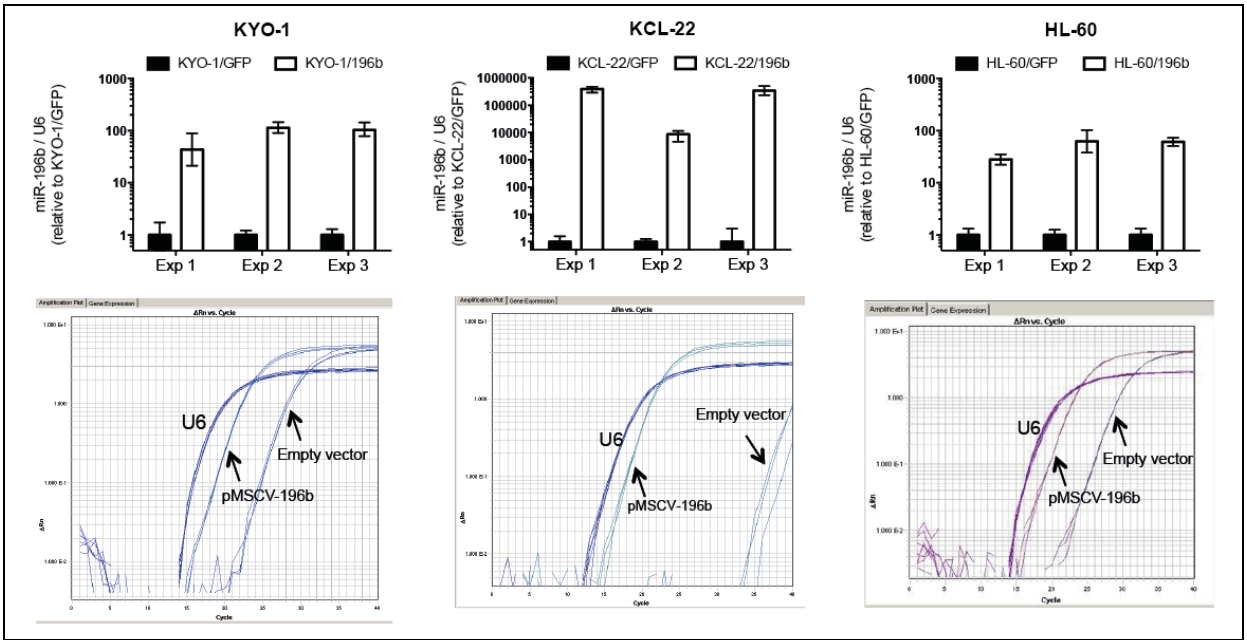

Fig 3.15: Over-expression of miR-196b. The pMSCV-puro-gfp-miR196b vector was used to over-express miR-196b in the KYO-1, KCL-22 and HL-60 cell lines. Over-expression was confirmed by qRT-PCR using the $\Delta\Delta C_T$ method. MiR-196b expression was divided by *RNU6B* expression and normalised to 1 against the GFP-control cell line. The top graphs (in $\log_{10}$-scale) show the mean ± range of relative miR-196b expression for three independent experiments for the three cell lines. The raw amplification plots are shown in the graphs below. *RNU6B* and miR-196b amplification curves are labelled (the amplification curves for *RNU6B* overlap for each set of cell lines).

Over-expression of miR-196b caused a three-fold reduction in proliferation of the CML cell lines. However, a similar phenotype was observed in the BCR-ABL negative, HL-60 cell line. This suggests that the inhibition of growth is independent of BCR-ABL expression.

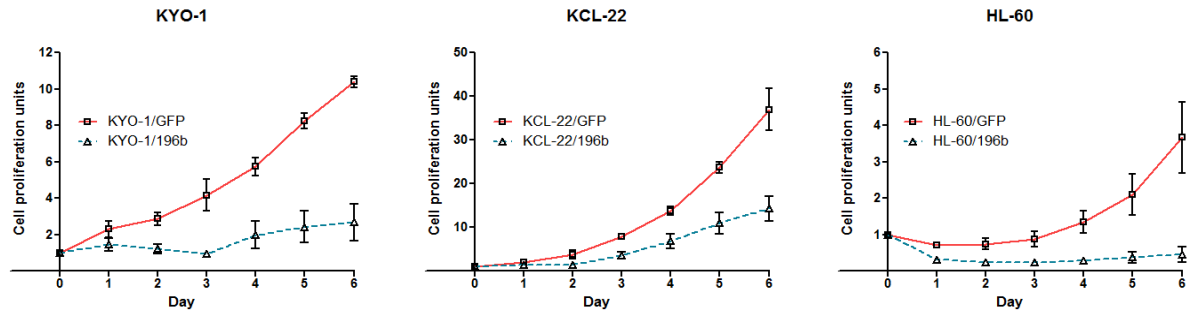

Fig 3.16: MiR-196b inhibits cell proliferation. The effect on proliferation for miR-196b over-expressing cell lines was measured using the Cell-Titer-Glo® assay. Fifty thousand miR-196b or empty vector control cells were seeded in a 24-well plate in triplicate. Cells were pipette mixed and the Cell-Titre-Glo® assay was performed in triplicate for each well over six days. This assay was performed for each independent miR-196b over-expression experiment. The graph above shows the means of the three independent experiments ± SEM (n = 3). These data were normalised to 1 against the day 0 – when the cells were plated.

BCR-ABL protein levels were quantified on day 6 of the proliferation experiment in order to examine any possible regulation by miR-196. In the KYO-1 cell lines there was no consistent reduction in BCR-ABL expression upon miR-196b over-expression. Two of the three experiments showed no change; however, there was a 50% reduction of BCR-ABL expression in experiment three (Fig 3.17, left). Similarly, experiment 1 in the KCL-22 experiments showed a large reduction in BCR-ABL protein levels, while there was no change in BCR-ABL expression in the other two experiments (Fig 3.17, centre). Quantification of miR-196b over-expression shows no aberrant miR-196b induction in the experiments where a reduction of BCR-ABL was observed (Fig 3.15).

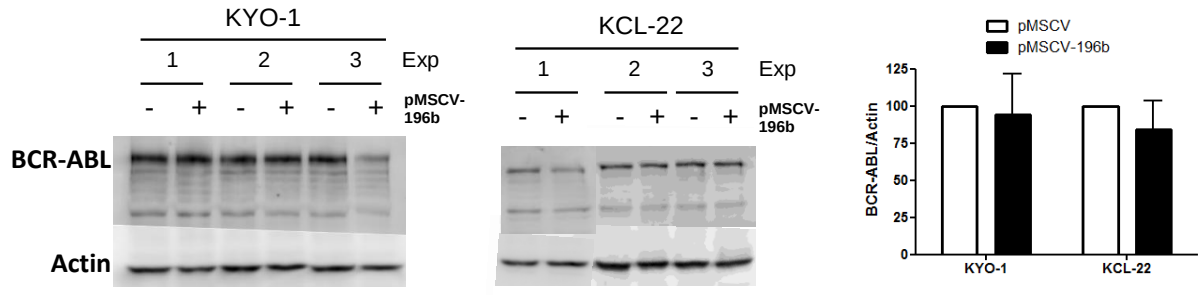

Fig 3.17: Over-expression of miR-196b did not change endogenous BCR-ABL expression. Relative BCR-ABL expression was determined in KYO-1 and KCL-22 miR-196b and empty-control cell lines. Western blots show BCR-ABL and Actin expression for three independent transfections. Minus: pMSCV empty vector, plus: pMSCV miR-196b expression vector. The graph shows mean ± SEM (n = 3). BCR-ABL expression was divided by Actin expression and normalised to 100 against empty vector control. Exp, experiment.

Quantification of miR-196b expression was obtained on day 6 (along with BCR-ABL expression), so it is possible that miR-196b levels fluctuate over time, which may explain the experiments where BCR-ABL levels were reduced. For the last experiment in KCL-22 cells, miR-196b levels were quantified at days 3, 6, and 13 post-sort for GFP.

In this experiment, miR-196b expression dropped 17% from day 3 to day 6 post-sort, and 18% from day 6 to day 13 (Fig 3.18). These changes were not significant, but they suggest (not surprisingly, given that miR-196b is detrimental to the cell (Fig 3.16)) that there is a selection bias towards lower miR-196b expression.

Therefore, the lack of rapid changes in miR-196b expression and the observation that experiment two had a lower induction of miR-196b than experiment one (where a reduction in BCR-ABL was observed) make it unlikely that a miR-196b-dosage effect was responsible for the result in experiment one differing from that in experiments two and three.

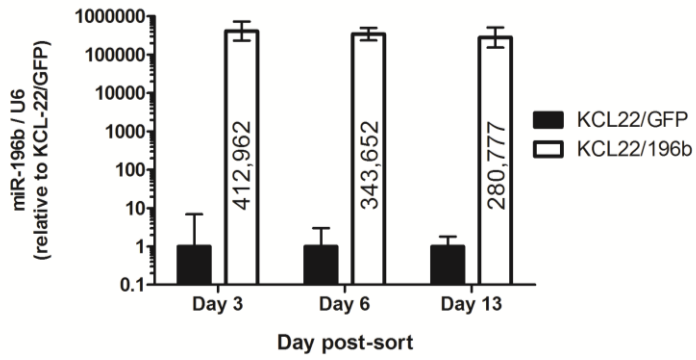

Fig 3.18: Expression levels of miR-196b in miR-196b-transduced KCL-22 cells. At day 3, 6 and 13 after GFP cell selection, miR-196b expression was determined by qRT-PCR using the $\Delta\Delta C_T$ method. MiR-196b expression was divided by *RNU6B* expression and normalised to 1 against the GFP-control cell line. The graph (in $\log_{10}$-scale) shows the mean ± range of relative miR-196b expression for the three time points described in one experiment.

3.3.3.5 AGO2 RIP-SEQ

Genome-wide AGO2 RIP-SEQ data were shown in the previous chapter for *ABL1*. AGO2 is a core component of the RISC, and therefore AGO2-RNA interactions are indicative of microRNA-RNA interactions. Where two or more AGO2 RIP-SEQ reads cluster, TargetScan was used to predict putative microRNA-*ABL1* 3'UTR interactions. Because the RIP-SEQ reads encompass discrete regions of the 3'UTR, we reduced the stringency of the predictions by removing the requirement that the microRNA must bind in a species conserved region of

the 3'UTR. Predicted microRNA binding sites were annotated in Fig 2.27 (pg 82-3). Briefly, miR-378, 411, 196, 19, 320, 361, 141/200 and miR-30 binding sites overlapped with the RIP-SEQ data (Table 3.4). Because those data only recently became freely available, it has not been possible to functionally validate these microRNAs in detail (with exception to miR-141). Therefore, any evidence linking these microRNAs with CML is included in Table 3.4.

Table 3.4: AGO2 RIP-SEQ data analysis

MicroRNA	**Position of AGO2 RIP-SEQ cluster***	**Experimental evidence?**	**Luciferase mapping overlap?** (Fig 2.29)
miR-19	141-190	-Upregulated in BC *vs.* Healthy controls[†]	No. Region was activating in luciferase mapping experiments
miR-196		-Specifically interacts with predicted binding site[#] Does not control endogenous BCR-ABL[#] -Downregulated in imatinib resistant patients^	
miR-378		n/a	
miR-411		-Downregulated in imatinib resistant patients^	
miR-320	1526-1570	n/a	No
miR-361		n/a	
miR-30	1930-1992	-Does not interact with predicted binding site[#] -Downregulated in imatinib resistant patients^	Yes. Region could reduce reporter expression
miR-141/200		-Downregulated in imatinib resistant patients^	

*Position within the ABL1 3'UTR, where 1 is the first nucleotide after the stop codon.
data from this thesis
^ Enériz, *et al.*[230]. [†]Polákova, *et al.*[229].
n/a, not available.

3.3.3.5.1 Transient transfection of miR-141 in K-562 cells

Dr Cameron Bracken and colleagues (Centre for Cancer Biology, Adelaide) have performed an AGO RIP-SEQ experiment that compared RNA bound to the AGO proteins in the parental MDA-MB231 breast cancer cell line and following induction of miR-141 levels (Cameron Bracken *et. al*, unpublished data). They kindly allowed us access to their data. Their results show a substantial enrichment of sequence reads that map at a predicted miR-141 binding site within the *ABL1* 3'UTR in the miR-141 induced cells. This also supports previous AGO RIP-

SEQ data shown in Fig 2.27. It has also been shown that miR-141 is downregulated in imatinib-resistant patients[230]. Through this collaboration we had access to reagents that could modulate miR-141 levels. This allowed us to examine whether or not miR-141 regulates BCR-ABL expression.

As the K-562 cell line is difficult to transfect (5% transfection efficiency with a GFP plasmid, see Fig 2.14, pg 60), K-562 cells were transfected with a Cy3-labelled (red fluorescent) Pre-miR in order to examine transfection efficiency of small molecules. Using a fluorescent-microscope, we observed that the majority of cells were Cy3 positive (Fig 3.19, A-B). When the same experiment was performed using non-fluorescent Pre-miRs, the cells were not fluorescent (Fig 3.19, C-D), indicative that we can use fluorescence-microscopy to estimate transfection efficiency, and that we achieve a high-transfection efficiencies using Pre-miRs. Therefore we should be able to detect changes in BCR-ABL expression upon miR-141 transfection. Two days after transfection of miR-141 at 10 or 100 nM, there was no reduction in BCR-ABL (or ABL) expression compared to a scrambled control, or untransfected K-562 cells (Fig 3.19, E). Therefore, miR-141 does not appear to control BCR-ABL expression despite the aforementioned results from the RIP-SEQ experiments. As with the miR-125 experiments (2.3.7.2), in order to dismiss the interaction between miR-141 and the 3'UTR, induction of this microRNA to significant levels should be confirmed, in addition to showing an effect against a *bone fide* miR-141 target.

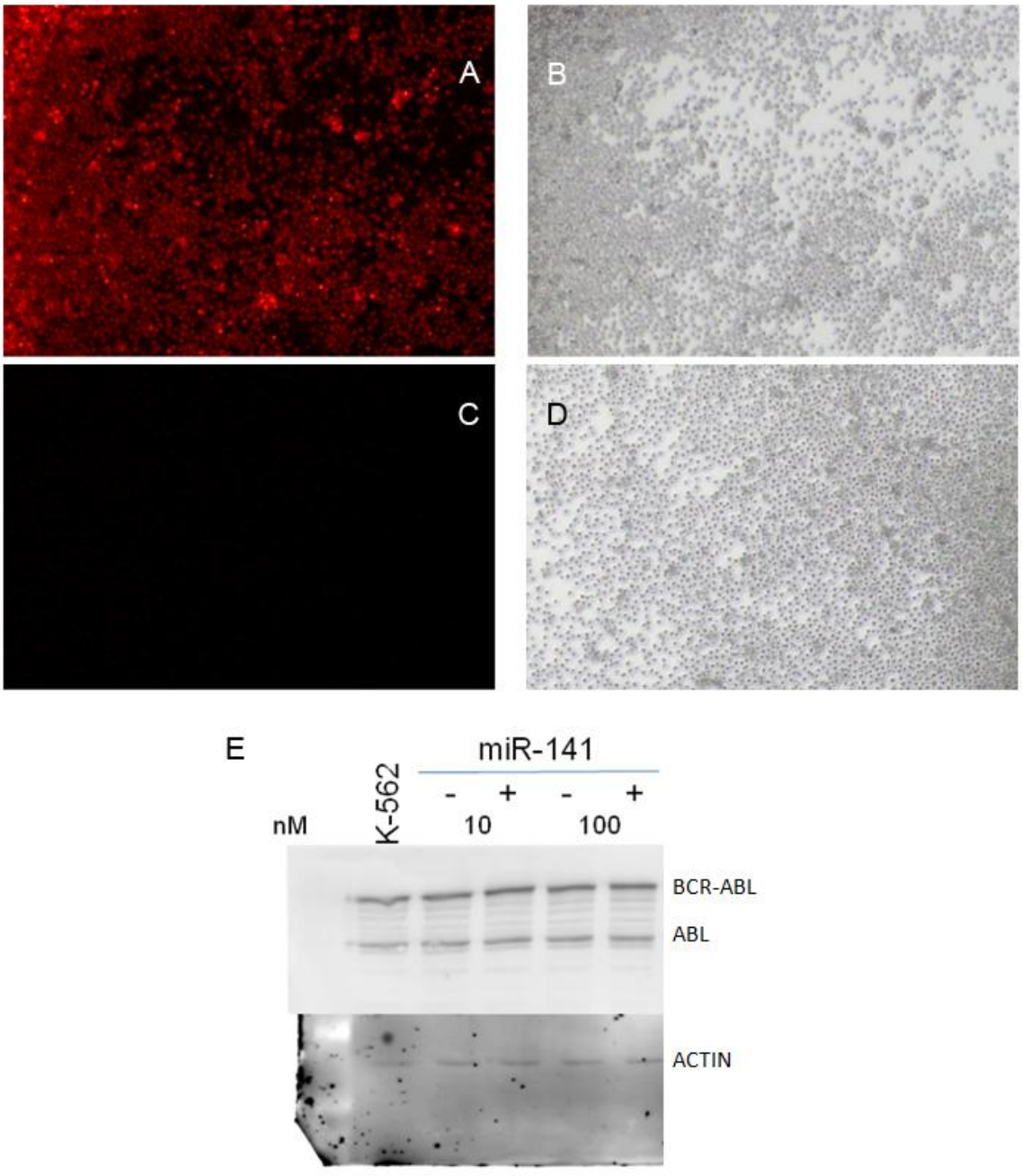

Fig 3.19: MiR-141 does not affect endogenous BCR-ABL expression. (**A-B**) Cy3 labelled Pre-miR negative control (9.2 nM) was transfected into K-562 cells, which were then visualised on a CKX41 microscope (Olympus, Mount Waverley, Australia) with a mercury lamp, and external camera. (**A**) Cells visualised using the lamp and red filter, or (**B**) white light. (**C-D**) 100 nM miR-141 mimic (non-fluorescent) was transfected into K-562 cells, which were then visualised on a CKX41 microscope with a mercury lamp, and external camera. (**C**) Cells visualised using the lamp and red filter, or (**D**) white light. (**E**) BCR-ABL protein expression was determined two days following transfection of either a negative control microRNA mimic or miR-141 mimic. Western blot shows BCR-ABL, ABL and Actin expression from one experiment using either 10 or 100 nM microRNA mimics. K-562: untransfected cells, minus: negative control microRNA, plus: miR-141 mimic.

3.4 Discussion

With the knowledge that the *BCR-ABL* 3'UTR was repressive (chapter 2), and the *ABL1* moiety appears to control the stability of the *BCR-ABL* transcript, microRNAs became a 'prime suspect' as regulators of BCR-ABL expression. Throughout the course of this study, other groups have reported changes in microRNA expression in disease progression, that is CP *vs.* BC[229], in CML patients resistant to TKI-therapy[229,230], and in different haemopoietic cell compartments[277]. So it is not ill-conceived to suggest that alterations in microRNA expression may play a role in these key events in CML. Given the consequence of BCR-ABL expression levels in those processes, we therefore focused on identifying microRNAs that could control BCR-ABL expression. This aim was novel at the start of this project, as there were no published studies on microRNA regulation of BCR-ABL. To date, there are two reports on this topic[173,174].

Our investigation led us to study the effect that miR-29, 30, 125, 141, 196 (and 203) had on BCR-ABL expression. These microRNAs were predicted to interact with the *BCR-ABL* 3'UTR by TargetScan software, or AGO2 RIP-SEQ in the case of miR-141. Unfortunately we have yet to identify a microRNA that is capable of regulating BCR-ABL expression.

Using a luciferase reporter method, we showed that miR-29 and 196 could specifically interact with luciferase reporters harbouring their predicted binding sites (Fig 3.11). On the other hand, miR-30 and 203 did not interact with their predicted sites (Fig 3.10). When the microRNAs were over-expressed in cell lines expressing BCR-ABL, we did not observe any striking effects on BCR-ABL expression. The results for miR-29 and 196 were disappointing, however these microRNAs did not interact with a region of the 3'UTR that was repressive in luciferase mapping experiments (Fig 2.29). Therefore, it might not be surprising that these microRNAs did not control BCR-ABL expression. Our experiments did show that miR-196b had a dramatic effect on proliferation in myeloid cells (Fig 3.16). This finding may be of interest for myeloid biology.

One caveat in the microRNA experiments was the lack of a positive control (due to time constraints). In order to completely rule out these microRNAs as regulators of BCR-ABL, analysis of *bone fide* targets for these microRNAs (such as CDC42, targeted by miR-29[283] and HOX-B7, targeted by miR-196[284]) should be performed in future work.

Recent availability of AGO2 RIP-SEQ data on the doRiNA database provides an alternate method for microRNA prediction. A number of RIP-SEQ reads from AGO2 immuno-precipitation experiments mapped to the *ABL1* 3'UTR. Using TargetScan, nine predicted microRNA binding sites were found within these RIP-SEQ reads (Table 3.4), including sites for miR-30 and 196. We examined published microRNA array data from several CML-related studies, in order to obtain further evidence for these microRNAs in CML. Five of the nine microRNAs were downregulated in imatinib resistant patients (miR-30, 141/200, 196 and 411)[229,230]. If those microRNAs were actual targets of BCR-ABL, reduced expression of these microRNAs in imatinib resistant patients would theoretically allow for enhanced BCR-ABL expression. This would be of interest given that enhanced BCR-ABL expression is believed to play a role in imatinib resistance. We have already studied miR-30, 141 and 196 and found no evidence that they control BCR-ABL expression. We observed that over-expression of miR-196b reduced cell-proliferation. So, downregulation of miR-196 in imatinib resistant CML could act by promoting cell survival, and reduce sensitivity of CML cells to imatinib. As it is unknown whether or not miR-411 can control BCR-ABL expression, functional experiments to resolve this gap should be considered in the future.

We had time to investigate miR-141's effect on BCR-ABL expression. This microRNA was chosen based on interesting data from doRiNA/TargetScan database analysis, the imatinib-microRNA expression study[230], and miR-141/AGO2 RIP-SEQ data (Bracken, *et al.*, unpublished data). K-562 cells were transfected with a miR-141 microRNA-mimic, and then BCR-ABL protein expression examined. However these experiments did not provide evidence that miR-141 regulates BCR-ABL expression (Fig 3.19).

False positives

When this project commenced, the bioinformatics-luciferase approach was the only technique readily available to identify microRNA-target interactions[285]. It has been widely-used in published studies to successfully identify functional microRNA interactions[286]. We used TargetScan software to generate a shortlist of microRNAs to study; however none of these microRNAs showed any effect on endogenous BCR-ABL expression – 'false-positives'. There are other prediction algorithms available for example, MicroCosm (www.ebi.ac.uk/enright-srv/microcosm/), DIANAmT (http://diana.cslab.ece.ntua.gr/), and

microRNA.org (www.microrna.org). However, due to time constraints, we only investigated TargetScan-predicted microRNAs. MicroRNA target predictions for *ABL1* using the aforementioned algorithms are in Appendix C. There was some overlap between the databases compared with TargetScan. For example, the DIANAmT program also identified miR-29, 30, 141/200, 196 and 203 as potential targets of *ABL1*. MicroRNA.org also predicted miR-30, 141/200, 196 and 203. Interestingly, there was no overlap between TargetScan and MicroCosm.

From our results, it is clear that a sequence complementary to a microRNA seed sequence does not always translate into a functional binding site. The site may not be accessible to microRNA targeting due to steric hindrance or competition from RNA-binding proteins or other non-coding RNAs[287]. Thus, using other algorithms may result in further false positives. However, without an alternate strategy, the next step would be to test the predictions of the other target prediction algorithms.

Fortunately, unbiased approaches have recently been developed to capture microRNA-target interactions in a cellular context, and appear to be a promising method for identify *bone fide* interactions[288-290]. The method involves tagging the 3'UTR using an RNA-aptamer, followed by enrichment of the tagged-3'UTR and associated microRNAs. Next-gen sequencing or microRNA arrays can be used to identify isolated microRNAs. Validation of functional interactions is then achieved using luciferase experiments and microRNA over-expression in cell lines. This approach has the added advantage that it can also be used to identify RNA-binding proteins or long non-coding RNA interactions (we used this strategy to isolate RNA-binding proteins (see chapter 4)). Therefore, it is strongly recommended to perform this technique in the context of the *BCR-ABL* 3'UTR in the future.

Another tactic to predict microRNAs of interest is to use expression arrays to highlight microRNA changes during stages of disease, treatment or development[291,292], and then correlate these data with bioinformatics predictions. For example, if miR-x is downregulated in the transition from CP to BC (where BCR-ABL expression increases), it could be hypothesised that this microRNA regulates BCR-ABL. If miR-x also has a predicted binding site in BCR-ABL, it would strengthen the rationale for further study. When we commenced this project such data were not available. Thus, we could only perform this in retrospect (Table 3.4). It is anticipated that additional microRNA expression arrays for CML will

become available in the future. This will make it easier to design approaches for the study of microRNAs by limiting candidate microRNAs to those relevant to CML.

miR-203

Intriguingly, we did not detect miR-203's effect on BCR-ABL expression using either luciferase assays (Fig 3.10) or miR-203 over-expression studies (Fig 3.14). Our findings are at odds with published studies by Bueno, *et al.*[173] and Iraci, *et al.*[174]. They reported that miR-203 specifically interacts with the *BCR-ABL* 3'UTR and reduces protein expression. Furthermore, Craig, *et al.* recently showed that miR-203 can reduce ABL protein levels[293].

In contrast to Bueno *et al.*[173], our luciferase experiments did not show that miR-203 interacted with its *ABL1* 3'UTR-predicted binding site (Fig 3.10), or with a full length *ABL1* 3'UTR luciferase reporter (data not shown). We then attempted to replicate the miR-203 over-expression experiments as reasonably as possible. Notably, we obtained the miR-203 expression vector used in the Bueno, *et al.* study, to generate cell lines that stably over-expressed miR-203. In K-562 cells we achieved $4x10^5$ fold over-expression, therefore we do not believe a lack of expression was the reason behind the discrepancy in our results. The only caveat in our work was the absence of a control experiment showing miR-203 targeting a known target. If this experiment was performed, it would strengthen our findings.

In addition, Dr. Duncan Hewett performed a comprehensive methylation analysis of the miR-203 promoter, and found no methylation of miR-203 in CML patient or cell line samples (data not shown). Instead, our results showed epigenetic silencing of miR-203 in Ph- (BCR-ABL negative) myeloid cell lines (data not shown). Two other studies have also reported a lack of miR-203 epigenetic silencing in CML[294,295]. The reasons for the discordance between the findings on miR-203 among different groups are not known.

In terms of BCR-ABL inhibition via miR-203, the reduction of BCR-ABL shown by Bueno, *et al.* was modest considering the phenotype[173]. In the K-562 cell line, over-expression of miR-203 caused a mean reduction of BCR-ABL by 20% (with a 20% standard deviation) (Fig 3.14, pg 118). This is suggestive that in one experiment there was no reduction in BCR-ABL expression, yet complete inhibition of cell growth was observed in each of their K-562 proliferation experiments (Fig 3.14). Those results are similar to what we observed after over-expressing miR-196 and may be indicative of a BCR-ABL independent mechanism. To address this, miR-203 over-expression should be performed in healthy and

CML primary cells. This will show if miR-203 controls BCR-ABL expression *ex vivo*, and if miR-203 over-expression does not alter cell growth of healthy cells (but inhibits CML cell growth).

Of interest, Bueno, *et al.* showed that demethylating agents Aza and PBA, dramatically reduced both ABL and BCR-ABL protein expression[173]. The rationale for that experiment was to restore miR-203 expression in CML cell lines, reduce BCR-ABL expression and inhibit cell growth. The results followed their hypothesis that if miR-203 expression is increased, BCR-ABL and ABL expression decrease. However the increase in miR-203 expression by the demethylation agents was 10-times less than that achieved by miR-203 over-expression, and yet demethylating agents resulted in a far superior reduction of BCR-ABL expression. Therefore it appears that a regulator of BCR-ABL (that is not miR-203) is responsive to demethylating agents in CML cells. This may give rise to an additional strategy to find regulators of BCR-ABL, as well as a way to target BCR-ABL expression.

Final remarks

Out of the microRNAs we have investigated, none of them showed the potential to regulate endogenous BCR-ABL expression. These microRNAs can be ruled out completely upon validation of our system. That is, can these microRNAs modulate the expression of a 'real' target? If TargetScan predicted microRNAs which in fact regulated BCR-ABL, the approach we undertook (which was the standard methodology at the time[285]) should have been sufficient to detect them. The reliance on *in silico* candidate selection is thought to be the contributing factor behind our unsuccessful initial search. The development of a method to generate microRNA candidates based on a cellular-context appears to circumvent this critical limitation. We are currently optimising this method in our laboratory and anticipate a more successful list of candidate microRNAs to investigate.

Chapter 4

Developing an assay to identify *ABL1* 3'UTR binding proteins

4.1 Introduction

4.1.1 RNA-binding proteins

A transcript is bound by RNA-binding proteins throughout its existence – from transcription to degradation[296,297]. These proteins affect RNA processing, localisation, translation and stability ultimately controlling gene expression (Fig 4.1). To date, over 900 RNA-binding proteins have been characterised in humans[298]. A number of studies have showed that these proteins are involved in development[197,299] and disease[143,300], including leukaemia[197]. Thus in addition to microRNAs, we are also interested in identifying protein interactions with the *BCR-ABL* 3'UTR. To achieve this, we started to develop an assay capable of isolating and identifying *BCR-ABL* 3'UTR RNA-binding proteins. Following this we would then determine the importance of these proteins in CML.

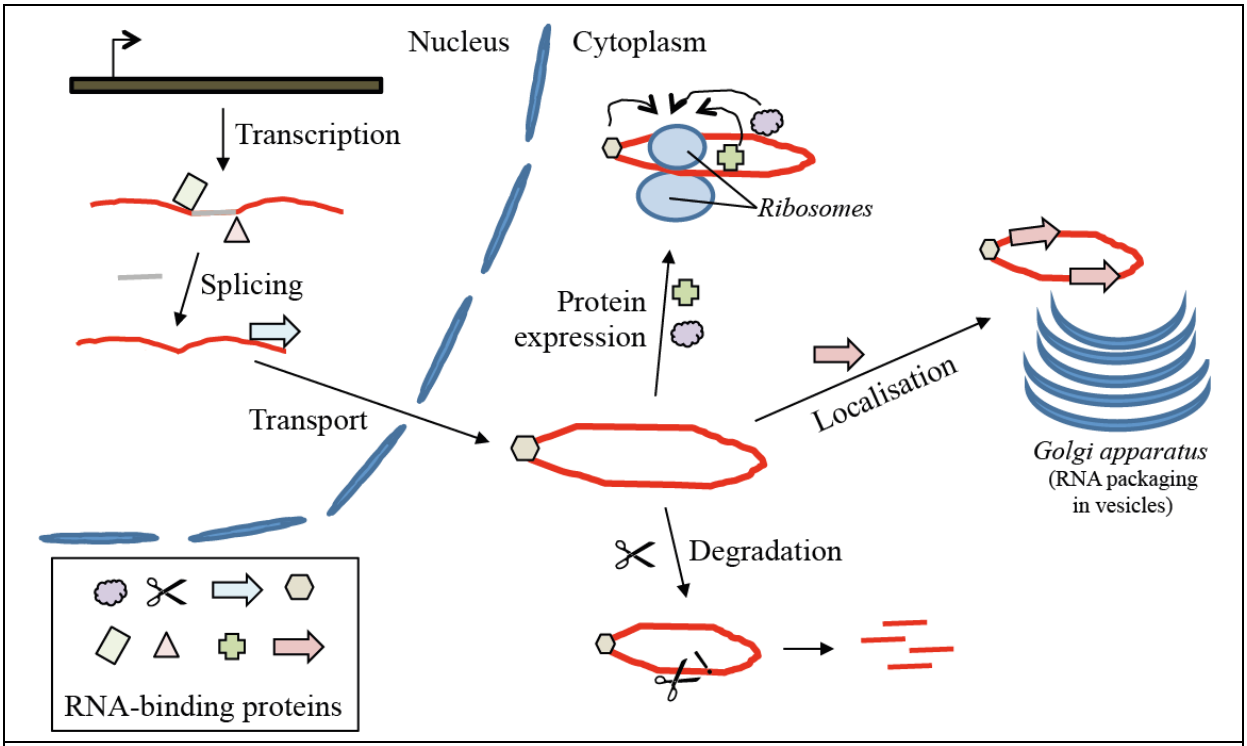

Fig 4.1: RNA-binding proteins are essential for RNA control and function. Throughout a transcript's (red line/circle) life, it is bound by RNA-binding proteins (various shapes). These proteins govern key roles such as RNA splicing, export to the cytoplasm and organelle localisation. These proteins can also govern the stability of the gene, and how much protein is translated from a particular gene-transcript. The brown hexagon represents the RNA capping proteins.

RBDs are critical for proteins to interact with RNA. These interactions are facilitated by van der Waal forces and hydrogen-bonding between the protein domain's amino acid side chains and the RNA[301,302]. There are over 40 RBDs characterised in human proteins[303]. The two best characterised are the RRM (RNA recognition motif), and the KH (K homology) domains (Fig 4.2)[301,302]. The RRM consists of a highly-conserved β-α-β-β-α-β protein structure and is found in over 400 human RNA-binding proteins[301,303]. The KH type I domain, found in eukaryotes, contains a β-α-α-β-β-α protein structure[302], and is found in approximately 40 human RNA-binding proteins[303].

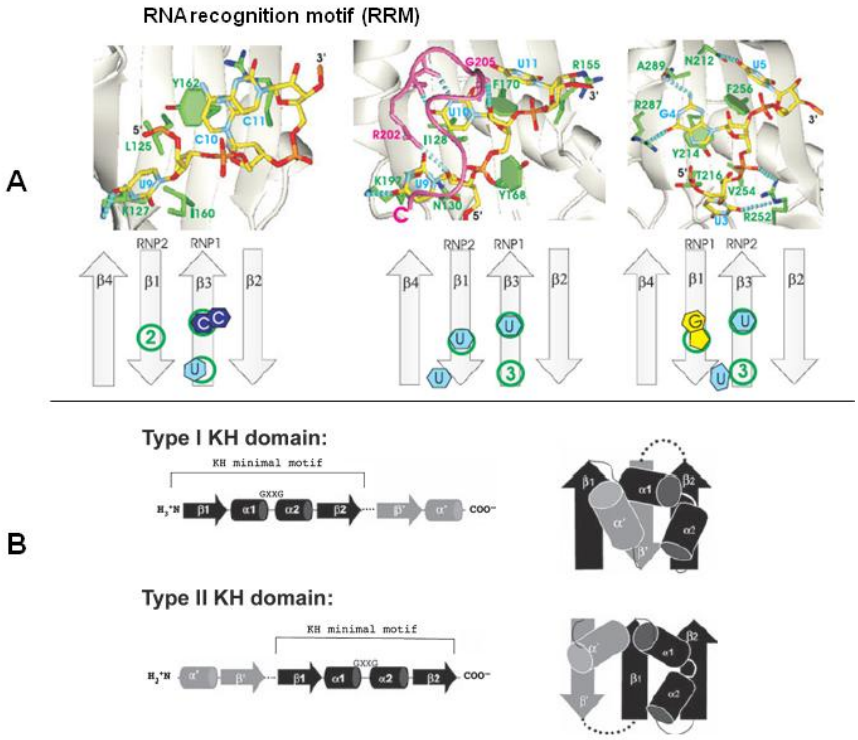

Fig 4.2: The RRM and KH RBDs. (**A**) Chemical structures of protein-RNA interactions for the RNA recognition motif (RRM). The top images show a schematic of the RNA-RRM interaction for three RNAs. RNA is shown in yellow, and the RRM is shown as beta-sheets and green residues that interact with RNA. The bottom images are diagrams of how the RNA nucleotides interact with the RRM residues. Nucleotides are represented by their sugar chemical structure, and the residues that interact with RNA are shown as green circles. Image from Maris, *et al.*[301], used with permission from John Wiley and Sons (Appendix D). (**B**) Diagrams of the Type I and type II KH domain structures. The Type I KH domain consists of a β-α-α-β-β-α protein structure, and is predominantly found in eukaryotes[302]. The α1, α2-helices and β2-sheet are responsible for direct RNA interactions[302]. The type II KH domain consists of an α-β-β-α-α-β protein structure, and predominantly found in prokaryotes[302]. The core KH structure, β-α-α-β (black), is arranged in a slightly different orientation between the two types of KH domains. Image from Valverde *et al*[302], used with permission from John Wiley and Sons (Appendix D).

4.1.2 RNA-binding proteins in development and disease

Gene regulatory control due to RNA-binding protein-mediated changes in RNA stability, alternate splicing and localisation have important consequences in both disease and development. A significant proportion of research regarding RNA-binding proteins and development involves the nervous system[299]. However, there are other examples of RNA-binding protein involvement during muscle and skeletal development[304,305], during wound healing[306,307] and in haemopoiesis[197].

The role of RNA-binding proteins in disease is less established compared to that of microRNAs, but disruptions in RNA-binding protein are known to feature in disease. Over-expression of Sam68 is a marker of poor prognosis in breast[308], cervix[309] and renal cell[310] cancers. Sam68 interacts with RNA by its (KH domain-containing) STAR/GSG RBD[311,312], and is known to regulate mRNA splicing, localisation and translation[313-315]. Aberrant Sam68-medated splicing of *CyclinD1*[316] and *BCL-X*[317] are known to disrupt cell proliferation and apoptosis, and is thought to contribute to disease pathogenesis[316,317].

TTP is an AU-RE binding protein (mentioned in chapter 2) which is known to interact with an extended AU-RE within 3'UTRs: AUAUUUAUA, and to control mRNA stability[189,318]. Current research is suggestive that TTP is a tumour suppressor. Downregulation of TTP is observed in several cancers comparing tumour cells with non-tumour matched samples[319], and expression of TTP in tumour cells suppresses their growth[320-322]. TTP knock-out mice develop normally, but succumb to a hyper-TNF-α phenotype[323] and show prolonged expression of cytokine mRNAs[324]. These phenotypes can in part be explained by TTP directly controlling the stability of a repertoire of cytokine transcripts including TNF-α[325], IFN-γ[326] and IL-2, -6 and -10[327-329].

4.1.2.1 RNA-binding proteins in chronic myeloid leukaemia

A few studies have reported the involvement of RNA-binding proteins in CML-biology. Inhibition of C/EBPα by hnRNP E2 was the first report involving the RNA-binding function of an RNA-binding protein in CML[100,101]. As described in 1.4.3.1.1 (pg 12), in CML, this process is dependent on the expression level of BCR-ABL. High BCR-ABL levels result in an induction of hnRNP E2 expression, hnRNP E2 inhibits the expression of C/EBPα, which in turn inhibits myeloid differentiation[100,101]. Those findings highlighted the importance of both BCR-ABL dosage and RNA-binding protein involvement in the biology of CML.

BCR-ABL kinase activity regulates both the expression and function of the FUS (or TLS) protein in CML[330,331]. FUS is a DNA and RNA binding protein, which was initially identified as a CHOP (or C/EBPε) fusion-partner in human liposarcoma[332,333]. It was, however, the DNA-binding properties of FUS that were first studied in relation to CML. BCR-ABL-mediated PKCβII phosphorylation of FUS affected the DNA-binding activity of FUS[330], and increased the stability of the FUS protein via inhibition of Jun mediated proteolysis[330]. In addition, knockdown of FUS reduced growth-factor independent colony formation and tumourigenesis, and restored differentiation in BCR-ABL expressing myeloid cells[331]. FUS binds an RNA 'GGUG' consensus sequence[334] and has a known role in regulating splicing and localisation of mRNA[335,336]. It is still uncertain whether FUS binding of RNA serves the same purpose in CML, but it would be predicted that this function may also control CML pathogenesis.

In the CML cell line K-562, knockdown of the RNA-binding protein IGF2BP3 (also known as IMP3) inhibited cell growth and promoted apoptosis, suggesting a possible role in CML[337]. It was later shown that IGF2BP3 enhances cell survival, in part, through IGF-II[338]. RIP-SEQ data suggest that IGF2BP1-3 interacts with the *BCR-ABL* 3'UTR (Fig 2.26, pg 81). Therefore, IGF2BP3 stabilisation of *BCR-ABL* mRNA may play a role in the phenotype observed in K-562 cells following IGF2BP2 knowndown.

Finally, two groups simultaneously showed that Musashi-2 was involved in CML-BC. Musashi-2 is an RNA-binding protein with two RRM domains[339], and has been recently linked to HSC development[340]. In CML, expression of Musashi-2 is markedly upregulated in blast crisis, and functions to inhibit *NUMB* translation[341,342]. Knockdown of Musashi-2 or ectopic NUMB expression attenuated BC transformation in CML mice models[341,342].

4.1.2.2 Modulation of BCR-ABL stability by RNA-binding proteins

As mentioned in chapter 2, a number of RNA-binding proteins have been shown to interact with *ABL1* 3'UTR RNA (Fig 2.26, pg 81). Leading to an important question, do RNA-binding proteins *functionally* interact with *BCR-ABL* RNA?

As RNA is always bound by protein[296], the *BCR-ABL* transcript *will* be bound by proteins. However it is unknown what involvement, if any, these proteins play in the control of BCR-ABL expression levels. In a rationale similar to that for microRNA interactions with

BCR-ABL, identification of proteins that alter BCR-ABL expression will have important implications for the biology of CML.

Our initial experiments focussed on the 3'UTR, because this is a known hub for proteins that regulate RNA stability[146]. Our approach was to tag *BCR-ABL* 3'UTR RNA, and then isolate proteins from cellular lysates that interact with the labelled 3'UTR. The next section provides a brief background surrounding the experimental method.

4.1.3 Methods for RNA-binding protein isolation

The standard approach for identifying RNA-binding proteins that bind to a particular RNA sequence involves tagging the RNA, purifying the RNA-protein complexes, and mass spectrometry identification (Fig 4.3). In general, this approach has been successful in capturing proteins bound to RNA[210,343,344]. Of note though, most of the RNA baits have been relatively small (<500bp) compared to the 2 kb *ABL1* 3'UTR. It was anticipated that the large size of the RNA bait would increase the complexity of the RNA-protein complexes and require careful optimisation. Identification of RNA-binding proteins bound to the 2.5 kb *LDL receptor* 3'UTR[210] provides a precedent that it is possible to isolate proteins this way (that study used biotinylated RNA).

There are different tagging methods available, which allow for slight variations of protein capture. They include RNA aptamers, allowing *in vivo* protein capture, and biotinylation which is less laborious, but only allows *in vitro* protein capture. The two methods are compared in Table 4.1.

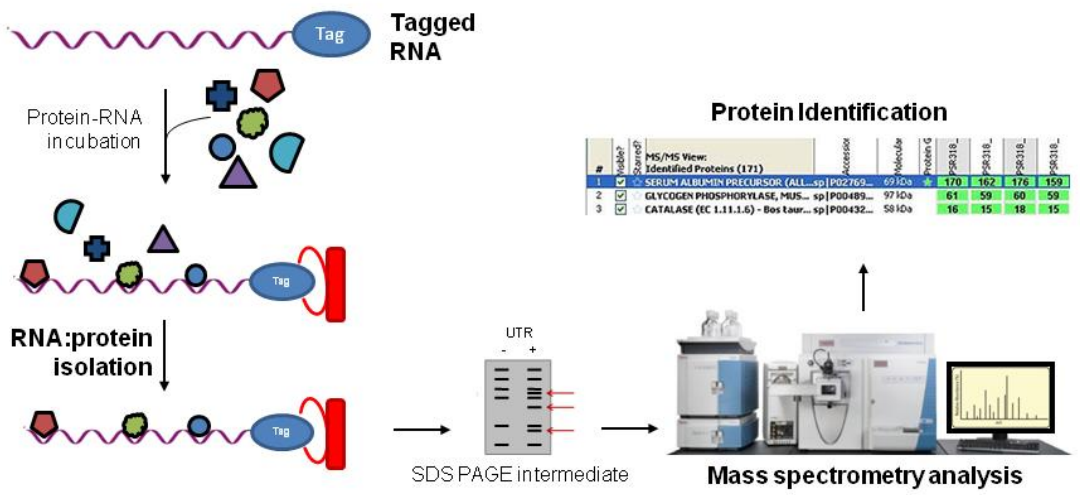

Fig 4.3: Schematic of the current methodology for identification of RNA-binding protein interactions with an RNA of interest. To isolate RNA-binding proteins from an RNA bait, the RNA is tagged using the methods discussed in this section. The tagged RNA is then incubated with cell proteins (depicted as coloured shapes). RNA-protein complexes are purified using the RNA tag, followed by visualisation of eluted proteins via SDS-PAGE. Identification of proteins can be achieved using high-resolution LC-MS/MS (see 4.1.3.3).

Table 4.1: Summary of current RNA tagging methods

	RNA aptamer	**Biotinylation**
RNA-tag	• 3’ or 5’ end of the RNA • Intra-RNA (requires secondary structure information)	• 3’ or 5’ end of the RNA • Incorporated into RNA • Biotinylated oligo-probe
Template	• PCR product (IVT only) • DNA template of interest in a suitable expression plasmid. Aptamer positioned 5’/3’/intra RNA of interest	• PCR product • DNA template of interest in a plasmid suitable for IVT
RNA source	• IVT • Intracellular transcription	• IVT • Oligo-synthesis
RNA-protein capture	• *In vitro* • *In vivo*	• *In vitro*
Isolation of RNA-protein complex	• Streptavidin (S1-class aptamers) • Streptomycin (StreptoTag) • MS2 coat protein (MS2 binding motif	• Streptavidin
IVT, *in vitro* transcription.		

4.1.3.1 RNA aptamers

An aptamer is a nucleic acid sequence (DNA or RNA) that interacts with a specific protein. A number of RNA aptamers have been developed in order to affinity-purify RNA sequences[345,346]. This has application to RNA-binding protein capture.

4.1.3.1.1 Streptavidin aptamers

Srisawat and Engelke designed an assay to identify aptamers that bind streptavidin[345]. A library of 84 nt RNAs were designed with a central 40 nt variable region. RNAs that bound streptavidin were enriched and sequenced to identify two aptamers named "S1" and "S13"[345]. The S1 and S13 aptamers have a binding affinity of 20 and 7 x 10^{-8} M respectively. This is compared to the biotin-streptavidin affinity of 10^{-14} M (the strongest biological interaction known)[347]. S1-tagged RNA has been used to identify RNA-binding proteins bound to *TNFα*[343] and *RPR1*[348]. Lioka, *et al.* developed a next-gen S1-tag, which was tethered to a tRNA in order to preserve the S1 tag structure[349]. They showed that the next-gen S1 tag was more effective than the original S1-tag and biotin-tagging for isolation of a known RNA-protein interaction. They then isolated RNA-binding proteins bound to the *CRB3* 3'UTR.

4.1.3.1.2 StreptoTag

The StreptoTag was developed in a similar approach to the S1 aptamer and binds streptomycin with an affinity of 10^{-6} M[350]. The aptamer allows the RNA to be immobilised on a streptomycin column followed by RNA-binding protein capture and isolation[346]. It was further shown that the StreptoTag reduces non-specific binding found with biotin tagging[346].

4.1.3.1.3 MS2 coat protein aptamer

The MS2 coat protein is an RNA-binding protein expressed by bacteriophage MS2. This protein recognises a specific RNA stem-loop structure present in its (own) viral RNA[351]. Many studies have taken advantage of this interaction to purify protein-RNA complexes[352]. This approach involves tagging the RNA with the MS2-stem-loop, followed by affinity purification of the tagged-RNA using a fusion-MS2 protein. Examples of fusion-MS2 proteins are maltose-binding protein/MS2 and GST/MS2 allowing for the use of amylose and glutathione bead purification respectively[290]. This approach can be performed *in vitro*[352] or *in vivo*[290]. Furthermore, the technique involves a protein-RNA interaction (MS2-coat protein and

MS2-stem-loop), which serves as a positive control to demonstrate that the experimental setup can isolate protein-RNA interactions. That is, if enrichment of MS2-stem-loop-tagged RNA is successful, this is indicative that the sample contains stable protein-RNA complexes. The MS2-aptamer approach has been used to isolate both RNA-RNA and RNA-protein interactions[290].

4.1.3.2 Biotinylation

Biotin tagging of RNA (Fig 4.4) utilises the biotin-streptavidin interaction (Fig 4.4, A), which is the strongest non-covalent biological interaction known. RNA can be end-labelled with a biotinylated bisphosphate-nucleotide, or the transcription reaction substituted with a biotinylated nucleotide – labelling the RNA throughout (Fig 4.4, B). Another approach uses a biotinylated oligonucleotide complementary to the RNA of interest (Fig 4.4, C;[353]). Biotinylation has been used to isolate RNA-binding proteins from *LDL receptor*[210], *NPM1*[160] and *AANAT*[354] RNA.

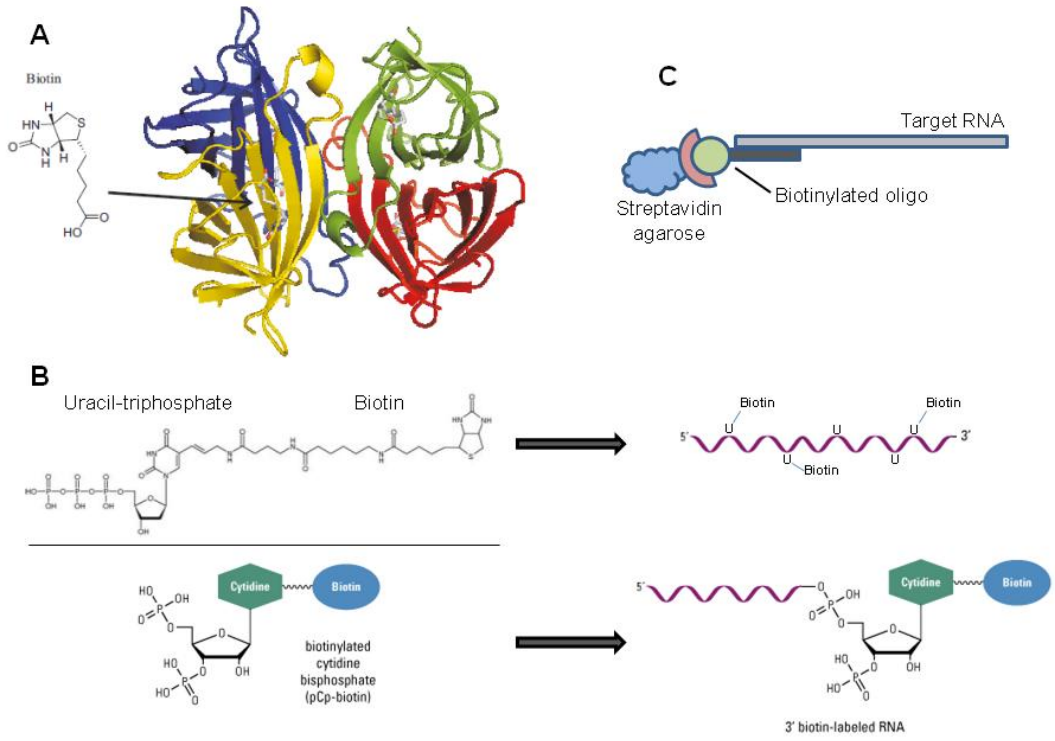

Fig 4.4: Isolation of RNA-binding proteins using biotin. (**A**) Model of the biotin-steptavidin (tetrameric) interaction. Each monomer subunit of streptavidin is shown in a difference colour. Image obtained and used with permission Franziska Luschtinetz (Appendix D). (**B**) Biotin incorporation into an RNA molecule (top), or 3' end labelling of an RNA molecule (bottom). Biotin-incorporation occurs during the *in vitro* transcription reaction, whereas 3' end labelling involves ligation of a biotin-tagged nucleotide to an RNA molecule. RNA molecule shown in purple. U, uracil. Biotin-uracil-triphosphate structure obtained from the ENZO-scientific webpage (www.enzolifesciences.com), and used with permission (Appendix D). Biotinylated cytidine bisphosphate molecule obtained from the Piercenet webpage (www.piercenet.com) and used with permission (Appendix D). (**C**) Biotinylated-oligonucleotide "probes" that are complementary to the target RNA are another approach used to indirectly label RNA, and isolate RNA-binding proteins.

4.1.3.3 Mass spectrometry-based identification of proteins

Mass spectrometry is used to identify proteins captured from tagged RNA. The exact approach is determined by the equipment available to the mass spectrometry facility. The approach available for this study was liquid chromatography-electrospray ionisation ion-trap mass spectrometry (LC-eSI-IT).

Mass spectrometry is used to determine a compound's mass to charge ratio (m/z). The first step is to ionise the compound so it has a positive charge. The ions are then sent through the mass spectrometer with a particular kinetic energy. Finally, they are deflected by a

magnetic field based on their mass, which is followed by ion detection and plotting of intensity *vs*. m/z[355].

Protein identification by mass spectrometry involves analysis of trypsinised peptides. Trypsin will cleave the C-terminal-side peptide bond of lysine and arginine amino acids (unless the next amino acid is proline)[356]. Therefore a protein can be identified by calculating the mass of the fragments observed. However this becomes difficult in samples containing multiple proteins. This is because the m/z spectrum will contain multiple ions produced by multiple proteins. Therefore, it is only possible to differentiate the largest ions from separate proteins. These large ions contain multiple amino acids, and this reduces the resolution of the information obtained (it may be possible to identify an ions amino acid composition, but not the sequence of the amino acids).

Tandem mass spectrometry (or MS-MS), utilises multiple mass spectrometers to overcome these limitations[357]. The MS-MS technique used in this study was LC-eSI-IT. In this technique (illustrated in Fig 4.5), HPLC is used to pre separate complex mixtures prior to mass spectrometry. Electrospray ionised peptides are sent to the first mass spectrometer (an ion trap), which selects individual ions from the sample (by time). One-by-one, these ions are further fragmented by collision–induced dissociation (CID) and detected by a second mass spectrometer. Ions formed by CID will produce a spectrum of ions, including ions fragmented at the peptide bond. These ions are detected by the Orbitrap™ mass spectrometer, from which sequence information can be obtained[357].

The XCalibur™ software (Thermo Scientific) is used to analyse mass spectrometry data and derive sequence information. The Mascot search engine (www.matrixscience.com) interprets the sequence data to determine protein identity.

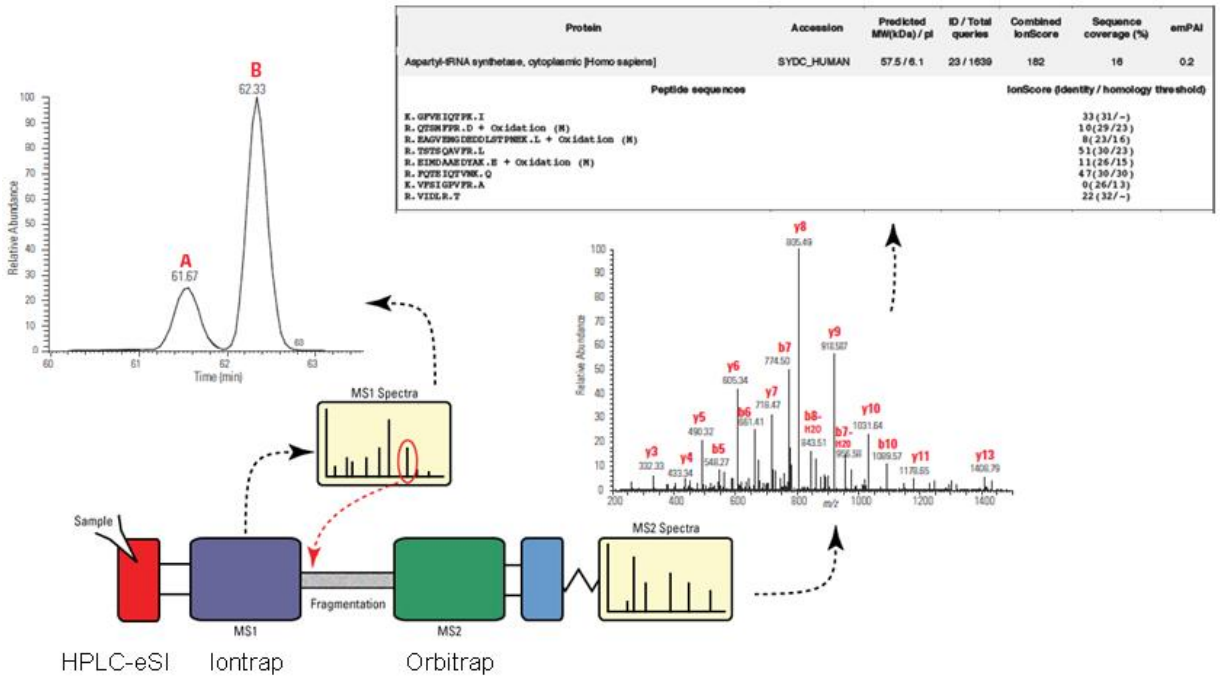

Fig 4.5: Mass spectrometry-based identification of proteins from complex samples. A complex mixture of proteins can be isolated using LC-eSI-IT MS-MS. The sample is first separated by HPLC, which sends a "steady stream" of peptides to the electrospray instrument (eSI; red box) to produce ions for the first mass spectrometer (MS1) (ion trap, purple box). This mass spectrometer selects particular ions (in our case based on time), and individually sends these ions for further fragmentation by collision–induced dissociation (producing a peptide spectra of a individual ion, which are analysed by a second mass spectrometer (MS2) (Orbitrap; green box). The spectra from MS2 are then mapped with peptide databases for protein identification. Spectra and mass spectrometry-work through obtained from ThermoScientific (http://www.thermoscientific.com), and used with permission (Appendix D).

4.2 Methods

4.2.1 Developing an assay to capture RNA-binding proteins that interact with the *BCR-ABL* 3'UTR.

To identify proteins that bind to the *BCR-ABL* 3'UTR, a number of approaches were attempted based on isolating proteins bound to 'tagged' *BCR-ABL* 3'UTR RNA. We utilised the S1-tag and biotinylated nucleotide incorporation. Both of these methods were streptavidin-agarose based, therefore we could use similar techniques for each method.

4.2.2 Cell culture

K-562 and HeLa cells were cultured as per Appendix A.14.

4.2.3 S1 RNA-aptamer

4.2.3.1 S1-aptamer constructs

It is recommended that the S1-tag is inserted intra-3'UTR, at the end of a stem-loop structure[358]. Mfold software (http://mobyle.pasteur.fr/cgi-bin/portal.py?#forms::mfold) predicted a stem-loop within nt 116-136 of the 3'UTR. Therefore, the minimal S1-tag sequence was cloned into nt 124 of the *ABL1* 3'UTR i.e., positioning the tag at the end of the stem-loop structure. Furthermore, the S1-tag/3'UTR was downstream of the *Renilla* luciferase gene.

4.2.3.1.1 Cloning the S1-tag into the pUC19 intermediate

Initially the S1-tag sequence was cloned into pUC19 as a readily available source for cloning (pUC19-S1).

4.2.3.1.1.1 Oligonucleotide duplex annealing

The minimal S1-tag sequence is 44-nt long, therefore two complementary oligonucleotides were designed containing the tag sequence flanked by *Eco*RI restriction sites for cloning (Table 4.2). The two complementary oligonucleotides were first annealed to form a double stranded duplex. Lyophilised S1-EcoRI_F and S1-EcoRI_R oligonucleotides were diluted to 200 nM in TE. Each oligonucleotide (25 µL) was placed in a 1.5 mL micro-centrifuge tube and heated to 90°C for 20 min and then allowed to cool to room temperature for approximately 3 h (switching off the heat block).

4.2.3.1.1.2 *Eco*RI restriction digest

pUC19 (5 µg) and annealed duplex (2 µL) were digested with *Eco*RI (20 U), in 1x BSA, 1x *Eco*RI buffer and water (up to 20 µL). The digests were incubated at 37°C for 2 h. CIP (10 U) was added to the pUC19 digest and incubated at 37°C for 15 min.

4.2.3.1.1.3 DNA purification, ligation and transformation

*Eco*RI/CIP-treated pUC19 DNA was purified by agarose gel extraction according to Appendix A.9. *Eco*RI-treated duplex was purified on an Illustra™ Microspin™ G-25 column (GE Healthcare) according to the manufacturer's instructions. The duplex was ligated into pUC19 according to Appendix A.10, using 2 µL of purified pUC19, and 1 µL of 1/50-diluted

purified duplex. The ligation was then transformed into electrocompetent cells as per Appendix A.11.

4.2.3.1.1.4 DNA plasmid prep

pUC19-S1 was obtained using the DNA plasmid prep method as per Appendix A.13**.** Presence of the S1-tag was confirmed by digesting each isolated clone (3 µL) with *Eco*RI (5 U) for 1 h, followed by agarose gel electrophoresis. Presence of a 50-bp band was indicative of the S1 being present. As this vector was only used as a source of S1-tagged DNA, the orientation of the S1-tag was not important. Moreover, only full length oligo-duplexes will clone into the *Eco*RI site, therefore sequencing was not performed. Bulk quantities of pUC19-S1 were obtained using the HiSpeed® Plasmid Midi Kit (QIAGEN) according to the manufacturer's instructions.

4.2.3.1.2 Cloning the S1-tag into the pBluescript II SK+ intermediate

An S1-tag duplex flanked by *Not*I sites (Table 4.2) was cloned into the *Not*I site of pBluescript II SK+ (pBSII-S1) based on the method for pUC19 (see 4.2.3.1.1).

Table 4.2: Oligonucleotides used for insertion of the S1-tag into the *BCR-ABL* 3'UTR

Oligonucleotide	**Sequence (5' – 3')**
S1-EcoRI_F	**GAATTC**ACCGACCAGAATCATGCAAGTGCGTAAGA TAGTCGCGGGCCGGG**GAATTC**
S1-EcoRI_R	**GAATTC**CCCGGCCCGCGACTATCTTACGCACTTGC ATGATTCTGGTCGGT**GAATTC**
S1-NotI_F	**GCGGCCGC**ACCGACCAGAATCATGCAAGTGCGTAA GATAGTCGCGGGCCGGG**GCGGCCGC**
S1-NotI_R	**GCGGCCGC**CCCGGCCCGCGACTATCTTACGCACTT GCATGATTCTGGTCGGT**GCGGCCGC**
ABL3'UTR.EcoRI.124 (F)	GGCCCAGGAGCTCTGC*GAATTC*CAGAGCTGAGGGC CCTG
ABL3'UTR.EcoRI.124 (R)	CAGGGCCCTCAGCTCTG*GAATTC*GCAGAGCTCCTG GGCC
Restriction sites in bold Restriction site introduced by mutagenesis underlined. Nucleotides altered in italics.	

4.2.3.1.3 Cloning the S1-tag into the full length ABL1 3'UTR

An *Eco*RI site was introduced into nt 124-129 of the *ABL1* 3'UTR downstream of *Renilla* by PCR mutagenesis (Appendix A.3), using primers in Table 4.2 to afford phRL-ABL3'UTR-EcoRI.124. The S1-tag was cloned into phRL-ABL3'UTR-EcoRI.124 to produce phRL-ABL3'UTR-S1 by a similar approach to 4.2.3.1.1.

Briefly, phRL-ABL3'UTR-EcoRI.124 (2 µg) and pUC19-S1 (2 µg) were digested with *Eco*RI (20 U) for 2 h. CIP (10 U) was added to the phRL-ABL3'UTR-EcoRI.124 digest and incubated at 37°C for 15 min. Both DNAs were purified by gel extraction, and 6 µL S1-tag DNA was ligated with 2 µL phRL-ABL3'UTR-EcoRI.124. Presence of the S1-tag in the 3'UTR and orientation was confirmed by sequencing Appendix A.4.

4.2.3.2 Transient transfection: luciferase assay

HeLa cells were seeded in 24-well plates 18 h pre-transfection (10^5/mL/well). The following day, cells were transfected as per Table 4.3 using the Lipofectamine™ transfection reagent according to the manufacturer's instructions. Cells were harvested 48 h post-transfection and luciferase readings obtained as per Appendix A.15. Statistical analysis was carried out using a one-tailed t-test using Prism 5 software.

Table 4.3: Transfection conditions (per well)

Renilla construct	3.2 fmol
pGL3-control*	500 ng
pUC19+	Up to 1 µg DNA
Lipofectamine™	3 µL
n	Quadruplicate
*Firefly transfection control +DNA filler	

4.2.3.3 S1-aptamer enrichment assay 1

4.2.3.3.1 Transfection of HeLa cells with phRL-ABL3'UTR-S1

HeLa cells (10^6 per dish in 5 mL) were seeded in two 10 cm dishes (BD Biosciences, San Jose, CA, USA) 18 h prior to transfection. The following day, cells were transfected with 5 µg of phRL-ABL3'UTR-S1 using Lipofectamine™ (15 µL, 3:1 ratio) according to the

manufacturer's instructions. Forty-eight hours post transfection, cells from each dish were trypsinised (Appendix A.14) and transferred to separate 10-mL centrifuge tubes. Cells from one of the tubes were resuspended in 600 µL TRIzol® (Invitrogen), for RNA extraction. The cells in the other tube were resuspended in 100 µL NP40 lysis buffer with 10x protease inhibitor (10 µL) and PSMF (1 µL), for protein analysis. The lysates were kept on ice and vortex-mixed every 10 min for 30 min. Lysates were then centrifuged (20800g, 10 min, 4^{o}C) and the supernatants collected in fresh tubes.

Protein amount was determined using the Bradford assay (BIO-RAD) according to the manufacturer's instructions.

4.2.3.3.2 Streptavidin agarose S1-tagged RNA enrichment

The HeLa protein lysate was incubated with streptavidin agarose to enrich for S1-tagged RNA. To reduce streptavidin binding proteins, avidin (3.5 µg, Sigma) was added to 350 µg protein lysate in a 1.5-mL microcentrifuge tube (the S1-tag does not bind avidin, only streptavidin[358]). Following a 10-min incubation on ice, streptavidin agarose (10 µL) was added to the tube, and left on ice for 1 h with occasional gentle mixing.

After 1 h, the agarose beads were centrifuged (4000g, 5 min, 4°C), the supernatant was collected and stored at -70°C, and the beads were washed 5 times with 1x NP40 buffer (20x bed-volume). To each wash, 200 µL TRIzol® were added and stored at -70°C. Five resin volumes (bed-volumes) of NP40 were added to the remaining beads, which were then transferred to an Ultrafree-MC 0.45 µM spin column (Millipore). The beads were washed twice with 5 bed-volumes of NP40 buffer. S1-tagged RNA was eluted from the streptavidin agarose by incubation for 1 h with 5 mM D-biotin (20 µL, Sigma). The spin column was centrifuged to collect the eluent, which was mixed with 200 µL TRIzol®.

4.2.3.4 S1-aptamer enrichment assay 2

A number of changes were made to the assay, and are underlined in the text below.

4.2.3.4.1 Transfection of HeLa cells with phRL-ABL3'UTR-S1

HeLa cells ($\underline{3x10^{6}}$ per dish in 5 mL) were seeded in <u>a 10 cm dish</u> 18 h prior to transfection. The following day, cells were transfected with <u>10 µg</u> of phRL-ABL3'UTR-S1 using Lipofectamine™ (<u>30 µL</u>, 3:1 ratio) according to the manufacturer's instructions. Forty-eight

hours post transfection, HeLa cells were trypsinised, then resuspended in 100 µL NP40 lysis buffer with 10x protease inhibitors (10 µL) and PSMF (1 µL). The lysate was kept on ice and vortex-mixed every 10 min for 30 min. Following centrifugation (20800g, 10 min, 4^{o}C), the supernatant was collected in a fresh tube. Protein amount was determined using the Bradford assay (BIO-RAD) according to the manufacturer's instructions.

4.2.3.4.2 Streptavidin agarose S1-tagged RNA enrichment

To reduce streptavidin binding proteins, avidin (10 µg) was added to 1000 µg protein lysate in a 1.5 mL microcentrifuge tube. Following a 10-min incubation on ice, streptavidin agarose (10 µL) was added to the tube, and left on ice for 1 h with occasional gentle mixing.

After 1 h, the agarose beads were transferred to an Ultrafree-MC 0.45 µM spin-column and centrifuged (4000g, 5 min, 4°C). The beads were washed in the filter five times with 20-bed volumes of 1x NP40 buffer. To each wash, 200 µL TRIzol® were added and stored at -70°C. S1-tagged RNA was eluted from the streptavidin agarose by incubation for 1 h with 5 mM D-biotin (20 µL). The spin-column was centrifuged to collect the eluent, which was mixed with 200 µL TRIzol®. In addition, the beads were washed from the spin column and mixed with 200 µL TRIzol®.

4.2.3.5 RNA isolation

RNA was isolated from TRIzol® mixes as per Appendix A.5. RNA yields were then quantified using the NanoDrop™ 1000 spectrophotometer. To remove plasmid DNA, samples were DNase treated before cDNA synthesis. Two units of DNase I (New England Biolabs) and 1.1 µL DNase-buffer were added to 10 µL RNA (~700 ng). Samples were then incubated at 37°C for 30 min. Then, 1.3 µL 0.5M ethylenediaminetetraacetic acid (EDTA) were added to each sample to stop the reaction, followed by heat-inactivation at 65°C for 10 min.

4.2.3.5.1 cDNA synthesis

cDNA synthesis was performed using Superscript™ II and Oligo(dT)15 primers (Promega) as per Appendix A.7.

4.2.3.5.2 Quantitative PCR

Renilla RNA was quantified by qRT-PCR, using a custom assay according to Appendix A.8. The primer and probe sequences are in Table 4.4.

Table 4.4: qRT-PCR primer and probe sequences for *Renilla* RNA quantification

	Sequence (5' – 3')
Forward primer	CCTCACCGCTTGGTTCGA
Reverse primer	TCGTGGCCCACAAAGATGAT
Probe	*FAM*-CTGAACCTTCCAAAGAA-*TAMRA*
FAM: 5' fluorophore TAMRA: 3' quencher	

4.2.3.5.3 G6PD qualitative PCR

G6PD was amplified using the primers in Table 4.5. The PCR was performed as per Appendix A.1.

Table 4.5: Primers to amplify *G6PD* mRNA

	Sequence (5' – 3')
G6PD Forward (Exon 7)	CCGCATCGACCACTACCTGGGCAAG
G6PD Reverse (Exon 9)	GTTCCCCACGTACTGGCCCAGGACCA

4.2.3.6 Streptavidin agarose binding assay

In vitro transcribed S1-tag RNA or a biotinylated oligonucleotide (Table 4.6) were incubated with streptavidin agarose, and then electrophoresed on a 10% TBE non-denaturing acrylamide gel (Appendix B).

4.2.3.6.1 In vitro transcription

S1-tag RNA was *in vitro* transcribed using the T7-MEGAshortscript™ *in vitro* transcription kit (Ambion) according to the manufacturer's instructions. Transcription template was amplified by PCR from pBSII-S1. The PCR was performed according to Appendix A.2, using the primers (T7-S1-NotI_for and S1-NotI_rev) in Table 4.6. The PCR product was gel purified as per Appendix A.9, and 100nM (~200 ng) used in the transcription reaction. The

transcription reaction was performed at 37°C for 5 h, and RNA purified by phenol-chloroform extraction/alcohol precipitation (as per kit's instructions).

Table 4.6: Oligonucleotide sequences used in the streptavidin binding assay

	Sequence (5' – 3')
T7-S1-NotI_for	TAATACGACTCACTATAGGGGCGGCCGCACCGACCAGAA
S1-NotI_rev	GCGGCCGCCCCGGCCCGCG
Biotinylated-oligonucleotide	5'biotin–TTTCTCCCCACTTTAGATC
T7 promoter underlined	

4.2.3.6.2 Binding assay

S1-tagged RNA (2.5 µg) or biotinylated oligonucleotide (350 ng) were incubated with 10 µL streptavidin agarose, and 5 µL NP40 buffer or 5 µL 50 mM D-biotin (in 1x NP40 buffer) for 1.5 h at room temperature. 1.5 µL 10x RNA loading buffer (40% glycerol, 1.45% bromophenol blue, in 1x NP40 buffer) were then added to the samples prior to electrophoresis.

4.2.3.6.3 Non-denaturing polyacrylamide-gel electrophoresis

Samples were loaded on a 10% non-denaturing TBE-polyacrylamide gel (Appendix B) and electrophoresed (150 V, 30 min), using the Mini-PROTEAN® Tetra Cell apparatus (BIO-RAD) in 1x TBE buffer (Appendix B). RNA and DNA bands were visualised by SYBR® Green II RNA stain (Invitrogen), according to the manufacturer's instructions.

4.2.4 Biotinylation of *BCR-ABL* 3'UTR RNA

4.2.4.1 T7 promoter-driven *BCR-ABL* 3'UTR vectors

The full length *ABL1* 3'UTR was cloned into the *Xba*I and *Not*I sites of pBluescript II SK+ in a similar approach to that described on 4.3.2.1. Briefly, phRL-ABL3'UTR (2 µg) and pBluescript II SK+ (2 µg) were digested with 20 U of *Xba*I and *Not*I-HF. CIP (10 U) was added to the pBluescript II SK+ digest and incubated at 37°C for 15 min. *ABL1* 3'UTR and pBluescript II SK+ DNA were purified by gel extraction as per Appendix A.9, then ligated as per Appendix A.10 to afford pBSII-ABL3'UTR(F). Plasmid identity was confirmed by sequencing Appendix A.4. Similarly, pBSII-ABL3'UTR(R) was obtained as above. However,

phRL-ABL3'UTR (reverse) was digested with *Xba*I, and the *ABL* 3'UTR was cloned into the *Xba*I site of pBluescript II SK+ in the reverse orientation.

4.2.4.2 *In vitro* transcription

ABL1 3'UTR (forward and reverse orientation) RNA was *in vitro* transcribed using the T7-MEGAscript™ *in vitro* transcription kit (Ambion) according to the manufacturer's instructions. The transcription reaction used either PCR product or plasmid as a template. PCR product was obtained as per 4.2.3.6.1 using the primers in Table 4.7. Plasmids from 4.2.4.1 (10 µg) were digested with *Not*I (80 U) in 1x NEB 3 buffer, 1x BSA and water (up to 100 µL). The plasmids were purified by alcohol precipitation (Appendix A.16). The transcription reaction was performed at 37°C overnight, using 200 ng PCR or 1 µg linearised plasmid template and, if the RNA was biotinylated, 0.5 M bio-16-UTP (Enzo Life Sciences, Farmingdale, NY, USA). RNA was purified by phenol-chloroform extraction/alcohol precipitation (as per kit's instructions).

UTP-biotin (0.5 M) randomly biotinylates 1.5% of the 3'UTR (6.5% of the 479 uracils in the *ABL1* 3'UTR are biotinylated), so approximately 30 biotinylated uracils are present in each 3'UTR RNA.

Table 4.7: Primers used to amplify *in vitro* transcription templates

	Sequence (5' – 3') (forward primer first)
T7-ABL 3'UTR (forward orientation)	TAATACGACTCACTATAGGCAGCAGTCAGGGGTCAG ATCTGCTCTAGATTCTAATGTAAACACTGATTTATTTA
T7-ABL 3'UTR (reverse orientation)	TAATACGACTCACTATAGGTTCTAATGTAAACACTG GTGCAGTCTAGACAGCAGTCAGGGGTCAGGTG
Forward sequence T7 promoter underlined	

4.2.4.3 Streptavidin agarose binding assay

Water, non-biotinylated *ABL1* 3'UTR RNA (5 µg), or biotinylated *ABL1* 3'UTR RNA (5 µg) were incubated with streptavidin agarose (25 µL, pre-washed twice with 1x PBS) in 50 µL RNA-binding protein assay buffer (RBP-assay buffer) (Table 4.8). The binding-assay was performed in 1.5 mL RNase-free microcentrifuge tubes (Quality Scientific Plastics, San Diego, CA, USA) for 2 h on ice. A further 50 µL RBP-assay buffer were added, and the

agarose beads were then centrifuged (1000g, 5 min). The supernatant was collected in 200 µL TRIzol®, and the beads washed twice more with 100 µL RBP-assay buffer (both collected in TRIzol®). Then, 100 µL RBP-assay buffer (4 mM D-biotin and 2% SDS) was added to the beads. Each tube was incubated at room temperature for 15 min followed by 65°C for 20 min. The supernatant was transferred to a new tube with TRIzol®. In addition, TRIzol® was also added to the beads.

RNA was isolated from each TRIzol® sample as per Appendix A.5 in a final volume of 20 µL. Five µL RNA sample were mixed with 5 µL 1x RNA loading buffer (supplied with the *in vitro* transcription kit), and loaded onto a 1.2% TBE-agarose gel and electrophoresed (50V, 2 h). RNA was visualised with ethidium bromide (Sigma).

Table 4.8: RBP-assay buffer

Component	For 10 mL	Final conc (mM)
HEPES (1 M)	100 µL	10.0
Potassium acetate (1 M)	900 µL	90.0
Magnesium chloride (0.5 M)	30 µL	1.5
Potassium chloride (1 M)	400 µL	40.0
Dithiothreitol (2.5 M)	25 µL	2.5
Water (RNA-grade)	up to 10 mL	-
See Appendix B for manufacturer details of each component		

4.2.4.4 RNA-binding protein pullout assay

Based on Olanich, *et al.*[160], seven RNA-binding protein isolations were performed using biotinylated RNA. Each isolation followed a core protocol (below); however optimisation of the assays required variations that are detailed in Table 4.9. These experiments used K-562 cell extract prepared using NP-40 lysis buffer (2.2.6.1).

Table 4.9: Variable conditions for each RNA-binding protein pullout assay

Assay	I	II	III	IV	V	VI	VII
In vitro transcription							
Template: PCR	✓	✓					
Template: linearised plasmid			✓	✓	✓	✓	✓
Binding assay							
Protein amount (mg)	1.0	1.0	0.5	0.25	0.25	0.25	0.25
tRNA addition							✓
RNaseOUT™							✓
RNA amount (µg)	20	20	10	10	10	10	10
65°C RNA pre-incubation			✓	✓	✓	✓	✓
Washes	5	5	4	4	4	4	4
Gel							
10% polyacrylamide gel (6 cm)	✓						
7.5% polyacrylamide gel (20 cm)		✓	✓	✓	✓		
4-20% TGX gradient gel (8 cm)						✓	✓
Visualisation							
Silverstain volume (mL)	25	50	50	50	50	25	25
Scanner	✓						
Phone camera/light box		✓	✓	✓	✓	✓	✓

K-562 cell lysate was pre-cleared with 50 µL (PBS-washed) streptavidin agarose at 4^{o}C overnight, in 400 µL RBP-assay buffer, to remove streptavidin binding proteins. The following day, RNA was heated to 65^{o}C for 5 min and cooled to room temperature. Pre-cleared protein was then added to the RNA and incubated at 4^{o}C for 1.5 h. The RNA-protein mix was then added to 50 µL PBS-washed streptavidin agarose and incubated at 4^{o}C for 2 h.

Samples were washed with 400 µL RBP-assay buffer, then resuspended in protein sample buffer.

4.2.4.4.1 TCA precipitation

Proteins were precipitated from the collected washes using trichloroacetic acid. To each of the washes, 250 µL of trichloroacetic acid (Sigma) per mL were added and the tubes left on ice for 10 min. Tubes were centrifuged (10600g, 5min, 4^{o}C), the supernatant was removed, and acetone (1 mL, Merck) added. Tubes were centrifuged (20800g, 5min, 4^{o}C) and the pellet resuspended in protein sample buffer.

4.2.4.4.2 Protein gel electrophoresis

Bead samples were boiled at 95^{o}C for 5 min and loaded on the gel. The Full-Range Rainbow™ marker was used to estimate protein size. The gel was electrophoresed at 150 V until the 12-kDa band reached the end of the gel, according to the parameters in Table 4.10.

Table 4.10: Parameters for gel electrophoresis

Size	%	Composition	Casting and electrophoresis equipment
Small (8 cm)	10 or 7.5	Resolving: 6 mL* Stacking gel*	mini-PROTEAN
Large (20 cm)	7.5	Resolving: 20 mL* Stacking gel*	PROTEAN II xi Cell
Small (8 cm)	4-20	TBX (precast)†	mini-PROTEAN
All gels run in tris-glycine running buffer (Appendix B) * Gel recipes in appendix B †TBX precast gel (BIO-RAD)			

4.2.4.4.3 Silver staining

Following electrophoresis, excess gel was removed by a scalpel (if necessary). Then protein bands were visualised using the Pierce Silver Stain kit (Thermo Scientific, Rockford, IL USA) as per the manufacturer's instructions.

4.2.4.4.4 Gel image capture

The image of the gel in the first assay was captured using the CanoScan™ LiDE 60 scanner (Canon Inc, Surrey, UK). Other gels were captured using the X6 phone camera (Nokia, Brisbane, Australia). A light box (Genetic Research Instrumentation Ltd, Essex, UK) was also used to improve image quality.

4.2.5 Next generation S1 aptamer

4.2.5.1 T7 promoter-driven tethered-S1-aptamer *BCR-ABL* 3'UTR vectors

A vector containing the tethered-S1-aptamer in pcDNA3 (pcDNA3-tRSA) was kindly provided by Prof. Ian Macara (University of Virginia, USA). The aptamer was shuttled into *Kpn*I/*Eco*RI sites in pBSII-ABL3'UTR(F) and pBSII-ABL3'UTR(R). pBSII-ABL3'UTR(F) was digested with *Eco*RI/*Xba*I to remove the polylinker between the aptamer and the 3'UTR. This was not possible for pBSII-ABL3'UTR(R) because it has two *Xba*I sites flanking the 3'UTR.

pBSII-ABL3'UTR(F) and (R), (2 µg) and pcDNA3-tRSA (5 µg) were digested with 20 U of *Kpn*I-HF and *Eco*RI-HF in 1x BSA, 1x NEB buffer 4 and water (up to 20 µL). The digests were incubated at 37°C for 1 h. CIP (1 µL) was added to the pBSII-ABL3'UTR digests and incubated at 37°C for 15 min. pBSII-ABL3'UTR and aptamer DNA was purified by gel extraction as per Appendix A.9, and ligated as per Appendix A.10. The pBSII-tRSA-ABL3'UTR(F) vector was digested with *Eco*RI-HF and *Xba*I (as above), and blunt ends were created using T4 polymerase (Appendix A.17) and ligated as per (appendix A.10). Plasmids were confirmed by sequencing Appendix A.4.

4.2.5.2 *In vitro* transcription

Next-gen-S1 tagged *ABL1* 3'UTR (forward and reverse orientation) RNA was *in vitro* transcribed using the T7-MEGAscript™ *in vitro* transcription kit according to the manufacturer's instructions. The transcription template was linearised plasmid. Plasmids from 4.2.5.1 (4 µg) were digested with *Not*I-HF (40 U) in 1x NEB buffer 4, 1x BSA and water (up to 50 µL). The plasmids were purified by alcohol precipitation (Appendix A.16). The transcription reaction was performed at 37°C overnight, using 1 µg linearised plasmid template. RNA was purified by phenol-chloroform extraction/alcohol precipitation (as per kit's instructions).

Next-gen-S1-tag RNA was *in vitro* transcribed using the T7-MEGAshortscript™ i*n vitro* transcription kit according to the manufacturer's instructions. The transcription reaction was performed at 37°C overnight, using 1 µg linearised pcDNA3-tRSA plasmid template (see above). RNA was purified by phenol-chloroform extraction/alcohol precipitation (as per kit's instructions).

4.2.5.3 Streptavidin agarose binding assay

This was done as per 4.2.4.3, except that the RNAs were heated at 65^{o}C for 5 min prior to addition of streptavidin agarose. Bands were quantified using Scion Image software (v4.0.2b. Scion Corporation, Frederick, MD, USA)

4.2.5.4 RNA-binding protein pullout assay (assay VIII)

K-562 cell lysate was pre-cleared with 10 µg/mg avidin, 100 µg tRNA (10x RNA amount) (Ambion) and RNase inhibitor, RNaseOUT™ (200 U) (Invitrogen) at 4^{o}C for 30 min.

Next-gen-S1-tagged forward-and-reverse-orientation 3'UTR RNA (10 µg) was heated at 65^{o}C for 5 min, then cooled to room temperature in 300 µL RBP-assay buffer. Each RNA was then added to separate tubes containing 50 µL PBS-washed streptavidin agarose and RNaseOUT™ (200 U); 4^{o}C for 30 min. The beads were washed twice with 200 µL RBP-assay buffer. Then 1 mg (200 µL) of the pre-cleared lysate was added to each tube and left at 4^{o}C for 1.5 h.

Agarose beads were washed four times with RBP-assay buffer, and resuspended in protein sample buffer (100 µL) and 5 mM D-biotin.

4.2.5.4.1 Protein gel electrophoresis

Bead samples were boiled at 95^{o}C for 5 min, then 20 µL was loaded on a 4-20% TBX gradient gel as per 4.2.4.4.2. The gel was silver-stained and photographed as per 4.2.4.4.3 and 4.2.4.4.3 respectively.

4.2.6 Mass spectrometry

The Adelaide Proteomics Centre electrophoresed the samples on a gradient gel and excised out a band approximately 60 kDa for LC-eSI-IT mass spectrometry. The complete methods are described in Appendix C.

4.3 Results

Our method for isolating proteins bound to the *ABL1* 3'UTR used an RNA-tagging approach. For each of the *ABL1* 3'UTR RNA tags, initial experiments tested their ability to isolate the RNA. Then if the tag was suitable, the tagged RNA was used to try and capture RNA-binding proteins.

4.3.1 The S1-RNA aptamer

The potential for the S1-tag to capture proteins bound to RNA *in vivo* made it an ideal candidate for labelling *ABL1* 3'UTR RNA. We incorporated the S1-tag into an *ABL1* 3'UTR expression vector within a predicted stem-loop structure as recommended by Walker, *et al.*[358]. Before the tag was used for enriching *ABL1* 3'UTR RNA, it was first examined if insertion of the tag altered the regulatory potential and thus protein interactions of the 3'UTR.

4.3.1.1 Intra *ABL1* 3'UTR insertion of the S1-tag does not affect luciferase expression

Altering the 3'UTR via insertion of the S1-tag may change its structure or properties. This may block the binding of key factors that interact with the *ABL1* 3'UTR, and thus prevent their identification. We compared the reporter activity of phRL-ABL3'UTR and phRL-ABL3'UTR-S1 to see if the reporter activity was dramatically altered by the S1-tag insertion. The results in Fig 4.6 show that insertion of the S1-tag does not considerably alter *ABL1* 3'UTR reporter activity. This suggested that the insertion of the S1-tag did not disturb the binding of important binding factors to the *ABL1* 3'UTR.

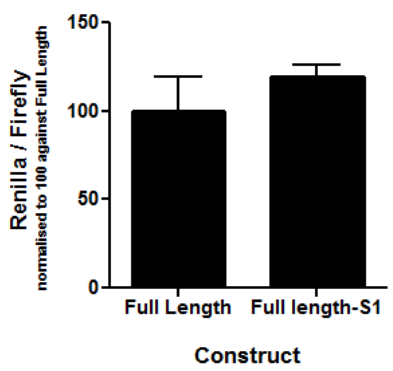

Fig 4.6: Insertion of the S1-tag does not interfere with ABL1 3'UTR reporter activity. HeLa cells were transfected with the wildtype full length *ABL1* 3'UTR reporter and a full length *ABL1* 3'UTR reporter containing the S1-tag. Luciferase activity was then measured 48 h post-transfection. The graph shows relative Renilla luciferase activity normalised to 100 against full length *ABL1* 3'UTR.

4.3.1.2 Streptavidin agarose did not enrich S1-tagged RNA

Since insertion of the S1-tag did not alter the function of the *ABL1* 3'UTR, S1-tagged RNA enrichment by streptavidin was examined using qRT-PCR. *Renilla* was quantified from HeLa cells transfected with phRL-ABL3'UTR-S1, along with the first and last washes, and the final elution of the enrichment assay. Only a modest enrichment was observed between the final

wash and elution samples, and most of the *Renilla* RNA was detected in the first wash (Fig 4.7).

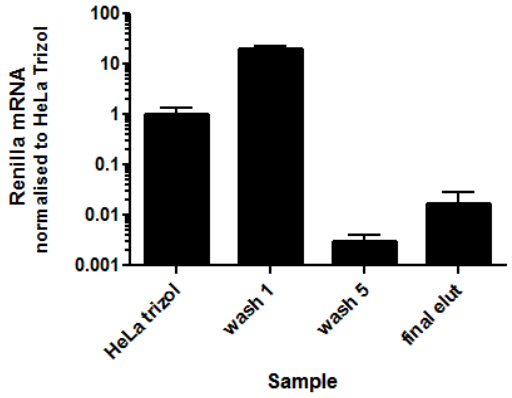

Fig 4.7: Quantification of *Renilla* RNA following streptavidin enrichment of cell extract, from HeLa cells transfected with the S1-tag *ABL1* 3'UTR vector (experiment 1). HeLa cells transfected with the S1-tag-*ABL1* 3'UTR vector (0.35 µg) were harvested 48 h post-transfection. The cell lysate was incubated with streptavidin agarose beads in order to enrich for S1-tagged RNA. RNA samples were obtained from the bead washes, and final biotin elution. In addition, an identical transfection was performed, with the cells collected in TRIzol® 48 h post-transfection, to serve as an input control (HeLa trizol). *Renilla* mRNA was quantified by qRT-PCR using RNA isolated from the HeLa trizol input control sample, and wash 1, wash 5, and the final elution sample from the streptavidin agarose enrichment experiment. The graph shows *Renilla* mRNA normalised to 1 against the HeLa trizol sample. Data represent the mean ± SD for each qRT-PCR performed in triplicate. *Renilla* mRNA levels are relative to the amount of RNA used in the cDNA reaction.

To improve the enrichment, protein input was increased from 0.35 to 1.0 mg. In addition, qRT-PCR was performed for each step of the enrichment assay. The PCRs also included a 'no reverse transcriptase' control. This experiment showed that there was no difference between *Renilla* mRNA expression plus or minus reverse transcriptase (Fig 4.8). This is indicative that either the majority of the PCR signal was from plasmid DNA not removed by DNase treatment, and/or the cDNA synthesis was unsuccessful.

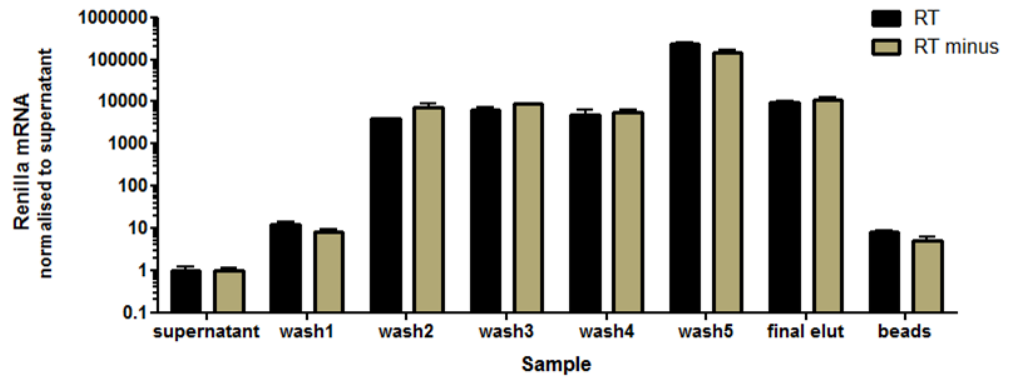

Fig 4.8: Quantification of *Renilla* RNA following streptavidin enrichment of cell extract, from HeLa cells transfected with the S1-tag *ABL1* 3'UTR vector (experiment 2). Similar to Fig 4.7, HeLa cells were transfected with the S1-tag-*ABL1* 3'UTR vector (1 µg), and then harvested 48 h post-transfection. In this experiment *Renilla* mRNA was quantified in each stage of the experiment, and included a no reverse transcriptase (RT minus) cDNA control. The top graph shows *Renilla* mRNA normalised to 1 against the 'supernatant' sample. Data represent the mean ± SD for each qRT-PCR performed in triplicate. *Renilla* mRNA levels are relative to the amount of RNA used in the cDNA reaction.

To show that the reverse transcription reaction was successful, a qualitative *G6PD* PCR was performed using primers that amplify a region of 343 bp in *G6PD* cDNA, or 636 bp in genomic DNA. A 350 bp band was observed for the two cDNA reactions containing reverse transcriptase, but not for the cDNAs lacking reverse transcriptase (Fig 4.9). Therefore, the cDNA synthesis was successful, and the signal in the *Renilla* qRT-PCRs was most likely due to plasmid contamination.

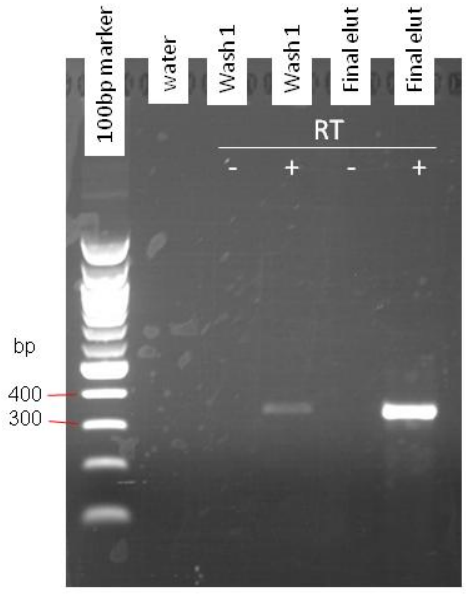

Fig 4.9: Qualitative PCR for *G6PD*, to check the integrity of the cDNA synthesis reaction. The wash 1 and final elution reverse transcriptase (RT) positive and negative cDNA reactions were used as a template for a qualitative PCR that amplified G6PD mRNA across several introns. PCRs were electrophoresed on a 1% TBE-agarose gel containing ethidium bromide in order to visualise DNA. No bands were observed in the RT minus lanes, indicative of no genomic DNA contamination in the isolated RNA.

A simple binding assay was developed to replace the PCR-based method for determining the binding capability of the S1-tag to streptavidin agarose. The S1-tag (only the minimal S1-sequence without the 3'UTR) was *in vitro* transcribed. The binding assay consisted of three conditions: RNA, RNA-streptavidin agarose and RNA-streptavidin agarose-biotin. Each sample was then electrophoresed on a non-denaturing TBE gel to preserve the S1-tag's conformation. RNA bound to streptavidin agarose should not migrate through the gel because the agarose-beads remain in the wells. The gel in (Fig 4.10, A) shows that the S1-tag did not bind streptavidin – a strong band was present in each lane. The assay was validated using a biotinylated oligonucleotide (a positive control for streptavidin binding). In this experiment, addition of the streptavidin beads to the oligonucleotide prevented the DNA from migrating through the gel, and, furthermore, addition of biotin competed out the oligonucleotide from the beads (Fig 4.10, B). These results show that the S1-tag does not bind to streptavidin in our system, and thus is not suitable for RNA-binding protein capture.

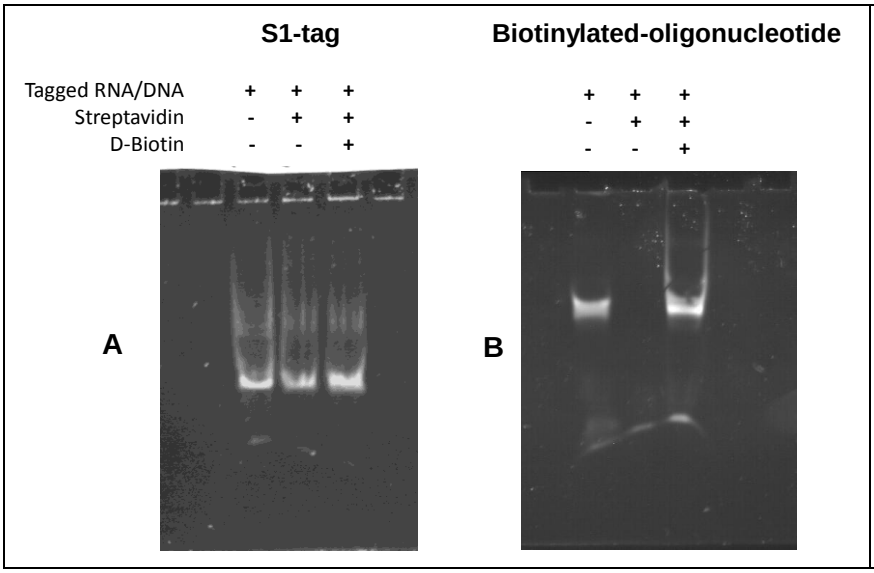

Fig 4.10: Streptavidin agarose failed to interact with S1-tag RNA. (**A**) S1-tag RNA was heated to 65°C and then incubated in the presence or absence of streptavidin agarose and biotin. These samples were then electrophoresed on a 10% non-denaturing TBE-acrylamide gel. (**B**) Same as **A**, except using a biontinylated-oligonucleotide.

4.3.2 Biotinylation of the *BCR-ABL* 3'UTR

Although the S1-tag does not bind streptavidin in our hands (Fig 4.10, A), the experiment involving the biotinylated-oligonucleotide (Fig 4.10, B) suggested that a biotin tag might be more suitable to isolate *ABL1* 3'UTR RNA. The biotin-tagged oligonucleotide strongly bound streptavidin, which was reversible upon addition of free biotin. The only drawback to this

approach is that the RNA-binding protein capture can only be performed *in vitro*, using cell extracts.

4.3.2.1 Streptavidin agarose enriched biotinylated RNA

In vitro transcribing the *ABL1* 3'UTR in the presence of 0.5 M biotinylated uracil randomly introduced approximately 30 biotin molecules into the 3'UTR (4.2.4.2). A slightly modified binding assay from 4.3.1.2 was performed to determine if biotinylated full-length *ABL1* 3'UTR RNA could bind streptavidin. The assay included *ABL1* 3'UTR which was not biotinylated as a control. After incubating the RNA with streptavidin, the streptavidin agarose was washed twice, and the RNA was then eluted with biotin/SDS[359].

Unbiotinylated RNA did not bind streptavidin agarose: most of it was visualised in the first wash (Fig 4.11). In contrast, the majority of the biotinylated RNA was visualised in the elution sample, indicative that the RNA strongly bound streptavidin. These results demonstrate that biotin-tagged RNA has the potential for capturing proteins bound to *ABL1* 3'UTR RNA.

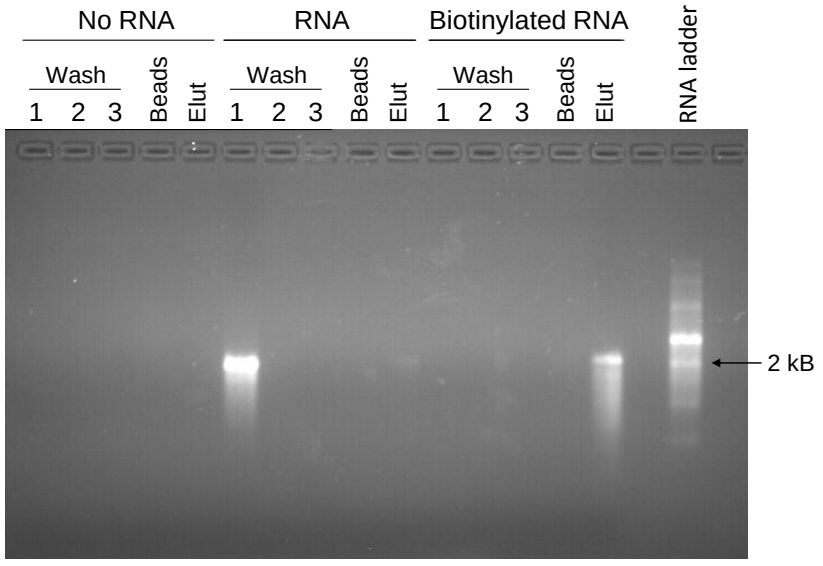

Fig 4.11: Biotinylated RNA can be captured by streptavidin agarose. RNA *in vitro*-transcribed in the presence or absence of biotinylated uracil was incubated with streptavidin agarose. The beads were washed, and RNA was then eluted with 2% SDS, 5mM D-biotin for 15 min at room temperature, then 65°C for 20 min, as recommended by Rybak, *et al.*[359]. Each step was collected in TRIzol® for RNA isolation. The RNA was then electrophoresed on a 1% TBE-agarose gel along with the ssRNA ladder. A no-RNA control was also included to show that the beads were not contaminated with RNA.

4.3.2.2 Optimisation of RNA-binding protein capture using biotin-tagged *ABL1* 3'UTR RNA

The RNA-binding protein capture assay involved mixing biotinylated *ABL1* 3'UTR with K-562 cell extract. Streptavidin agarose was then added to bind the *ABL1* 3'UTR. The unbound protein was then removed, and the beads washed five times to remove residual unbound protein. In the first assay, unbound protein, the five washes and the beads (containing RNA and captured protein) were electrophoresed on a 10% polyacrylamide gel (Fig 4.12). The gel shows that unbound proteins are removed by the second wash. In the beads lane, there is a silver stain smear throughout the lane, indicative that RNA-binding proteins were captured. There is a contaminant that is increasingly present from washes 3-5. This is thought to be the streptavidin beads, because bead-loss occurred during the washes. Also, the beads lane contains the remaining beads, and also has a large smear around the same molecular weight as washes 3-5. Although the beads should not migrate through the gel (see 4.3.2.1), it is possible that the TCA precipitation degraded/altered the streptavidin agarose, allowing contaminants to migrate through the gel.

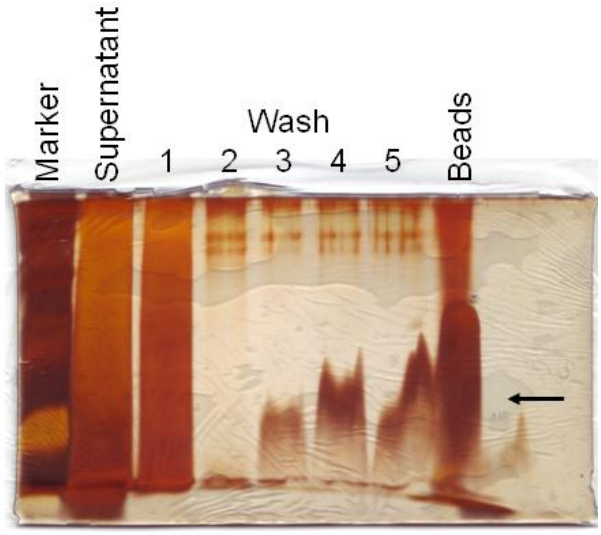

Fig 4.12: Silver-stained gel for each stage of RNA-binding protein isolation assay I. Biotinylated *ABL1* 3'UTR RNA was incubated with K-562 cell extract and streptavidin agarose. Several washes were performed to remove protein not bound to the 3'UTR. Protein samples from each step of the assay were electrophoresed on an 8-cm 10% SDS-PAGE gel, and protein visualised by silver-staining using the Pierce silver-staining kit. Marker was the full-range molecular weight marker - but was over-exposed during silver staining. Image captured on the LiDE-60 scanner. The contaminant described in the text is denoted by an arrow.

To try to observe discrete bands, the size of the gel was increased from 8 to 20 cm. In this experiment, the reverse 3'UTR RNA control was included to look for proteins specific to the forward 3'UTR sample. Increasing the gel size allowed for better protein separation,

however none of the bands were specific to the forward 3'UTR sample (Fig 4.13). These proteins may bind to streptavidin, or bind to RNA in a non-specific manner.

The contaminant was not present in this gel, increasing the likelihood it was indeed the streptavidin agarose. In this gel only the supernatant of the beads sample was loaded. Greater care was also taken to avoid bead-loss during the washes, illustrated by the lack of bands in the Wash 5 sample (also included to show that no protein remained after five washes).

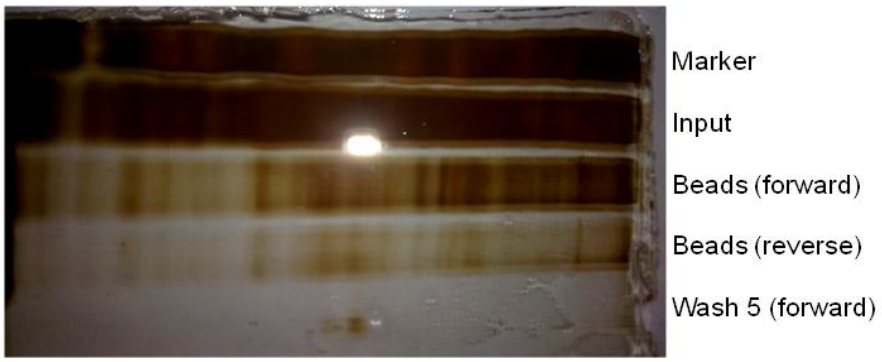

Fig 4.13: RNA-binding protein isolation assay II. Biotinylated *ABL1* 3'UTR RNA (forward and reverse orientation) was incubated with K-562 cell extract and streptavidin agarose. To enrich for proteins bound to the 3'UTR, several washes were performed to remove unbound protein. On the gel above, 1.0 mg K-562 protein (equiv to input), protein eluted from the final beads fraction and protein from wash 5 (TCA precipitated; from the forward orientation experiment) were electrophoresed on a 20-cm 7.5% SDS-PAGE gel. Protein was then visualised by silver-staining. 'Marker' corresponds to Full-Range Rainbow™ molecular weight marker. Image captured using the camera on a Nokia-X6 phone.

The next assay was scaled by half to reduce the amount of protein and RNA required per assay. The amount of washes was reduced to four due to the scaling-down of the experiment, and to avoid bead-loss (thus sample loss). This experiment further examined the effect of heating the RNA (and allowing it to cool to 37°C) to induce secondary structure prior to addition of cellular-proteins. A no-RNA control was also included to show that the proteins visible in the elution fraction bound the RNA, rather than the streptavidin-agarose. It is unclear if pre-heating the RNA altered protein binding, because the unheated RNA sample was over-exposed (Fig 4.14). However, heating the RNA did not appear to degrade it, as protein bands are visible. The 'No RNA' lane had smearing and could not be analysed.

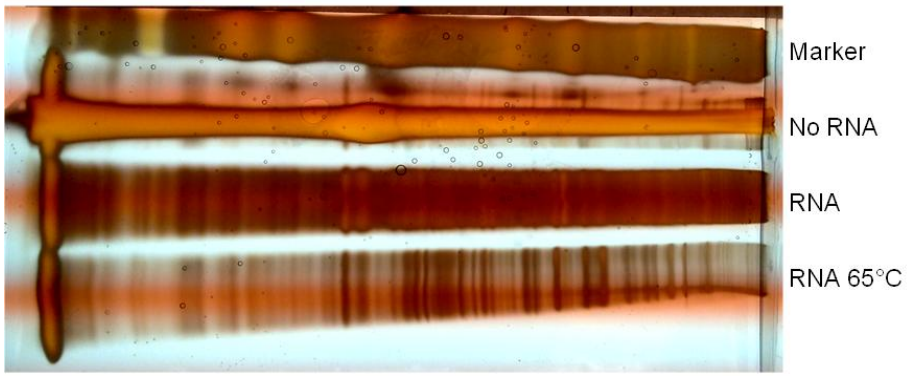

Fig 4.14: RNA-binding protein isolation assay III. Biotinylated *ABL1* 3'UTR RNA ("melted" (65°C) and "non-melted") was incubated with K-562 cell extract and streptavidin agarose. A no-RNA control was also included, to indicate if proteins were binding to the streptavidin beads in the absence of RNA. To enrich for proteins bound to the 3'UTR, several washes were performed to remove unbound protein. On the gel above, protein from the final beads fraction for each experiment was electrophoresed on a 20-cm 7.5% SDS-PAGE gel. Protein was then visualised by silver-staining. 'Marker' corresponds to Full-Range Rainbow™ molecular weight marker. Image captured using the camera on a Nokia-X6 phone. A light-box was used to improve visualisation of the silver-stained bands.

It was important to know which bands were present because they interacted with the streptavidin beads (protein bands found in the elution fraction in the presence or absence of RNA). Therefore the assay was performed with beads alone and biotinylated 3'UTR. Because the protein amount appears to be in excess, the protein input was halved from 500 to 250 µg. The 'No RNA' sample had fewer bands than the RNA sample in this experiment, similar to the previous gel (Fig 4.15). This suggests that pre-blocking the cell lysate with streptavidin beads removed most of the streptavidin-binding proteins from the assay.

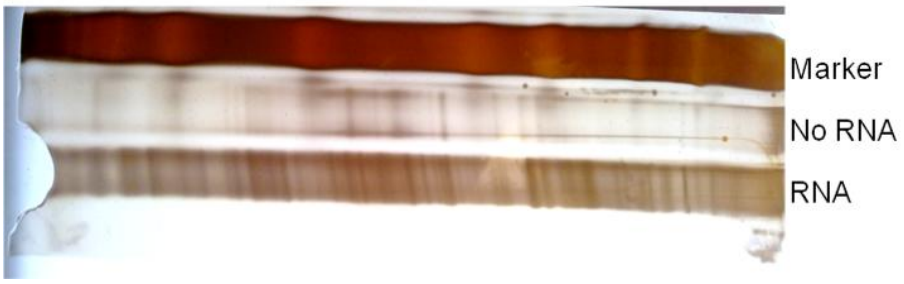

Fig 4.15: RNA-binding protein isolation assay IV. Biotinylated *ABL1* 3'UTR RNA was incubated with K-562 cell extract and streptavidin agarose. A no-RNA control was also included, to indicate if proteins were binding to the streptavidin beads in the absence of RNA. To enrich for proteins bound to the 3'UTR, several washes were performed to remove unbound protein. On the gel above, protein from the final beads fraction for each experiment was electrophoresed on a 20-cm 7.5% SDS-PAGE gel. Protein was visualised by silver-staining. 'Marker' corresponds to Full-Range Rainbow™ molecular weight marker. An image of the gel was captured using the camera on a Nokia-X6 phone and a light-box.

Next, the reverse orientation 3'UTR RNA was included in order to identify bands specific to the forward orientation 3'UTR. The gel for this experiment did not run as well as the previous ones. However, it was seen for the third time, that the 'No RNA' sample contained much less protein than the RNA-containing samples (Fig 4.16). This provides further evidence that the proteins observed in the RNA lanes are binding the tagged RNA and not the streptavidin beads.

Fig 4.16: RNA-binding protein isolation assay V. Biotinylated *ABL1* 3'UTR RNA (forward and reverse orientation) was incubated with K-562 cell extract and streptavidin agarose. A no-RNA control was also included, to indicate if proteins were binding to the streptavidin beads in the absence of RNA. To enrich for proteins bound to the 3'UTR, several washes were performed to remove unbound protein. Protein from the final beads' fraction for each experiment was electrophoresed on a 20-cm 7.5% SDS-PAGE gel. Proteins were visualised by silver-staining. 'Marker' corresponds to Full-Range Rainbow™ molecular weight marker. An image of the gel was captured using the camera on a Nokia-X6 phone and a light-box. The silver-stain "splotch" on the left hand side of each 'RNA', and the 'no RNA' lanes, is presumed to be bromo-phenol blue, present in the loading buffer.

In the next assay, samples were run on a 4-20% gradient TGX precast gel. It was predicted that this gel would improve the resolution of the bands observed, in addition to reducing inconsistencies between gels. Other advantages of this gel are that the smaller size allows the use of the mini-PROTEAN gel apparatus, which is less laborious than the PROTEAN II xi Cell apparatus. A smaller gel also reduces the amount of reagents required for running and staining the gel. Furthermore, the precast gel is keratin-free which should benefit downstream mass spectrometry analysis.

As expected, the protein bands were much sharper when run on the gradient gel. However, high and low molecular weight proteins were not visible, and there were no bands specific to the forward RNA (Fig 4.17).

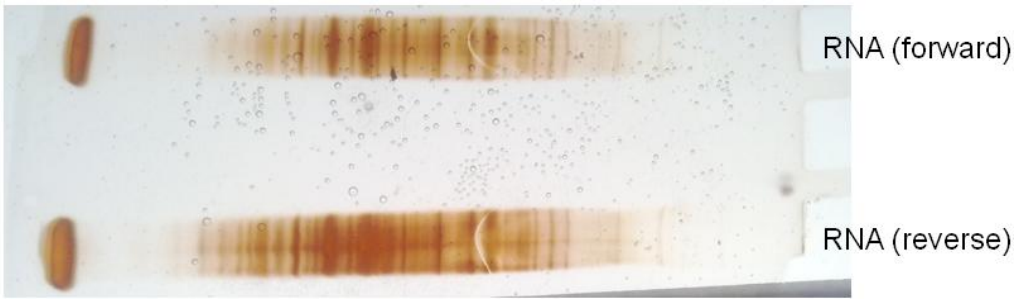

Fig 4.17: RNA-binding protein isolation assay VI. Biotinylated *ABL1* 3'UTR RNA (forward and reverse orientation) was incubated with K-562 cell extract and streptavidin agarose. To enrich for proteins bound to the 3'UTR, several washes were performed to remove unbound protein. On the gel above, protein from the final beads fraction for each experiment was electrophoresed on an 8-cm 4-20% TGX gradient gel (BIO-RAD). Protein was visualised by silver-staining. An image of the gel was captured using the camera on a Nokia-X6 phone and a light-box. Protein size marker not shown.

To try to reduce non-specific protein binding to the RNA, tRNA was added during protein pre-clearing with streptavidin as a sink for non-specific RNA binding proteins. RNAse inhibitors were also included in the assay in case RNA degradation caused non-specific protein binding. The gel (Fig 4.18) appears to have fewer bands than the previous gel (Fig 4.17). However it is unclear if this is was due to less protein in the sample, silver staining development, or if non-specific binding was reduced. Again, there were no bands specific to the forward RNA sample.

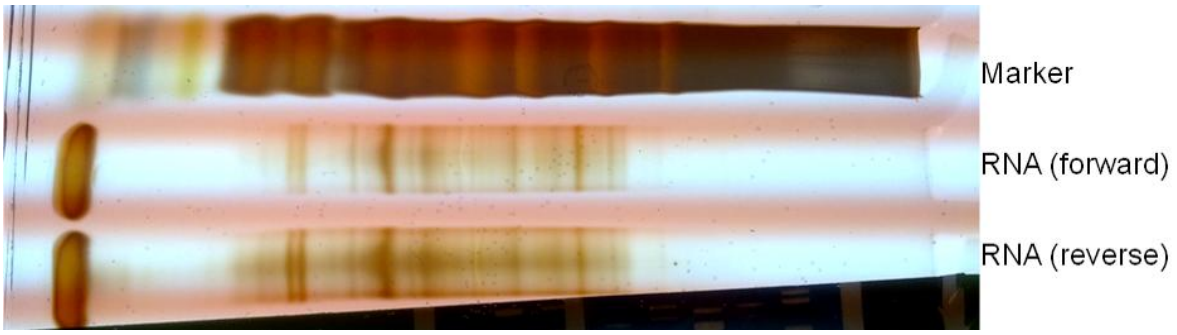

Fig 4.18: RNA-binding protein isolation assay VII. Biotinylated *ABL1* 3'UTR RNA (forward and reverse orientation) was incubated with K-562 cell extract and streptavidin agarose. To enrich for proteins bound to the 3'UTR, several washes were performed to remove unbound protein. On the gel above, protein from the final beads fraction for each experiment was electrophoresed on an 8-cm 4-20% TGX gradient gel. Marker corresponds to Full-Range Rainbow™ molecular weight marker. Protein was visualised by silver-staining. An image of the gel was captured using the camera on a Nokia-X6 phone and a light-box. Horizontal lines are refresh-rate blemishes from the light-box.

4.3.3 Next-gen tRNA-tethered-S1-tag

The previous binding assays involving biotinylated RNA paved the way for optimising key technical aspects of the RNA-binding protein capture assay. However, these experiments did not identify any protein bands specific for *ABL1* 3'UTR RNA. A possible explanation involves the structure of the RNA. Approximately 30 biotinylated uracils are present throughout the *ABL1* 3'UTR (4.2.4.2). Thus, there will be multiple anchor-points between the RNA and streptavidin beads. This may alter the secondary structure and/or make regions of the 3'UTR inaccessible to RNA-binding proteins. It also forces a bias against proteins which bind to motifs containing uracils or near uracil-containing motifs, such as AU-RE binding proteins. Therefore, using the next-gen tethered-tRNA S1-tag to end label the 3'UTR might increase the success of capturing *ABL1* 3'UTR-specific RNA-binding proteins.

4.3.3.1 Streptavidin agarose enriched tRNA-tethered-S1-tagged RNA

A streptavidin-binding assay was used to determine the binding capability of the next-gen S1-tag alone or when fused to the end of the *ABL1* 3'UTR. One-third of the next-gen S1-tag RNA bound to the streptavidin beads (Fig 4.19, A, C). Upon addition of the 3'UTR in the forward or reverse orientation approximately 15% of the tagged RNA bound to the beads (Fig 4.19, B, C). The experiment also showed that two washes removed most of the unbound RNA (Fig 4.19, A, B).

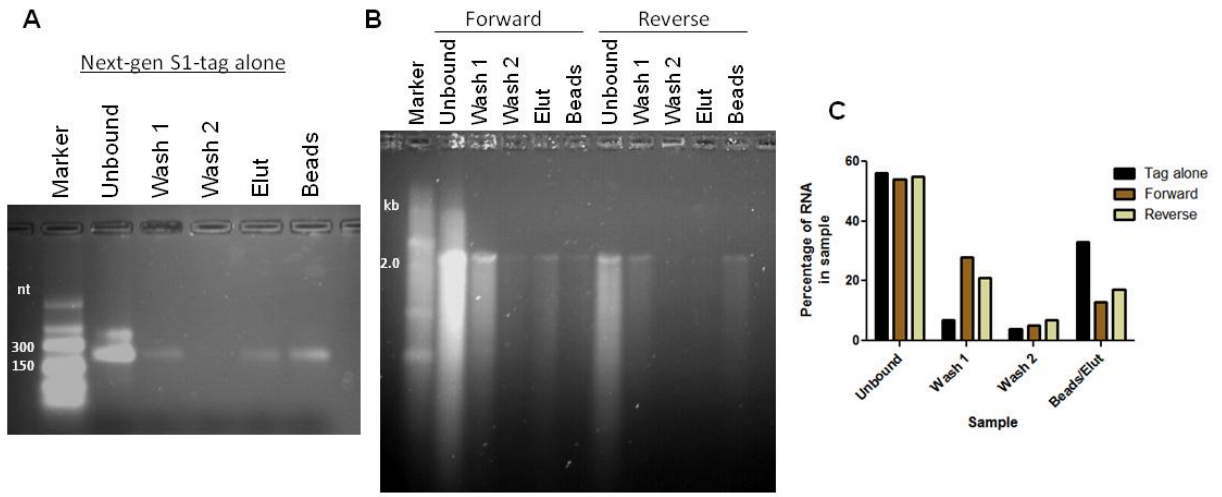

Fig 4.19: Next-gen S1-tagged RNA can be captured by streptavidin agarose. (**A**) The next gen S1-tag (alone) was *in vitro* transcribed and incubated with streptavidin agarose. The beads were washed, and then RNA was eluted with 2% SDS, 5mM D-biotin for 15 min at room temperature, followed by 65°C for 20 min, as recommended by Rybak, *et al.*[359]. Each step was collected in TRIzol® for RNA isolation. The RNA was then electrophoresed on a 1% TBE-agarose gel along with a low range ssRNA ladder. (**B**) Same as **A**, but the next-generation S1-tagged *ABL1* 3'UTR RNA (forward and reverse orientation) was *in vitro* transcribed, and treated as above. The RNA was then electrophoresed on a 1% TBE-agarose gel along with the ssRNA ladder. (**C**) Quantification of the percentage RNA amount in each sample. Bead and elution fractions were grouped together because the RNA was not eluted from the beads in the RNA-binding protein isolation experiments. It was done in these experiments to show it was possible to elute RNA from the beads. The 200 nt (S1-tag) and 2000 nt (S1-tag-3'UTR) bands were quantified using Scion Image software (v4.0.2b. Scion Corporation)

4.3.3.2 RNA-binding protein isolation

The banding patterns of proteins isolated using the next-gen S1-tag appeared similar to the biotin-tag. However, in the next-gen tag experiment, there was a band of approximately 60 kDa that appeared specific to the forward 3'UTR sample (Fig 4.20). The samples were then sent to the mass spectrometry facility in order to identify the corresponding protein.

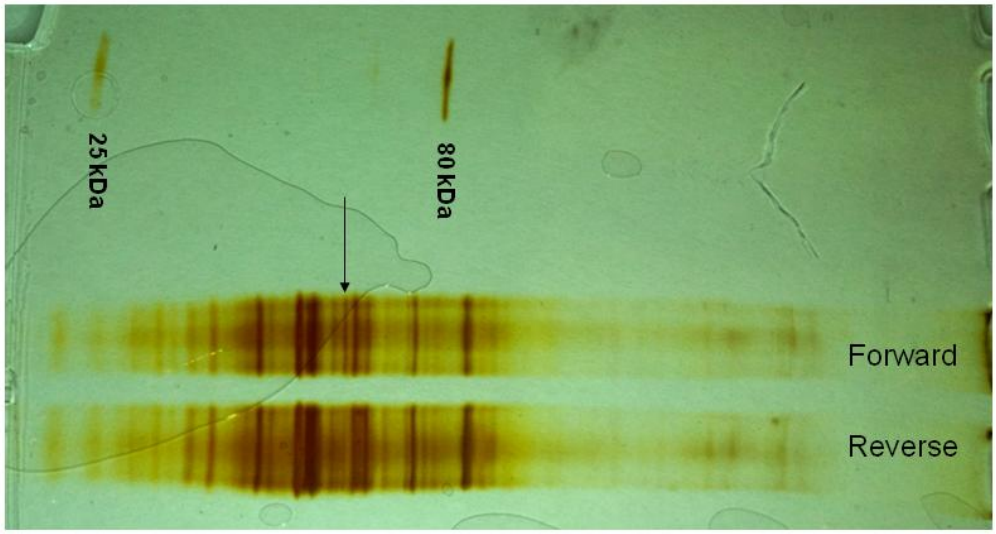

Fig 4.20: RNA-binding protein isolation assay VIII. Next-generation S1-tagged *ABL1* 3'UTR RNA (forward and reverse orientation) was incubated with K-562 cell extract and streptavidin agarose. To enrich for proteins bound to the 3'UTR, several washes were performed to remove unbound protein. On the gel above, protein from the final beads fraction for each experiment was electrophoresed on an 8-cm 4-20% TGX gradient gel. Marker was "protein ladder 10-250 kDa" – however only the most intense markers: 25 and 80 kDa were visualised. Protein was then visualised by silver-staining. An image of the gel was captured using the camera on a Nokia-X6 phone and a light-box. Arrow indicates a protein band present in the forward orientation RNA lane, but not the reverse orientation lane.

The samples were electrophoresed on a 4-12% gel at the mass spectrometry facility. A band of a similar size (as in Fig 4.20), appeared more predominant in the forward sample compared to the reverse 3'UTR sample (Fig 4.21). This band was cut out for LC-eSI-IT mass spectrometry.

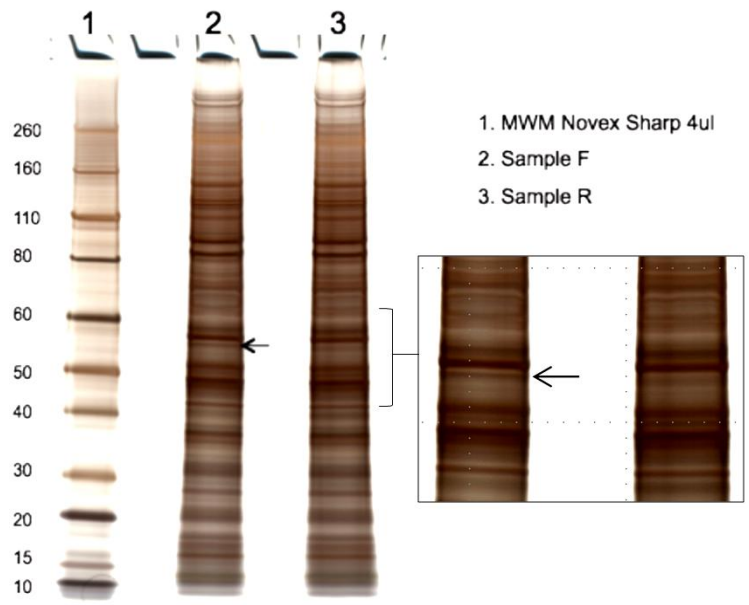

Fig 4.21: Samples from RNA-binding protein isolation assay VIII electrophoresed for mass-spectrometry. Samples from Fig 4.20 were re-electrophoresed on a 4-12% bis-tris gradient gel in 1x MOPS buffer by mass-spectrometry facility staff (see Appendix C). Sample F and Sample R correspond to forward and reverse orientation *ABL1* 3'UTR RNA sample respectively. Part of the gel (right) is enlarged to highlight a protein band more predominant in the forward orientation RNA lane. This band is of a similar size to the band highlighted in Fig 4.20.

4.3.3.3 Mass spectrometry analysis

LC-eSI-IT mass spectrometry was performed on the band of interest. Table 4.11 details the proteins identified in the forward sample. The subsequent table (Table 4.12) sorts the proteins by ionscore, which is based on the sequence coverage, peptide matches and relates to the probability of the protein identification. The top protein hit was Aspartyl-tRNA synthetase (Table 4.12). The Genecards, Uniprot and PubMed internet-based databases were used to find evidence that these proteins could interact with RNA (Table 4.12). Of the proteins identified, only four showed evidence of RNA-binding properties (Aspartyl-tRNA synthetase, ATP synthase alpha, tRNA-splicing ligase RtcB homolog and Inosine-5'-monophosphate dehydrogenase 2 (known as IMPDH2)) (Table 4.12). Of these proteins, only IMPDH2 is a realistic candidate for regulation of *BCR-ABL*, as discussed below.

Table 4.11: Proteins identified by mass spectrometry sorted alphabetically

Protein (sorted alphabetically)	Accession (_HUMAN)	MW	Sequence coverage (%)	Peptide matches
Adenylyl cyclise-associated protein 1	CAP1	65.7	7	4
Aspartyl-tRNA synthetase, cytoplasmic	SYDC	57.5	16	8
ATP synthase alpha, mitochondrial	ATPA	59.8	11	7
Chromosomal transmission fidelity protein 8 homolog isoform 2	CTF8A	63.1	4	4
Inosine-5'-monophosphate dehydrogenase 2	IMDH2	62.3	10	2
Nicalin	NCLN	50.0	4	2
Protein disulphide-isomerase A3	PDIA3	57.1	11	6
Protein phosphatase 1F	PPM1F	57.8	6	2
T-complex protein 1 subunit beta	TCPB	53.7	8	3
tRNA-splicing ligase RtcB homolog	RTCB	66.2	10	3

Table 4.12: Proteins identified by mass spectrometry sorted by ionscore

Protein (sorted by ionscore*)	Accession (_HUMAN)	MW	Sequence coverage (%)	Peptide matches	RNA binding#
Aspartyl-tRNA synthetase, cytoplasmic	SYDC	57.5	16	8	Yes
ATP synthase alpha, mitochondrial	ATPA	59.8	11	7	Yes
Protein disulphide-isomerase A3	PDIA3	57.1	11	6	No
tRNA-splicing ligase RtcB homolog	RTCB	66.2	10	3	Yes
T-complex protein 1 subunit beta	TCPB	53.7	8	3	No
Protein phosphatase 1F	PPM1F	57.8	6	2	No
Nicalin	NCLN	50.0	4	2	No
Chromosomal transmission fidelity protein 8 homolog isoform 2	CTF8A	63.1	4	4	No
Adenylyl cyclise-associated protein 1	CAP1	65.7	7	4	No
Inosine-5'-monophosphate dehydrogenase 2	IMPDH2	62.3	10	2	Yes^

*ionscore relates to the probability that the prediction is correct, and is based on both sequence coverage and peptide matches.
^ assumption based from[360]
# Protein considered to bind RNA based on evidence from www.genecards.org, www.uninprot.org, and http://www.ncbi.nlm.nih.gov/pubmed.
Keratin hits (four) excluded from table
MW, molecular weight.

4.4 Discussion

This chapter described the establishment of an assay to capture proteins that interact with the *BCR-ABL* 3'UTR. The basis of this approach was to use the 3'UTR as a bait and affinity

purify interacting proteins. This strategy has been successfully used to identify RNA-protein interactions with the 3'UTR[160,210,343,344,353].

Unfortunately our assay failed to generate a list of candidate proteins that could potentially regulate BCR-ABL expression. For example, Li, *et al.*'s study yielded approximately 30 potential protein interactions with biotinylated-*LDL receptor* 3'UTR RNA[210]. From that study's published gel photo, ten of the protein bands were conspicuously present in the 3'UTR sample[210]. Based on length (the *LDL receptor* 3'UTR is 2.5 kb) that study is the best comparative example for the *ABL1* 3'UTR. The only significant difference between Li, *et al.*'s and our approach is the time of protein-RNA complex formation: 16 h compared with 3 h, respectively[210]. We based our biotinylation-tag experiments on the system from Olanich, *et al*., which successfully identified proteins bound to the *NPM1* 3'UTR[160]. Because our difficulty was with non-specific protein interactions, increasing the time of RNA-protein complex formation would not improve our assay.

What worked

Despite not generating a list of candidate proteins which regulate BCR-ABL, a number of logistical parameters were optimised. We showed that the biotin-tagged RNA had a high affinity for the streptavidin beads (Fig 4.11). In our hands, we found that the next-gen S1-tag (Fig 4.19), but not the minimal S1-tag sequence (Fig 4.10, A), could bind streptavidin (albeit poorly relative to biotin-tagged RNA). Cellular proteins did not bind non-specifically to the streptavidin beads (Fig 4.14-16). And, the washes successfully removed unbound protein (Fig 4.12 and 4.13).

In addition, we optimised some of the equipment to run the assay. We found that using 4-20% TGX gradient gels, instead of 8- or 20-cm (non-gradient) SDS gels, provide optimal protein band separation. With the lack of a proper image capture apparatus, we used a light box and mobile phone camera to visualise the bands more clearly and obtain gel images. Furthermore, the sample we sent to the mass spectrometry facility was relatively keratin-free. The top hits were genuine proteins-hits and not keratin contamination, thus highlighting the cleanliness of our experimental technique (Appendix C).

Where is our list of candidates?

Even though (to the best of our ability) we used protocols that have isolated protein-RNA interactions, our experiments were not as successful. We failed to observe discrete bands between the forward and reverse 3'UTR bait RNAs. Possible explanations include the binding buffer not being stringent enough, the reverse 3'UTR RNA also interacting with many proteins, or the *in vitro* nature of the assay preventing *bone fide* protein-RNA interactions.

The silver-stain gel protein-fingerprints in both our and Olanich, *et al.*'s study exhibit many bands (Fig 4.12-21;[160]), which may suggest that the binding buffer is not stringent enough. However, in Olanich, *et al.*'s study, there are a number of bands that are clearly specific to a particular sample[160]. Altering the salt concentration of the binding buffer is one way to alter the stringency of the assay. Increasing the salt concentration of the binding buffer will disrupt the ionic interactions between protein and RNA and thus the stringency of the assay[361]. Future experiments should include a salt gradient in the washing stages to try to remove weakly bound proteins and increase the potential for differential bands between the two RNA bait samples.

Although the reverse strand of the *ABL1* 3'UTR (probably) does not exist in the cell, it has a larger repressive effect on Renilla expression than the forward orientation 3'UTR (data not shown). Therefore, it does interact with regulatory molecules. We considered the reverse orientation a suitable candidate for a negative control (prior to the knowledge of its regulatory activity) due to it being identical in size. Other studies have used coding sequences[210] and intronic sequences[349] as their 'negative control'. Coincidently, the size of the *LDL receptor* coding sequence is almost identical to the 3'UTR making it an ideal control. In comparison, the *ABL1* coding sequence is approximately 4kb (double the size of the 3'UTR). If the salt gradient optimisation fails to improve the assay, switching the negative control to the *ABL1* coding sequence should be considered.

The pullout assay is entirely *in vitro*. Cell extract is mixed with tagged-RNA in a tube and then subjected to purification. These conditions may favour binding of non-specific RNA-chaperone proteins over proteins that specifically control RNA stability. For example, the RISC microRNA machinery may only be formed in a cellular context, or important protein-RNA interactions may only occur in a particular location in the cell. Although the next-gen S1-tag allows for expression inside the cell, we opted to initially perform this experiment *in vitro*. The difficulty to transfect haemopoietic cells, or stably over express the

ABL1 3'UTR in these cells (data not shown) were the reasons for using the *in vitro* approach. Another strategy is to use a biotin-probe for the *BCR-ABL* transcript (Fig 4.4). This approach involves purification of *BCR-ABL* mRNA-protein complexes from cell extracts using a biotin-tagged oligonucleotide-probe specific to *BCR-ABL*. This method was used to identify proteins that interact with the 3'UTR of dengue virus RNA[353]. Successful knockdown of BCR-ABL using siRNAs designed against the *BCR-ABL* e13a2 and e14a2 transcripts[114,116,119] suggests that the biotin-probe can access the *BCR-ABL* junction. Furthermore, this strategy would allow for specific-purification of the *BCR-ABL* transcript, rather than the *ABL1* 3'UTR alone. In addition, any type of cell extracts, including from primary CML cells are suitable for this method. This poses as an exciting strategy to identify clinically relevant protein-RNA interactions in the context of the entire *BCR-ABL* transcript.

Isolation of a 60 kDa band

In the last experiment, using next-gen S1-tagged RNA, a band of approximately 60 kDa was differentially observed in the forward orientation 3'UTR sample (Fig 4.21). Mass spectrometry identification produced a number of hits for this protein (Table 4.11), the top three being Aspartyl-tRNA synthetase, ATP synthase alpha (mitochondrial) and PDIA3 (also known as GRP58). Aspartyl-tRNA synthetase is required for aminoacylation (joining amino acids to tRNA molecules)[362]. As the next-gen S1-tag consists of the S1-tag tethered to a tRNA molecule, Aspartyl-tRNA synthetase may have been trying to add an amino acid to the RNA-tag. ATP synthase alpha was eliminated as a *bone fide* interactor of the 3'UTR based on it being a mitochondrial protein. PDIA3 is involved in protein folding and loading peptides into the major histocompatibility complex (class I)[363] and there is no evidence that is can interact with RNA (Table 4.12). Based on this, it was also excluded.

After the top three proteins, the peptide-matches in the mass spectrometry data decrease significantly (Table 4.12). Therefore, discussion will be limited to the two proteins with known RNA-binding potential. tRNA-splicing ligase RtcB homolog (also known as HSPC117) is another tRNA-related protein involved in tRNA splicing[364], thus this protein is unlikely to have relevance for BCR-ABL regulation. Finally, IMPDH2 is involved in the synthesis of guanine nucleotides, interact with polysomes[365] and assumed to bind RNA[360]. Even though IMPDH2 is the lowest-scored protein, it is the closest link with mRNA regulation. Recently, IMPDH1 (an isoenzyme to IMPDH2) was found to act as a C/T-rich

transcription factor[366]. This was of interest as the domain responsible for transcriptional regulation is the most variable moiety between IMPDH1 and 2[367]. As IMPDH2 is known to interact with RNA and polysomes, it may interact with and regulate RNA instead of DNA.

Future work could determine the binding potential of these proteins using gel-shift experiments. This strategy would involve three conditions: 1) labelled *ABL1* 3'UTR RNA, 2) labelled *ABL1* 3'UTR RNA mixed with cellular extract (or recombinant protein), and 3) RNA/protein and an antibody against the candidate protein. If the protein binds to the 3'UTR, the RNA will move slower through the gel compared to RNA alone. A super-shift in the antibody sample would confirm that the candidate protein is interacting with the *ABL1* 3'UTR.

Final remarks

The logistical aspects of the assay have been optimised. It now remains to determine the ideal parameters for isolation of *BCR-ABL* 3'UTR-interacting proteins. Recommendations for further optimisation include:

- A salt gradient to determine the ideal stringency of the assay buffer
- Use of another control RNA, for example from a published study, which does not interact with many proteins
- Biotin-probe approach to capture cellular interactions *in vivo*
- Switch to the MS2-aptamer approach (4.1.3.1.3), which has been used to enrich both RNA-protein and RNA-RNA interactions[290]
- Continuing review of published protein RIP-SEQ data to mine for putative protein interactions with BCR-ABL (chapter 2, 2.3.11, pg 77)

Chapter 5

Conclusions

5.1 Overall conclusions

CML is caused by the deregulated tyrosine kinase activity of the BCR-ABL fusion protein, the derivative of a translocation between chromosomes 9 and 22. BCR-ABL 'dosage' has been associated with both disease progression and response to TKI therapy, which are both key events for the pathogenesis of CML. Surprisingly, little is known about the regulation of BCR-ABL expression, either at the transcriptional or post-transcriptional level. This study focused on one of the two evident starting points to improve our understanding on how BCR-ABL expression is controlled – the *ABL1* 3'UTR (the other being the *BCR* promoter, which our laboratory is also investigating in a parallel project). The findings in this thesis add to the foundation built by the early investigations into BCR-ABL expression in the mid-1980s and early 1990s.

The first aim of this project was to identify the function of the *ABL1* 3'UTR. Our data showed, for the first time, that addition of the *ABL1* 3'UTR to the *Renilla* or *Firefly* genes markedly reduced their expression (except in the KCL-22 cell line). This demonstrated that the *ABL1* 3'UTR was repressive. In addition, the *ABL1* 3'UTR sequence was required in the mRNA for its maximum repression to occur. These experiments were consistent with published data regarding the stabilities of *ABL*, *BCR* and *BCR-ABL* transcripts. Notably, these data showed that the *ABL1* 3'UTR sequence is repressive and located within a region responsible for controlling *BCR-ABL* mRNA stability.

This study also looked at a potential link between BCR-ABL kinase inhibition and the 3'UTR. Although the 3'UTR did not appear to be responsive to imatinib, our results suggest that BCR-ABL kinase inhibition may affect the expression of BCR-ABL via the *BCR* 5'UTR. These findings may provide the rationale for further work to dissect this mechanism, and/or determine if second-generation TKIs may also play a role in BCR-ABL expression.

Generation of reporter constructs with serial deletions of the *ABL1* 3'UTR aimed to identify regions within the 3'UTR which can affect gene expression. In particular, we mapped two regions, 96-nt (839-935) and 142-nt (1116-1257) that showed strong repressive activity. In addition, our mapping experiments suggest that the first 500 nt contains a stabilising/activating element. We coupled some findings from the 3'UTR-mapping experiment with publically available results for global RNA and protein interactions. In particular, we investigated the possible regulation of *ABL1* by miR-125 and TTP, an RNA-

binding protein. Those experiments found that a consensus AU-RE/TTP site within the *ABL1* 3'UTR has a small influence on gene expression. Therefore, TTP or a AU-RE binding protein may play a fine-tuning role in regulating BCR-ABL expression. A list of potential protein and microRNA regulators of *ABL1* based on bioinformatics data are listed in Table 5.1 and Table 5.2, respectively. As more data regarding interactomes between mRNA and RNAs, and mRNA and proteins becomes available, it will become easier to use existing knowledge to better understand gene-expression networks, as well as providing a platform to study unknown networks (i.e., BCR-ABL regulation).

Table 5.1: Proteins marked for further study

Protein	Notes
TTP	Predicted binding site is located within a region of the *ABL1* 3'UTR that exhibits regulatory activity. Deletion of the predicted binding site for TTP rescues reporter expression. TTP expression is reduced in BC *vs*. CP[197]. TTP is known to control the stability of mRNA[189], therefore an increase in TTP expression in BC may provide a mechanism for enhanced BCR-ABL expression in disease progression
ELAVL-1	RIP-SEQ experiments show that ELAVL-1 can interact with the *ABL1* 3'UTR. ELAVL-1 expression increases in BC *vs*. CP[197]. ELAVL-1 has a known role in stabilising mRNA[206,207], therefore an increase in ELAVL-1 expression in BC may provide a mechanism for enhanced BCR-ABL expression in disease progression. May co-localise with hnRNP-C to inhibit TIA/TIAL-1 mediated splicing of the *ABL1* 3'UTR[214].
hnRNP-C	RIP-SEQ experiments show that hnRNP-C can interact with the *ABL1* 3'UTR. hnRNP-C has a known role in stabilising mRNA[202-204], therefore an increase in hnRNP-C expression in BC may provide a mechanism for enhanced BCR-ABL expression in disease progression. May co-localise with ELAVL-1 to inhibit TIA/TIAL-1 mediated splicing of the *ABL1* 3'UTR[214].
TIA/TIAL-1	RIP-SEQ experiments show that TIA/TIAL-1 can interact with the *ABL1* 3'UTR, in particular at the splice donor and acceptor sites of the 3'RACE-mapped interstitial splice event in the 3'UTR. TIA/TIAL-1 have a well-documented role in mRNA splicing[212].

Table 5.2: MicroRNAs marked for further study

MicroRNA	Notes
miR-19	Predicted to interact with the *ABL1* 3'UTR within a region that shows a RIP-SEQ hit for AGO. miR-19 is up-regulated in BC[230].
miR-320	Predicted to interact with the *ABL1* 3'UTR within a region that shows a RIP-SEQ hit for AGO.
miR-361	Predicted to interact with the *ABL1* 3'UTR within a region that shows a RIP-SEQ hit for AGO.
miR-378	Predicted to interact with the *ABL1* 3'UTR within a region that shows a RIP-SEQ hit for AGO.
miR-411	Predicted to interact with the *ABL1* 3'UTR within a region that shows a RIP-SEQ hit for AGO. miR-411 is down-regulated in BC[230].

The use of RNA-aptamers or RNA-tags had the hallmarks of a useful strategy for identification of protein and/or microRNA interactions. However, it did not prove to be the case in our hands, as we were unable to isolate specific proteins that interacted with the *ABL1* 3'UTR. The use of *in silico* microRNA-target prediction was equally unsuccessful. The last two goals set out for this thesis hinged on the success of these methods. Unfortunately, these approaches are still the current gold-standard to identify regulators that interact with an RNA molecule. We did, however, optimise over-expression of microRNAs in CML cells, as well as the logistical aspects of the RNA-tag approach. Therefore, we can effectively evaluate any future candidate microRNA targets of BCR-ABL. Likewise, we are also in the position to quickly adapt to new RNA-tagging techniques or optimisation strategies if they become available.

The following points summarise our findings regarding the control of BCR-ABL expression via its 3'UTR:

- The *ABL1* moiety plays an important role in *BCR-ABL* mRNA stability.
- The *ABL1* 3'UTR is overall, repressive (except in the KCL-22 cell line).
    - These findings agree with those from Collins *et al*., who showed that *ABL1* sequences do not contribute to *BCR-ABL* mRNA stability in KCL-22 cells[194].
- The presence of the *ABL1* 3'UTR sequence is required in the mRNA for its full repressive activity.

- Discrete regions of the *ABL1* 3'UTR are responsible for controlling gene expression
    - A stabilising/activating element resides within the first 500 nt
    - A repressive element is located within a ~96 nt region (839-935)
    - Another repressive element is located within a ~141 nt region (1116-1257)
    - Repressive regions might be under control of a "balancer" similar to the *HNF4α* gene
- TTP or a AU-RE binding protein may regulate BCR-ABL expression.
- The major *ABL1* 3'UTR species is the NCBI/Ensembl-annotated, 1992 nt sequence after the *ABL1* stop codon.
- The *ABL1* 3'UTR sequence is not duplicated in (does not blast against) the human genome.
- No evidence that miR-29, 30, 125, 141/200, 196, 203 control BCR-ABL expression.

5.2 Future directions: *Q & A*

This section addresses a few of the key questions generated by this study.

Which microRNAs and/or proteins functionally interact with the *BCR-ABL* 3'UTR?

Although our described efforts have been unsuccessful, there are still a number of strategies available to answer this question. The most promising is switching to an *in vivo* approach to streamline RNA-RNA and protein-RNA identification. This would allow for identification of endogenous cellular RNA-protein complexes rather than complexes that are formed *in vitro*, in a test-tube. The next-gen S1-tag, MS2-tag or biotin-probe capture techniques are all compatible with an *in vivo* method (Table 4.1).

For protein identification, a number of recommendations were discussed in chapter 4, such as increasing the stringency of the buffer, changing the 'negative-reference' RNA, switching to either a biotin-probe or MS2 capture approach. A further improvement relates to the resolution of comparing the test (tagged-*ABL1* 3'UTR) and control (tagged-antisense *ABL1* 3'UTR) samples. The resolution of the protein samples can be increased using 2-dimensional (2D) SDS PAGE, or stable isotope labelling by amino acids in cell culture (SILAC) coupled with MS-MS. In the 2D-gel approach, the protein-pullout assay is performed in exactly the same manner as described in chapter 4. However, the final test and control samples are labelled with a different fluorescent dye and electrophoresed on a 2D-

PAGE gel increasing the resolution of protein separation. Differential spots on the gel are then excised and identified using mass spectrometry (Fig 5.1, A). The SILAC-approach follows a similar principle, but uses isotope-labelling of proteins instead of fluorescent dyes. The control RNA is mixed with unlabelled proteins, whereas the test RNA is mixed with carbon-13 and nitrogen-15 heavy isotope labelled proteins. The final control and test protein samples are mixed together and analysed in a single MS-MS run. This allows for quantification of heavy *vs.* light proteins, and identification of proteins enriched in the test sample (Fig 5.1, B). The SILAC approach has been successfully employed in the identification of protein-RNA interactions[368,369].

To identify RNAs that interact with the 3'UTR, switching from *in silico* to *in vivo* candidate selection is the best 'active' strategy that one can undertake. This would involve cellular expression of tagged control and test RNA, followed by UV-crosslinking and enrichment of tagged-RNA-RNA complexes. Bound RNA is then sequenced using next-gen sequencing techniques (for example on the Ion-Torrent, Applied Biosystems). Functional analysis (i.e, over-expression or knock-down of the RNA of interest) will confirm if they are genuine regulators of BCR-ABL expression. A 'passive' approach is to mine newly published AGO RIP-SEQ experiments, to identify putative microRNA targets of *ABL1*.

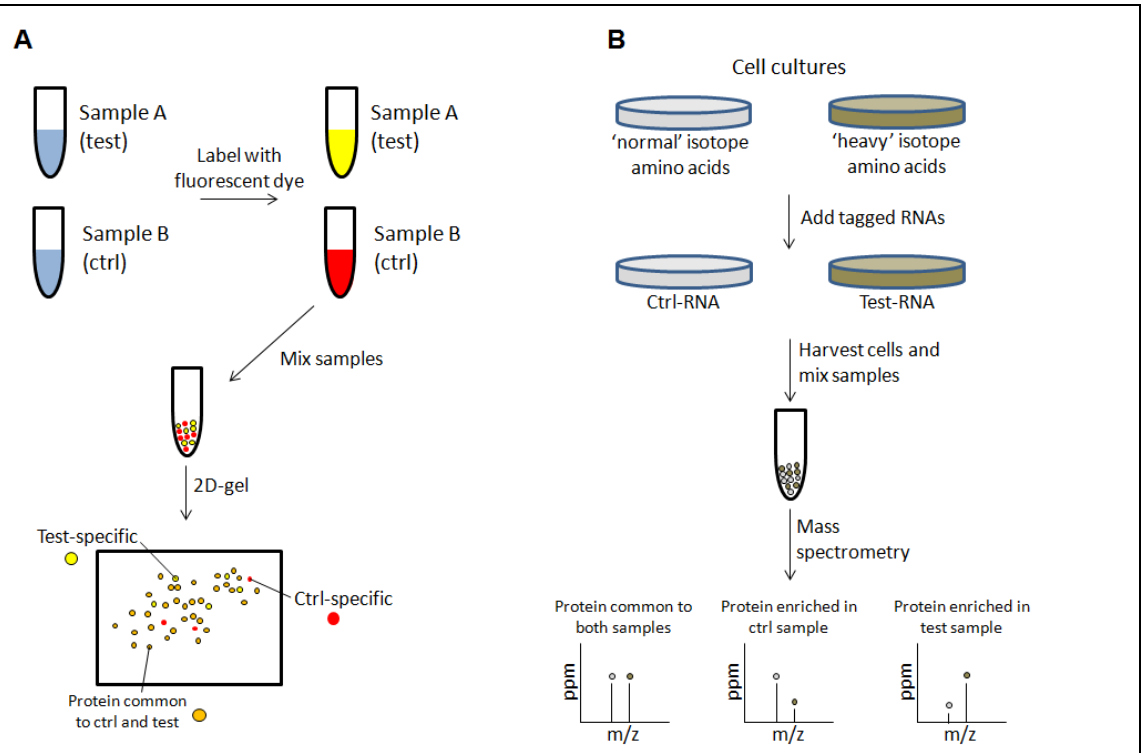

Fig 5.1: Approaches available to increase the resolution of protein sample separation. (**A**) Workflow for fluorescent labelling and 2D-gel protein separation. Protein enrichment using tagged RNA would be performed exactly as before. However, the final sample would be labelled with a fluorescent dye. In this case, test-proteins enriched from tagged-*ABL1* 3'UTR RNA are labelled with a yellow dye, and proteins enriched from a tagged-control RNA are labelled red. The samples are then mixed and separated on a 2D-gel. An ideal result is visualisation of test-specific (yellow) spots on the gel, which would be then identified using mass spectrometry. (**B**) Workflow for the SILAC approach. Tagged-control and *ABL1* 3'UTR RNA would be expressed in cells cultured in normal (or light) isotope amino acids (grey), or heavy isotope amino acids (brown), respectively. Proteins bound to the RNA would be enriched by affinity purification, then mixed together and analysed by mass-spectrometry. Comparison of proteins' relative abundance (parts per million, or ppm) will identify proteins that are common amongst both samples, or specific to either the control or test RNA sample.

What if the RNA-tags are unable to identify 3'UTR-interactors?

It is possible that even after further optimisation of our assay, we are still unable to identify factors that interact with the 3'UTR. In this case, we may be forced to use alternate strategies. One possible approach utilises cell lines that stably express GFP fused to the *ABL1* 3'UTR. These cell lines could be treated with either siRNA against a library of RNA-binding proteins, or microRNAs. Screening these cell lines for GFP expression levels will identify potential targets of the *ABL1* 3'UTR. Performing this exact experiment in a cell line expressing GFP

alone, will filter out 3'UTR-independent alterations in GFP expression. Another approach which has been used to identify regulators of IL-3[370], involves exposing the GFP/3'UTR cell line to a mutagen (e.g. ICR191, a frame-shift mutagen). Over time, it is expected that the bulk population's GFP signature will change as particular factors are mutated. In this case, if a factor that negatively regulates gene expression by the *ABL1* 3'UTR is mutated, GFP expression will increase, and *visa versa*. Thus, selection of high and low GFP-expressing cells, followed by mutation analysis will provide a list of candidate factors that regulate gene expression via the *ABL1* 3'UTR. These approaches have the added advantage that they can also identify indirect targets of the 3'UTR, or 'regulators of other regulators' that directly interact with the 3'UTR. This may uncover a complex regulatory network for BCR-ABL expression.

There are a few alternate approaches which may answer general questions about the *ABL1* 3'UTR. One of these was mentioned in chapter 2, and involved knockdown of Dicer in conjunction with transfection of the luciferase *ABL1* 3'UTR reporter. Changes in luciferase reporter expression upon Dicer knockdown would implicate the microRNA pathway in the regulation of BCR-ABL, either by direct binding of the microRNA to the 3'UTR, or indirectly altering the expression of a 3'UTR-binding factor. Again, an identical experiment using a luciferase reporter that does not contain the 3'UTR would filter out 3'UTR-independent candidates. Finally, labelled *ABL1* 3'UTR RNA could be mixed with cellular extract and used in gel-shift experiments. This experiment would demonstrate that proteins interact with the 3'UTR, and has been performed for the *β-F1-ATPase*[344] and *LDL receptor*[210] 3'UTRs. The gel-shift may provide a tool to optimise the isolation of RNA-protein complexes (i.e., buffer conditions, use of different control RNAs). In addition, this technique may also allow for super-shifting of RNA-protein complexes in the gel-shift assay using antibodies against known RNA-binding proteins, such as TTP, or ELAVL-1.

Does TTP regulate BCR-ABL expression?

In chapter 2 it was suggested to advance TTP through the pipeline in Fig 1.5 based on our luciferase data (Fig 2.21) and array data showing that TTP expression is reduced in BC[197]. This would involve modulation of TTP expression and to look for alterations in BCR-ABL expression, and, subsequently, establish if TTP directly interacts with BCR-ABL. To address this, knock-down and/or over-expression of TTP should be performed in CML cells. Based on

our data from the luciferase experiments, it would be predicted that increased TTP expression would decrease BCR-ABL expression and, conversely, knock-down of TTP would increase BCR-ABL expression. Additional work should include measurement of cell proliferative effects due to manipulation of TTP expression, as well as investigating if altered TTP expression can synergise with TKI-induced cell death. To show that TTP directly binds to the *ABL1* 3'UTR, gel-shift assays can be performed (see above) using labelled *ABL1* 3'UTR RNA and a TTP-antibody. Positive results from these experiments could provide the rationale to consider TTP as a potential therapeutic target in CML. The TTP site encompasses an AU-RE that is bound by other proteins. Therefore in an approach similar to above, AU-RE binding proteins could be examined for their ability to regulate BCR-ABL.

Why does the *ABL1* 3'UTR act differently in KCL-22 cells?

The *ABL1* 3'UTR has no effect on reporter expression in the KCL-22 cell line, whereas it is repressive in every other cell line tested. One explanation is that the KCL-22 cell line lacks a repressor or expresses an activator (or both) which acts via the *ABL1* 3'UTR. This possibility is strengthened by the observation that in KCL-22 cells, deletion of the first 499 nt of the 3'UTR restores the repressive activity of the 3'UTR. The reasons why this would be 'exclusive' to KCL-22, are not clear. However, it is interesting to note that KCL-22 is also unique among CML cell lines for being intrinsically resistant to imatinib-induced cell death[73,103]. Whether the two phenomena are related remains to be investigated.

Notwithstanding this 'coincidence', this cell line could be used as a tool to identify the regulator(s) involved. One strategy to utilise this phenomenon involves differential display of proteins that interact with the *ABL1* 3'UTR between KCL-22 cells and any other cell in which the *ABL1* 3'UTR is repressive. This idea would involve either the SILAC or 2D-gel experiments that were explained in Fig 5.1. Instead of comparing forward and reverse 3'UTR RNA, one would compare proteins from KCL-22 cells with (for example) proteins from K-562 cells. One would then look for changes in protein interactomes between the cell lines to identify putative regulators of BCR-ABL. Therefore, the KCL-22 cell line would add another 'filter' to the protein pullout assay in terms of identifying functional regulators, and not just pulling out whichever protein binds to the 3'UTR.

Final remarks

I think that understanding the mechanisms that govern BCR-ABL expression will be an important achievement in terms of CML biology. It will provide insights into the role of enhanced BCR-ABL expression in disease progression, and may also help to understand mechanisms of TKI resistance. In the future it may also allow for alternate therapeutic strategies to combat not only CML, but generate technology which can be applied to other diseases of low biological complexity (i.e., one or a few genomic lesions).

Appendix A: Common experimental protocols

Manufacturers' details for chemicals are listed in Appendix B.16.

A.1 PCR: AmpliTaq® Gold polymerase

Table A.1: AmpliTaq® PCR setup

Component	Volume
AmpliTaq Gold® DNA Polymerase	0.1 µL (0.2 U)
10 x PCR buffer#	2.0 µL
dNTPs (2.5 mM, iNtRON^)	1.6 µL
$MgCl_2$# (25 mM)	1.2 µL
Primer (forward) (20 µM)	1.0 µL
Primer (reverse) (20 µM)	1.0 µL
Template	*
PCR grade water	up to 20 µL
* template type: genomic (200 ng), plasmid (1 ng), cDNA (1 µL, undiluted cDNA) # supplied with enzyme ^ iNtRON Biotechnology (Daejoen, South Korea)	

Notes:

- For the purpose of cloning, five 20 µL reactions were performed; 20 µL was run on an agarose gel to confirm the correct product was synthesised, and the remainder was used for cloning.
- PCR setup in 200 µL flat top tubes.

A.2 PCR: Phusion® High-Fidelity DNA Polymerase

Table A.2: Phusion PCR setup

Component	Volume
Phusion® High-Fidelity DNA Polymerase	0.1 µL (0.2 U)
5 x Phusion® High-Fidelity DNA Polymerase buffer	4.0 µL
dNTPs (2.5 mM, iNtRON)	1.6 µL
Primer (forward) (20 µM)	1.0 µL
Primer (reverse) (20 µM)	1.0 µL
Template	*
PCR grade water	up to 20 µL
* template type: genomic (200 ng), plasmid (1 ng), cDNA (1 µL, undiluted cDNA)	

Notes:

- For the purpose of cloning, five 20 µL reactions were performed; 20 µL was run on an agarose gel to confirm the correct product was synthesised, and the remainder was used for cloning.
- PCR setup in 200 µL flat top tubes (Scientific Specialities Inc. Lodi, CA, USA)

A.3 PCR: mutagenesis

This PCR-method was based on the Quikchange™ mutagenesis kit instructions (QIAgen), using PfuUltra™ polymerase (Agilent Technologies, Mulgrave, Australia).

Table A.3.1: Mutagenesis PCR setup

Component	Volume
PfuUltra™ Fusion HotStart DNA Polymerase	1 µL (2.5 U)
10 x PfuUltra™ buffer	5.0 µL
dNTPs (2.5 mM, iNtRON)	1.0 µL
Primer (forward) (25 ng / µL)	5.0 µL
Primer (reverse) (25 ng / µL)	5.0 µL
Template	300 ng
PCR grade water	up to 50 µL

Table A.3.2: PCR cycle conditions

Temperature	Time	
95^{o}C	30 sec	
95^{o}C	50 sec	22 cycles
50^{o}C	50 sec	
68^{o}C	2 min / kb	

Ten microlitres of the PCR was collected for agarose gel analysis, then 20 U of *Dpn*I was added to the remaining 40 µL, and incubated at 37^{o}C for 2 h to digest DNA that was not synthesised in the PCR (i.e., plasmid DNA). Ten microlitres of *Dpn*I-treated and untreated PCR were electrophoresed on a 1% agarose gel to ensure that *Dpn*I digestion was successful. Then, 2 µL of the *Dpn*I-treated DNA was transformed into TOP10 electro-competent cells (see Appendix A.11). DNA plasmid prep (see Appendix A.13) was preformed for isolation of a clone that harbours the desired mutation. Mutagenesis was confirmed by sequencing, and bulk quantities of the plasmid were isolated using the HiSpeed® MIDI kit.

A.4 PCR: Sequencing

DNA vectors were sequenced to confirm their identity. The sequencing PCR was performed as outlined below. The extension products were precipitated and sent to the sequencing facility (Molecular Pathology, IMVS).

Table A.4.1: Sequencing PCR setup

Component	Volume
Ready Reaction Premix^ (2.5x)*	2 µL
BigDye sequencing buffer^ (5x)	4 µL
Primer (3.2 pmol)	1 µL
Template	250-500 ng
PCR grade water	up to 20 µL
* contains enzyme ^ Applied Biosystems	

Table A.4.2: PCR cycle conditions

Temperature	Time	
96^{o}C	1 min	
96^{o}C	10 sec	25 cycles
50^{o}C	5 sec	
60^{o}C	4 min	

The extension products were purified using isopropanol. To the PCR, 75% isopropanol (80 µL) was added, followed by vortex-mixing, and then the sample was left at room temperature for 20 min. The sample was then centrifuged (20800g, 22°C, 15 min). After removal of the supernatant, 75% isopropanol (250 µL) was added followed by centrifugation (20800g, 22°C, 5 min). Then the supernatant was aspirated and the pellet was air dried. The sample was then sent to the sequencing facility, where the sequence run was performed on a 3730xl DNA sequencer (Applied Biosystems) according to the manufacturer's instructions.

A.5 RNA isolation

RNA isolation from cell material was performed using the TRIzol® reagent. Cells were lysed in the TRIzol® reagent, 10^7 cells/mL of TRIzol®. Cells were then frozen at -80°C for at least 24 h.

After thawing the sample, 200 µL of chloroform/mL of TRIzol® was added to the tube, followed by vigorous mixing for 15 sec. The tube was placed at room temperature for 10

min, and then centrifuged (20800g, 4°C, 15 min). The top (aqueous layer) was transferred to a new microcentrifuge tube and mixed with an equal volume of isopropanol. The tube was then placed at -20°C for at least 1 h to precipitate the RNA. After precipitation, the tube was centrifuged (20800g, 4°C, 10 min). The supernatant was then aspirated and the RNA pellet was washed with two volumes of ethanol (75%), and centrifuged (7600g, 4°C, 5 min). Following removal of ethanol, the pellet was air dried and resuspended in PCR-grade water.

A.6 Genomic DNA isolation

Cells (10^6) were resuspended in 500 µL lysis buffer (Appendix B) and incubated at 55ºC overnight. The following day, an equal volume of phenol:chloroform isoamyl alcohol (25:24:1) was added followed by a brief vortex mix and centrifugation (15700g, 5 min). The supernatant was transferred to a new tube and an equal volume of chloroform was added, followed by another vortex mix and centrifugation (15700g, 5 min). The supernatant was transferred to a new tube and precipitated with an equal volume of isopropanol. The DNA precipitate was collected with a sterile loop (Sarstedt) and dipped in 70% ethanol. The DNA (on the loop) was then placed in TE and allowed to resuspend for 5 minutes.

A.7 cDNA synthesis

Synthesis of cDNA was performed using SuperScript™ II (Invitrogen). Oligo(dT)15 primers (500 ng) or Random hexamer primer (50 ng; Geneworks), and 1 µL of 10 nM dNTPs were added to total RNA (up to 5 µg), and then made up to 12 µL with PCR-grade water. The mix was then heated at 65°C for 5 min, followed by rapid cooling on ice. After a brief centrifugation; 5x first strand buffer (4 µL), 0.1 M dithiothreitol (2 µL), and 200 units of SuperScript™ II (1 µL) were added to the reaction-tube; followed by incubation at 42°C for 50 min. The reaction is inactivated by heating at 75°C for 15 min.

A.8 qRT-PCR

All qRT-PCRs were performed on the 7900HT Real-Time PCR system (Applied Biosystems). cDNAs (5 µL) were added to a MicroAmp® Optical 96-Well Reaction Plate (Applied Biosystems). The reaction master-mix (Table A.8.1) for the appropriate custom primers/probe or commercial primers/probe were then added to the cDNA samples. The 96-well plate was

sealed using a MicroAmp® optical adhesive film (Applied Biosystems), and loaded on to the 7900HT machine for qRT-PCR according to the manufacturer's instructions.

Table A8.1: qRT-PCR reaction master mix

Custom primer/probe		Commercial primer/probe	
Component	**Volume**	**Component**	**Volume**
2x universial master-mix	10.0 µL	2x universial master-mix	10.0 µL
Primer (forward, 20 µM)	0.9 µL	Primer/probe mix	1.0 µL
Primer (reverse, 20 µM)	0.9 µL		
Probe (10 µM)	0.5 µL		
Water	upto 15 µL	Water	upto 15 µL
Custom primers from Geneworks Universal master mix, custom and commercial probes from Applied Biosystems			

Table A.8.2: Primer and probe reagents for qRT-PCR

Gene	Custom/ commercial	Assay part number
miR-196b	Commercial	TM496
RNU6b	Commercial	TM1093
BCR-ABL	Custom	-
G-USB	Custom	-
Renilla	Custom	-

A.9 Gel purification

DNA of interest (a maximum of 20 µL per well) in DNA load buffer (Appendix B) were loaded on a TBE-agarose gel (Appendix B) containing ethidium bromide. Electrophoresis was carried out until excision was possible. Standard voltages and agarose percentages are listed below in Table A.9. The gel was then placed in a UV box and the desired DNA product(s) were excised using a scalpel. Then DNA extracted using the QIAgen gel extraction kit according to the manufacturers' instructions to afford the DNA in 30 µL volume of TE.

Table A.9: Gel running conditions

Gel size (Biorad)	Voltage
5 x 10 cm	60
15 x 10 cm	75
Band size (bp)	**Agarose percentage**
0-500	2%
500-1000	1.5%
1000-4000	1%
4000<	0.8%

A.10 Ligation reactions

Table A.10: Ligation reaction setup

Component	Volume
Purified DNA vector backbone	2 µL*
Purified DNA insert	6 µL
10x T4 ligase buffer	1 µL
T4 ligase (New England Biolabs)	1 µL (40 U)
* 8 µL vector backbone used for plasmid self-ligation.	

Reaction carried out at room temperature overnight (except for plasmid self ligation, which was performed at room temperature for 5 h).

A.11 Transformation: electro-competent cells

Two microlitres of ligation reaction was added to One-Shot® TOP10 electro-competent cells (50 µL), then transferred to a 2 mm cuvette (BTX Harvard Apparatus, Holliston, MA). The electroporation was performed using the BIO-RAD gene pulser, set to 2.5 V and 25 µFD, which was connected to a BIO-RAD pulse controller set to 200 Ω. Care was taken to keep all reagents on ice until electroporation. Following electroporation, Luria Broth (LB) (Sigma) (950 µL) was added to the cuvette, then transferred to a 1.5 mL centrifuge tube and incubated at 37^{o}C for 1 h. Transformations were plated on ampicillin-LB agar plates, and left overnight at 37^{o}C.

A.12 Transformation: chemical competent cells

Fifty microlitres of DH5α *E.coli* chemical competent cells (kindly provided by Vicki Wilczek) were thawed on ice, then 5 µL of ligation reaction was added to the cells. This

mixture was left on ice for 30 min; then the mixture was heated to 42^{o}C for 1.5 min, placed on ice for 2 min. LB (450 µL) was then added to the transformed cells, which were then incubated at 37^{o}C for 1 h. The transformation was plated on an ampicillin-LB agar plate and left overnight at 37^{o}C.

A.13 DNA plasmid prep

The alkaline lysis mini prep method (http://bacpac.chori.org/bacpacmini.htm) was used to isolate desired DNA plasmid clones from transformation agar plates.

Single colonies were picked from an agar plate using a sterile 200 µL micropipette tip, and placed into 10 mL centrifuge tubes containing 2mL LB and 0.1 mg/mL ampicillin. The tubes were left at 37^{o}C overnight. The next day, the cultures were transferred to 1.5 mL microcentrifuge tubes and centrifuged (15700g, 1 min), followed by removal of the supernatant. The *E.coli* pellet was then resuspended in 300 µL of buffer P1 (Appendix B). Buffer P2 (300 µL) (Appendix B) was added to the tubes and the tubes left at room temperature for 5 min. Then, 300 µL of buffer P3 (Appendix B) was added to the tube, the tubes were inverted twice and placed on ice for 5 min. The tubes were then centrifuged (15700g, 10 min, 4^{o}C). To a new tube, 700 µL supernatant was added to 700 µL cold isopropanol and left on ice for 5 min. Tubes were then centrifuged (15700g, 15 min, 4^{o}C). After aspiration of the supernatant, 500 µL of 70% ethanol was added, followed by another centrifugation (15700g, 5 min, 4^{o}C). Supernatant was aspirated and pellet air dried for 15 min. The DNA was then resuspended in 30 µL TE.

A.14 Cell Culture

Suspension cell lines (Table A.14) were maintained at exponential growth at 37^{o}C and 5% CO_2, in RPMI-1640 media (Appendix B).

Adherent cell lines, HeLa and 293T, were maintained at exponential growth at 37^{o}C at 5% CO_2; in DMEM media (Appendix B). Passaging was achieved by aspiration of media, addition of 5 mL PBS, then the PBS was removed and cells were treated with trypsin (0.05%) (Invitrogen) for 5 min at 37^{o}C. Fresh media was added to the trypsinised cells which were then transferred to a 50-mL centrifuge tube. Cells were centrifuged (250g, 5 min), then resuspended in fresh media and seeded at 2x10^{5} cells/mL.

Table A.14: Cell lines used in experiments (human)

Suspension cell line	Notes
BV-173	CML blast crisis, lymphoid
HEL	Erythroleukemia
HL-60	Promyelocytic leukaemia
K-562	CML blast crisis, erythroid
KCL-22	CML blast crisis, myeloid
KG-1	Acute myeloid leukaemia
KT-1	CML blast crisis, myeloid (*ABL1* negative)
KYO-1	CML blast crisis, myeloid (*ABL1* negative)
Jurkat-LT	Acute lymphoblastic leukaemia
LAMA-84	CML blast crisis, myeloid (*ABL1* negative)
THP-1	Acute myeloid leukaemia
U-937	Histiocytic lymphoma

A.15 Luciferase reporter assay

Cells transfected with luciferase constructs were harvested at 24 or 48 h post-transfection. The cells were washed either in 250 µL PBS (24 well plate) or 500 µL PBS (6-well plate). Then, the cells were lysed using Passive Lysis Buffer (supplied with the luciferase assay system) and gently mixed for 15 min at room temperature. Lysated were stored at -20ºC for at least 18 h prior to luciferase readings.

Luciferase readings were obtained using the Dual-Luciferase Reporter Assay System (Promega) and T-20/20 luminometer (Table A.15) (Turner Designs, Sunnyvale, CA, USA). Ten microlitres of cell lysate was added to 50 µL LAR-II in a 1.5 mL microcentrifuge tube, and pipette-mixed. The Firefly activity was then obtained using the luminometer. To obtain the Renilla activity, 50 µL Stop & Glo® Reagent was added to the tube, followed by vortex-mixing and luciferase reading obtained using the luminometer.

Table A.15: Luminometer setup

Mode	DLR
Sensitivity	30-100%*
Delay	2 s
Integration	10 s
Replicates	1^{+}

*Cell-type and transfection specific. The Firefly activity from one of the samples is measured and set to 100-500 luciferase units or 100% if lower than 100. The Renilla reading is almost always higher than Firefly, therefore the sensitivity must not be set too high in order for the Renilla reading to be within the range of measurement.
$^{+}$Replicate function not used. Samples read individually and grouped into replicates during analysis.

A.16 Purification of linearised plasmid for *in vitro* transcription

Plasmid DNA (10 µg) harbouring the desired DNA-template sequence was linearised as described in the relevant methods section. The DNA was then purified following addition of PCR-grade water (15 µL), glycogen (5 µL, 25 ng; Ambion), 3 M ammonium acetate (5 µL; Ambion) and 100% ethanol (100 µL). The mix was vortex-mixed and placed at -20°C for at least 30 min. The tube was then centrifuged (20800g, 4°C, 15 min), and then the supernatant removed. To the pellet, 70% ethanol (300 µL) was added followed by centrifugation (20800g, 4°C, 15 min). Supernatant was removed, pellet allowed to air dry. The DNA was resuspended in 11 µL PCR-grade water. DNA yield was determined using the NanoDrop apparatus.

A.17 End-fill

T4 polymerase (New England Biolabs) was used to create blunt (or end-filled) double-stranded DNA molecules that have been restriction-enzyme digested. The endfill reaction was performed following the restriction digest by adding dNTPs (4 µL, 2.5 mM), up to 49 µL water, and T4 polymerase (1 µL, 3 U). The reaction was left at 16°C for 15 min, followed by heat inactivation of T4 polymerase and restriction enzyme(s) at 75°C for 20 min.

Appendix B: Reagents and solutions

Manufacturers' details for chemicals are listed in Appendix B.16.

B.1 Protein sample buffer (for 2x)

Component	Amount	Final concentration
Tris (1 M, pH 6.8)	0.625 mL	0.125 M
SDS (10%)	4.000 mL	4%
Glycerol	2.000 mL	20%
Dithiothreitol (2.5 M)	0.800 mL	0.200 M
Bromophenol blue (1%)	0.200 mL	0.02%
Water	up to 10 mL	

B.2 Tris-glycine running buffer (for 5x)

Component	Amount	Final concentration
Tris	30.3 g	0.125 M
SDS (10%)	100 mL	4.0%
Glycine	144.2 g	0.5%
Water	up to 2 L	

B.3 Western transfer buffer

Component	Amount
Tris	14.50 g
SDS (10%)	7.5 mL
Glycine	5.84 g
Methonol	100 mL
Water	up to 2 L

B.4 TBS-T (for 5x)

Component	Amount	Final concentration
Tris	15 g	12.5 mM
Sodium chloride	40 g	69.0 mM
Potassium chloride	1 g	1.4 mM
Tween-20	5 mL	0.1%
Water	up to 1 L	

B.5 TBE buffer (for 5x)

Component	Amount	Final concentration
Tris	107.8 g	890 mM
Boric Acid	55.0 g	890 mM
EDTA	5.8 g	25 mM
Water	up to 1 L	

B.6 TBE-agarose gels (horizontal)

TBE-agarose gels were made for electrophoresis using the Mini-Sub® Cell GT apparatus (BIO-RAD). A 5x stock solution of TBE buffer was diluted to 0.5x, to a final volume of 50 mL (10 x 5 cm gel) or 150 mL (10 x 15 mL) in a 250 mL conical flask (SCHOTT, Frenchs Forest, Australia). Agarose (Sigma) was then added to the TBE solution and microwave-heated until boiling. The TBE-agarose was then transferred to a Mini-Gel caster (BIO-RAD) using the appropriate UV-transparent gel tray and comb (BIO-RAD).

B.7 TBE-polyacrylamide non-denaturing gels (vertical)

Non-denaturing TBE-polyacrylamide gels (10%) were made for electrophoresis on the Mini-PROTEAN Tetra Cell apparatus using the recipe below.

Component	**Amount**
5x TBE buffer	3.00 mL
Acrylamide/Bis (29:1, 40%)	3.40 mL
Diethylpyrocarbonate (DEPC)-treated water*	10.00 mL
Ammonium persulfate	0.05 mL
TEMED	0.01 mL
* DEPC added water at a final concentration of 0.1%. The solution is incubated for 2 h at 37ºC followed by autoclaving.	

B.8 SDS PAGE gel

Table B.6.1: Resolving gel

	7.5%		10%
Component	**Amount**		
Gel size	*8 cm*	*20 cm*	*8 cm*
Tris-HCl (1.5 M, pH 8.8)	1.25 mL	5.00 mL	1.25 mL
SDS (10%)	0.05 mL	0.10 mL	0.05 mL
Acrylamide/Bis (37.5:1, 40%)	0.96 mL	3.76 mL	1.25 mL
Ammonium persulfate	0.02 mL	0.03 mL	0.02 mL
TEMED	0.01 mL	0.02 mL	0.01 mL
Water	2.74 mL	10.96 mL	3.03 mL

Table B.6.2 Stacking gel

	4%	
Component	**Amount**	
Gel size	*8 cm*	*20 cm*
Tris-HCl (0.5 M, pH 8.8)	1.25 mL	2.52 mL
SDS (10%)	0.05 mL	0.10 mL
Acrylamide/Bis (37.5:1, 40%)	0.50 mL	1.00 mL
Ammonium persulfate	0.02 mL	0.02 mL
TEMED	0.01 mL	0.02 mL
Water	3.17 mL	6.46 mL

B.9 DNA load buffer (for 10x)

Component	Amount
Bromophenol Blue (1%)	0.25 mL
SDS (10%)	0.50 mL
EDTA (0.5 M)	0.20 mL
Glycerol	40% (w/v)
Water	5.95 mL

B.10 DNA lysis buffer

Component	Amount
EDTA (0.5 M)	0.5 mL
Sodium chloride (5 M)	2.0 mL
Tris pH 7.0	5.0 mL
SDS (10%)	1.0 mL
Water	41.5 mL

B.11 P1 (for plasmid preparation)

Component	Amount
EDTA (0.5 M)	1.0 mL
Tris (1 M)	2.5 mL
RNase A	0.05 g
Water	46.5 mL
Solution filtered using a 0.45 µM filter.	

B.12 P2 (for plasmid preparation)

Component	Amount
Sodium hydroxide (10 M)	0.8 mL
SDS (10%)	4.0 mL
Water	35.2 mL
Solution filtered using a 0.45 µM filter.	

B.13 P3 (for plasmid preparation)

Component	Amount
Potassium acetate (5 M)	30.00 mL
Acetic acid, glacial	5.75 mL
Water	14.25 mL

B.14 TE buffer

Component	Amount
Tris 1 M	0.50 mL
EDTA 0.5 M	0.05 mL
Water	49.45 mL

B.15 Cell culture media

RPMI-media (10% FCS)	
Component	**Amount**
RPMI-1640 media	One bottle
Fetal calf serum	50 mL
L-Glutamine	2 mM
Penicillin	50 U/mL
Streptomycin	500 µg/mL
DMEM-media (10% FCS)	
Component	**Amount**
DMEM media	One bottle
Fetal calf serum	50 mL
L-Glutamine	2 mM
Penicillin	50 U/mL
Streptomycin	500 µg/mL

B.16 Chemical manufacturer details

Component	Manufacturer
Acetic acid, glacial	Ajax Finechem[#]
Ampicilin	Sigma
Boric acid	Sigma
Bromophenol blue	Sigma
Chloroform	Ajax Finechem[#]
Dithiothreitol	Invitrogen
DMEM (cell culture media)	Invitrogen
EDTA	VWR international^
Ethanol	Chem-Supply*
Glycerol	Sigma
Glycine	BIO-RAD
HEPES	Invitrogen
L-Glutamine	Invitrogen
Magnesium chloride	Sigma
Methanol	Chem-Supply*
Penicilin	Invitrogen
Phenol:chloroform isoamyl alcohol (25:24:1)	Sigma
Potassium acetate	Sigma
Potassium chloride	Sigma
RMPI-1640 (cell culture media)	Invitrogen
RNAse A	Sigma
SDS	BIO-RAD
Sodium chloride	Sigma
Sodium hydroxide	Chem-Supply*
Streptomycin	Invitrogen
Tris	Sigma
Tween-20	BIO-RAD
*Chem-Supply (Port Adelaide, Australia) ^VWR international (Poole, UK) [#]Ajax Finechem (Auckland, New Zealand)	

Appendix C: Supplementary data

C.1 Additional microRNA target predictions for the *ABL1* 3'UTR

MicroCosm (www.ebi.ac.uk/enright-srv/microcosm/)

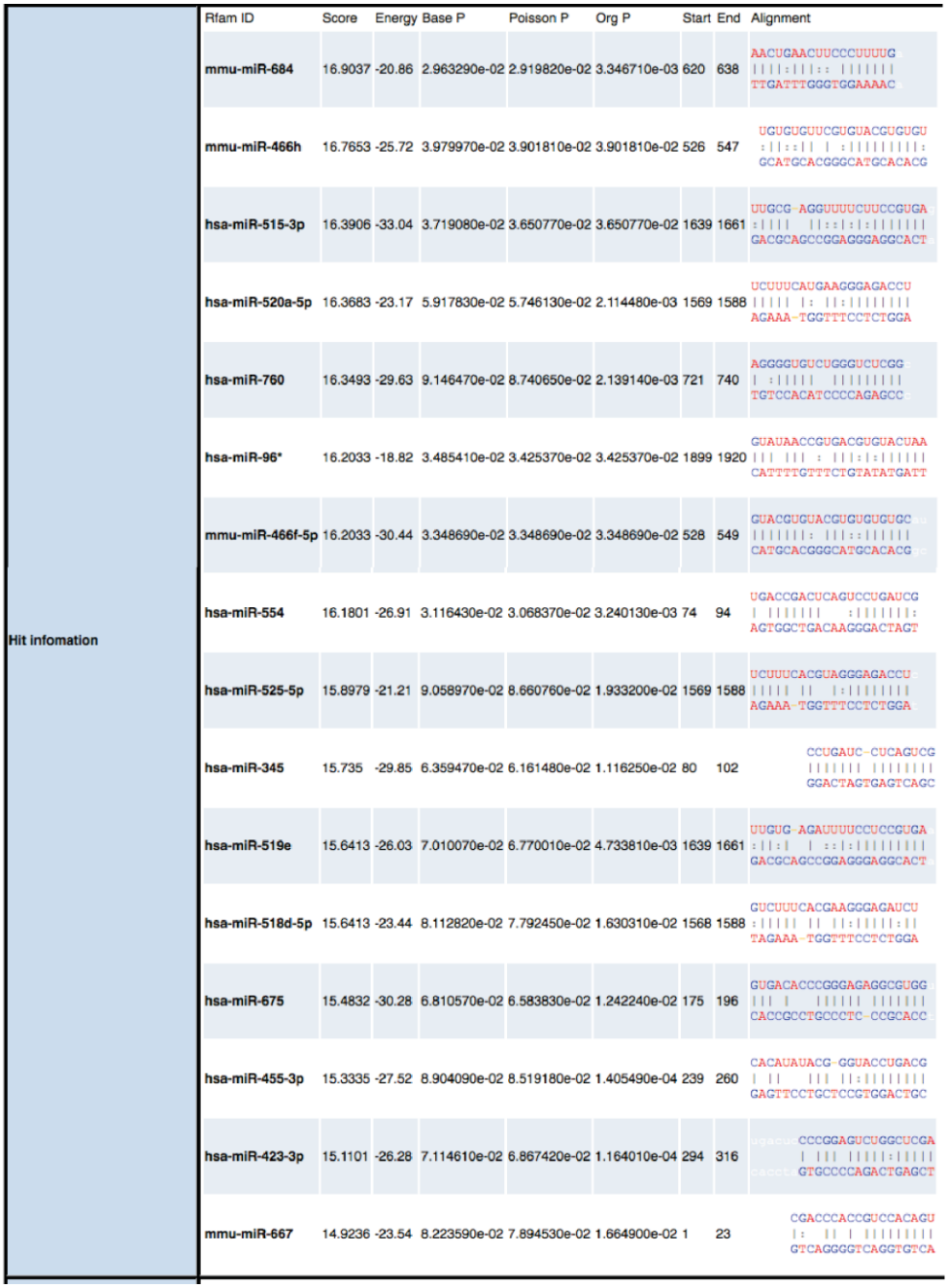

	Rfam ID	Score	Energy	Base P	Poisson P	Org P	Start	End	Alignment
Hit infomation	mmu-miR-684	16.9037	-20.86	2.963290e-02	2.919820e-02	3.346710e-03	620	638	AACUGAACUUCCCUUUUG TTGATTTGGGTGGAAAAC
	mmu-miR-466h	16.7653	-25.72	3.979970e-02	3.901810e-02	3.901810e-02	526	547	UGUGUGUUCGUGUACGUGUGU GCATGCACGGGCATGCACACG
	hsa-miR-515-3p	16.3906	-33.04	3.719080e-02	3.650770e-02	3.650770e-02	1639	1661	UUGCG-AGGUUUUCUUCCGUGA GACGCAGCCGGAGGGAGGCACT
	hsa-miR-520a-5p	16.3683	-23.17	5.917830e-02	5.746130e-02	2.114480e-03	1569	1588	UCUUUCAUGAAGGGAGACCU AGAAA-TGGTTTCCTCTGGA
	hsa-miR-760	16.3493	-29.63	9.146470e-02	8.740650e-02	2.139140e-03	721	740	AGGGGUGUCUGGGUCUCGG- TGTCCACATCCCCAGAGCC-
	hsa-miR-96*	16.2033	-18.82	3.485410e-02	3.425370e-02	3.425370e-02	1899	1920	GUAUAACCGUGACGUGUACUAA CATTTTGTTTCTGTATATGATT
	mmu-miR-466f-5p	16.2033	-30.44	3.348690e-02	3.348690e-02	3.348690e-02	528	549	GUACGUGUACGUGUGUGUGC-U CATGCACGGGCATGCACACG-C
	hsa-miR-554	16.1801	-26.91	3.116430e-02	3.068370e-02	3.240130e-03	74	94	UGACCGACUCAGUCCUGAUCG AGTGGCTGACAAGGGACTAGT
	hsa-miR-525-5p	15.8979	-21.21	9.058970e-02	8.660760e-02	1.933200e-02	1569	1588	UCUUUCACGUAGGGAGACCU- AGAAA-TGGTTTCCTCTGGA
	hsa-miR-345	15.735	-29.85	6.359470e-02	6.161480e-02	1.116250e-02	80	102	CCUGAUC-CUCAGUCG GGACTAGTGAGTCAGC
	hsa-miR-519e	15.6413	-26.03	7.010070e-02	6.770010e-02	4.733810e-03	1639	1661	UUGUG-AGAUUUUCCUCCGUGA GACGCAGCCGGAGGGAGGCACT
	hsa-miR-518d-5p	15.6413	-23.44	8.112820e-02	7.792450e-02	1.630310e-02	1568	1588	GUCUUUCACGAAGGGAGAUCU TAGAAA-TGGTTTCCTCTGGA
	hsa-miR-675	15.4832	-30.28	6.810570e-02	6.583830e-02	1.242240e-02	175	196	GUGACACCCGGGAGAGGCGUGG CACCGCCTGCCCTC-CCGCACC
	hsa-miR-455-3p	15.3335	-27.52	8.904090e-02	8.519180e-02	1.405490e-04	239	260	CACAUAUACG-GGUACCUGACG GAGTTCCTGCTCCGTGGACTGC
	hsa-miR-423-3p	15.1101	-26.28	7.114610e-02	6.867420e-02	1.164010e-04	294	316	ugacuc CCCGGAGUCUGGCUCGA cacccu GTGCCCCAGACTGAGCT
	mmu-miR-667	14.9236	-23.54	8.223590e-02	7.894530e-02	1.664900e-02	1	23	CGACCCACCGUCCACAGU GTCAGGGGTCAGGTGTCA

microRNA.org (www.microrna.org)

DIANA-mT (http://diana.cslab.ece.ntua.gr/)

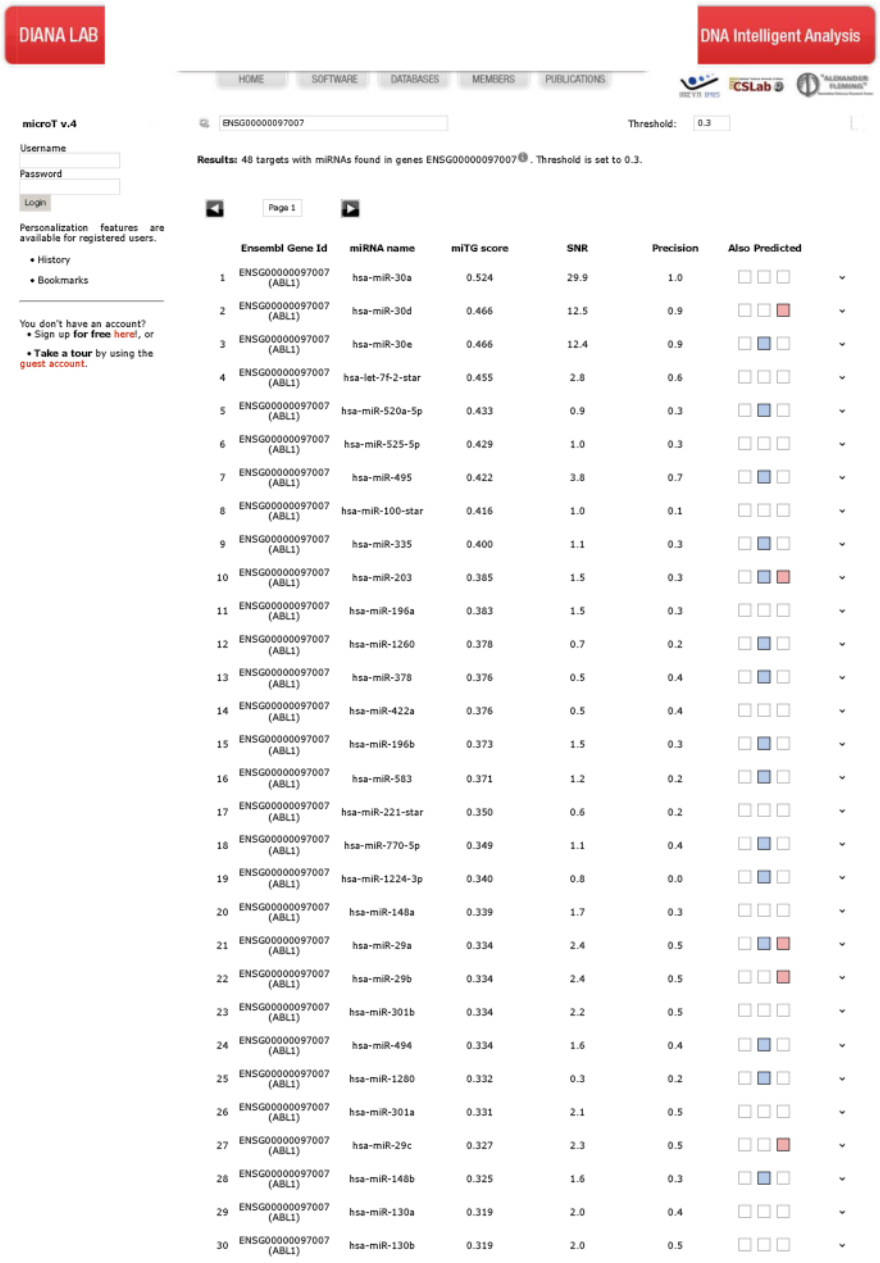

	Ensembl Gene Id	miRNA name	miTG score	SNR	Precision	Also Predicted
1	ENSG00000097007 (ABL1)	hsa-miR-30a	0.524	29.9	1.0	
2	ENSG00000097007 (ABL1)	hsa-miR-30d	0.466	12.5	0.9	
3	ENSG00000097007 (ABL1)	hsa-miR-30e	0.466	12.4	0.9	
4	ENSG00000097007 (ABL1)	hsa-let-7f-2-star	0.455	2.8	0.6	
5	ENSG00000097007 (ABL1)	hsa-miR-520a-5p	0.433	0.9	0.3	
6	ENSG00000097007 (ABL1)	hsa-miR-525-5p	0.429	1.0	0.3	
7	ENSG00000097007 (ABL1)	hsa-miR-495	0.422	3.8	0.7	
8	ENSG00000097007 (ABL1)	hsa-miR-100-star	0.416	1.0	0.1	
9	ENSG00000097007 (ABL1)	hsa-miR-335	0.400	1.1	0.3	
10	ENSG00000097007 (ABL1)	hsa-miR-203	0.385	1.5	0.3	
11	ENSG00000097007 (ABL1)	hsa-miR-196a	0.383	1.5	0.3	
12	ENSG00000097007 (ABL1)	hsa-miR-1260	0.378	0.7	0.2	
13	ENSG00000097007 (ABL1)	hsa-miR-378	0.376	0.5	0.4	
14	ENSG00000097007 (ABL1)	hsa-miR-422a	0.376	0.5	0.4	
15	ENSG00000097007 (ABL1)	hsa-miR-196b	0.373	1.5	0.3	
16	ENSG00000097007 (ABL1)	hsa-miR-583	0.371	1.2	0.2	
17	ENSG00000097007 (ABL1)	hsa-miR-221-star	0.350	0.6	0.2	
18	ENSG00000097007 (ABL1)	hsa-miR-770-5p	0.349	1.1	0.4	
19	ENSG00000097007 (ABL1)	hsa-miR-1224-3p	0.340	0.8	0.0	
20	ENSG00000097007 (ABL1)	hsa-miR-148a	0.339	1.7	0.3	
21	ENSG00000097007 (ABL1)	hsa-miR-29a	0.334	2.4	0.5	
22	ENSG00000097007 (ABL1)	hsa-miR-29b	0.334	2.4	0.5	
23	ENSG00000097007 (ABL1)	hsa-miR-301b	0.334	2.2	0.5	
24	ENSG00000097007 (ABL1)	hsa-miR-494	0.334	1.6	0.4	
25	ENSG00000097007 (ABL1)	hsa-miR-1280	0.332	0.3	0.2	
26	ENSG00000097007 (ABL1)	hsa-miR-301a	0.331	2.1	0.5	
27	ENSG00000097007 (ABL1)	hsa-miR-29c	0.327	2.3	0.5	
28	ENSG00000097007 (ABL1)	hsa-miR-148b	0.325	1.6	0.3	
29	ENSG00000097007 (ABL1)	hsa-miR-130a	0.319	2.0	0.4	
30	ENSG00000097007 (ABL1)	hsa-miR-130b	0.319	2.0	0.5	

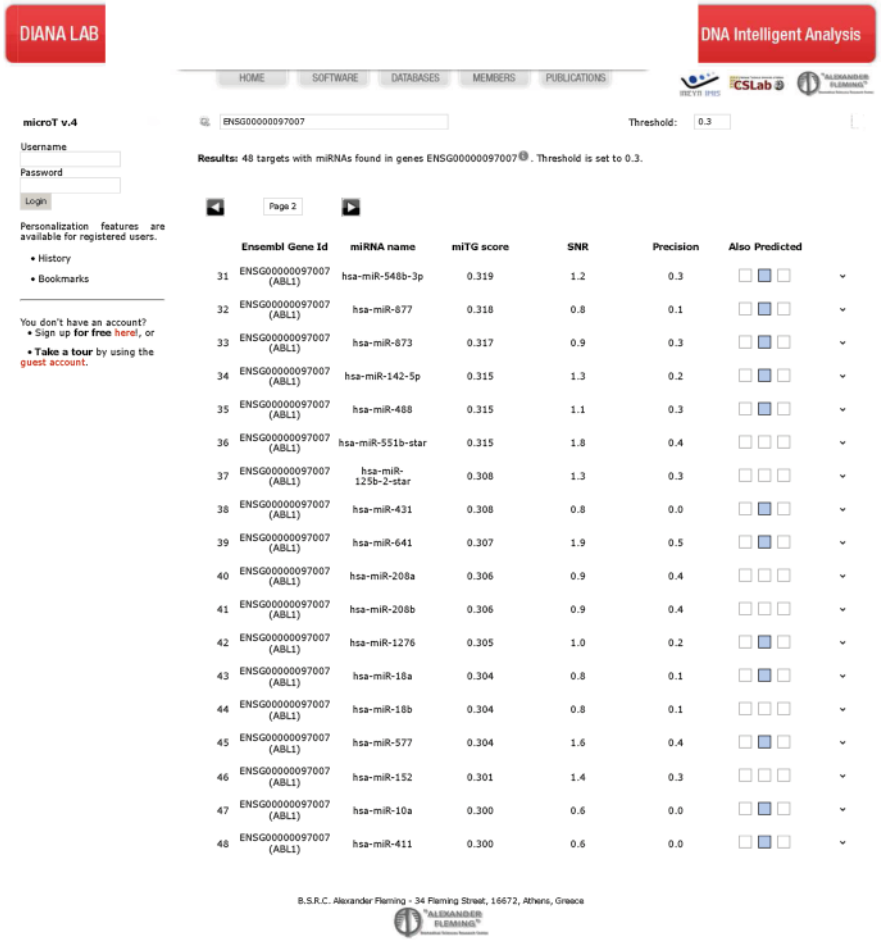

DIANA LAB

DNA Intelligent Analysis

HOME SOFTWARE DATABASES MEMBERS PUBLICATIONS

microT v.4

Username

Password

Login

Personalization features are available for registered users.

- History
- Bookmarks

You don't have an account?
- Sign up **for free** here!, or
- **Take a tour** by using the guest account.

ENSG00000097007 Threshold: 0.3

Results: 48 targets with miRNAs found in genes ENSG00000097007. Threshold is set to 0.3.

Page 2

	Ensembl Gene Id	miRNA name	miTG score	SNR	Precision	Also Predicted
31	ENSG00000097007 (ABL1)	hsa-miR-548b-3p	0.319	1.2	0.3	
32	ENSG00000097007 (ABL1)	hsa-miR-877	0.318	0.8	0.1	
33	ENSG00000097007 (ABL1)	hsa-miR-873	0.317	0.9	0.3	
34	ENSG00000097007 (ABL1)	hsa-miR-142-5p	0.315	1.3	0.2	
35	ENSG00000097007 (ABL1)	hsa-miR-488	0.315	1.1	0.3	
36	ENSG00000097007 (ABL1)	hsa-miR-551b-star	0.315	1.8	0.4	
37	ENSG00000097007 (ABL1)	hsa-miR-125b-2-star	0.308	1.3	0.3	
38	ENSG00000097007 (ABL1)	hsa-miR-431	0.308	0.8	0.0	
39	ENSG00000097007 (ABL1)	hsa-miR-641	0.307	1.9	0.5	
40	ENSG00000097007 (ABL1)	hsa-miR-208a	0.306	0.9	0.4	
41	ENSG00000097007 (ABL1)	hsa-miR-208b	0.306	0.9	0.4	
42	ENSG00000097007 (ABL1)	hsa-miR-1276	0.305	1.0	0.2	
43	ENSG00000097007 (ABL1)	hsa-miR-18a	0.304	0.8	0.1	
44	ENSG00000097007 (ABL1)	hsa-miR-18b	0.304	0.8	0.1	
45	ENSG00000097007 (ABL1)	hsa-miR-577	0.304	1.6	0.4	
46	ENSG00000097007 (ABL1)	hsa-miR-152	0.301	1.4	0.3	
47	ENSG00000097007 (ABL1)	hsa-miR-10a	0.300	0.6	0.0	
48	ENSG00000097007 (ABL1)	hsa-miR-411	0.300	0.6	0.0	

B.S.R.C. Alexander Fleming - 34 Fleming Street, 16672, Athens, Greece

C.2 Mass spectrometry data

ADELAIDE PROTEOMICS CENTRE

Mass Spectrometry Report

30th November 2011

For: Bradley Chereda
Job: 11-103

Sample preparation

The indicated band was excised from the gel manually (Figure 1), washed in 500 μL of 50 mM ammonium bicarbonate (NH4HCO3) and processed as follows:

- 30 mM potassium ferricyanide and 100 mM sodium thiosulfate
- Reduced with 0.5 μmol dithiothretiol (DTT) in 100 mM ammonium bicarbonate
- Alkylated with 2.75 μmol iodoacetamide (IAA) in 100 mM ammonium bicarbonate
- Digested with 100 ng of sequencing grade modified trypsin (Promega) in 5 mM ammonium bicarbonate + 10% acetonitrile (ACN)
- Extracted with 1% formic acid (FA) in water, 1%FA in 50% ACN and 100% ACN

The volumes of the resulting peptide extracts were reduced by vacuum centrifugation to approximately 1 μL.

Liquid chromatography-electrospray ionisation ion-trap (LC-eSI-IT) mass spectrometry

Data acquisition – Orbitrap - ESI Mass spectrometry (MS)

Vacuum concentrated samples were resuspended with 0.1%FA in 2% ACN to total volume of ~8 μL. LC-eSI-IT MS/MS was performed using an online Ultimate 3000 RSL HPLC (Dionex, Germany) and LTQ Orbitrap XL ETD mass spectrometer (Thermo Fisher Scientific Inc., MA). The HPLC and Mass Spectrometer are connected using the Nanospray Source I (Thermo Fisher Scientific) and a nanospray emitter (New Objective, MA). The column used was Acclaim® PepMap RSLC 75 μm x 15 cm (Dionex) as the analytical column and Acclaim® PepMap RSLC 75 μm x 2 cm as the enrichment column

5 microlitres of sample was loaded on the enrichment column at a flow rate of 3 μL/min in Mobile Phase A (0.1% FA in 2% v/v ACN) and resolved with 4-55% B gradient of Mobile Phase B (0.1% FA in 80% w/v ACN) over 25 minutes at a flow rate of 300 nL/min.

Ionisable species ($300 < m/z < 2000$) were trapped and the six most intense ions eluting at the time were individually selected for fragmentation by collision-induced dissociation. Active exclusion was used to exclude an already fragmented precursor ion from selection for a period of 15 seconds.

Peter Hoffmann 830 35507 Peter.Hoffmann@adelaide.edu.au
Sandra Hack 830 34903 Sandra.Hack@adelaide.edu.au

Adelaide Proteomics Centre
School of Molecular & Biomedical Science
Molecular Life Science building 1.50
University of Adelaide, SA, 5005

Data analysis

Data analysis was performed using the XCalibur software (Version 2.0.7,Thermo Fisher Scientific). MS/MS spectra were extracted and submitted to the Mascot search engine using Proteome Discoverer (Version 1.3,Thermo Fisher Scientific), search parameters were as shown in Table 1.

Results

The protein identities of the band is summarised in Table 1. This Table includes information about:

- The name of the identified protein and the organism from which the protein was identified
- The accession number of the protein in the database
- The combined ion score for all queries (i.e., MS/MS spectra) matched to a single protein.
- The number of queries that were matched to a single protein and the total number of queries resulting from that LC-eSI-IT MS run.
- The sequences of the identified peptides
- The independent ion scores for each of the matched peptides and the cut off score, whereby peptides with ion scores above this threshold indicate identity or extensive homology. The Identity threshold is calculated for each peptide at the significance level of 0.05 meaning that peptide matches with scores above the Identity Threshold have a 5% chance of being incorrect.
- The exponentially modified protein abundance index (emPAI value) as an approximate measure of relative quantitation. This is calculated from the number of observed peptides relative to that predicted from the matched sequence. In general, higher scores indicate greater relative abundance in that sample (i.e., the gel spot or band). Developed by Ishihama and colleagues, the key publication is Ishihama *et al*, 2005, Molecular & Cellular Proteomics, 4, 1265-1272.
- The predicted molecular weight (MW) and isoelectric point (pI) of the matched protein based on the values provided in the MASCOT Summary Report

Protein identifications were made on the basis of having at least two matching unique peptides with individual ion score above the homology threshold. These unique peptides were required to have different sequences or different variations of the same sequence, for example, containing a modified residue or missed cleavage site. Multiple charge states were not considered as unique. Identities assigned based on only a single peptide hit should be considered as tentative and further experimental evidence is required to confirm their presence in the sample. Identification of Keratin is typically due to background levels of contamination.

Report prepared by:

Note: All samples (gels, digests, etc.) not completely used for the analysis are stored at the APC for 12 months and then discarded.

Peter Hoffmann
Sandra Hack

Peter.Hoffmann@adelaide.edu.au
Sandra.Hack@adelaide.edu.au

Adelaide Proteomics Centre
School of Molecular & Biomedical Science
Molecular Life Science building 1.50
University of Adelaide, SA, 5005

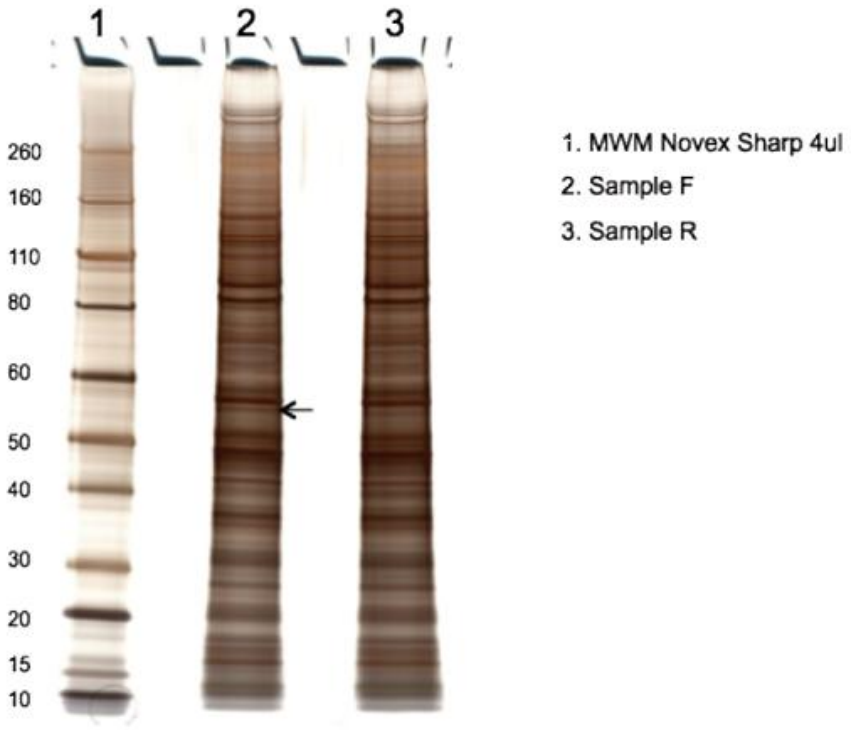

Figure 1 The frozen samples were placed in the sonicating water bath to thaw for 30 sec, centrifuged at 14000G for 60 sec and 20ul of supernatant removed and made up to 30ul with 7ul LDS loading buffer and 3ul 0.5M DTT. They were heated at 95ºC for 10min and each sample loaded in entirety. The Invitrogen NuPage™ 4-12% bis-tris gel was run at 180V in 1 x MOPS running buffer for 60 min. The gel was subsequently fixed for 1.5 hour and silver stained using the Invitrogen SilverQuest™ silver stain kit.

Peter Hoffmann 830 35507 Peter.Hoffmann@adelaide.edu.au
Sandra Hack 830 34903 Sandra.Hack@adelaide.edu.au
Adelaide Proteomics Centre
School of Molecular & Biomedical Science
Molecular Life Science building 1.50
University of Adelaide, SA, 5005

Table 1

Combined LC-eSI-IT MS MASCOT search results summary.

Sample reference: File Name: 111130_11-103_1_5uL.RAW		Mascot parameters Database: SwissProt Taxonomy: . . . . . Homo sapiens (human) Enzyme: Trypsin (2 missed cleavages) Fixed modifications: Carbamidomethyl (C) Variable modifications: Oxidation (M) Mass tolerances: MS 0.1Da, MS/MS 0.6Da (Monoisotopic)				
Protein	**Accession**	**Predicted MW(kDa) / pI**	**ID / Total queries**	**Combined IonScore**	**Sequence coverage (%)**	**emPAI**
Aspartyl-tRNA synthetase, cytoplasmic [Homo sapiens]	SYDC_HUMAN	57.5 / 6.1	23 / 1639	182	16	0.2
Peptide sequences				**IonScore (Identity / homology threshold)**		
K.GFVEIQTPK.I				33(31/-)		
R.QTSMFPR.D + Oxidation (M)				10(29/23)		
R.EAGVEMGDEDDLSTPNEK.L + Oxidation (M)				8(23/16)		
R.TSTSQAVFR.L				51(30/23)		
R.EIMDAAEDYAK.E + Oxidation (M)				11(26/15)		
R.FQTEIQTVNK.Q				47(30/30)		
K.VFSIGPVFR.A				0(26/13)		
R.VIDLR.T				22(32/-)		
Protein	**Accession**	**Predicted MW(kDa) / pI**	**ID / Total queries**	**Combined IonScore**	**Sequence coverage (%)**	**emPAI**
ATP synthase subunit alpha, mitochondrial [Homo sapiens]	ATPA_HUMAN	59.8 / 9.2	27 / 1639	141	11	0.2
Peptide sequences				**IonScore (Identity / homology threshold)**		
R.VVDALGNAIDGK.G				16(31/15)		
K.AVDSLVPIGR.G				31(29/-)		
R.LTELLK.Q				9(32/22)		
K.APGIIPR.I				25(28/22)		
R.QMSLLLR.R + Oxidation (M)				17(31/28)		
R.VLSIGDGIAR.V				24(31/30)		
R.ELIIGDR.Q				20(32/-)		
Protein	**Accession**	**Predicted MW(kDa) / pI**	**ID / Total queries**	**Combined IonScore**	**Sequence coverage (%)**	**emPAI**
Protein disulfide-isomerase A3 [Homo sapiens]	PDIA3_HUMAN	57.1 / 6.0	17 / 1639	135	11	0.2

Peter Hoffmann 830 35507 Peter.Hoffmann@adelaide.edu.au
Sandra Hack 830 34903 Sandra.Hack@adelaide.edu.au

Adelaide Proteomics Centre
School of Molecular & Biomedical Science
Molecular Life Science building 1.50
University of Adelaide, SA, 5005

Peptide sequences	IonScore (Identity / homology threshold)
K.SEPIPESNDGPVK.V	6(29/13)
R.LAPEYEAAATR.L	46(31/29)
K.QAGPASVPLR.T	44(29/-)
K.DPNIVIAK.M	20(29/20)
K.GIVPLAK.V	16(27/14)
K.KKAQEDL.-	4(32/20)

Protein	Accession	Predicted MW(kDa) / pI	ID / Total queries	Combined IonScore	Sequence coverage (%)	emPAI
Keratin, type I cytoskeletal 10 [Homo sapiens]	K1C10_HUMAN	59.0 / 5.1	36 / 1639	123	12	0.2

Peptide sequences	IonScore (Identity / homology threshold)
R.LKYENEVALR.Q	35(30/27)
K.IRLENEIQTYR.S	20(30/25)
R.LENEIQTYR.S	1(30/14)
R.ALEESNYELEGK.I	11(29/19)
R.LAADDFR.L	37(31/26)
R.SLLEGEGSSGGGGR.G	10(30/18)
K.YYKTIDDLK.N	4(31/21)
R.LASYLDK.V	4(30/22)

Protein	Accession	Predicted MW(kDa) / pI	ID / Total queries	Combined IonScore	Sequence coverage (%)	emPAI
Keratin, type II cytoskeletal 1 [Homo sapiens]	K2C1_HUMAN	71.3 / 5.9	18 / 1639	117	8	0.1

Peptide sequences	IonScore (Identity / homology threshold)
K.AEAESLYQSK.Y	22(30/19)
R.SLVNLGGSKSISISVAR.G	21(27/15)
R.TNAENEFVTIKK.D	19(30/22)
K.SISISVAR.G	15(32/26)
K.AQYEDIAQK.S	8(30/15)
K.SLNNQFASFIDKVR.F	19(29/18)

Protein	Accession	Predicted MW(kDa) / pI	ID / Total queries	Combined IonScore	Sequence coverage (%)	emPAI
tRNA-splicing ligase RtcB homolog [Homo sapiens]	RTCB_HUMAN	66.2 / 8.2	10 / 1639	103	10	0.2

Peptide sequences	IonScore (Identity / homology threshold)
K.LVMEEAPESYK.N + Oxidation (M)	18(29/17)

Peter Hoffmann 830 35507 Peter.Hoffmann@adelaide.edu.au
Sandra Hack 830 34903 Sandra.Hack@adelaide.edu.au

Adelaide Proteomics Centre
School of Molecular & Biomedical Science
Molecular Life Science building 1.50
University of Adelaide, SA, 5005

R.TNLDESDVQPVK.E R.SSMTFLTR.Q + Oxidation (M)						37(30/23) 46(31/-)	
Protein		**Accession**	**Predicted MW(kDa) / pI**	**ID / Total queries**	**Combined IonScore**	**Sequence coverage (%)**	**emPAI**
Keratin, type II cytoskeletal 8 [Homo sapiens]		K2C8_HUMAN	56.8 / 5.6	21 / 1639	94	8	0.1
Peptide sequences					**IonScore (Identity / homology threshold)**		
R.ISSSSFSR.V						47(29/-)	
K.LVSESSDVLPK.-						13(31/21)	
K.FASFIDKVR.F						15(30/24)	
K.LLEGEESR.L						14(31/28)	
Protein		**Accession**	**Predicted MW(kDa) / pI**	**ID / Total queries**	**Combined IonScore**	**Sequence coverage (%)**	**emPAI**
T-complex protein 1 subunit beta [Homo sapiens]		TCPB_HUMAN	53.7 / 5.5	14 / 1639	89	8	0.1
Peptide sequences					**IonScore (Identity / homology threshold)**		
R.VDNIIK.A						20(32/28)	
R.DASLMVTNDGATILK.N + Oxidation (M)						20(29/19)	
K.NIGVDNPAAK.V						38(30/-)	
Protein		**Accession**	**Predicted MW(kDa) / pI**	**ID / Total queries**	**Combined IonScore**	**Sequence coverage (%)**	**emPAI**
Protein phosphatase 1F [Homo sapiens]		PPM1F_HUMAN	57.8 / 6.0	9 / 1639	77	6	0.1
Peptide sequences					**IonScore (Identity / homology threshold)**		
R.VAEELVAAAR.E						66(31/-)	
K.QVPLAAR.A						11(28/-)	
Protein		**Accession**	**Predicted MW(kDa) / pI**	**ID / Total queries**	**Combined IonScore**	**Sequence coverage (%)**	**emPAI**
Nicalin [Homo sapiens]		NCLN_HUMAN	50.0 / 5.0	6 / 1639	77	4	0.1
Peptide sequences					**IonScore (Identity / homology threshold)**		
R.AMAAVPQDVVR.Q + Oxidation (M)						39(31/-)	
R.NAVLNTEAR.T						34(31/-)	

Peter Hoffmann 830 35507 Peter.Hoffmann@adelaide.edu.au
Sandra Hack 830 34903 Sandra.Hack@adelaide.edu.au
Adelaide Proteomics Centre
School of Molecular & Biomedical Science
Molecular Life Science building 1.50
University of Adelaide, SA, 5005

Protein	Accession	Predicted MW(kDa) / pI	ID / Total queries	Combined IonScore	Sequence coverage (%)	emPAI
Chromosome transmission fidelity protein 8 homolog isoform 2 [Homo sapiens]	CTF8A_HUMAN	63.1 / 6.4	10 / 1639	73	4	0.1
Peptide sequences					**IonScore (Identity / homology threshold)**	
R.AGGLLGAGPDPR.G					10(30/19)	
R.DPSMASFPR.G + Oxidation (M)					7(30/21)	
R.SGFLGTNPAPR.S					27(31/18)	
R.GGGPMGPGSGPNLR.A + Oxidation (M)					26(29/22)	

Protein	Accession	Predicted MW(kDa) / pI	ID / Total queries	Combined IonScore	Sequence coverage (%)	emPAI
Keratin, type II cytoskeletal 2 epidermal [Homo sapiens]	K22E_HUMAN	51.4 / 12.4	10 / 1639	69	9	0.1
Peptide sequences					**IonScore (Identity / homology threshold)**	
R.GFSSGSAVVSGGSR.R					35(29/24)	
K.FASFIDKVR.F					15(30/24)	
R.SLVGLGGTK.S					4(32/20)	
R.STSSFSCLSR.H					14(29/19)	

Protein	Accession	Predicted MW(kDa) / pI	ID / Total queries	Combined IonScore	Sequence coverage (%)	emPAI
Adenylyl cyclase-associated protein 1 [Homo sapiens]	CAP1_HUMAN	65.7 / 8.1	11 / 1639	67	7	0.0
Peptide sequences					**IonScore (Identity / homology threshold)**	
K.NSLDCEIVSAK.S					21(30/-)	
K.INSITVDNCK.K					5(30/13)	
R.ALLVTASQCQQPAENK.L					7(29/20)	
K.LVTTVTEIAG.-					36(31/30)	

Protein	Accession	Predicted MW(kDa) / pI	ID / Total queries	Combined IonScore	Sequence coverage (%)	emPAI
Inosine-5'-monophosphate dehydrogenase 2 [Homo sapiens]	IMDH2_HUMAN	52.3 / 8.2	6 / 1639	67	10	0.1
Peptide sequences					**IonScore (Identity / homology threshold)**	
K.VAQGVSGAVQDK.G					30(31/21)	
K.EANEILQR.S					36(31/-)	

Peter Hoffmann 830 35507 Peter.Hoffmann@adelaide.edu.au
Sandra Hack 830 34903 Sandra.Hack@adelaide.edu.au

Adelaide Proteomics Centre
School of Molecular & Biomedical Science
Molecular Life Science building 1.50
University of Adelaide, SA, 5005

Appendix D: Permissions

This section includes correspondence regarding the use of figures in this thesis which are not my own (personal contact information within the correspondence was removed).

Applied Biosystems, Fig 3.6

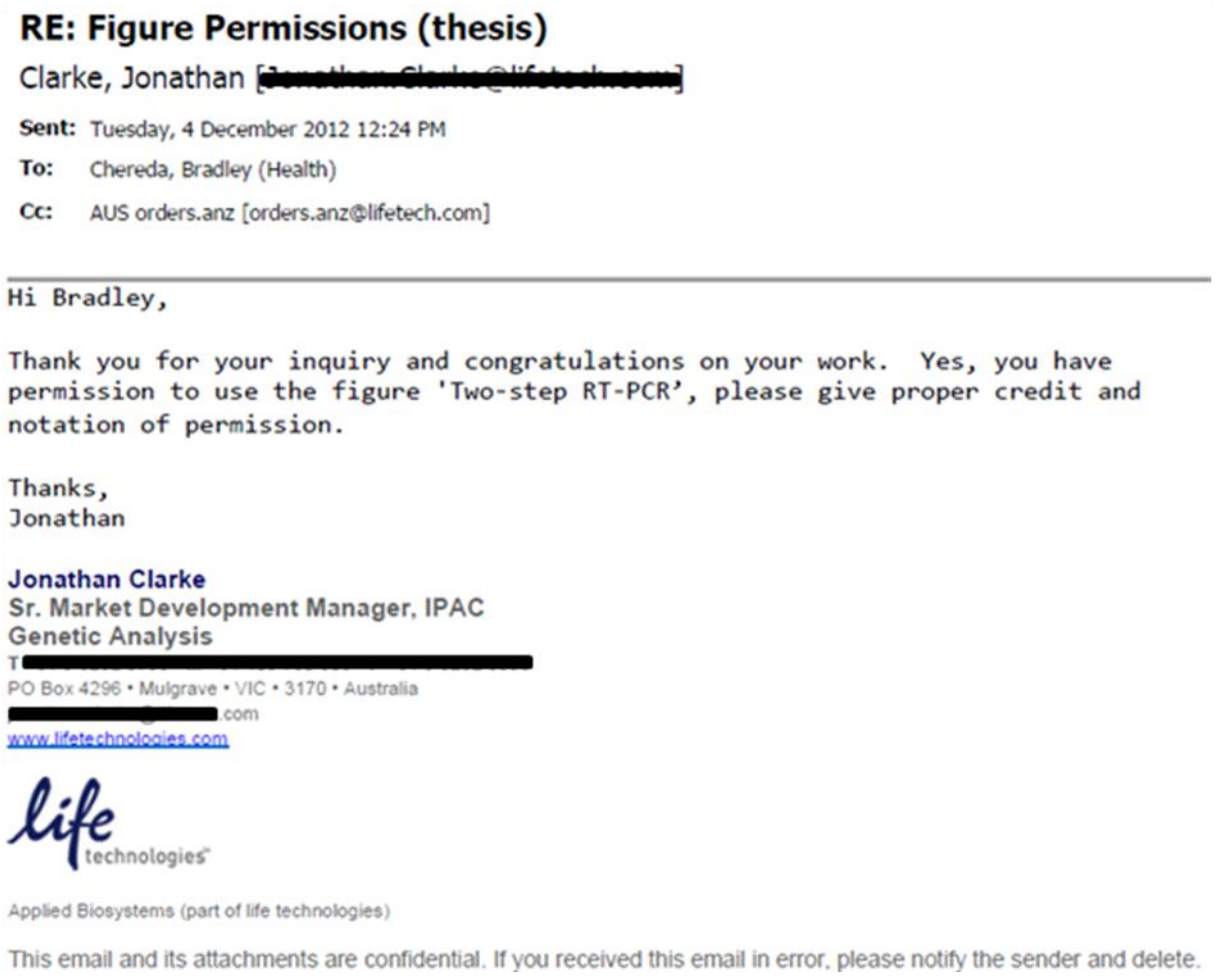

RE: Figure Permissions (thesis)

Clarke, Jonathan [redacted]

Sent: Tuesday, 4 December 2012 12:24 PM

To: Chereda, Bradley (Health)

Cc: AUS orders.anz [orders.anz@lifetech.com]

Hi Bradley,

Thank you for your inquiry and congratulations on your work. Yes, you have permission to use the figure 'Two-step RT-PCR', please give proper credit and notation of permission.

Thanks,
Jonathan

Jonathan Clarke
Sr. Market Development Manager, IPAC
Genetic Analysis
T [redacted]
PO Box 4296 • Mulgrave • VIC • 3170 • Australia
[redacted].com
www.lifetechnologies.com

life technologies

Applied Biosystems (part of life technologies)

Bueno, *et al*. Fig 3.14

ELSEVIER LICENSE
TERMS AND CONDITIONS

May 10, 2012

This is a License Agreement between Bradley Chereda ("You") and Elsevier ("Elsevier") provided by Copyright Clearance Center ("CCC"). The license consists of your order details, the terms and conditions provided by Elsevier, and the payment terms and conditions.

All payments must be made in full to CCC. For payment instructions, please see information listed at the bottom of this form.

Supplier	Elsevier Limited The Boulevard,Langford Lane Kidlington,Oxford,OX5 1GB,UK
Registered Company Number	1982084
Customer name	Bradley Chereda
Customer address	IMVS main building, Frome Rd Adelaide, S.A 5000
License number	2905290494883
License date	May 10, 2012
Licensed content publisher	Elsevier
Licensed content publication	Cancer Cell
Licensed content title	Genetic and Epigenetic Silencing of MicroRNA-203 Enhances*ABL1*and*BCR-ABL1*Oncogene Expression
Licensed content author	María J. Bueno,Ignacio Pérez de Castro,Marta Gómez de Cedrón,Javier Santos,George A. Calin,Juan C. Cigudosa,Carlo M. Croce,José Fernández-Piqueras,Marcos Malumbres
Licensed content date	10 June 2008
Licensed content volume number	13
Licensed content issue number	6
Number of pages	11
Start Page	496
End Page	506
Type of Use	reuse in a thesis/dissertation
Portion	figures/tables/illustrations
Number of figures/tables /illustrations	2
Format	both print and electronic
Are you the author of this Elsevier article?	No
Will you be translating?	No
Order reference number	001
Title of your thesis/dissertation	Control of BCR-ABL expression

Maris, *et al*. Fig 4.2, A

Copyright Clearance Center RightsLink®

Home | Account Info | Help

Title: The RNA recognition motif, a plastic RNA-binding platform to regulate post-transcriptional gene expression

Author: Christophe Maris,Cyril Dominguez,Frédéric H.-T. Allain

Publication: FEBS Journal

Publisher: John Wiley and Sons

Date: Apr 21, 2005

Logged in as:
Bradley Chereda
Account #:
3000532029

LOGOUT

Order Completed

Thank you very much for your order.

This is a License Agreement between Bradley Chereda ("You") and John Wiley and Sons ("John Wiley and Sons"). The license consists of your order details, the terms and conditions provided by John Wiley and Sons, and the payment terms and conditions.

Get the printable license.

License Number	2919670727464
License date	May 31, 2012
Licensed content publisher	John Wiley and Sons
Licensed content publication	FEBS Journal
Licensed content title	The RNA recognition motif, a plastic RNA-binding platform to regulate post-transcriptional gene expression
Licensed content author	Christophe Maris,Cyril Dominguez,Frédéric H.-T. Allain
Licensed content date	Apr 21, 2005
Start page	2118
End page	2131
Type of use	Dissertation/Thesis
Requestor type	University/Academic
Format	Print and electronic
Portion	Figure/table
Number of figures/tables	1
Original Wiley figure/table number(s)	Fig 3a
Will you be translating?	No
Order reference number	
Total	0.00 USD

Valverde, *et al*. Fig 4.2, B

JOHN WILEY AND SONS LICENSE TERMS AND CONDITIONS

Dec 03, 2012

This is a License Agreement between Bradley Chereda ("You") and John Wiley and Sons ("John Wiley and Sons") provided by Copyright Clearance Center ("CCC"). The license consists of your order details, the terms and conditions provided by John Wiley and Sons, and the payment terms and conditions.

All payments must be made in full to CCC. For payment instructions, please see information listed at the bottom of this form.

License Number	2923991396906
License date	Jun 07, 2012
Licensed content publisher	John Wiley and Sons
Licensed content publication	FEBS Journal
Book title	
Licensed content author	Roberto Valverde,Laura Edwards,Lynne Regan
Licensed content date	Apr 15, 2008
Start page	2712
End page	2726
Type of use	Dissertation/Thesis
Requestor type	University/Academic
Format	Print and electronic
Portion	Figure/table
Number of figures/tables	1
Number of extracts	
Original Wiley figure/table number(s)	Fig 1
Will you be translating?	No

Franziska Luschtinetz, Fig 4.4, A

Re: E-Mail über Kontaktformular (www.luschtinetz.com)

Franziska Luschtinetz [redacted]

Sent: Saturday, 2 June 2012 11:43 PM
To: Chereda, Bradley (Health)
Attachments: biotin-Streptavidin.pdf (2 MB) [Open as Web Page]

Hi Bradley,

sure, you can use the picture 2.3 from my PhD thesis. Please just reference it:

title: Cyaninfarbstoffe als Fluoreszenzsonden in biomimetischen und biologischen Systemen: Fluoreszenz-Korrelations-Spektroskopie und Fluoreszenzanisotropie Untersuchungen, Universität Potsdam
author: Franziska Luschtinetz
date: 2010

and the software PyMol (and maybe also the crystal structure database). Attached you can find the pdf from the picture (I used pdfTeX for my PhD and don't have jpeg-files)

I used the software PyMol for the creation of this picture.
http://pymol.org/educational/
The crystal structure of biotin streptavidin can be found in the protein database (I used PDB 1SWD). With these you can change the picture yourself and also create videos from it.

Good luck with your thesis and greetings from Munich.

Franziska

ENZO scientific, Fig 4.4, B (uracil triphosphate molecule)

FW: WG: Contact from Enzolifesciences

Maurice Weidling [redacted]

Sent: Wednesday, 4 July 2012 1:05 AM

To: Chereda, Bradley (Health)

Cc: Walter Isler [redacted]; Adrian Rea [redacted]

Hi Bradley,

you can use the chemical structure pls just reference Enzo.

Thank you very much in advance :)

Best
Maurice

>-----Original Message-----
>From: Chereda, Bradley (Health)
>[mailto:[redacted].au]
>Sent: Montag, 2. Juli 2012 06:34
>To: Maurice Weidling
>Subject: RE: WG: Contact from Enzolifesciences
>
>Hello,
>Sorry I have been away.
>I was wanting to use the chemical structure from:
>http://www.enzolifesciences.com/fileadmin/reports/els_c6ed28b812.pdf
>
>Thanks,
>Bradley.
>

Piece (Thermo Scientific), Fig 4.4, B (biotinylated cytidine) and Fig 4.5 (mass spectrometry)

Permission to use a Thermo Fisher Scientific figure in your thesis

Schubert, Holly J. [m]

Sent: Friday, 1 June 2012 7:18 PM

To: Chereda, Bradley (Health)

Dear Bradley Chereda:

You have one-time, limited permission from Thermo Fisher Scientific to use three images from our www.piercenet.com website in your forthcoming thesis, tentatively titled "Characterisation of the BCR-ABL 3'untranslated region." The images are:
http://www.piercenet.com/media/Tandem%20Mass%20Spec-650px.jpg
http://www.piercenet.com/media/LC-MS-MS-460px.jpg
http://www.piercenet.com/media/pCp-RNA-Biotin-Rxn.gif

If I can be of further assistance, please let me know. I wish you much success with completing your thesis!

Best wishes,
Holly

Holly Schubert
Director, Marketing Communications
Biosciences Division

Thermo Fisher Scientific
3747 N Meridian Road
PO Box 117
Rockford, IL 61105
Direct Tel:
Fax: 815-987-3949
Email: her.com
www.thermoscientific.com

References

1. Ben-Neriah Y, Daley GQ, Mes-Masson AM, Witte ON, Baltimore D. The chronic myelogenous leukemia-specific P210 protein is the product of the bcr/abl hybrid gene. Science. 1986;233:212-214.
2. Daley GQ, Van Etten RA, Baltimore D. Induction of chronic myelogenous leukemia in mice by the P210bcr/abl gene of the Philadelphia chromosome. Science. 1990;247:824-830.
3. Gambacorti-Passerini C, le Coutre P, Mologni L, et al. Inhibition of the ABL kinase activity blocks the proliferation of BCR/ABL+ leukemic cells and induces apoptosis. Blood Cells Mol Dis. 1997;23:380-394.
4. Deininger MW. Signal Transduction Inhibitors in Chronic Myeloid Leukaemia. Myeloproliferative Disorders. New York: Springer Berlin Heidelberg; 2007:75-102.
5. Druker BJ, Guilhot F, O'Brien SG, et al. Five-year follow-up of patients receiving imatinib for chronic myeloid leukemia. N Engl J Med. 2006;355:2408-2417.
6. Leukaemia Foundation. Chronic myeloid leukaemia. Vol. 2012. Windsor, Queensland, Australia: Leukaemia Foundation; 2008.
7. Faquharson M, Shepherd P. Clinical Features of CML. Myeloproliferative Disorders. New York: Springer Berlin Heidelberg; 2007:59-74.
8. Druker BJ, Tamura S, Buchdunger E, et al. Effects of a selective inhibitor of the Abl tyrosine kinase on the growth of Bcr-Abl positive cells. Nat Med. 1996;2:561-566.
9. Melo JV, Barnes DJ. Chronic myeloid leukaemia as a model of disease evolution in human cancer. Nat Rev Cancer. 2007;7:441-453.
10. Jamieson CH, Ailles LE, Dylla SJ, et al. Granulocyte-macrophage progenitors as candidate leukemic stem cells in blast-crisis CML. N Engl J Med. 2004;351:657-667.
11. Perrotti D, Jamieson C, Goldman J, Skorski T. Chronic myeloid leukemia: mechanisms of blastic transformation. J Clin Invest. 2010;120:2254-2264.
12. Skorski T. Genetic mechanisms of chronic myeloid leukemia blastic transformation. Curr Hematol Malig Rep. 2012;7:87-93.
13. Melo JV, Barnes DJ. Chronic Myeloid Leukemia: Biology of Advanced Phase. Myeloproliferative Disorders. New York: Springer Berlin Heidelberg; 2007:37-59.
14. Nagar B, Hantschel O, Young MA, et al. Structural basis for the autoinhibition of c-Abl tyrosine kinase. Cell. 2003;112:859-871.
15. Schindler T, Bornmann W, Pellicena P, Miller WT, Clarkson B, Kuriyan J. Structural mechanism for STI-571 inhibition of abelson tyrosine kinase. Science. 2000;289:1938-1942.
16. Deininger M, Buchdunger E, Druker BJ. The development of imatinib as a therapeutic agent for chronic myeloid leukemia. Blood. 2005;105:2640-2653.
17. Branford S, Hughes TP, Rudzki Z. Monitoring chronic myeloid leukaemia therapy by real-time quantitative PCR in blood is a reliable alternative to bone marrow cytogenetics. Br J Haematol. 1999;107:587-599.
18. Hughes TP, Hochhaus A, Branford S, et al. Long-term prognostic significance of early molecular response to imatinib in newly diagnosed chronic myeloid leukemia: an analysis from the International Randomized Study of Interferon and STI571 (IRIS). Blood. 2010;116:3758-3765.
19. Mahon FX, Rea D, Guilhot J, et al. Discontinuation of imatinib in patients with chronic myeloid leukaemia who have maintained complete molecular remission for at least 2

years: the prospective, multicentre Stop Imatinib (STIM) trial. Lancet Oncol. 2010;11:1029-1035.
20. Larson RA, Hochhaus A, Hughes TP, et al. Nilotinib vs imatinib in patients with newly diagnosed Philadelphia chromosome-positive chronic myeloid leukemia in chronic phase: ENESTnd 3-year follow-up. Leukemia;26:2197-2203.
21. Hochhaus A, O'Brien SG, Guilhot F, et al. Six-year follow-up of patients receiving imatinib for the first-line treatment of chronic myeloid leukemia. Leukemia. 2009;23:1054-1061.
22. Gorre ME, Mohammed M, Ellwood K, et al. Clinical resistance to STI-571 cancer therapy caused by BCR-ABL gene mutation or amplification. Science. 2001;293:876-880.
23. von Bubnoff N, Peschel C, Duyster J. Resistance of Philadelphia-chromosome positive leukemia towards the kinase inhibitor imatinib (STI571, Glivec): a targeted oncoprotein strikes back. Leukemia. 2003;17:829-838.
24. Lange T, Park B, Willis SG, Deininger MW. BCR-ABL kinase domain mutations in chronic myeloid leukemia: not quite enough to cause resistance to imatinib therapy? Cell Cycle. 2005;4:1761-1766.
25. Giles FJ, Abruzzese E, Rosti G, et al. Nilotinib is active in chronic and accelerated phase chronic myeloid leukemia following failure of imatinib and dasatinib therapy. Leukemia. 2010;24:1299-1301.
26. Gruber FX, Ernst T, Porkka K, et al. Dynamics of the emergence of dasatinib and nilotinib resistance in imatinib-resistant CML patients. Leukemia. 2012;26:172-177.
27. O'Hare T, Eide CA, Deininger MW. Bcr-Abl kinase domain mutations, drug resistance, and the road to a cure for chronic myeloid leukemia. Blood. 2007;110:2242-2249.
28. Copland M, Hamilton A, Elrick LJ, et al. Dasatinib (BMS-354825) targets an earlier progenitor population than imatinib in primary CML but does not eliminate the quiescent fraction. Blood. 2006;107:4532-4539.
29. Jorgensen HG, Allan EK, Jordanides NE, Mountford JC, Holyoake TL. Nilotinib exerts equipotent antiproliferative effects to imatinib and does not induce apoptosis in CD34+ CML cells. Blood. 2007;109:4016-4019.
30. Bhatia R, Holtz M, Niu N, et al. Persistence of malignant hematopoietic progenitors in chronic myelogenous leukemia patients in complete cytogenetic remission following imatinib mesylate treatment. Blood. 2003;101:4701-4707.
31. Graham SM, Jorgensen HG, Allan E, et al. Primitive, quiescent, Philadelphia-positive stem cells from patients with chronic myeloid leukemia are insensitive to STI571 in vitro. Blood. 2002;99:319-325.
32. Chu S, Li L, Singh H, Bhatia R. BCR-tyrosine 177 plays an essential role in Ras and Akt activation and in human hematopoietic progenitor transformation in chronic myelogenous leukemia. Cancer Res. 2007;67:7045-7053.
33. Hamilton A, Helgason GV, Schemionek M, et al. Chronic myeloid leukemia stem cells are not dependent on Bcr-Abl kinase activity for their survival. Blood. 2012;119:1501-1510.
34. Hiwase DK, Saunders VA, Nievergall E, Ross DD, White DL, Hughes TP. Dasatinib targets chronic myeloid leukemia-CD34+ progenitors as effectively as it targets mature cells. Haematologica. 2012.
35. Konig H, Holtz M, Modi H, et al. Enhanced BCR-ABL kinase inhibition does not result in increased inhibition of downstream signaling pathways or increased growth suppression in CML progenitors. Leukemia. 2008;22:748-755.

36. Corbin AS, Agarwal A, Loriaux M, Cortes J, Deininger MW, Druker BJ. Human chronic myeloid leukemia stem cells are insensitive to imatinib despite inhibition of BCR-ABL activity. J Clin Invest. 2011;121:396-409.
37. Chu S, McDonald T, Lin A, et al. Persistence of leukemia stem cells in chronic myelogenous leukemia patients in prolonged remission with imatinib treatment. Blood. 2011;118:5565-5572.
38. Balabanov S, Gontarewicz A, Keller G, et al. Abcg2 overexpression represents a novel mechanism for acquired resistance to the multi-kinase inhibitor Danusertib in BCR-ABL-positive cells in vitro. PLoS One. 2011;6:e19164.
39. Engler JR, Frede A, Saunders VA, Zannettino AC, Hughes TP, White DL. Chronic myeloid leukemia CD34+ cells have reduced uptake of imatinib due to low OCT-1 activity. Leukemia. 2010;24:765-770.
40. Jiang X, Zhao Y, Smith C, et al. Chronic myeloid leukemia stem cells possess multiple unique features of resistance to BCR-ABL targeted therapies. Leukemia. 2007;21:926-935.
41. Brendel C, Scharenberg C, Dohse M, et al. Imatinib mesylate and nilotinib (AMN107) exhibit high-affinity interaction with ABCG2 on primitive hematopoietic stem cells. Leukemia. 2007;21:1267-1275.
42. Nowell PC, Hungerford DA. A minute chromosome in human chronic granulocytic leukemia. Science. 1960;132:1497.
43. de Klein A, van Kessel AG, Grosveld G, et al. A cellular oncogene is translocated to the Philadelphia chromosome in chronic myelocytic leukaemia. Nature. 1982;300:765-767.
44. Groffen J, Stephenson JR, Heisterkamp N, de Klein A, Bartram CR, Grosveld G. Philadelphia chromosomal breakpoints are clustered within a limited region, bcr, on chromosome 22. Cell. 1984;36:93-99.
45. Score J, Calasanz MJ, Ottman O, et al. Analysis of genomic breakpoints in p190 and p210 BCR-ABL indicate distinct mechanisms of formation. Leukemia. 2010;24:1742-1750.
46. Balatzenko G, Vundinti BR, Margarita G. Correlation between the type of bcr-abl transcripts and blood cell counts in chronic myeloid leukemia - a possible influence of mdr1 gene expression. Hematol Rep. 2011;3:e3.
47. Melo JV. The diversity of BCR-ABL fusion proteins and their relationship to leukemia phenotype. Blood. 1996;88:2375-2384.
48. Elliott SL, Taylor KM, Taylor DL, et al. Cytogenetic response to alpha-interferon is predicted in early chronic phase chronic myeloid leukemia by M-bcr breakpoint location. Leukemia. 1995;9:946-950.
49. Mills KI, MacKenzie ED, Birnie GD. The site of the breakpoint within the bcr is a prognostic factor in Philadelphia-positive CML patients. Blood. 1988;72:1237-1241.
50. Mills KI, Sproul AM, Leibowitz D, Burnett AK. Mapping of breakpoints, and relationship to BCR-ABL RNA expression, in Philadelphia-chromosome-positive chronic myeloid leukaemia patients with a breakpoint around exon 14 (b3) of the BCR gene. Leukemia. 1991;5:937-941.
51. Inokuchi K, Inoue T, Tojo A, et al. A possible correlation between the type of bcr-abl hybrid messenger RNA and platelet count in Philadelphia-positive chronic myelogenous leukemia. Blood. 1991;78:3125-3127.
52. Verschraegen CF, Kantarjian HM, Hirsch-Ginsberg C, et al. The breakpoint cluster region site in patients with Philadelphia chromosome-positive chronic myelogenous leukemia. Clinical, laboratory, and prognostic correlations. Cancer. 1995;76:992-997.

53. Lucas CM, Harris RJ, Giannoudis A, et al. Chronic myeloid leukemia patients with the e13a2 BCR-ABL fusion transcript have inferior responses to imatinib compared to patients with the e14a2 transcript. Haematologica. 2009;94:1362-1367.
54. Rozman C, Urbano-Ispizua A, Cervantes F, et al. Analysis of the clinical relevance of the breakpoint location within M-BCR and the type of chimeric mRNA in chronic myelogenous leukemia. Leukemia. 1995;9:1104-1107.
55. Fioretos T, Nilsson PG, Aman P, et al. Clinical impact of breakpoint position within M-bcr in chronic myeloid leukemia. Leukemia. 1993;7:1225-1231.
56. Dowding C, Guo AP, Maisin D, Gordon MY, Goldman JM. The effects of interferon-alpha on the proliferation of CML progenitor cells in vitro are not related to the precise position of the M-BCR breakpoint. Br J Haematol. 1991;77:165-171.
57. Opalka B, Wandl UB, Kloke O, Beer U, Seeber S, Niederle N. No correlation between site of breakpoint in the BCR gene and platelet counts in Philadelphia chromosome-positive CML. Leuk Res. 1992;16:937-939.
58. Chan LC, Karhi KK, Rayter SI, et al. A novel abl protein expressed in Philadelphia chromosome positive acute lymphoblastic leukaemia. Nature. 1987;325:635-637.
59. Saglio G, Guerrasio A, Rosso C, et al. New type of Bcr/Abl junction in Philadelphia chromosome-positive chronic myelogenous leukemia. Blood. 1990;76:1819-1824.
60. Weerkamp F, Dekking E, Ng YY, et al. Flow cytometric immunobead assay for the detection of BCR-ABL fusion proteins in leukemia patients. Leukemia. 2009;23:1106-1117.
61. Gleissner B, Gokbuget N, Bartram CR, et al. Leading prognostic relevance of the BCR-ABL translocation in adult acute B-lineage lymphoblastic leukemia: a prospective study of the German Multicenter Trial Group and confirmed polymerase chain reaction analysis. Blood. 2002;99:1536-1543.
62. Verstovsek S, Lin H, Kantarjian H, et al. Neutrophilic-chronic myeloid leukemia: low levels of p230 BCR/ABL mRNA and undetectable BCR/ABL protein may predict an indolent course. Cancer. 2002;94:2416-2425.
63. McGahon A, Bissonnette R, Schmitt M, Cotter KM, Green DR, Cotter TG. BCR-ABL maintains resistance of chronic myelogenous leukemia cells to apoptotic cell death. Blood. 1994;83:1179-1187.
64. Bedi A, Zehnbauer BA, Barber JP, Sharkis SJ, Jones RJ. Inhibition of apoptosis by BCR-ABL in chronic myeloid leukemia. Blood. 1994;83:2038-2044.
65. Daley GQ, Baltimore D. Transformation of an interleukin 3-dependent hematopoietic cell line by the chronic myelogenous leukemia-specific P210bcr/abl protein. Proc Natl Acad Sci U S A. 1988;85:9312-9316.
66. Sirard C, Laneuville P, Dick JE. Expression of bcr-abl abrogates factor-dependent growth of human hematopoietic M07E cells by an autocrine mechanism. Blood. 1994;83:1575-1585.
67. Bunting KD. STAT5 signaling in normal and pathologic hematopoiesis. Front Biosci. 2007;12:2807-2820.
68. Ferbeyre G, Moriggl R. The role of Stat5 transcription factors as tumor suppressors or oncogenes. Biochim Biophys Acta. 2011;1815:104-114.
69. Carlesso N, Frank DA, Griffin JD. Tyrosyl phosphorylation and DNA binding activity of signal transducers and activators of transcription (STAT) proteins in hematopoietic cell lines transformed by Bcr/Abl. J Exp Med. 1996;183:811-820.
70. Chai SK, Nichols GL, Rothman P. Constitutive activation of JAKs and STATs in BCR-Abl-expressing cell lines and peripheral blood cells derived from leukemic patients. J Immunol. 1997;159:4720-4728.

71. Wolff NC, Ilaria RL, Jr. Establishment of a murine model for therapy-treated chronic myelogenous leukemia using the tyrosine kinase inhibitor STI571. Blood. 2001;98:2808-2816.
72. Hoelbl A, Schuster C, Kovacic B, et al. Stat5 is indispensable for the maintenance of bcr/abl-positive leukaemia. EMBO Mol Med;2:98-110.
73. Deininger MW, Goldman JM, Lydon N, Melo JV. The tyrosine kinase inhibitor CGP57148B selectively inhibits the growth of BCR-ABL-positive cells. Blood. 1997;90:3691-3698.
74. Shah NP, Kasap C, Weier C, et al. Transient potent BCR-ABL inhibition is sufficient to commit chronic myeloid leukemia cells irreversibly to apoptosis. Cancer Cell. 2008;14:485-493.
75. Barnes DJ, Schultheis B, Adedeji S, Melo JV. Dose-dependent effects of Bcr-Abl in cell line models of different stages of chronic myeloid leukemia. Oncogene. 2005;24:6432-6440.
76. Modi H, McDonald T, Chu S, Yee JK, Forman SJ, Bhatia R. Role of BCR/ABL gene-expression levels in determining the phenotype and imatinib sensitivity of transformed human hematopoietic cells. Blood. 2007;109:5411-5421.
77. Keeshan K, Cotter TG, McKenna SL. High Bcr-Abl expression prevents the translocation of Bax and Bad to the mitochondrion. Leukemia. 2002;16:1725-1734.
78. Steelman LS, Pohnert SC, Shelton JG, Franklin RA, Bertrand FE, McCubrey JA. JAK/STAT, Raf/MEK/ERK, PI3K/Akt and BCR-ABL in cell cycle progression and leukemogenesis. Leukemia. 2004;18:189-218.
79. Bovolenta C, Testolin L, Benussi L, Lievens PM, Liboi E. Positive selection of apoptosis-resistant cells correlates with activation of dominant-negative STAT5. J Biol Chem. 1998;273:20779-20784.
80. Franke TF, Kaplan DR, Cantley LC. PI3K: downstream AKTion blocks apoptosis. Cell. 1997;88:435-437.
81. Amarante-Mendes GP, Jascur T, Nishioka WK, Mustelin T, Green DR. Bcr - Abl-mediated resistance to apoptosis is independent of PI 3-kinase activity. Cell Death Differ. 1997;4:548-554.
82. Hoover RR, Gerlach MJ, Koh EY, Daley GQ. Cooperative and redundant effects of STAT5 and Ras signaling in BCR/ABL transformed hematopoietic cells. Oncogene. 2001;20:5826-5835.
83. Koptyra M, Cramer K, Slupianek A, Richardson C, Skorski T. BCR/ABL promotes accumulation of chromosomal aberrations induced by oxidative and genotoxic stress. Leukemia. 2008;22:1969-1972.
84. Amos TA, Lewis JL, Grand FH, Gooding RP, Goldman JM, Gordon MY. Apoptosis in chronic myeloid leukaemia: normal responses by progenitor cells to growth factor deprivation, X-irradiation and glucocorticoids. Br J Haematol. 1995;91:387-393.
85. Bedi A, Barber JP, Bedi GC, et al. BCR-ABL-mediated inhibition of apoptosis with delay of G2/M transition after DNA damage: a mechanism of resistance to multiple anticancer agents. Blood. 1995;86:1148-1158.
86. Skorski T. BCR/ABL, DNA damage and DNA repair: implications for new treatment concepts. Leuk Lymphoma. 2008;49:610-614.
87. Skorski T. Genomic instability: The cause and effect of BCR/ABL tyrosine kinase. Curr Hematol Malig Rep. 2007;2:69-74.

88. Cramer K, Nieborowska-Skorska M, Koptyra M, et al. BCR/ABL and other kinases from chronic myeloproliferative disorders stimulate single-strand annealing, an unfaithful DNA double-strand break repair. Cancer Res. 2008;68:6884-6888.
89. Dierov J, Sanchez PV, Burke BA, et al. BCR/ABL induces chromosomal instability after genotoxic stress and alters the cell death threshold. Leukemia. 2009;23:279-286.
90. Koptyra M, Falinski R, Nowicki MO, et al. BCR/ABL kinase induces self-mutagenesis via reactive oxygen species to encode imatinib resistance. Blood. 2006;108:319-327.
91. Nowicki MO, Falinski R, Koptyra M, et al. BCR/ABL oncogenic kinase promotes unfaithful repair of the reactive oxygen species-dependent DNA double-strand breaks. Blood. 2004;104:3746-3753.
92. Cooke MS, Evans MD, Dizdaroglu M, Lunec J. Oxidative DNA damage: mechanisms, mutation, and disease. FASEB J. 2003;17:1195-1214.
93. Deutsch E, Dugray A, AbdulKarim B, et al. BCR-ABL down-regulates the DNA repair protein DNA-PKcs. Blood. 2001;97:2084-2090.
94. Slupianek A, Schmutte C, Tombline G, et al. BCR/ABL regulates mammalian RecA homologs, resulting in drug resistance. Mol Cell. 2001;8:795-806.
95. Barnes DJ, Palaiologou D, Panousopoulou E, et al. Bcr-Abl expression levels determine the rate of development of resistance to imatinib mesylate in chronic myeloid leukemia. Cancer Res. 2005;65:8912-8919.
96. Gaiger A, Henn T, Horth E, et al. Increase of bcr-abl chimeric mRNA expression in tumor cells of patients with chronic myeloid leukemia precedes disease progression. Blood. 1995;86:2371-2378.
97. Marega M, Piazza RG, Pirola A, et al. BCR and BCR-ABL regulation during myeloid differentiation in healthy donors and in chronic phase/blast crisis CML patients. Leukemia. 2010;24:1445-1449.
98. Andrews DF, 3rd, Collins SJ. Heterogeneity in expression of the bcr-abl fusion transcript in CML blast crisis. Leukemia. 1987;1:718-724.
99. Neviani P, Santhanam R, Trotta R, et al. The tumor suppressor PP2A is functionally inactivated in blast crisis CML through the inhibitory activity of the BCR/ABL-regulated SET protein. Cancer Cell. 2005;8:355-368.
100. Chang JS, Santhanam R, Trotta R, et al. High levels of the BCR/ABL oncoprotein are required for the MAPK-hnRNP-E2 dependent suppression of C/EBPalpha-driven myeloid differentiation. Blood. 2007;110:994-1003.
101. Guerzoni C, Bardini M, Mariani SA, et al. Inducible activation of CEBPB, a gene negatively regulated by BCR/ABL, inhibits proliferation and promotes differentiation of BCR/ABL-expressing cells. Blood. 2006;107:4080-4089.
102. Eiring AM, Harb JG, Neviani P, et al. miR-328 functions as an RNA decoy to modulate hnRNP E2 regulation of mRNA translation in leukemic blasts. Cell. 2010;140:652-665.
103. Mahon FX, Deininger MW, Schultheis B, et al. Selection and characterization of BCR-ABL positive cell lines with differential sensitivity to the tyrosine kinase inhibitor STI571: diverse mechanisms of resistance. Blood. 2000;96:1070-1079.
104. Desplat V, Belloc F, Lagarde V, et al. Overproduction of BCR-ABL induces apoptosis in imatinib mesylate-resistant cell lines. Cancer. 2005;103:102-110.
105. Tang C, Schafranek L, Watkins DB, et al. Tyrosine kinase inhibitor resistance in chronic myeloid leukemia cell lines: investigating resistance pathways. Leuk Lymphoma. 2011;52:2139-2147.

106. Ren R. Mechanisms of BCR-ABL in the pathogenesis of chronic myelogenous leukaemia. Nat Rev Cancer. 2005;5:172-183.
107. Zhang P, Iwasaki-Arai J, Iwasaki H, et al. Enhancement of hematopoietic stem cell repopulating capacity and self-renewal in the absence of the transcription factor C/EBP alpha. Immunity. 2004;21:853-863.
108. Dobbs TA, Tainer JA, Lees-Miller SP. A structural model for regulation of NHEJ by DNA-PKcs autophosphorylation. DNA Repair (Amst);9:1307-1314.
109. Jin S, Kharbanda S, Mayer B, Kufe D, Weaver DT. Binding of Ku and c-Abl at the kinase homology region of DNA-dependent protein kinase catalytic subunit. J Biol Chem. 1997;272:24763-24766.
110. Keeshan K, Mills KI, Cotter TG, McKenna SL. Elevated Bcr-Abl expression levels are sufficient for a haematopoietic cell line to acquire a drug-resistant phenotype. Leukemia. 2001;15:1823-1833.
111. Melo JV, Ross DM. Minimal residual disease and discontinuation of therapy in chronic myeloid leukemia: can we aim at a cure? Hematology Am Soc Hematol Educ Program. 2011;2011:136-142.
112. Chomel JC, Sorel N, Guilhot J, Guilhot F, Turhan AG. BCR-ABL expression in leukemic progenitors and primitive stem cells of patients with chronic myeloid leukemia. Blood. 2012;119:2964-2965; author reply 2965-2966.
113. Kumari A, Brendel C, Hochhaus A, Neubauer A, Burchert A. Low BCR-ABL expression levels in hematopoietic precursor cells enable persistence of chronic myeloid leukemia under imatinib. Blood. 2012;119:530-539.
114. Scherr M, Battmer K, Winkler T, Heidenreich O, Ganser A, Eder M. Specific inhibition of bcr-abl gene expression by small interfering RNA. Blood. 2003;101:1566-1569.
115. Wohlbold L, van der Kuip H, Miething C, et al. Inhibition of bcr-abl gene expression by small interfering RNA sensitizes for imatinib mesylate (STI571). Blood. 2003;102:2236-2239.
116. Zhelev Z, Bakalova R, Ohba H, et al. Suppression of bcr-abl synthesis by siRNAs or tyrosine kinase activity by Glivec alters different oncogenes, apoptotic/antiapoptotic genes and cell proliferation factors (microarray study). FEBS Lett. 2004;570:195-204.
117. Elmaagacli AH, Koldehoff M, Peceny R, et al. WT1 and BCR-ABL specific small interfering RNA have additive effects in the induction of apoptosis in leukemic cells. Haematologica. 2005;90:326-334.
118. Koldehoff M, Steckel NK, Beelen DW, Elmaagacli AH. Therapeutic application of small interfering RNA directed against bcr-abl transcripts to a patient with imatinib-resistant chronic myeloid leukaemia. Clin Exp Med. 2007;7:47-55.
119. Murao S, Diala I, Fujii M. Suppression of bcr-abl mRNA by chemically modified siRNA. Nucleic Acids Symp Ser (Oxf). 2008:499-500.
120. Koldehoff M, Elmaagacli AH. Therapeutic targeting of gene expression by siRNAs directed against BCR-ABL transcripts in a patient with imatinib-resistant chronic myeloid leukemia. Methods Mol Biol. 2009;487:451-466.
121. McLaughlin J, Cheng D, Singer O, et al. Sustained suppression of Bcr-Abl-driven lymphoid leukemia by microRNA mimics. Proc Natl Acad Sci U S A. 2007;104:20501-20506.
122. Laneuville P, Heisterkamp N, Groffen J. Expression of the chronic myelogenous leukemia-associated p210bcr/abl oncoprotein in a murine IL-3 dependent myeloid cell line. Oncogene. 1991;6:275-282.

123. Voncken JW, Kaartinen V, Pattengale PK, Germeraad WT, Groffen J, Heisterkamp N. BCR/ABL P210 and P190 cause distinct leukemia in transgenic mice. Blood. 1995;86:4603-4611.
124. Zhu QS, Heisterkamp N, Groffen J. Unique organization of the human BCR gene promoter. Nucleic Acids Res. 1990;18:7119-7125.
125. Shah NP, Witte ON, Denny CT. Characterization of the BCR promoter in Philadelphia chromosome-positive and -negative cell lines. Mol Cell Biol. 1991;11:1854-1860.
126. Law JA, Jacobsen SE. Establishing, maintaining and modifying DNA methylation patterns in plants and animals. Nat Rev Genet. 2010;11:204-220.
127. Dawson MA, Kouzarides T. Cancer epigenetics: from mechanism to therapy. Cell. 2012;150:12-27.
128. Strahl BD, Allis CD. The language of covalent histone modifications. Nature. 2000;403:41-45.
129. Andreassi C, Riccio A. To localize or not to localize: mRNA fate is in 3'UTR ends. Trends Cell Biol. 2009;19:465-474.
130. Jackson RJ, Hellen CU, Pestova TV. The mechanism of eukaryotic translation initiation and principles of its regulation. Nat Rev Mol Cell Biol. 2010;11:113-127.
131. Sanyal A, Lajoie BR, Jain G, Dekker J. The long-range interaction landscape of gene promoters. Nature. 2012;489:109-113.
132. Spitz F, Furlong EE. Transcription factors: from enhancer binding to developmental control. Nat Rev Genet. 2012;13:613-626.
133. Chen J, Kastan MB. 5'-3'-UTR interactions regulate p53 mRNA translation and provide a target for modulating p53 induction after DNA damage. Genes Dev. 2010;24:2146-2156.
134. Smith L, Coleman LJ, Cummings M, et al. Expression of oestrogen receptor beta isoforms is regulated by transcriptional and post-transcriptional mechanisms. Biochem J. 2010;429:283-290.
135. Proudfoot NJ. Ending the message: poly(A) signals then and now. Genes Dev. 2011;25:1770-1782.
136. Marzluff WF, Wagner EJ, Duronio RJ. Metabolism and regulation of canonical histone mRNAs: life without a poly(A) tail. Nat Rev Genet. 2008;9:843-854.
137. Beaudoing E, Freier S, Wyatt JR, Claverie JM, Gautheret D. Patterns of variant polyadenylation signal usage in human genes. Genome Res. 2000;10:1001-1010.
138. Wu X, Brewer G. The regulation of mRNA stability in mammalian cells: 2.0. Gene. 2012;500:10-21.
139. Gallie DR. The cap and poly(A) tail function synergistically to regulate mRNA translational efficiency. Genes Dev. 1991;5:2108-2116.
140. Filipowicz W, Bhattacharyya SN, Sonenberg N. Mechanisms of post-transcriptional regulation by microRNAs: are the answers in sight? Nat Rev Genet. 2008;9:102-114.
141. Fabian MR, Sonenberg N, Filipowicz W. Regulation of mRNA translation and stability by microRNAs. Annu Rev Biochem. 2010;79:351-379.
142. Esteller M. Non-coding RNAs in human disease. Nat Rev Genet. 2011;12:861-874.
143. Lukong KE, Chang KW, Khandjian EW, Richard S. RNA-binding proteins in human genetic disease. Trends Genet. 2008;24:416-425.
144. Lunde BM, Moore C, Varani G. RNA-binding proteins: modular design for efficient function. Nat Rev Mol Cell Biol. 2007;8:479-490.
145. Anko ML, Neugebauer KM. RNA-protein interactions in vivo: global gets specific. Trends Biochem Sci. 2012;37:255-262.

146. Mazumder B, Seshadri V, Fox PL. Translational control by the 3'-UTR: the ends specify the means. Trends Biochem Sci. 2003;28:91-98.
147. Mayr C, Bartel DP. Widespread shortening of 3'UTRs by alternative cleavage and polyadenylation activates oncogenes in cancer cells. Cell. 2009;138:673-684.
148. Lopez de Silanes I, Quesada MP, Esteller M. Aberrant regulation of messenger RNA 3'-untranslated region in human cancer. Cell Oncol. 2007;29:1-17.
149. Chin LJ, Ratner E, Leng S, et al. A SNP in a let-7 microRNA complementary site in the KRAS 3' untranslated region increases non-small cell lung cancer risk. Cancer Res. 2008;68:8535-8540.
150. Mishra PJ, Banerjee D, Bertino JR. MiRSNPs or MiR-polymorphisms, new players in microRNA mediated regulation of the cell: Introducing microRNA pharmacogenomics. Cell Cycle. 2008;7:853-858.
151. Zhang L, Liu Y, Song F, et al. Functional SNP in the microRNA-367 binding site in the 3'UTR of the calcium channel ryanodine receptor gene 3 (RYR3) affects breast cancer risk and calcification. Proc Natl Acad Sci U S A. 2011;108:13653-13658.
152. Gong J, Tong Y, Zhang HM, et al. Genome-wide identification of SNPs in microRNA genes and the SNP effects on microRNA target binding and biogenesis. Hum Mutat. 2012;33:254-263.
153. Di Giammartino DC, Nishida K, Manley JL. Mechanisms and consequences of alternative polyadenylation. Mol Cell. 2011;43:853-866.
154. Chowdhury B, Krishnan S, Tsokos CG, et al. Stability and translation of TCR zeta mRNA are regulated by the adenosine-uridine-rich elements in splice-deleted 3' untranslated region of zeta-chain. J Immunol. 2006;177:8248-8257.
155. Thiele A, Nagamine Y, Hauschildt S, Clevers H. AU-rich elements and alternative splicing in the beta-catenin 3'UTR can influence the human beta-catenin mRNA stability. Exp Cell Res. 2006;312:2367-2378.
156. Yoon OK, Hsu TY, Im JH, Brem RB. Genetics and regulatory impact of alternative polyadenylation in human B-lymphoblastoid cells. PLoS Genet. 2012;8:e1002882.
157. Wiestner A, Tehrani M, Chiorazzi M, et al. Point mutations and genomic deletions in CCND1 create stable truncated cyclin D1 mRNAs that are associated with increased proliferation rate and shorter survival. Blood. 2007;109:4599-4606.
158. Deshpande A, Pastore A, Deshpande AJ, et al. 3'UTR mediated regulation of the cyclin D1 proto-oncogene. Cell Cycle. 2009;8:3584-3592.
159. Poliseno L, Salmena L, Zhang J, Carver B, Haveman WJ, Pandolfi PP. A coding-independent function of gene and pseudogene mRNAs regulates tumour biology. Nature. 2010;465:1033-1038.
160. Olanich ME, Moss BL, Piwnica-Worms D, Townsend RR, Weber JD. Identification of FUSE-binding protein 1 as a regulatory mRNA-binding protein that represses nucleophosmin translation. Oncogene. 2010;30:77-86.
161. Mighell AJ, Smith NR, Robinson PA, Markham AF. Vertebrate pseudogenes. FEBS Lett. 2000;468:109-114.
162. Mercer TR, Wilhelm D, Dinger ME, et al. Expression of distinct RNAs from 3' untranslated regions. Nucleic Acids Res. 2011;39:2393-2403.
163. Cuneo A, Ferrant A, Michaux JL, et al. Philadelphia chromosome-positive acute myeloid leukemia: cytoimmunologic and cytogenetic features. Haematologica. 1996;81:423-427.

164. Zuna J, Zaliova M, Muzikova K, et al. Acute leukemias with ETV6/ABL1 (TEL/ABL) fusion: poor prognosis and prenatal origin. Genes Chromosomes Cancer. 2010;49:873-884.
165. Barbouti A, Ahlgren T, Johansson B, et al. Clinical and genetic studies of ETV6/ABL1-positive chronic myeloid leukaemia in blast crisis treated with imatinib mesylate. Br J Haematol. 2003;122:85-93.
166. La Starza R, Trubia M, Testoni N, et al. Clonal eosinophils are a morphologic hallmark of ETV6/ABL1 positive acute myeloid leukemia. Haematologica. 2002;87:789-794.
167. Eyre T, Schwab CJ, Kinstrie R, et al. Episomal amplification of NUP214-ABL1 fusion gene in B-cell acute lymphoblastic leukemia. Blood. 2012;120:4441-4443.
168. Graux C, Stevens-Kroef M, Lafage M, et al. Heterogeneous patterns of amplification of the NUP214-ABL1 fusion gene in T-cell acute lymphoblastic leukemia. Leukemia. 2009;23:125-133.
169. Chiaretti S, Tavolaro S, Ghia EM, et al. Characterization of ABL1 expression in adult T-cell acute lymphoblastic leukemia by oligonucleotide array analysis. Haematologica. 2007;92:619-626.
170. Inokuchi K, Wakita S, Hirakawa T, et al. RCSD1-ABL1-positive B lymphoblastic leukemia is sensitive to dexamethasone and tyrosine kinase inhibitors and rapidly evolves clonally by chromosomal translocations. Int J Hematol. 2011;94:255-260.
171. Andrews DF, 3rd, Tompkins CK, Hendrickson SL, Singer JW. Cloning and sequencing of the human c-abl 3' untranslated region. Oncogene. 1990;5:441-444.
172. Nobrega MA, Pennacchio LA. Comparative genomic analysis as a tool for biological discovery. J Physiol. 2004;554:31-39.
173. Bueno MJ, Perez de Castro I, Gomez de Cedron M, et al. Genetic and epigenetic silencing of microRNA-203 enhances ABL1 and BCR-ABL1 oncogene expression. Cancer Cell. 2008;13:496-506.
174. Iraci I, Valli E, Gherardi S, et al. Suppression of Bcr-Abl Expression in CML by a Panel of miRNAs. ASH. New Orleans, LA, USA; 2009.
175. Andrews DF, 3rd, Nemunaitis J, Tompkins C, Singer JW. Effect of 5-azacytidine on gene expression in marrow stromal cells. Mol Cell Biol. 1989;9:2748-2751.
176. Andrews DF, 3rd, Nemunaitis JJ, Singer JW. Recombinant tumor necrosis factor alpha and interleukin 1 alpha increase expression of c-abl protooncogene mRNA in cultured human marrow stromal cells. Proc Natl Acad Sci U S A. 1989;86:6788-6792.
177. Westin EH, Wong-Staal F, Gelmann EP, et al. Expression of cellular homologues of retroviral onc genes in human hematopoietic cells. Proc Natl Acad Sci U S A. 1982;79:2490-2494.
178. Ponzetto C, Wolgemuth DJ. Haploid expression of a unique c-abl transcript in the mouse male germ line. Mol Cell Biol. 1985;5:1791-1794.
179. Meijer D, Hermans A, von Lindern M, et al. Molecular characterization of the testis specific c-abl mRNA in mouse. EMBO J. 1987;6:4041-4048.
180. Oppi C, Shore SK, Reddy EP. Nucleotide sequence of testis-derived c-abl cDNAs: implications for testis-specific transcription and abl oncogene activation. Proc Natl Acad Sci U S A. 1987;84:8200-8204.
181. Gregory PA, Bert AG, Paterson EL, et al. The miR-200 family and miR-205 regulate epithelial to mesenchymal transition by targeting ZEB1 and SIP1. Nat Cell Biol. 2008;10:593-601.
182. Pillai RS, Bhattacharyya SN, Artus CG, et al. Inhibition of translational initiation by Let-7 MicroRNA in human cells. Science. 2005;309:1573-1576.

183. Gomez-Benito M, Loayza-Puch F, Oude Vrielink JA, Odero MD, Agami R. 3'UTR-mediated gene silencing of the Mixed Lineage Leukemia (MLL) gene. PLoS One. 2011;6:e25449.
184. Rulcova J, Zmekova V, Zemanova Z, Klamova H, Moravcova J. The effect of total-ABL, GUS and B2M control genes on BCR-ABL monitoring by real-time RT-PCR. Leuk Res. 2007;31:483-491.
185. Nwagwu M, Nana M. Ribonucleic acid synthesis in embryonic chick muscle, rates of synthesis and half-lives of transfer and ribosomal RNA species. J Embryol Exp Morphol. 1980;56:253-267.
186. Scotto-Lavino E, Du G, Frohman MA. 3' end cDNA amplification using classic RACE. Nat Protoc. 2006;1:2742-2745.
187. Wirsing A, Senkel S, Klein-Hitpass L, Ryffel GU. A systematic analysis of the 3'UTR of HNF4A mRNA reveals an interplay of regulatory elements including miRNA target sites. PLoS One. 2011;6:e27438.
188. Marit G, Cao Y, Froussard P, et al. Increased liposome-mediated gene transfer into haematopoietic cells grown in adhesion to stromal or fibroblast cell line monolayers. Eur J Haematol. 2000;64:22-31.
189. Lai WS, Parker JS, Grissom SF, Stumpo DJ, Blackshear PJ. Novel mRNA targets for tristetraprolin (TTP) identified by global analysis of stabilized transcripts in TTP-deficient fibroblasts. Mol Cell Biol. 2006;26:9196-9208.
190. Syed AS, D'Antonio M, Ciccarelli FD. Network of Cancer Genes: a web resource to analyze duplicability, orthology and network properties of cancer genes. Nucleic Acids Res. 2010;38:D670-675.
191. Kawaji H, Kasukawa T, Fukuda S, et al. CAGE Basic/Analysis Databases: the CAGE resource for comprehensive promoter analysis. Nucleic Acids Res. 2006;34:D632-636.
192. Ray D, Kazan H, Chan ET, et al. Rapid and systematic analysis of the RNA recognition specificities of RNA-binding proteins. Nat Biotechnol. 2009;27:667-670.
193. Lin Y, Li Z, Ozsolak F, et al. An in-depth map of polyadenylation sites in cancer. Nucleic Acids Res. 2012;40:8460-8471.
194. Collins S, Coleman H, Groudine M. Expression of bcr and bcr-abl fusion transcripts in normal and leukemic cells. Mol Cell Biol. 1987;7:2870-2876.
195. Suresh S, McCallum L, Lu W, Lazar N, Perbal B, Irvine AE. MicroRNAs 130a/b are regulated by BCR-ABL and downregulate expression of CCN3 in CML. J Cell Commun Signal. 2011;5:183-191.
196. Yuan H, Wang Z, Gao C, et al. BCR-ABL gene expression is required for its mutations in a novel KCL-22 cell culture model for acquired resistance of chronic myelogenous leukemia. J Biol Chem. 2010;285:5085-5096.
197. Baou M, Norton JD, Murphy JJ. AU-rich RNA binding proteins in hematopoiesis and leukemogenesis. Blood. 2011;118:5732-5740.
198. Ulitsky I, Shkumatava A, Jan CH, Sive H, Bartel DP. Conserved function of lincRNAs in vertebrate embryonic development despite rapid sequence evolution. Cell. 2011;147:1537-1550.
199. Young LE, Moore AE, Sokol L, Meisner-Kober N, Dixon DA. The mRNA stability factor HuR inhibits microRNA-16 targeting of COX-2. Mol Cancer Res. 2012;10:167-180.
200. Kedde M, van Kouwenhove M, Zwart W, Oude Vrielink JA, Elkon R, Agami R. A Pumilio-induced RNA structure switch in p27-3' UTR controls miR-221 and miR-222 accessibility. Nat Cell Biol. 2010;12:1014-1020.

201. Kedde M, Strasser MJ, Boldajipour B, et al. RNA-binding protein Dnd1 inhibits microRNA access to target mRNA. Cell. 2007;131:1273-1286.
202. Kim JH, Paek KY, Choi K, et al. Heterogeneous nuclear ribonucleoprotein C modulates translation of c-myc mRNA in a cell cycle phase-dependent manner. Mol Cell Biol. 2003;23:708-720.
203. Lee EK, Kim HH, Kuwano Y, et al. hnRNP C promotes APP translation by competing with FMRP for APP mRNA recruitment to P bodies. Nat Struct Mol Biol. 2010;17:732-739.
204. Shetty S. Regulation of urokinase receptor mRNA stability by hnRNP C in lung epithelial cells. Mol Cell Biochem. 2005;272:107-118.
205. Kulkarni M, Ozgur S, Stoecklin G. On track with P-bodies. Biochem Soc Trans. 2010;38:242-251.
206. Uren PJ, Burns SC, Ruan J, Singh KK, Smith AD, Penalva LO. Genomic analyses of the RNA-binding protein Hu antigen R (HuR) identify a complex network of target genes and novel characteristics of its binding sites. J Biol Chem. 2011;286:37063-37066.
207. Choi HJ, Yang H, Park SH, Moon Y. HuR/ELAVL1 RNA binding protein modulates interleukin-8 induction by muco-active ribotoxin deoxynivalenol. Toxicol Appl Pharmacol. 2009;240:46-54.
208. Thomas MA, Preece DM, Bentel JM. Androgen regulation of the prostatic tumour suppressor NKX3.1 is mediated by its 3' untranslated region. Biochem J. 2010;425:575-583.
209. Oh-hashi K, Hirata Y, Kiuchi K. Characterization of 3'-untranslated region of the mouse GDNF gene. BMC Mol Biol. 2012;13:2.
210. Yashiro T, Yokoi Y, Shimizu M, Inoue J, Sato R. Chenodeoxycholic acid stabilization of LDL receptor mRNA depends on 3'-untranslated region and AU-rich element-binding protein. Biochem Biophys Res Commun. 2011;409:155-159.
211. Himmelreich H, Mathys A, Wodnar-Filipowicz A, Kalberer CP. Post-transcriptional regulation of ULBP1 ligand for the activating immunoreceptor NKG2D involves 3' untranslated region. Hum Immunol. 2011;72:470-478.
212. Wang Z, Kayikci M, Briese M, et al. iCLIP predicts the dual splicing effects of TIA-RNA interactions. PLoS Biol. 2010;8:e1000530.
213. Izquierdo JM. Hu antigen R (HuR) functions as an alternative pre-mRNA splicing regulator of Fas apoptosis-promoting receptor on exon definition. J Biol Chem. 2008;283:19077-19084.
214. Izquierdo JM. Heterogeneous ribonucleoprotein C displays a repressor activity mediated by T-cell intracellular antigen-1-related/like protein to modulate Fas exon 6 splicing through a mechanism involving Hu antigen R. Nucleic Acids Res. 2010;38:8001-8014.
215. Friedman RC, Farh KK, Burge CB, Bartel DP. Most mammalian mRNAs are conserved targets of microRNAs. Genome Res. 2009;19:92-105.
216. Kozomara A, Griffiths-Jones S. miRBase: integrating microRNA annotation and deep-sequencing data. Nucleic Acids Res. 2011;39:D152-157.
217. Bartel DP. MicroRNAs: target recognition and regulatory functions. Cell. 2009;136:215-233.
218. Lee RC, Feinbaum RL, Ambros V. The C. elegans heterochronic gene lin-4 encodes small RNAs with antisense complementarity to lin-14. Cell. 1993;75:843-854.
219. Wightman B, Ha I, Ruvkun G. Posttranscriptional regulation of the heterochronic gene lin-14 by lin-4 mediates temporal pattern formation in C. elegans. Cell. 1993;75:855-862.
220. Ambros V. microRNAs: tiny regulators with great potential. Cell. 2001;107:823-826.
221. Ebert MS, Sharp PA. Roles for microRNAs in conferring robustness to biological processes. Cell. 2012;149:515-524.

222. Olsen PH, Ambros V. The lin-4 regulatory RNA controls developmental timing in Caenorhabditis elegans by blocking LIN-14 protein synthesis after the initiation of translation. Dev Biol. 1999;216:671-680.
223. Bissels U, Bosio A, Wagner W. MicroRNAs are shaping the hematopoietic landscape. Haematologica. 2012.
224. Liao R, Sun J, Zhang L, et al. MicroRNAs play a role in the development of human hematopoietic stem cells. J Cell Biochem. 2008;104:805-817.
225. Han YC, Park CY, Bhagat G, et al. microRNA-29a induces aberrant self-renewal capacity in hematopoietic progenitors, biased myeloid development, and acute myeloid leukemia. J Exp Med. 2010;207:475-489.
226. Ooi AG, Sahoo D, Adorno M, Wang Y, Weissman IL, Park CY. MicroRNA-125b expands hematopoietic stem cells and enriches for the lymphoid-balanced and lymphoid-biased subsets. Proc Natl Acad Sci U S A. 2010;107:21505-21510.
227. Zhao H, Wang D, Du W, Gu D, Yang R. MicroRNA and leukemia: tiny molecule, great function. Crit Rev Oncol Hematol. 2010;74:149-155.
228. Venturini L, Battmer K, Castoldi M, et al. Expression of the miR-17-92 polycistron in chronic myeloid leukemia (CML) CD34+ cells. Blood. 2007;109:4399-4405.
229. Machova Polakova K, Lopotova T, Klamova H, et al. Expression patterns of microRNAs associated with CML phases and their disease related targets. Mol Cancer. 2011;10:41.
230. San Jose-Eneriz E, Roman-Gomez J, Jimenez-Velasco A, et al. MicroRNA expression profiling in Imatinib-resistant Chronic Myeloid Leukemia patients without clinically significant ABL1-mutations. Mol Cancer. 2009;8:69.
231. Millar AA, Waterhouse PM. Plant and animal microRNAs: similarities and differences. Funct Integr Genomics. 2005;5:129-135.
232. Havens MA, Reich AA, Duelli DM, Hastings ML. Biogenesis of mammalian microRNAs by a non-canonical processing pathway. Nucleic Acids Res. 2012;40:4626-4640.
233. Loeb GB, Khan AA, Canner D, et al. Transcriptome-wide miR-155 Binding Map Reveals Widespread Noncanonical MicroRNA Targeting. Mol Cell. 2012.
234. Lee Y, Kim M, Han J, et al. MicroRNA genes are transcribed by RNA polymerase II. EMBO J. 2004;23:4051-4060.
235. Rodriguez A, Griffiths-Jones S, Ashurst JL, Bradley A. Identification of mammalian microRNA host genes and transcription units. Genome Res. 2004;14:1902-1910.
236. Corcoran DL, Pandit KV, Gordon B, Bhattacharjee A, Kaminski N, Benos PV. Features of mammalian microRNA promoters emerge from polymerase II chromatin immunoprecipitation data. PLoS One. 2009;4:e5279.
237. Olive V, Jiang I, He L. mir-17-92, a cluster of miRNAs in the midst of the cancer network. Int J Biochem Cell Biol. 2010;42:1348-1354.
238. Cai X, Hagedorn CH, Cullen BR. Human microRNAs are processed from capped, polyadenylated transcripts that can also function as mRNAs. RNA. 2004;10:1957-1966.
239. Kim YK, Kim VN. Processing of intronic microRNAs. EMBO J. 2007;26:775-783.
240. Gregory RI, Yan KP, Amuthan G, et al. The Microprocessor complex mediates the genesis of microRNAs. Nature. 2004;432:235-240.
241. Yeom KH, Lee Y, Han J, Suh MR, Kim VN. Characterization of DGCR8/Pasha, the essential cofactor for Drosha in primary miRNA processing. Nucleic Acids Res. 2006;34:4622-4629.
242. Zeng Y, Cullen BR. Structural requirements for pre-microRNA binding and nuclear export by Exportin 5. Nucleic Acids Res. 2004;32:4776-4785.

243. Yi R, Qin Y, Macara IG, Cullen BR. Exportin-5 mediates the nuclear export of pre-microRNAs and short hairpin RNAs. Genes Dev. 2003;17:3011-3016.
244. Hutvagner G, McLachlan J, Pasquinelli AE, Balint E, Tuschl T, Zamore PD. A cellular function for the RNA-interference enzyme Dicer in the maturation of the let-7 small temporal RNA. Science. 2001;293:834-838.
245. Kok KH, Ng MH, Ching YP, Jin DY. Human TRBP and PACT directly interact with each other and associate with dicer to facilitate the production of small interfering RNA. J Biol Chem. 2007;282:17649-17657.
246. Koscianska E, Starega-Roslan J, Krzyzosiak WJ. The role of Dicer protein partners in the processing of microRNA precursors. PLoS One. 2012;6:e28548.
247. Lee Y, Hur I, Park SY, Kim YK, Suh MR, Kim VN. The role of PACT in the RNA silencing pathway. EMBO J. 2006;25:522-532.
248. Chendrimada TP, Gregory RI, Kumaraswamy E, et al. TRBP recruits the Dicer complex to Ago2 for microRNA processing and gene silencing. Nature. 2005;436:740-744.
249. Haase AD, Jaskiewicz L, Zhang H, et al. TRBP, a regulator of cellular PKR and HIV-1 virus expression, interacts with Dicer and functions in RNA silencing. EMBO Rep. 2005;6:961-967.
250. Kim VN. MicroRNA biogenesis: coordinated cropping and dicing. Nat Rev Mol Cell Biol. 2005;6:376-385.
251. Hu HY, Yan Z, Xu Y, et al. Sequence features associated with microRNA strand selection in humans and flies. BMC Genomics. 2009;10:413.
252. Biasiolo M, Sales G, Lionetti M, et al. Impact of host genes and strand selection on miRNA and miRNA* expression. PLoS One. 2011;6:e23854.
253. Eulalio A, Huntzinger E, Nishihara T, Rehwinkel J, Fauser M, Izaurralde E. Deadenylation is a widespread effect of miRNA regulation. RNA. 2009;15:21-32.
254. Wu L, Fan J, Belasco JG. MicroRNAs direct rapid deadenylation of mRNA. Proc Natl Acad Sci U S A. 2006;103:4034-4039.
255. Liu J, Valencia-Sanchez MA, Hannon GJ, Parker R. MicroRNA-dependent localization of targeted mRNAs to mammalian P-bodies. Nat Cell Biol. 2005;7:719-723.
256. Walters RW, Bradrick SS, Gromeier M. Poly(A)-binding protein modulates mRNA susceptibility to cap-dependent miRNA-mediated repression. RNA. 2010;16:239-250.
257. Lewis BP, Burge CB, Bartel DP. Conserved seed pairing, often flanked by adenosines, indicates that thousands of human genes are microRNA targets. Cell. 2005;120:15-20.
258. Ambros V, Bartel B, Bartel DP, et al. A uniform system for microRNA annotation. RNA. 2003;9:277-279.
259. Grimson A, Farh KK-H, Johnston WK, Garrett-Engele P, Lim LP, Bartel DP. MicroRNA Targeting Specificity in Mammals: Determinants beyond Seed Pairing. Molecular cell. 2007;27:91-105.
260. John B, Enright AJ, Aravin A, Tuschl T, Sander C, Marks DS. Human MicroRNA Targets. PLoS Biol. 2004;2:e363.
261. Betel D, Koppal A, Agius P, Sander C, Leslie C. Comprehensive modeling of microRNA targets predicts functional non-conserved and non-canonical sites. Genome Biol. 2010;11:R90.
262. Maragkakis M, Reczko M, Simossis VA, et al. DIANA-microT web server: elucidating microRNA functions through target prediction. Nucleic Acids Research. 2009;37:W273-W276.
263. Griffiths-Jones S, Saini HK, van Dongen S, Enright AJ. miRBase: tools for microRNA genomics. Nucleic Acids Res. 2008;36:D154-158.

264. Georgantas RW, 3rd, Hildreth R, Morisot S, et al. CD34+ hematopoietic stem-progenitor cell microRNA expression and function: a circuit diagram of differentiation control. Proc Natl Acad Sci U S A. 2007;104:2750-2755.
265. Romania P, Lulli V, Pelosi E, Biffoni M, Peschle C, Marziali G. MicroRNA 155 modulates megakaryopoiesis at progenitor and precursor level by targeting Ets-1 and Meis1 transcription factors. Br J Haematol. 2008;143:570-580.
266. Lu J, Guo S, Ebert BL, et al. MicroRNA-mediated control of cell fate in megakaryocyte-erythrocyte progenitors. Dev Cell. 2008;14:843-853.
267. Fazi F, Rosa A, Fatica A, et al. A minicircuitry comprised of microRNA-223 and transcription factors NFI-A and C/EBPalpha regulates human granulopoiesis. Cell. 2005;123:819-831.
268. Gutierrez NC, Sarasquete ME, Misiewicz-Krzeminska I, et al. Deregulation of microRNA expression in the different genetic subtypes of multiple myeloma and correlation with gene expression profiling. Leukemia. 2010;24:629-637.
269. Rhyasen GW, Starczynowski DT. Deregulation of microRNAs in myelodysplastic syndrome. Leukemia. 2012;26:13-22.
270. Garzon R, Volinia S, Liu CG, et al. MicroRNA signatures associated with cytogenetics and prognosis in acute myeloid leukemia. Blood. 2008;111:3183-3189.
271. Cimmino A, Calin GA, Fabbri M, et al. miR-15 and miR-16 induce apoptosis by targeting BCL2. Proc Natl Acad Sci U S A. 2005;102:13944-13949.
272. Starczynowski DT, Kuchenbauer F, Argiropoulos B, et al. Identification of miR-145 and miR-146a as mediators of the 5q- syndrome phenotype. Nat Med. 2010;16:49-58.
273. Mu P, Han YC, Betel D, et al. Genetic dissection of the miR-17~92 cluster of microRNAs in Myc-induced B-cell lymphomas. Genes Dev. 2009;23:2806-2811.
274. Mi S, Li Z, Chen P, et al. Aberrant overexpression and function of the miR-17-92 cluster in MLL-rearranged acute leukemia. Proc Natl Acad Sci U S A. 2010;107:3710-3715.
275. Hayashita Y, Osada H, Tatematsu Y, et al. A polycistronic microRNA cluster, miR-17-92, is overexpressed in human lung cancers and enhances cell proliferation. Cancer Res. 2005;65:9628-9632.
276. Hong L, Lai M, Chen M, et al. The miR-17-92 cluster of microRNAs confers tumorigenicity by inhibiting oncogene-induced senescence. Cancer Res. 2010;70:8547-8557.
277. Agirre X, Jimenez-Velasco A, San Jose-Eneriz E, et al. Down-regulation of hsa-miR-10a in chronic myeloid leukemia CD34+ cells increases USF2-mediated cell growth. Mol Cancer Res. 2008;6:1830-1840.
278. Lopotova T, Zackova M, Klamova H, Moravcova J. MicroRNA-451 in chronic myeloid leukemia: miR-451-BCR-ABL regulatory loop? Leuk Res. 2011;35:974-977.
279. Bader AG, Brown D, Stoudemire J, Lammers P. Developing therapeutic microRNAs for cancer. Gene Ther. 2011;18:1121-1126.
280. Broderick JA, Zamore PD. MicroRNA therapeutics. Gene Ther. 2012;18:1104-1110.
281. Garzon R, Marcucci G, Croce CM. Targeting microRNAs in cancer: rationale, strategies and challenges. Nat Rev Drug Discov. 2010;9:775-789.
282. Carlesso N, Griffin JD, Druker BJ. Use of a temperature-sensitive mutant to define the biological effects of the p210BCR-ABL tyrosine kinase on proliferation of a factor-dependent murine myeloid cell line. Oncogene. 1994;9:149-156.
283. Park SY, Lee JH, Ha M, Nam JW, Kim VN. miR-29 miRNAs activate p53 by targeting p85 alpha and CDC42. Nat Struct Mol Biol. 2009;16:23-29.

284. Braig S, Mueller DW, Rothhammer T, Bosserhoff AK. MicroRNA miR-196a is a central regulator of HOX-B7 and BMP4 expression in malignant melanoma. Cell Mol Life Sci. 2010;67:3535-3548.
285. Kuhn DE, Martin MM, Feldman DS, Terry AV, Jr., Nuovo GJ, Elton TS. Experimental validation of miRNA targets. Methods. 2008;44:47-54.
286. Hsu SD, Lin FM, Wu WY, et al. miRTarBase: a database curates experimentally validated microRNA-target interactions. Nucleic Acids Res. 2011;39:D163-169.
287. Pasquinelli AE. MicroRNAs and their targets: recognition, regulation and an emerging reciprocal relationship. Nat Rev Genet. 2012;13:271-282.
288. Vo NK, Dalton RP, Liu N, Olson EN, Goodman RH. Affinity purification of microRNA-133a with the cardiac transcription factor, Hand2. Proc Natl Acad Sci U S A. 2010;107:19231-19236.
289. Liu H, Zhang S, Lin H, Jia R, Chen Z. Identification of microRNA-RNA interactions using tethered RNAs and streptavidin aptamers. Biochem Biophys Res Commun. 2012;422:405-410.
290. Yoon JH, Srikantan S, Gorospe M. MS2-TRAP (MS2-tagged RNA affinity purification): Tagging RNA to identify associated miRNAs. Methods. 2012;58:81-87.
291. Huang JC, Babak T, Corson TW, et al. Using expression profiling data to identify human microRNA targets. Nat Methods. 2007;4:1045-1049.
292. Gennarino VA, Sardiello M, Avellino R, et al. MicroRNA target prediction by expression analysis of host genes. Genome Res. 2009;19:481-490.
293. Craig VJ, Cogliatti SB, Rehrauer H, Wundisch T, Muller A. Epigenetic silencing of microRNA-203 dysregulates ABL1 expression and drives Helicobacter-associated gastric lymphomagenesis. Cancer Res. 2011;71:3616-3624.
294. Chim CS, Wan TS, Wong KY, Fung TK, Drexler HG, Wong KF. Methylation of miR-34a, miR-34b/c, miR-124-1 and miR-203 in Ph-negative myeloproliferative neoplasms. J Transl Med. 2011;9:197.
295. Chim CS, Wong KY, Leung CY, et al. Epigenetic inactivation of the hsa-miR-203 in haematological malignancies. J Cell Mol Med. 2011;15:2760-2767.
296. Dreyfuss G, Kim VN, Kataoka N. Messenger-RNA-binding proteins and the messages they carry. Nat Rev Mol Cell Biol. 2002;3:195-205.
297. Janga SC, Mittal N. Construction, structure and dynamics of post-transcriptional regulatory network directed by RNA-binding proteins. Adv Exp Med Biol. 2010;722:103-117.
298. Galante PA, Sandhu D, de Sousa Abreu R, et al. A comprehensive in silico expression analysis of RNA binding proteins in normal and tumor tissue: Identification of potential players in tumor formation. RNA Biol. 2009;6:426-433.
299. Agnes F, Perron M. RNA-binding proteins and neural development: a matter of targets and complexes. Neuroreport. 2004;15:2567-2570.
300. Carpenter B, MacKay C, Alnabulsi A, et al. The roles of heterogeneous nuclear ribonucleoproteins in tumour development and progression. Biochim Biophys Acta. 2006;1765:85-100.
301. Maris C, Dominguez C, Allain FH. The RNA recognition motif, a plastic RNA-binding platform to regulate post-transcriptional gene expression. FEBS J. 2005;272:2118-2131.
302. Valverde R, Edwards L, Regan L. Structure and function of KH domains. FEBS J. 2008;275:2712-2726.

303. Anantharaman V, Koonin EV, Aravind L. Comparative genomics and evolution of proteins involved in RNA metabolism. Nucleic Acids Res. 2002;30:1427-1464.
304. Liu Y, Szaro BG. hnRNP K post-transcriptionally co-regulates multiple cytoskeletal genes needed for axonogenesis. Development. 2011;138:3079-3090.
305. Figueroa A, Cuadrado A, Fan J, et al. Role of HuR in skeletal myogenesis through coordinate regulation of muscle differentiation genes. Mol Cell Biol. 2003;23:4991-5004.
306. Manieri NA, Drylewicz MR, Miyoshi H, Stappenbeck TS. Igf2bp1 is required for full induction of Ptgs2 mRNA in colonic mesenchymal stem cells in mice. Gastroenterology. 2012;143:110-121 e110.
307. Izumi K, Kurosaka D, Iwata T, et al. Involvement of insulin-like growth factor-I and insulin-like growth factor binding protein-3 in corneal fibroblasts during corneal wound healing. Invest Ophthalmol Vis Sci. 2006;47:591-598.
308. Song L, Wang L, Li Y, et al. Sam68 up-regulation correlates with, and its down-regulation inhibits, proliferation and tumourigenicity of breast cancer cells. J Pathol. 2010;222:227-237.
309. Li Z, Yu CP, Zhong Y, et al. Sam68 expression and cytoplasmic localization is correlated with lymph node metastasis as well as prognosis in patients with early-stage cervical cancer. Ann Oncol. 2012;23:638-646.
310. Zhang Z, Li J, Zheng H, et al. Expression and cytoplasmic localization of SAM68 is a significant and independent prognostic marker for renal cell carcinoma. Cancer Epidemiol Biomarkers Prev. 2009;18:2685-2693.
311. Lin Q, Taylor SJ, Shalloway D. Specificity and determinants of Sam68 RNA binding. Implications for the biological function of K homology domains. J Biol Chem. 1997;272:27274-27280.
312. Vernet C, Artzt K. STAR, a gene family involved in signal transduction and activation of RNA. Trends Genet. 1997;13:479-484.
313. Paronetto MP, Zalfa F, Botti F, Geremia R, Bagni C, Sette C. The nuclear RNA-binding protein Sam68 translocates to the cytoplasm and associates with the polysomes in mouse spermatocytes. Mol Biol Cell. 2006;17:14-24.
314. Bielli P, Busa R, Paronetto MP, Sette C. The RNA-binding protein Sam68 is a multifunctional player in human cancer. Endocr Relat Cancer. 2011;18:R91-R102.
315. Chawla G, Lin CH, Han A, Shiue L, Ares M, Jr., Black DL. Sam68 regulates a set of alternatively spliced exons during neurogenesis. Mol Cell Biol. 2009;29:201-213.
316. Paronetto MP, Cappellari M, Busa R, et al. Alternative splicing of the cyclin D1 proto-oncogene is regulated by the RNA-binding protein Sam68. Cancer Res. 2010;70:229-239.
317. Paronetto MP, Achsel T, Massiello A, Chalfant CE, Sette C. The RNA-binding protein Sam68 modulates the alternative splicing of Bcl-x. J Cell Biol. 2007;176:929-939.
318. Worthington MT, Pelo JW, Sachedina MA, Applegate JL, Arseneau KO, Pizarro TT. RNA binding properties of the AU-rich element-binding recombinant Nup475/TIS11/tristetraprolin protein. J Biol Chem. 2002;277:48558-48564.
319. Brennan SE, Kuwano Y, Alkharouf N, Blackshear PJ, Gorospe M, Wilson GM. The mRNA-destabilizing protein tristetraprolin is suppressed in many cancers, altering tumorigenic phenotypes and patient prognosis. Cancer Res. 2009;69:5168-5176.
320. Kim CW, Vo MT, Kim HK, et al. Ectopic over-expression of tristetraprolin in human cancer cells promotes biogenesis of let-7 by down-regulation of Lin28. Nucleic Acids Res. 2011;40:3856-3869.

321. Essafi-Benkhadir K, Onesto C, Stebe E, Moroni C, Pages G. Tristetraprolin inhibits Ras-dependent tumor vascularization by inducing vascular endothelial growth factor mRNA degradation. Mol Biol Cell. 2007;18:4648-4658.
322. Lee HH, Son YJ, Lee WH, et al. Tristetraprolin regulates expression of VEGF and tumorigenesis in human colon cancer. Int J Cancer. 2010;126:1817-1827.
323. Taylor GA, Carballo E, Lee DM, et al. A pathogenetic role for TNF alpha in the syndrome of cachexia, arthritis, and autoimmunity resulting from tristetraprolin (TTP) deficiency. Immunity. 1996;4:445-454.
324. Kratochvill F, Machacek C, Vogl C, et al. Tristetraprolin-driven regulatory circuit controls quality and timing of mRNA decay in inflammation. Mol Syst Biol. 2011;7:560.
325. Blackshear PJ, Lai WS, Kennington EA, et al. Characteristics of the interaction of a synthetic human tristetraprolin tandem zinc finger peptide with AU-rich element-containing RNA substrates. J Biol Chem. 2003;278:19947-19955.
326. Ogilvie RL, Sternjohn JR, Rattenbacher B, et al. Tristetraprolin mediates interferon-gamma mRNA decay. J Biol Chem. 2009;284:11216-11223.
327. Stoecklin G, Tenenbaum SA, Mayo T, et al. Genome-wide analysis identifies interleukin-10 mRNA as target of tristetraprolin. J Biol Chem. 2008;283:11689-11699.
328. Ogilvie RL, Abelson M, Hau HH, Vlasova I, Blackshear PJ, Bohjanen PR. Tristetraprolin down-regulates IL-2 gene expression through AU-rich element-mediated mRNA decay. J Immunol. 2005;174:953-961.
329. Zhao W, Liu M, D'Silva NJ, Kirkwood KL. Tristetraprolin regulates interleukin-6 expression through p38 MAPK-dependent affinity changes with mRNA 3' untranslated region. J Interferon Cytokine Res. 2011;31:629-637.
330. Perrotti D, Iervolino A, Cesi V, et al. BCR-ABL prevents c-jun-mediated and proteasome-dependent FUS (TLS) proteolysis through a protein kinase CbetaII-dependent pathway. Mol Cell Biol. 2000;20:6159-6169.
331. Perrotti D, Bonatti S, Trotta R, et al. TLS/FUS, a pro-oncogene involved in multiple chromosomal translocations, is a novel regulator of BCR/ABL-mediated leukemogenesis. EMBO J. 1998;17:4442-4455.
332. Crozat A, Aman P, Mandahl N, Ron D. Fusion of CHOP to a novel RNA-binding protein in human myxoid liposarcoma. Nature. 1993;363:640-644.
333. Rabbitts TH, Forster A, Larson R, Nathan P. Fusion of the dominant negative transcription regulator CHOP with a novel gene FUS by translocation t(12;16) in malignant liposarcoma. Nat Genet. 1993;4:175-180.
334. Colombrita C, Onesto E, Megiorni F, et al. TDP-43 and FUS RNA-binding proteins bind distinct sets of cytoplasmic messenger RNAs and differently regulate their post-transcriptional fate in motoneuron-like cells. J Biol Chem. 2012;287:15635-15647.
335. Zinszner H, Sok J, Immanuel D, Yin Y, Ron D. TLS (FUS) binds RNA in vivo and engages in nucleo-cytoplasmic shuttling. J Cell Sci. 1997;110 (Pt 15):1741-1750.
336. Rogelj B, Easton LE, Bogu GK, et al. Widespread binding of FUS along nascent RNA regulates alternative splicing in the brain. Sci Rep. 2012;2:603.
337. Liao B, Hu Y, Herrick DJ, Brewer G. The RNA-binding protein IMP-3 is a translational activator of insulin-like growth factor II leader-3 mRNA during proliferation of human K562 leukemia cells. J Biol Chem. 2005;280:18517-18524.
338. Liao B, Hu Y, Brewer G. RNA-binding protein insulin-like growth factor mRNA-binding protein 3 (IMP-3) promotes cell survival via insulin-like growth factor II signaling after ionizing radiation. J Biol Chem. 2011;286:31145-31152.

339. Nakamura M, Okano H, Blendy JA, Montell C. Musashi, a neural RNA-binding protein required for Drosophila adult external sensory organ development. Neuron. 1994;13:67-81.
340. de Andres-Aguayo L, Varas F, Kallin EM, et al. Musashi 2 is a regulator of the HSC compartment identified by a retroviral insertion screen and knockout mice. Blood. 2011;118:554-564.
341. Ito T, Kwon HY, Zimdahl B, et al. Regulation of myeloid leukaemia by the cell-fate determinant Musashi. Nature. 2010;466:765-768.
342. Kharas MG, Lengner CJ, Al-Shahrour F, et al. Musashi-2 regulates normal hematopoiesis and promotes aggressive myeloid leukemia. Nat Med. 2010;16:903-908.
343. Vasudevan S, Steitz JA. AU-rich-element-mediated upregulation of translation by FXR1 and Argonaute 2. Cell. 2007;128:1105-1118.
344. Ortega AD, Willers IM, Sala S, Cuezva JM. Human G3BP1 interacts with beta-F1-ATPase mRNA and inhibits its translation. J Cell Sci. 2010;123:2685-2696.
345. Srisawat C, Engelke DR. Streptavidin aptamers: affinity tags for the study of RNAs and ribonucleoproteins. RNA. 2001;7:632-641.
346. Bachler M, Schroeder R, von Ahsen U. StreptoTag: a novel method for the isolation of RNA-binding proteins. RNA. 1999;5:1509-1516.
347. Green NM. Avidin. Adv Protein Chem. 1975;29:85-133.
348. Xiao S, Day-Storms JJ, Srisawat C, Fierke CA, Engelke DR. Characterization of conserved sequence elements in eukaryotic RNase P RNA reveals roles in holoenzyme assembly and tRNA processing. RNA. 2005;11:885-896.
349. Iioka H, Loiselle D, Haystead TA, Macara IG. Efficient detection of RNA-protein interactions using tethered RNAs. Nucleic Acids Res. 2011;39:e53.
350. Wallace ST, Schroeder R. In vitro selection and characterization of streptomycin-binding RNAs: recognition discrimination between antibiotics. RNA. 1998;4:112-123.
351. Peabody DS. The RNA binding site of bacteriophage MS2 coat protein. EMBO J. 1993;12:595-600.
352. Keryer-Bibens C, Barreau C, Osborne HB. Tethering of proteins to RNAs by bacteriophage proteins. Biol Cell. 2008;100:125-138.
353. Lei Y, Huang Y, Zhang H, Yu L, Zhang M, Dayton A. Functional interaction between cellular p100 and the dengue virus 3' UTR. J Gen Virol. 2011;92:796-806.
354. Woo KC, Kim TD, Lee KH, et al. Modulation of exosome-mediated mRNA turnover by interaction of GTP-binding protein 1 (GTPBP1) with its target mRNAs. FASEB J. 2011;25:2757-2769.
355. Hoffmann Ed, Stroobant V. Mass Spectrometry: Principles and Applications (ed 3rd): Wiley; 2007.
356. Keil B. Proteolysis Data Bank: specificity of alpha-chymotrypsin from computation of protein cleavages. Protein Seq Data Anal. 1987;1:13-20.
357. Wang G, Wu WW, Zeng W, Chou CL, Shen RF. Label-free protein quantification using LC-coupled ion trap or FT mass spectrometry: Reproducibility, linearity, and application with complex proteomes. J Proteome Res. 2006;5:1214-1223.
358. Walker SC, Scott FH, Srisawat C, Engelke DR. RNA affinity tags for the rapid purification and investigation of RNAs and RNA-protein complexes. Methods Mol Biol. 2008;488:23-40.
359. Rybak JN, Scheurer SB, Neri D, Elia G. Purification of biotinylated proteins on streptavidin resin: a protocol for quantitative elution. Proteomics. 2004;4:2296-2299.

360. McLean JE, Hamaguchi N, Belenky P, Mortimer SE, Stanton M, Hedstrom L. Inosine 5'-monophosphate dehydrogenase binds nucleic acids in vitro and in vivo. Biochem J. 2004;379:243-251.
361. Noelting B. Methods in Modern Biophysics: Springer; 2009.
362. Giege R, Florentz C, Kern D, Gangloff J, Eriani G, Moras D. Aspartate identity of transfer RNAs. Biochimie. 1996;78:605-623.
363. Ni M, Lee AS. ER chaperones in mammalian development and human diseases. FEBS Lett. 2007;581:3641-3651.
364. Popow J, Englert M, Weitzer S, et al. HSPC117 is the essential subunit of a human tRNA splicing ligase complex. Science. 2011;331:760-764.
365. Mortimer SE, Xu D, McGrew D, et al. IMP dehydrogenase type 1 associates with polyribosomes translating rhodopsin mRNA. J Biol Chem. 2008;283:36354-36360.
366. Kozhevnikova EN, van der Knaap JA, Pindyurin AV, et al. Metabolic enzyme IMPDH is also a transcription factor regulated by cellular state. Mol Cell. 2012;47:133-139.
367. Colby TD, Vanderveen K, Strickler MD, Markham GD, Goldstein BM. Crystal structure of human type II inosine monophosphate dehydrogenase: implications for ligand binding and drug design. Proc Natl Acad Sci U S A. 1999;96:3531-3536.
368. Butter F, Scheibe M, Morl M, Mann M. Unbiased RNA-protein interaction screen by quantitative proteomics. Proc Natl Acad Sci U S A. 2009;106:10626-10631.
369. Lee N, Pimienta G, Steitz JA. AUF1/hnRNP D is a novel protein partner of the EBER1 noncoding RNA of Epstein-Barr virus. RNA. 2012;18:2073-2082.
370. Stoecklin G, Colombi M, Raineri I, et al. Functional cloning of BRF1, a regulator of ARE-dependent mRNA turnover. EMBO J. 2002;21:4709-4718.